

Statics and dynamics of skyrmions interacting with disorder and nanostructures

C. Reichhardt[✉] and C. J. O. Reichhardt[†]

*Theoretical Division and Center for Nonlinear Studies, Los Alamos National Laboratory,
Los Alamos, New Mexico 87545, USA*

M. V. Milošević[‡]

*NANOLab Center of Excellence, Department of Physics, University of Antwerp,
Groenenborgerlaan 171, B-2020 Antwerp, Belgium*

 (published 20 September 2022)

Magnetic skyrmions are topologically stable nanoscale particlelike objects that were discovered in 2009. Since that time, intense research interest in the field has led to the identification of numerous compounds that support skyrmions over a range of conditions spanning from cryogenic to room temperatures. Skyrmions can be set into motion under various types of driving, and the combination of their size, stability, and dynamics makes them ideal candidates for numerous applications. At the same time, skyrmions represent a new class of system in which the energy scales of the skyrmion-skyrmion interactions, sample disorder, temperature, and drive can compete. A growing body of work indicates that the static and dynamic states of skyrmions can be influenced strongly by pinning or disorder in the sample; thus, an understanding of such effects is essential for the eventual use of skyrmions in applications. The current state of knowledge regarding individual skyrmions and skyrmion assemblies interacting with quenched disorder or pinning is reviewed. The microscopic mechanisms for skyrmion pinning, including the repulsive and attractive interactions that can arise from impurities, grain boundaries, or nanostructures, are outlined. This is followed by descriptions of depinning phenomena, sliding states over disorder, the effect of pinning on the skyrmion Hall angle, the competition between thermal and pinning effects, the control of skyrmion motion using ordered potential landscapes such as one- or two-dimensional periodic asymmetric substrates, the creation of skyrmion diodes, and skyrmion ratchet effects. Highlighted are the distinctions arising from internal modes and the strong gyrotropic or Magnus forces that cause the dynamical states of skyrmions to differ from those of other systems with pinning, such as vortices in type-II superconductors, charge density waves, or colloidal particles. Throughout this review future directions and open questions related to the pinning and dynamics in skyrmion systems are also discussed.

DOI: [10.1103/RevModPhys.94.035005](https://doi.org/10.1103/RevModPhys.94.035005)

CONTENTS

I. Introduction	2	C. Avalanches	29
II. Pinning in Particlelike Systems	5	D. Continuum-based simulations of the dynamic phase diagram	30
III. Models of Skyrmions and Mechanisms of Skyrmion Pinning	7	E. Three-dimensional skyrmion dynamics	30
A. Particle-based approaches to skyrmion dynamics and pinning	8	F. Further directions for dynamic skyrmion phases with random disorder	31
IV. Micromagnetic Models	10	VII. Pinning and the Skyrmion Hall Angle	32
A. Pinning mechanisms	11	A. Thermal effects	36
B. Skyrmion pinning by individual versus extended defects and the role of the Magnus force	14	B. Future directions	37
C. Discussion	16	VIII. Nanostructured and Periodic Landscapes	38
V. Collective States and Skyrmion Lattices with Pinning	17	A. One-dimensional periodic substrates and speedup effects	39
A. Future directions	21	B. Skyrmions with 2D periodic pinning	42
VI. Depinning Dynamics of Skyrmions with Pinning	21	C. Further directions for 1D and 2D periodic substrates	44
A. Elastic and plastic depinning	23	D. Asymmetric arrays, diodes, and ratchets	46
B. Noise	27	E. Coupling skyrmions to other quasiperiodic lattice structures	47
		F. Single skyrmion manipulation	48
		IX. Future Directions	48
		X. Conclusion	49
		Acknowledgments	49
		References	49

[✉]reichhardt@lanl.gov

[†]cjrx@lanl.gov

[‡]milorad.milosevic@uantwerpen.be

I. INTRODUCTION

Skyrmions were first introduced by Tony Skyrme, whose goal was to obtain low-mass baryon particles from a nonlinear field theory in which the topological quantum number was identified with the baryon number. Skyrme showed that such excitations could be stabilized in a sigma model by introducing additional nonlinear terms (Skyrme, 1961, 1962). The concept of particlelike field solutions, which came to be called skyrmions, spread far beyond nuclear physics and has been applied in a wide variety of systems, including two-dimensional (2D) electron gases (Sondhi *et al.*, 1993; Brey *et al.*, 1995), Bose-Einstein condensates (Al Khawaja and Stoof, 2001), and liquid crystals (Ackerman *et al.*, 2014). The theoretically proposed existence of skyrmions in magnetic systems (Bogdanov and Yablonskii, 1989; Rößler, Bogdanov, and Pfleiderer, 2006) was confirmed experimentally in 2009 when neutron scattering experiments revealed a sixfold scattering pattern in the chiral magnet MnSi, indicating the presence of a collection of lines forming a 2D hexagonal skyrmion lattice (Mühlbauer *et al.*, 2009). Shortly afterward, direct Lorentz microscopy images of the skyrmion lattice were obtained in thin-film samples (Yu *et al.*, 2010). Since then, skyrmions with sizes ranging from micron scale down to 10 nm have been identified in a growing number of 2D, three-dimensional (3D), and layered materials (Heinze *et al.*, 2011; Yu *et al.*, 2011; Seki *et al.*, 2012; Milde *et al.*, 2013; Nagaosa and Tokura, 2013; Romming *et al.*, 2013; Jiang *et al.*, 2015; L. Wang *et al.*, 2018).

As an applied magnetic field is increased, a skyrmion lattice emerges from the helical state, remains stable over a range of temperatures and fields, and then disappears at the ferromagnetic transition (Mühlbauer *et al.*, 2009; Nagaosa and Tokura, 2013). The predicted spin structures of a skyrmion lattice and an individual skyrmion, shown schematically in Figs. 1(a) and 1(b), agree well with the initial Lorentz microscopy images in Figs. 1(c) and 1(d) of skyrmions that are approximately 90 nm in diameter (Yu *et al.*, 2010). These first observations of magnetic skyrmions were performed at temperatures near $T = 30$ K, but since that time numerous magnetic systems have been identified that support skyrmions at and above room temperature (Jiang *et al.*, 2015; Tokunaga *et al.*, 2015; Boulle *et al.*, 2016; Moreau-Luchaire *et al.*, 2016; Wiesendanger, 2016; Woo *et al.*, 2016; Soumyanarayanan *et al.*, 2017). Figure 2 shows images of room-temperature skyrmion bubbles of diameter close to a micron (Jiang *et al.*, 2015). The skyrmion lattice illustrated in Fig. 1 is composed of Bloch skyrmions stabilized by the bulk Dzyaloshinskii-Moriya interaction (DMI) (Finocchio *et al.*, 2016; Wiesendanger, 2016; Fert, Reyren, and Cros, 2017; Jiang, Chen *et al.*, 2017; Tokura and Kanazawa, 2021), while in the system in Fig. 2, as well as in general multilayer systems containing well-defined interfaces, bubblelike Néel skyrmions stabilized by an interfacial DMI appear (Zhang, Zhou *et al.*, 2020; Göbel, Mertig, and Tretiakov, 2021). There are also transitions from hexagonal to square skyrmion lattices (Yi *et al.*, 2009; Karube *et al.*, 2016; Nakajima, Oike *et al.*, 2017), as well as new types of particlelike textures such as a square meron lattice that transitions into a triangular skyrmion lattice (Yu, Koshibae *et al.*, 2018).

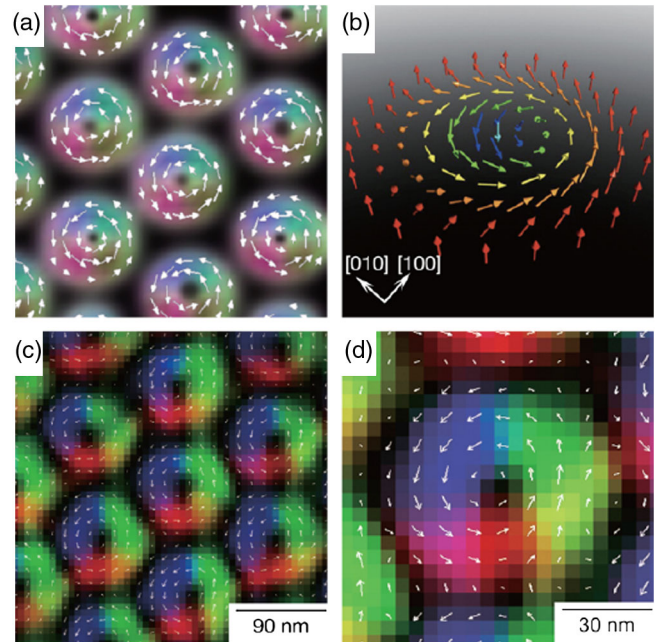


FIG. 1. Skyrmion crystal image obtained using Lorentz microscopy on thin-film $\text{Fe}_{0.5}\text{Co}_{0.5}\text{Si}$ near $T = 25$ K. (a) Spin structures predicted by simulation. (b) Schematic of the spin configuration in a single skyrmion. (c) Lorentz image of the skyrmion lattice. (d) Magnified view of panel (c). Here the skyrmions are on the order of 90 nm in diameter. From Yu *et al.*, 2010.

Skyrmions can be 2D in thin films (Mühlbauer *et al.*, 2009; Yu *et al.*, 2010), can have a layered or pancakelike structure in layered materials, can form 3D lines in bulk materials (Milde *et al.*, 2013; Park *et al.*, 2014; Zhang, van der Laan *et al.*, 2018; Birch *et al.*, 2020), and can assemble into 3D lattices of particlelike hedgehogs in certain bulk systems (Lin and Batista, 2018; Fujishiro *et al.*, 2019).

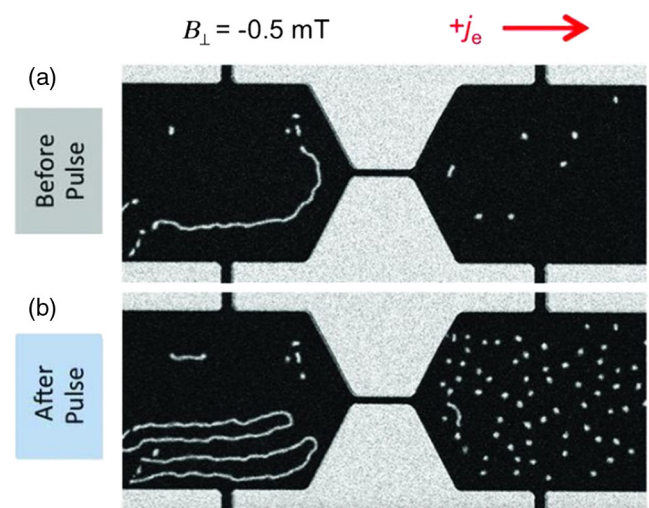


FIG. 2. Image of skyrmion creation at room temperature by passing current through a constriction. Here the skyrmions are approximately a micron in diameter. The constriction at the center of the image is $3 \mu\text{m}$ wide and $20 \mu\text{m}$ long. From Jiang *et al.*, 2015.

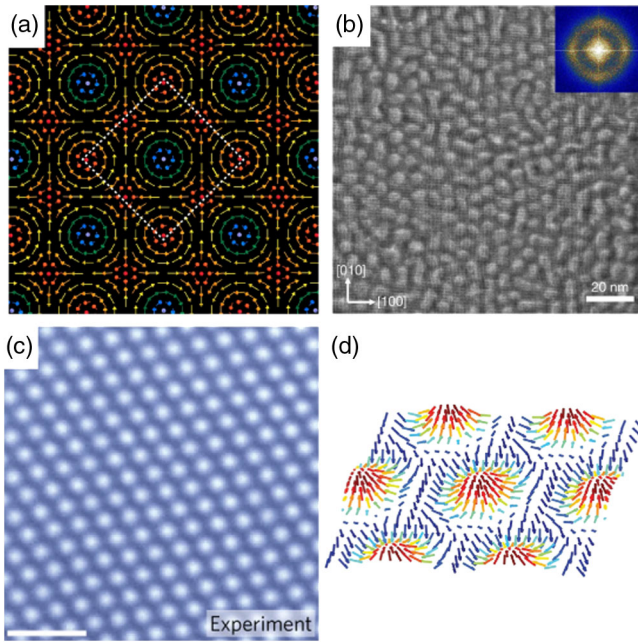


FIG. 3. Different types of skyrmionic textures in real space. (a) Schematic magnetization texture of a square meron lattice. The dashed square is about 100 nm on a side in a typical experiment. From Yu, Koshibae *et al.*, 2018. (b) Image of a polar skyrmion structure. From Das *et al.*, 2019. (c) Image of a half skyrmion lattice in a liquid-crystal system. The scale bar is 1 μm long. From Nych *et al.*, 2017. (d) Vector representation of the electric field for a Néel-type optical skyrmion that is roughly 500 nm in diameter. From Tsesses *et al.*, 2018.

Different species of skyrmions can exist (Leonov and Mostovoy, 2015), including biskyrmions (Yu *et al.*, 2014; Wang *et al.*, 2016; Takagi *et al.*, 2018), multiply charged skyrmions (Rybakov and Kiselev, 2019), antiskyrmions (Hoffmann *et al.*, 2017; Nayak *et al.*, 2017; Desplat, Kim, and Stamps, 2019; Peng *et al.*, 2020; Ritzmann *et al.*, 2020), antiferromagnetic skyrmions (Barker and Tretiakov, 2016; Zhang, Xia *et al.*, 2016; Akosa *et al.*, 2018), magnetic bilayer skyrmions (Zhang, Zhou, and Ezawa, 2016b), square vortex and skyrmion phases in antiferromagnets, (Li and Kovalev, 2020) elliptical skyrmions (Jena *et al.*, 2020; Xia *et al.*, 2020), meron lattices (Yu, Koshibae *et al.*, 2018; Gao *et al.*, 2020; Y. J. Wang *et al.*, 2020), half skyrmions (S. Zhang *et al.*, 2020; Jani *et al.*, 2021) bimerons (Zhang, Xia *et al.*, 2020; Jani *et al.*, 2021), hopfions (Wang, Qaiumzadeh, and Brataas, 2019; Liu *et al.*, 2020; Kent *et al.*, 2021), hedgehog textures (Fujishiro *et al.*, 2019; Zou, Zhang, and Tserkovnyak, 2020), and polar skyrmions (Das *et al.*, 2019). Skyrmions can be described by their winding number or topological index $N = (1/4\pi) \int \mathbf{m} \cdot [(\partial\mathbf{m}/\partial x) \times (\partial\mathbf{m}/\partial y)] dx dy$, where \mathbf{m} is a unit vector oriented in the direction of the local magnetic field (Braun, 2012). The skyrmion number is classified by the second homotopy group on a two-sphere $\pi_2(S^2)$. Skyrmions have $N = 1$, skyrmionium has a double twisted core and $N = 0$, (Zhang, Zhou, and Ezawa, 2016a; Zhang, Kronast *et al.*, 2018), and recently bimeronium was proposed to exist (Zhang *et al.*, 2021). Chiral bobbers resemble skyrmions,

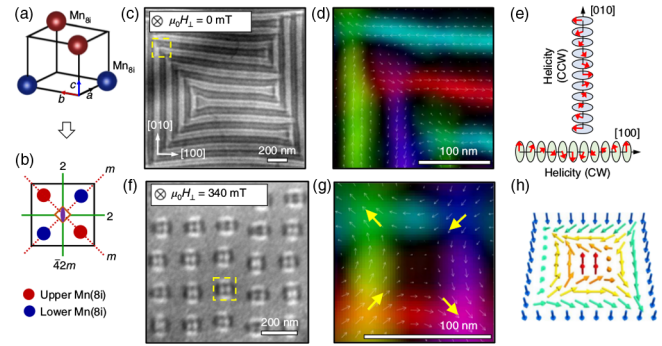


FIG. 4. Antiskyrmions with noncircular shapes can produce alternative lattice structures. (a),(b) Schematics of the magnetic Mn atom locations in $\text{Mn}_{1.4}\text{Pt}_{0.9}\text{Pd}_{0.1}\text{Sn}$. (c) Lorentz image of a helical stripe state. (d) The corresponding clockwise (CW) and counterclockwise (CCW) magnetization textures from the dashed yellow box in (c). (e) Illustration of the same helical state. (f) Square antiskyrmions forming a square lattice in a Lorentz image under an applied field of 340 mT. (g) The corresponding magnetization texture of the antiskyrmion in the dashed yellow box in (f), where large yellow arrows are Bloch lines. (h) Schematic illustration of the spin texture of the square antiskyrmion. From Peng *et al.*, 2020.

but their magnetic tube texture passes only partway through the bulk (Rybakov *et al.*, 2015; Zheng *et al.*, 2018). Skyrmions and similar quasiparticle textures arise in many nonmagnetic systems including graphene (Bömerich, Heinen, and Rosch, 2020; Zhou *et al.*, 2020), liquid crystals (Nych *et al.*, 2017; Duzgun, Selinger, and Saxena, 2018; Foster *et al.*, 2019), and optical (Tsesses *et al.*, 2018) and plasmonic systems (Davis *et al.*, 2020).

A variety of possible textures appear in Fig. 3, including a square meron lattice (Yu, Koshibae *et al.*, 2018) in Fig. 3(a), polar skyrmions (Das *et al.*, 2019) in Fig. 3(b), a half skyrmion lattice in a chiral liquid-crystal system (Nych *et al.*, 2017) in Fig. 3(c), and an optical skyrmion (Tsesses *et al.*, 2018) in Fig. 3(d). Magnetic half skyrmions, where the spin orientation rotates only by π , have half a unit of topological charge (Salomaa and Volovik, 1987; Hirata *et al.*, 2019; S. Zhang *et al.*, 2020; Jani *et al.*, 2021) and cannot exist in isolation. They are topologically confined as pairs that are equivalent to an elongated skyrmion if they are of the same topological charge. Liquid-crystal half skyrmions, which have a director field instead of a spin degree of freedom, resemble $N = 1$ magnetic skyrmions, and are unconfined. Isolated half skyrmions, known as merons and antimérons, of either Néel or Bloch character were recently found in antiferromagnetic systems (Jani *et al.*, 2021). Polar skyrmions are an electrical dipole version of magnetic skyrmions (Das *et al.*, 2019). Skyrmion textures are not always circular but can adopt other shapes that may modify the skyrmion lattice structure, as illustrated in Fig. 4, where the square symmetry of individual skyrmions in a $\text{Mn}_{1.4}\text{Pt}_{0.9}\text{Pd}_{0.1}\text{Sn}$ magnet produces a square skyrmion lattice (Peng *et al.*, 2020).

Skyrmions can be set into motion with an applied drive, such as the spin torque from a current. The skyrmion motion can be deduced from changes in the topological Hall effect (THE) (Schulz *et al.*, 2012; Liang *et al.*, 2015) or observed

through direct imaging (Jiang *et al.*, 2015, 2017; Woo *et al.*, 2016; Legrand *et al.*, 2017; Litzius *et al.*, 2017; Tolley, Montoya, and Fullerton, 2018; Woo *et al.*, 2018). It is also possible to move skyrmions with temperature gradients (Kong and Zang, 2013; Mochizuki *et al.*, 2014; Pöllath *et al.*, 2017; Z. Wang *et al.*, 2020), magnetic fields (Shen, Xia *et al.*, 2018; Zhang, Wang *et al.*, 2018; Casiraghi *et al.*, 2019), electric fields (White *et al.*, 2014; Kruchkov *et al.*, 2018; Ma *et al.*, 2019), microwaves (Wang *et al.*, 2015; Ikka, Takeuchi, and Mochizuki, 2018), spin waves (Zhang, Ezawa *et al.*, 2015; Zhang, Müller *et al.*, 2017; Shen, Zhang *et al.*, 2018), magnons (Psaroudaki and Loss, 2018), or acoustic waves (Nepal, Güngördü, and Kovalev, 2018). Because of their size scale, mobility, and stability at room temperature (Desplat *et al.*, 2018), skyrmions have great potential for use in a wide range of applications, such as racetrack memory (Fert, Cros, and Sampaio, 2013; Tomasello *et al.*, 2014; Fert, Reyren, and Cros, 2017; Müller, 2017; Everschor-Sitte *et al.*, 2018; Suess *et al.*, 2018, 2019), logic devices (Zhang, Ezawa, and Zhou, 2015; Luo, Song *et al.*, 2018; Liu *et al.*, 2019; Mankalale *et al.*, 2019), or novel computing architectures (Pinna *et al.*, 2018; Prychynenko *et al.*, 2018; Zázvorka *et al.*, 2019; Grollier *et al.*, 2020; Song *et al.*, 2020). Many of the proposed skyrmion-based devices would require the skyrmions to move through a nanostructured landscape in a highly controlled fashion.

A growing body of work indicates that, in many skyrmion systems, pinning and the effects of quenched disorder are important for determining both the static and dynamic skyrmion response (Nagaosa and Tokura, 2013; Wiesendanger, 2016; Woo *et al.*, 2016; Fert, Reyren, and Cros, 2017; Jiang *et al.*, 2017; Litzius *et al.*, 2017). Initial transport studies revealed only weak skyrmion-pinning effects, with a critical depinning force j_c in MnSi at $T = 28$ K of only $j_c \propto 10^6$ A/m² (Jonietz *et al.*, 2010; Schulz *et al.*, 2012), nearly 5 orders of magnitude smaller than the depinning force for magnetic domain walls (Tsoi, Fontana, and Parkin, 2003). In contrast, recent work by Woo *et al.* (2018) on room-temperature skyrmions in thin films revealed strong pinning with $j_c \propto 2.2 \times 10^{11}$ A/m². Similar high depinning thresholds observed in other systems (Hrabec *et al.*, 2017) indicate that a variety of skyrmion-pin interaction mechanisms arise in different materials that support skyrmions depending on the skyrmion size, the dimensionality, and the characteristics of the disorder in the sample. Magnetization and small-angle neutron scattering measurements (Kindervater *et al.*, 2020), along with resonant ultrasound spectroscopy (Luo, Lin *et al.*, 2018), indicate that the pinning potential can depend on the direction of the applied magnetic field. There have also been proposals for using defects or pinning to implement all-electrical detection of spin textures, including skyrmions, which would be valuable for applications (Fernandes, Bouhassoune, and Lounis, 2020).

Skyrmion motion and the skyrmion Hall effect (SkHE) can be strongly modified by pinning. The SkHE arises when the gyrotropic nature of the skyrmion dynamics causes the skyrmions to move at an angle called the skyrmion Hall angle (θ_{SkH}) with respect to the applied drive (Zang *et al.*, 2011; Iwasaki, Mochizuki, and Nagaosa, 2013b; Nagaosa and

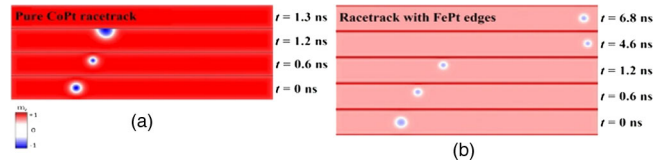


FIG. 5. Snapshots at different times of out-of-plane magnetization components from micromagnetic simulations of a skyrmion driven by a spin current applied parallel to a CoPt racetrack sample. (a) In a pure sample, the skyrmion travels to the edge and annihilates. (b) When the sample edge is lined with a repulsive material, the skyrmion is prevented from annihilating. From Lai *et al.*, 2017.

Tokura, 2013; Everschor-Sitte and Sitte, 2014). A skyrmion driven along a narrow strip by a current parallel to the strip does not follow the current but translates toward the strip edge. This sets a limit on the skyrmion speed since, for higher velocities, the skyrmion overcomes the edge barrier and annihilates, posing a problem for the use of skyrmions in strip-based devices (Iwasaki, Mochizuki, and Nagaosa, 2013a). In Fig. 5 we show images from micromagnetic simulations by Lai *et al.* (2017) of a skyrmion moving through a racetrack. For the pure sample in Fig. 5(a), the skyrmion travels toward the sample edge and is annihilated, but when the sample edges are rimmed with high crystalline anisotropy materials, as in Fig. 5(b), the skyrmion is repelled from the edge. Such repulsive interactions with nanostructures or engineered defect structures could enhance the performance of skyrmion-based devices (Purnama *et al.*, 2015; Juge *et al.*, 2021).

The motion of skyrmions through a strip can also be changed by placing pinning along the edges or in the bulk. Simulations (Müller and Rosch, 2015; Reichhardt, Ray, and Reichhardt, 2015a, 2015b; Reichhardt and Reichhardt, 2016; Kim and Yoo, 2017; Legrand *et al.*, 2017; Litzius *et al.*, 2020) and experiments (Jiang *et al.*, 2017; Litzius *et al.*, 2017, 2020; Woo *et al.*, 2018) show that the addition of pinning not only produces a finite depinning threshold for skyrmion motion but also generates a strong drive dependence of the skyrmion Hall angle, which increases from a small value at low drives to the pin-free intrinsic value $\theta_{\text{SkH}}^{\text{int}}$ as the drive increases. Pinning can also be detrimental since it increases the critical depinning force. Ideally, the skyrmions would remain in a fixed position and resist thermal wandering for arbitrarily long times at zero current while still moving at reasonable velocities above a critical current that is as low as possible. Pinning implies a trapping force; however, other forms of quenched disorder are possible, such as repulsive sites that deflect but do not pin the skyrmion. This type of quenched disorder could reduce the skyrmion Hall angle while still allowing motion under low currents.

Pinning effects can be beneficial under a variety of circumstances. The thermal and diffusive skyrmion motion observed in experiment (Nozaki *et al.*, 2019; Zázvorka *et al.*, 2019; Zhao *et al.*, 2020) need to be taken into account during device creation, particularly for smaller skyrmions. For example, a skyrmion serving as an information carrier in a memory device must remain locked in a specific location for long times, but room-temperature thermal motion could cause the

skyrmion to wander away and destroy the memory. Pinning could overcome the thermal effects over arbitrarily long times and make stable long-term memory possible. It would be ideal to have tunable pinning that would be absent when rapid motion of skyrmions is needed but strong when long-time stability of the skyrmion memory configuration is required. Different types of pinning have already been identified that have attractive, repulsive, radially symmetric, or radially asymmetric behavior. Devices could be created using nanoscale techniques to fabricate controlled pinning patterns in the form of lines or channels that guide skyrmions, periodic arrays that stabilize certain skyrmion configurations, or asymmetric pinning that produces skyrmion diodes, rectifiers, and logic devices. For future applications it is important to develop a thorough understanding of skyrmion pinning and dynamics.

Beyond applications, interacting skyrmions driven over pinning represent a class of systems in which collective and competing effects produce a rich variety of nonequilibrium dynamical phases (Fisher, 1998; Reichhardt and Reichhardt, 2017a). Skyrmion-skyrmion interactions favor a triangular skyrmion lattice, while the interactions of skyrmions with random pinning favor a disordered skyrmion structure, producing a competition between crystalline and glassy states even for static skyrmion configurations. Pinning opposes the skyrmion motion under an applied drive, and the competition between the pinning and driving forces generates complex dynamics near the depinning threshold. Additional competing effects appear when thermal fluctuations are important. Temperature can reduce the effectiveness of the pinning, favoring an ordered state, but can also disorder the skyrmion lattice.

In this review, we focus on aspects of pinning and dynamics in skyrmion systems. We highlight what is known currently about skyrmion pinning and the variety of mechanisms that can produce it, including changes in the DMI, atomic impurities, local anisotropy, sample thickness, damage tracks, missing spins, holes, or blind holes. We outline the microscopic models for pinning and skyrmion dynamics currently in use and show that skyrmions can have attractive, repulsive, or combined attractive and repulsive interactions with pointlike or linelike disorder. Throughout this review we discuss similarities and differences between skyrmions and other systems with pinning such as superconducting vortices, sliding charge density waves, Wigner crystals, and colloidal particles. In the absence of driving, we consider disorder-induced transitions from a skyrmion crystal to different types of glassy states. When a drive is added, we describe the different types of depinning that occur, ranging from elastic to plastic, as well as the effect of disorder on bulk transport measures such as velocity-force curves, the role of temperature, and creep effects. The effects of pinning on fluctuations, the skyrmion Hall angle, and the skyrmion-skyrmion interactions are also covered. In addition to sources of random disorder, we describe the pinning and dynamics of skyrmions on ordered structures such as 2D periodic, quasiperiodic, quasi-one-dimensional (quasi-1D) periodic, and 1D asymmetric substrates, which can produce commensurate and incommensurate states, soliton motion, and diode and ratchet effects.

In each section we discuss future directions including studies of skyrmions in bulk materials, skyrmion behavior in thin films with extended or point defects, the effects of nanostructured arrays with periodic or 1D modulation, the behavior of layered materials, the coupling of skyrmions to other topological defects such as vortices in type-II superconductors, and the effect of having different species of skyrmions coexist. Introduction of a columnar pinning landscape for 3D skyrmions could create a state analogous to the Bose glass found in type-II superconductors, cutting and entanglement effects, and the possibility of creating transformer geometries. We outline potential new measures for characterizing the skyrmion structures and dynamics that are borrowed from work in superconducting vortex dynamics, soft matter, and statistical physics, such as structural measures, force chains, jamming concepts, glassy effects, and defect proliferation.

Skyrmion physics is a vast topic encompassing many reviews that cover various other aspects of skyrmions. Broad reviews were given by Nagaosa and Tokura (2013), Bogdanov and Panagopoulos (2020), and Tokura and Kanazawa (2021). Materials supporting skyrmions were discussed by Li *et al.* (2021), while multilayers were treated by Jiang *et al.* (2017). Details of different skyrmionlike textures were given by Göbel, Mertig, and Tretiakov (2021). There have also been reviews on ways to create or delete skyrmions (Zhang, Zhou *et al.*, 2020; Marrows and Zeissler, 2021), imaging (Yu, 2021), collective spin excitations and magnonics (Garst, Waizner, and Grundler, 2017), nanoscale skyrmions (Wiesendanger, 2016), skyrmions in thin-film structures (Finocchio *et al.*, 2016), potential applications (Fert, Reyren, and Cros, 2017), memory technologies (Luo and You, 2021; Vakili *et al.*, 2021), the dynamics of magnetic excitations in chiral magnets (Lonsky and Hoffmann, 2020), and road maps for future directions (Back *et al.*, 2020).

II. PINNING IN PARTICLELIKE SYSTEMS

Systems with many interacting particles coupled to some form of disorder or pinning are known to exhibit rich static and dynamic phase behavior as a function of changing particle-particle interactions, disorder strength, and temperature. One of the best-studied examples of such systems is vortices in type-II superconductors (Blatter *et al.*, 1994), which have no Magnus force and are distinct from the vortices found in magnetic systems. In the absence of driving, superconducting vortices can form a triangular lattice, a weakly pinned Bragg glass in which the vortices remain elastic with topological order but still have glassy properties (Giamarchi and Le Doussal, 1995; Klein *et al.*, 2001), topologically disordered vortex glass states (Fisher, Fisher, and Huse, 1991; Henderson *et al.*, 1996; Nattermann and Scheidl, 2000; Ganguli *et al.*, 2015; Toft-Petersen *et al.*, 2018), entangled vortex lines (Nelson, 1988; Giller *et al.*, 1997), liquid states (Safar *et al.*, 1992; Cubitt *et al.*, 1993; Zeldov *et al.*, 1995), or reentrant liquid states (Banerjee *et al.*, 2000; Avraham *et al.*, 2001). Superconducting vortices in the presence of an external drive can exhibit elastic depinning, where the system transitions from a pinned crystal into a moving crystal state

(Bhattacharya and Higgins, 1993; Di Scala *et al.*, 2012; Reichhardt and Reichhardt, 2017a), or plastic depinning, where the moving state has a liquid structure (Jensen, Brass, and Berlinsky, 1988; Bhattacharya and Higgins, 1993; Matsuda *et al.*, 1996; Olson, Reichhardt, and Nori, 1998a; Fily *et al.*, 2010; Shaw *et al.*, 2012; Reichhardt and Reichhardt, 2017a). Plastically moving superconducting vortices at higher drives can transition into a moving crystalline (Bhattacharya and Higgins, 1993; Koshelev and Vinokur, 1994; Giamarchi and Le Doussal, 1996; Olson, Reichhardt, and Nori, 1998b; Reichhardt and Reichhardt, 2017a) or moving smectic phase (Balents, Marchetti, and Radzihovsky, 1998; Olson, Reichhardt, and Nori, 1998b; Pardo *et al.*, 1998). These different depinning and dynamical phase transitions produce distinct signatures in the bulk transport measures and velocity-force curves, as well as changes in the superconducting vortex lattice structure and fluctuations (Jensen, Brass, and Berlinsky, 1988; Bhattacharya and Higgins, 1993; Koshelev and Vinokur, 1994; Fisher, 1998; Olson, Reichhardt, and Nori, 1998b; Fily *et al.*, 2010; Di Scala *et al.*, 2012). Similar depinning and sliding dynamics occur in other systems of particlelike objects moving through quenched disorder, such as colloidal particles (Hu and Westervelt, 1995; Pertsinidis and Ling, 2008; Tierno, 2012), Wigner crystals (Williams *et al.*, 1991; Cha and Fertig, 1994, 1998; Kumar, Laitinen, and Hakonen, 2018), and certain pattern forming systems (Sengupta, Sengupta, and Menon, 2010; Morin *et al.*, 2017).

To highlight the similarities between skyrmions and other systems with pinning, in Fig. 6(a) we show a scanning tunneling microscopy image of a triangular superconducting vortex lattice (Hess *et al.*, 1989). In Fig. 6(b), a magneto-optical image reveals a disordered superconducting vortex structure. (Goa *et al.*, 2001). Figure 6(c) shows a colloidal triangular lattice observed with optical microscopy (Weiss, Larsen, and Grier, 1998), while in Fig. 6(d), the colloidal lattice is distorted by strong pinning, there are numerous topological defects, and the system forms a pinned glass (Pertsinidis and Ling, 2008). If the disorder is weak, as in Figs. 6(a) and 6(c), the particles depin without the generation of topological defects and flow elastically, while for strong disorder, as in Figs. 6(b) and 6(d), the particles depin plastically with large lattice distortions or with a coexistence of pinned and moving particles.

A crucial difference between skyrmions and the superconducting vortices or colloidal particles illustrated in Fig. 6 is the fact that skyrmions experience a strong nondissipative gyrotropic or Magnus force that generates a velocity component perpendicular to the net external forces acting on the skyrmion. We note that magnetic vortices in magnetic systems can also experience gyrotropic forces (Zvezdin, Belotelov, and Zvezdin, 2008). In many of the previously studied systems, the dynamics are overdamped and the particle velocity \mathbf{v}_d is strictly aligned with the net external force \mathbf{F}_{ext} , $\mathbf{v}_d = \alpha_d \mathbf{F}_{\text{ext}}$, where α_d is a damping constant. In a skyrmion system, the damping term is accompanied by a Magnus-force contribution of strength α_m to the velocity $\mathbf{v}_m = \alpha_m \hat{\mathbf{z}} \times \mathbf{F}_{\text{ext}}$, which generates a velocity component perpendicular to the applied force. The ratio α_m/α_d for skyrmions can be as large as 10 or even higher (Schulz *et al.*, 2012; Nagaosa and Tokura, 2013;

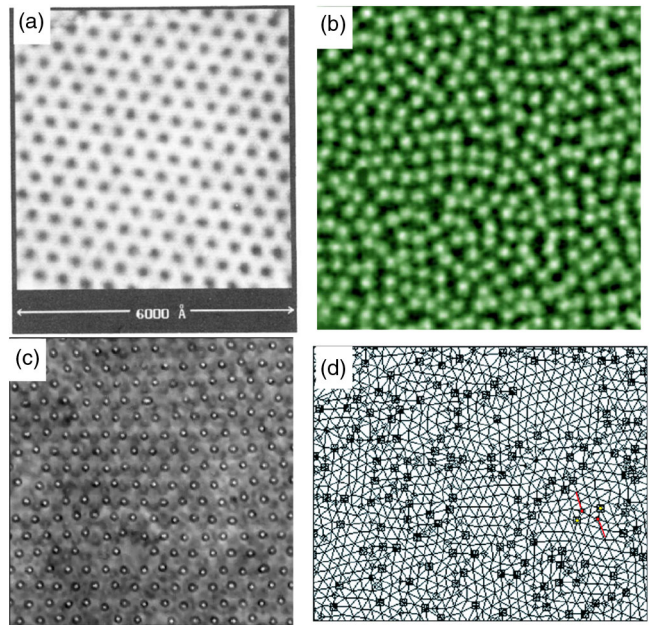


FIG. 6. (a) Scanning tunneling microscope image of an ordered superconducting vortex lattice. From Hess *et al.*, 1989. (b) Magneto-optical image of a disordered superconducting vortex lattice. From Goa *et al.*, 2001. (c) Optical microscope image of a colloidal lattice. From Weiss, Larsen, and Grier, 1998. (d) Delaunay triangulation from an optical microscope image of colloidal particle positions in a colloidal glass state. From Pertsinidis and Ling, 2008.

Everschor-Sitte and Sitte, 2014). One consequence of the Magnus force is the appearance of a SkHE in which the skyrmion moves at an angle θ_{SKH} with respect to the applied driving force. The intrinsic value of this angle derived from the Thiele equation (Thiele, 1973; Everschor-Sitte and Sitte, 2014; Brearton *et al.*, 2021) is $\theta_{\text{SKH}}^{\text{int}} = \tan^{-1}(\alpha_m/\alpha_d)$. The Magnus force affects both the skyrmion-skyrmion interactions and the motion of skyrmions through pinning sites. In Fig. 7(a) we show repulsively interacting particles initialized in a dense cluster and then allowed to move away from each other. In the overdamped limit with $\alpha_m = 0$ in Fig. 7(b), the particles move radially in the direction of the repulsive particle-particle interaction forces. In contrast, the particles in Fig. 7(c) have a finite Magnus force ($\alpha_m > 0$), which adds a strong rotational component to the radial displacement. If the dissipative term α_d were zero, only rotational motion of the particles would occur with no radial motion.

Many of the previously studied systems with pinning, including superconducting vortices, classical charges, and colloidal particles, are composed of stiff objects with negligible internal degrees of freedom, making a particle-based treatment of their dynamics appropriate. In contrast, skyrmions can exhibit excitations of internal modes (Onose *et al.*, 2012; Beg *et al.*, 2017; Garst, Waizner, and Grundler, 2017; Ikka, Takeuchi, and Mochizuki, 2018) or large distortions (Litzius *et al.*, 2017, 2020; Zeissler *et al.*, 2017; Gross *et al.*, 2018) that activate additional degrees of freedom, significantly impacting the statics and dynamics. Furthermore, moving skyrmions can emit spin waves that could modify the effective

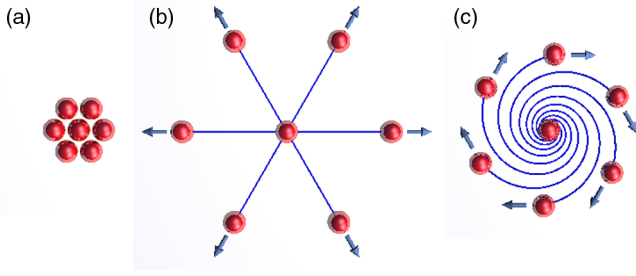


FIG. 7. Illustration of the difference between purely overdamped motion and motion with a Magnus force of strength α_m for particles with finite damping ($\alpha_d > 0$). (a) Initial dense cluster of particles. (b) Trajectories of overdamped particles with $\alpha_m = 0$ moving away from the center. (c) Trajectories of particles with a Magnus force $\alpha_m > 0$ moving away from the center, showing the emergence of nonconservative rotation.

skyrmion-skyrmion interactions (Schütte *et al.*, 2014; Koshibae and Nagaosa, 2018). The uniformity often associated with particle-based models may also not capture the behavior of a skyrmion system well. It is possible for skyrmions to coexist with a stripe phase or ferromagnetic domains (Müller *et al.*, 2017; Loudon *et al.*, 2018; Shibata *et al.*, 2018; Yu, Morikawa *et al.*, 2018), and in some systems there is considerable dispersion in the size of the skyrmions, making the skyrmion assembly effectively polydisperse (Karube *et al.*, 2018) This contrasts strongly with superconducting vortices, which are all the same size in a given sample.

III. MODELS OF SKYRMIONS AND MECHANISMS OF SKYRMION PINNING

An overall goal of any model is to identify universal features of skyrmions interacting with pinning or disorder; however, this is an open field and it is possible that there are several different fundamental rules depending on the details of the disorder and whether the skyrmion can be treated as a particle or as an emergent object that can be disordered or broken apart. The starting point for models of skyrmions is the energy functional (Bogdanov and Yablonskii, 1989)

$$\mathcal{H} = \int d\mathbf{r}^2 \left[\frac{J_{\text{ex}}}{2} (\nabla \mathbf{n})^2 + D \mathbf{n} \cdot \nabla \times \mathbf{n} - \mathbf{H}_a \cdot \mathbf{n} + H_{\text{dp}} \right], \quad (1)$$

where $\mathbf{n} = \mathbf{n}(\mathbf{r})$ indicates the direction of the normalized magnetization $\mathbf{n} = \mathbf{M}/M_s$, J_{ex} is the exchange term, D is the DMI produced by spin-orbit coupling, \mathbf{H}_a is the anisotropy term, and H_{dp} is the dipole-dipole interaction term

$$H_{\text{dp}} = -\frac{1}{2} \sum_{ij} \frac{\mu_0}{4\pi |\mathbf{r}_{ij}|^5} [3(\mathbf{n}_i \cdot \mathbf{r}_{ij})(\mathbf{n}_j \cdot \mathbf{r}_{ij}) - \mathbf{n}_i \cdot \mathbf{n}_j],$$

which in some cases can be stronger than the DMI interaction (Göbel, Henk, and Mertig, 2019). Additional terms can be added to represent pinning, thermal forces, gradient forces, and other effects. This Hamiltonian can be integrated as follows using the Landau-Lifshitz-Gilbert (LLG) equation (Tatara, Kohno, and Shibata, 2008):

$$\begin{aligned} \frac{d\mathbf{n}}{dt} = & \frac{pa^3}{2e} (\mathbf{j} \cdot \nabla) \mathbf{n} - \gamma \mathbf{n} \times \mathbf{B}_{\text{eff}} \\ & + \alpha \mathbf{n} \times \frac{d\mathbf{n}}{dt} - \frac{pa^3\beta}{2e} [\mathbf{n} \times (\mathbf{j} \cdot \nabla) \mathbf{n}]. \end{aligned} \quad (2)$$

The first term on the right-hand side of Eq. (2) gives the time-dependent motion of the magnetization, where \mathbf{j} is the spin-transfer-torque current, a is the lattice constant, p is the spin polarization of the electric current, and e is the elementary charge. The second term is the gyromagnetic interaction with the effective magnetic field $\mathbf{B}_{\text{eff}} = -(1/\gamma)\partial\mathcal{H}/\partial\mathbf{n}$, where γ is the gyromagnetic ratio. The third term is the Gilbert damping, and the final term is a coupling of the spins to the spin-polarized current \mathbf{j} of strength β .

Since it is computationally expensive to treat the full LLG equation, it is convenient to focus on the movement of the skyrmions without preserving the full underlying spin dynamics. In a particle-based skyrmion model, skyrmions are represented as point particles with dynamics that evolve according to the following equation of motion proposed by Thiele (1973) to describe a driven magnetic particle:

$$\mathcal{G} \times \dot{\mathbf{R}} + \alpha D \dot{\mathbf{R}} + m \ddot{\mathbf{R}} = \mathbf{F}_D. \quad (3)$$

In Eq. (3) \mathbf{F}_D is the driving force, α is the Gilbert damping of an individual spin, αD is the friction experienced by the skyrmion, and \mathcal{G} is the gyrocoupling term, analogous to the Coriolis force, that acts like a magnetic field applied perpendicular to the plane. The inertial term is proportional to the skyrmion mass m and can be neglected for small m . Additional second derivative terms can arise when internal modes of the skyrmion are excited. To derive Eq. (3), Thiele projected the LLG equation onto the translational modes of the spin texture, as described by Tomasello *et al.* (2014).

The Thiele equation can be extended with terms representing a substrate potential, field gradients, thermal forces, or gyrodamping (Schütte *et al.*, 2014). Because of its flexibility, the Thiele approach has been used to model the dynamics of single rigid skyrmions (Büttner *et al.*, 2015). The mass term is usually neglected since continuum simulations indicate that any inertial effects are small (Schütte *et al.*, 2014); however, future magnetic, soft matter, atomic, molecular, or optical skyrmion systems could be identified in which the mass term becomes important. In this case, new phenomena such as phonons or shock waves could arise. Examples of effects that appear in overdamped particle models when inertial effects are introduced can be found in the literature on frictional systems (Vanossi *et al.*, 2013).

In metallic systems, skyrmions can be driven by spin-torque interactions generated by an electric current. For the LLG approach, skyrmions that arise from localized d -electron spins are coupled to the current-carrying itinerant s electrons. In insulating or semiconducting systems, skyrmions can be driven by a thermal gradient, an electric field, or even optical trapping. The particle-based approach abstracts away the microscopic interactions producing the driving, and does not capture effects such as the distortion of skyrmions by the drive; however, additional terms could be added to the particle-based model in order to mimic such effects.

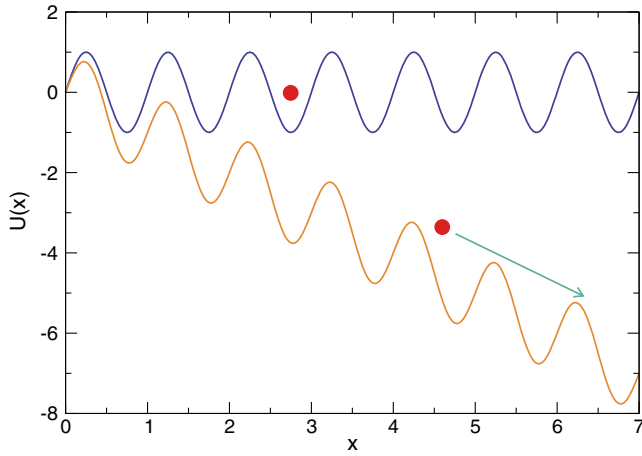


FIG. 8. The simplest system exhibiting depinning is an overdamped particle (filled circle) in a sinusoidal potential $U(x) = A \cos(kx)$ tilted by a driving force F_D . The particle is pinned when $F_D < F_c$ (upper blue curve), where F_c is the critical driving force that must be applied to enable the particle to slide. Steady state motion occurs when $F_D > F_c$ (lower orange curve).

A. Particle-based approaches to skyrmion dynamics and pinning

One of the simplest pictures of pinning and sliding dynamics is a model of a single particle in a tilted sinusoidal potential with period L . To further simplify the problem, consider an overdamped particle that obeys the following equation of motion:

$$\alpha_d \frac{dx}{dt} = -\frac{dU(x)}{dx} + F_D. \quad (4)$$

In Eq. (4) α_d is the damping constant, F_D is the external dc drive, and $U(x) = A \cos(kx)$, where $k = 2\pi/L$. When $A = 0$, the substrate disappears and the particle moves in the driving direction with velocity $v = F_D/\alpha_d$. When $A > 0$, there is a finite depinning threshold F_c and no steady state motion occurs unless $F_D > F_c$. If we set $A = A_0/k$, we obtain a critical force of $F_c = A_0$. For drives close to but above the critical force ($F_D \gtrsim F_c$), the particle slides with velocity $v \propto (F_D - F_c)^\beta$, where $\beta = 1/2$ (Fisher, 1985). At higher drives, as in Fig. 8, the velocity approaches the clean value limit of $v \propto F_D$.

Coupling to a thermal bath is modeled by adding a fluctuating force term $\eta(t)$ representing Langevin kicks. These obey the correlations $\langle \eta(t) \rangle = 0$ and $\langle \eta(t)\eta(t') \rangle = 2k_B T \delta(t - t')$, where k_B is the Boltzmann constant. When $F_D = 0$, the particle thermally hops left or right with equal probability according to an Arrhenius law, with instantaneous velocity $|v| \propto \exp(-U/k_B T)$ and zero average velocity. An applied drive biases the Arrhenius jumps to be larger in the driving direction, and the time-averaged velocity becomes finite. The potential $U(x)$ is replaced by $U(x) \pm U_D(x)$, where for a linear drive $U_D(x) = U(x) - F_D x$, and a creep regime emerges. The creep velocity for $F < F_c$ is of the form

$$v \propto C_A \exp\left(\frac{A - F_D}{kT}\right), \quad (5)$$

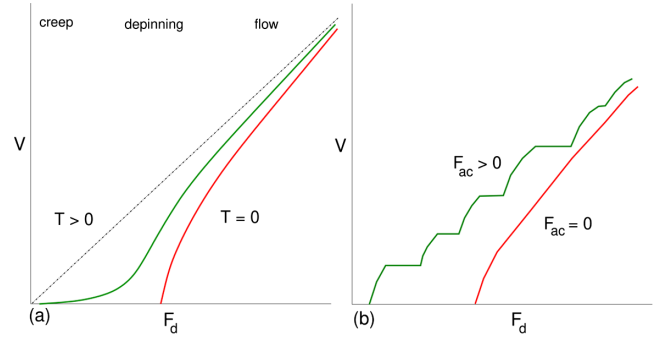


FIG. 9. (a) Schematic velocity v vs drive F_d curves for a system with a finite depinning threshold F_c at zero temperature ($T = 0$; lower red curve) and finite temperature ($T > 0$; upper green curve). Finite temperature creep occurs when the velocity remains nonzero for $F_d < F_c$. The $T > 0$ velocity-force curve changes shape near F_c at the crossover from creep to flow. The dashed line indicates the free-flow limit $v \propto F_d$ for a system with no pinning. (b) The same for particles moving over a periodic substrate with a finite depinning threshold F_c at zero temperature ($T = 0$). Lower red curve, response in the absence of ac driving; upper green curve, Shapiro steps appear when a finite ac drive is superimposed on the dc driving force.

where C_A is the attempt frequency. Figure 9(a) shows schematic velocity-force curves at $T = 0$ and $T > 0$. Even at finite temperatures, the velocity-force curves change noticeably at F_c when a crossover occurs from intermittently hopping creep motion for $F_D < F_c$ to continuous flow for $F_D > F_c$. An Arrhenius treatment of creep motion was proposed in Anderson-Kim models for superconducting vortices (Anderson and Kim, 1964). This approach can be modified for multiple interacting particles to capture collective creep, plastic creep, or glassy effects, which typically introduce a power law prefactor to the exponential velocity term (Feigel'man *et al.*, 1989; Luo and Hu, 2007).

It is possible to add other terms to Eq. (4), including substrate asymmetry or disorder as well as an inertial term $M d^2x/dt^2$, where M is the particle mass. If the dc drive is combined with an ac drive of the form $F^{\text{ac}} = A_{\text{ac}} \sin(\omega t)$, the well-known Shapiro step phenomenon appears in the form of steps in the velocity-force curves (Shapiro, 1963). In Fig. 9(b), we show a schematic velocity-force curve for combined dc and ac driving of particles over a periodic substrate, where velocity steps occur over fixed intervals of the dc drive amplitude. The Shapiro steps disappear for zero ac drive, and their widths oscillate as a function of ac drive amplitude or frequency. The substrate complexity can be increased by adding random disorder or by introducing 2D spatial variation, such as square or triangular pinning lattices. For an overdamped system, the 1D picture of depinning generally captures the behavior of a 1D or 2D substrate. This is not the case for skyrmions, since the Magnus force causes 2D skyrmions to exhibit different dynamics than their completely 1D counterparts.

The next level of complexity is to include multiple interacting or coupled particles, such as dimers or trimers connected by springs on a periodic 1D substrate. This resembles the well-known Frenkel-Kontorova model consisting of a 1D chain of

elastically coupled particles moving over a 1D periodic substrate (Braun and Kivshar, 1998). This model can be extended to describe a 1D string of particles or a 2D array of particles moving in two or three dimensions and coupled to a random substrate. For example, a 2D triangular array of skyrmions could be modeled as a 2D elastic lattice. In 3D, a single 1D linelike string could be modeled as an elastically coupled array of elements extending along the string length. Additional terms can be incorporated into the equation of motion to capture specific effects. When the particles are coupled by unbreakable elastic springs that do not allow neighbor exchanges, phase slips, or breaking of the lattice, the system is said to be in an elastic limit. Here the exact details of the particle-particle interactions can be ignored since the system is represented as a collection of harmonic springs. This approximation is appropriate when both the pinning and the temperature are sufficiently weak that only small lattice distortions occur. It has been applied to the depinning of directed lines (Ertaş and Kardar, 1996; Kardar, 1998), superconducting vortices (Dobramysl, Pleimling, and Täuber, 2014), sliding charge density waves (Fisher, 1985), models of friction (Vanossi *et al.*, 2013), and even plate tectonics (Carlson, Langer, and Shaw, 1994). For skyrmions, elastically coupled particle models can be used for 2D skyrmion lattices moving over weak disorder well below the temperature at which dislocations can be created thermally, as well as for individual or coupled 3D skyrmion lines. Additional terms such as the Magnus force can be inserted into the Frenkel-Kontorova model to capture long-wavelength features of the depinning and sliding states.

The next step beyond an elastically coupled system is models with pairwise particle-particle interactions that can be of short, intermediate, or long range. Such models allow neighbor exchange, dislocation generation, and other plastic or nonaffine events (Fisher, 1998; Reichhardt and Reichhardt, 2017a). Driven particle-based models that undergo depinning have been used extensively in a wide range of studies of hard matter systems, such as superconducting vortices, and soft matter systems, such as colloidal particles and granular matter (Reichhardt and Reichhardt, 2017a). Particle-based models capture realistic pairwise particle-particle interactions and permit transitions between elastic and plastic motion. They are also generally more computationally efficient than fully continuum models, such as micromagnetic skyrmion models; however, they neglect the small-scale degrees of freedom responsible for such phenomena as magnon generation and skyrmion shape changes, which can be important in skyrmion dynamics. The particle-particle interaction potentials are typically more complex than simple nearest-neighbor harmonic interactions and have a range that depends strongly on the microscopic details of the system. For example, in thin-film superconductors, the pairwise interactions between superconducting vortices are logarithmic, requiring all particles to interact with all other particles and with image charges, while in colloidal systems with strong screening a particle only interacts with its first or second nearest neighbors.

To capture particle-particle interactions in the Thiele approach, Lin *et al.* (2013b) proposed a particle-based model including skyrmion-skyrmion, skyrmion-pinning, and skyrmion-driving force interactions of the following form:

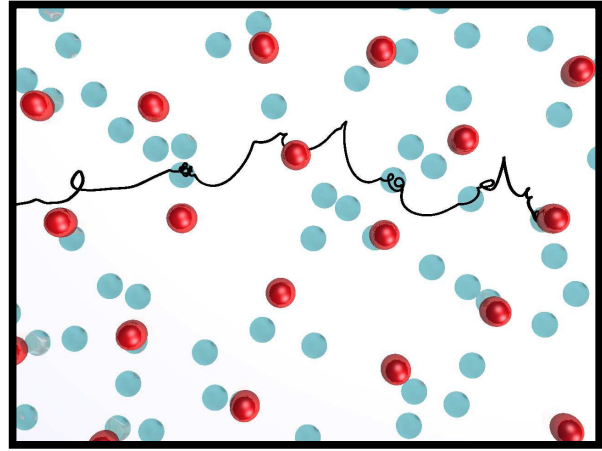


FIG. 10. Real-space image of skyrmions (red spheres) in a particle-based model driven through randomly arranged pinning sites (blue disks) in a plastic flow phase. The trajectory of a single skyrmion (black line) shows spiraling motions inside the pinning sites. From Reichhardt, Ray, and Reichhardt, 2015a.

$$\alpha_m \hat{z} \times \mathbf{v}_i + \alpha_d \mathbf{v}_i = \mathbf{F}_i^{ss} + \mathbf{F}_i^p + \mathbf{F}^D. \quad (6)$$

In Eq. (6) $\mathbf{v}_i = d\mathbf{r}_i/dt$ is the skyrmion velocity, α_d is the damping constant that aligns \mathbf{v}_i parallel to the external forces, and α_m is the strength of the Magnus term that aligns \mathbf{v}_i perpendicular to the external forces. When both α_d and α_m are finite, the skyrmions move at an angle called the intrinsic skyrmion Hall angle $\theta_{\text{SkH}}^{\text{int}} = \tan^{-1}(\alpha_m/\alpha_d)$ with respect to an externally applied driving force. Lin *et al.* (2013b) modeled the skyrmion-skyrmion interaction as a short-range repulsive force of the form $\mathbf{F}_i^{ss} = \sum_{j \neq i}^N K_1(r_{ij}) \hat{\mathbf{r}}_{ij}$, where K_1 is the modified Bessel function, $r_{ij} = |\mathbf{r}_i - \mathbf{r}_j|$ is the distance between skyrmions i and j , and $\hat{\mathbf{r}}_{ij} = (\mathbf{r}_i - \mathbf{r}_j)/r_{ij}$. Figure 10 shows a snapshot from a 2D particle-based skyrmion simulation model illustrating the skyrmion locations, pinning site locations, and the trajectory of one of the skyrmions, which undergoes rotational motion due to the Magnus force as it moves across the pinning sites (Reichhardt, Ray, and Reichhardt, 2015a). The model proposed by Lin *et al.* (2013b) has both advantages and disadvantages. It neglects inertial effects, changes in the skyrmion shape, magnon generation, and possible many-body interaction terms. On the other hand, it allows for greater computational efficiency than micromagnetic simulations do, permitting many thousands of skyrmions to be simulated over long periods of time. In many cases the particle-based model successfully captures the robust general features of the system.

Particle-based models can be substantially modified based on insight gained from micromagnetic simulations or experiments. For instance, the skyrmion interactions are typically modeled as a short-range repulsion; however, some micromagnetic simulations (Rózsa *et al.*, 2016; Loudon *et al.*, 2018; Leonov and Pappas, 2019) and experiments (Du *et al.*, 2018; Loudon *et al.*, 2018) show evidence of skyrmion clustering, suggesting that the skyrmion interactions are of longer range and could be modeled with a different potential. Some systems show a transition from a square to a triangular skyrmion lattice

(Takagi *et al.*, 2020), which can be modeled by including an additional higher order symmetry term in the pairwise potential of the following form (Olszewski *et al.*, 2018):

$$V(R, \theta) = K(r)[1 + A \cos^2(n_a\{\theta - \phi\}/2)]. \quad (7)$$

In Eq. (7) θ is the angle between the two skyrmions, ϕ is the rotation angle of the axis, and n_a is the number of symmetry directions in the potential, where $n_a = 4$ would favor square ordering. To capture the variation of skyrmion size found in some systems, a varying screening length λ_i with some distribution could be used in the interaction potential $K_1(r/\lambda_i)$. Three-body and multibody effects can be added by including higher order potentials such as a three-body $V_{i,j,k}$ extracted from micromagnetic simulations, in analogy to the techniques used to model such effects in colloidal systems (Sengupta, Sengupta, and Menon, 2010). The skyrmion dynamics can also be modified, such as by giving an antiskyrmion a fourfold modulation of its dissipative term or different dissipation terms for different directions of driving (Kovalev and Sandhoefner, 2018). Other studies have shown trochoidal skyrmion motion, some types of which can be modeled with particle-based approaches (Ritzmann *et al.*, 2018; Takagi *et al.*, 2020).

A variety of potentials can be used to represent the pinning term F_i^p , including short-range attraction (Lin *et al.*, 2013b), short-range repulsion, longer-range pinning arising from strain fields or magnetic interactions, sites with competing attraction and repulsion of the type observed in micromagnetic simulations (Müller and Rosch, 2015), or long-range smoothly varying landscapes. It is also possible to add a thermal term to the skyrmion equation of motion by introducing Langevin kicks (Brown, Täuber, and Pleimling, 2018; Reichhardt and Reichhardt, 2019b). A particle-based picture is appropriate when the pinning produces little distortion of the skyrmion since microscopic changes of the spin configurations by the pinning are treated in a mean field manner instead of directly. The microscopic interactions of a skyrmion with the pinning landscape are better captured with micromagnetic approaches.

In some cases, additional terms can be incorporated into the particle-based model to mimic microscopic effects, such as by representing breathing modes through a time dependence of the skyrmion interactions or the dissipative or Magnus-force magnitudes. Similarly, shape changes of skyrmions that become compressed or elongated in pinning sites can be modeled by modifying the particle-particle interactions when at least one of the skyrmions is inside a pinning site. Similar modifications could be applied for shape-changing skyrmions moving across a landscape. To represent skyrmion creation or annihilation, rules could be added defining certain conditions for the combination of external and pinning forces that, when met, would cause the removal or addition of a skyrmion. Magnon generation could be captured by introducing retarded potentials, a dynamical pairwise skyrmion-skyrmion interaction term, or multibody interaction effects. The particle-based model does not include the effect of tilting the magnetic field, internal skyrmion breathing modes, or large skyrmion distortions produced by pinning, driving, sample edges, or

skyrmion interactions. Particle-based simulations are maximally efficient when $\theta_{\text{SKH}}^{\text{int}} = 45^\circ$ such that the damping and Magnus terms are equal, since small simulation time steps are required when either term is small. For numerical stability, the time step should be small enough to ensure that a skyrmion moves at most 1/100 the distance of a pin radius or skyrmion lattice constant during a single simulation step. Particle-based simulations can generally access the time evolution over a length scale of up to 100 skyrmion lattice constants, or around 10 000 skyrmions. Larger systems can be studied with graphics processing unit resources. With simplified particle models in which only short-range nearest-neighbor pairwise repulsions are employed, simulation densities of up to 100 000 skyrmions can readily be accessed.

The particle description can be integrated directly to examine the skyrmion dynamics; however, in order to identify ground state configurations such as crystal, liquid, or pinning-stabilized disordered structures, Monte Carlo or simulated annealing methods (Kirkpatrick, Gelatt, and Vecchi, 1983) can be applied. Use of such methods does not guarantee that trapping in a metastable state cannot occur, and there are ongoing efforts to use stochastic LLG or energy pathway approaches to escape such traps. Even in experiment, long-lived metastable states can appear. In simulated annealing, the system is initialized in a high temperature rapidly diffusing state, and the temperature is gradually lowered to $T = 0$ or the desired final temperature. The cooling must be performed sufficiently slowly that the particles can explore phase space and find a configuration in or near a ground state. The cooling rate can be tested by first considering a pin-free system to determine whether the skyrmions are able to settle into a triangular lattice.

IV. MICROMAGNETIC MODELS

In micromagnetic simulations, the dynamics of the spin degrees of freedom described by the LLG equation are calculated directly in the presence of different interaction terms including exchange energy, DMI, anisotropy, and magnetic fields. For reviews and general background on micromagnetic simulations, see Fidler and Schrefl (2000) and Coey (2010), and for a review of spin-transfer torques, see Ralph and Stiles (2008). As an example of a micromagnetic simulation of skyrmion states, in Fig. 11 we show a hexagonal to square skyrmion lattice transition (Takagi *et al.*, 2020) induced by changing the external field B/B_c , where B_c is the field at which a uniform ferromagnetic state appears. This transition is visible in the magnetization m_z in Figs. 11(a)–11(d), the topological charge n_{sk} in Figs. 11(e)–11(h), and the energy distribution ϵ in Figs. 11(i)–11(l). At $B/B_c = 0.44$ in Figs. 11(a), 11(e), and 11(i), there is a well-defined particlelike skyrmion texture with circular skyrmions that form a triangular lattice. In this regime, particle-based models capture the same relevant details as micromagnetic models. In Figs. 11(b), 11(f), and 11(j) at $B/B_c = 0$, the skyrmions become elongated and begin to adopt hexagonal shapes in response to the formation of a triangular skyrmion lattice. At $B/B_c = -0.26$ in Figs. 11(c), 11(g), and 11(k), the skyrmions grow even larger with more pronounced hexagonal distortions, while for $B/B_c = -0.32$ in Figs. 11(d), and 11(h), and 11(l), the skyrmions are square in shape and

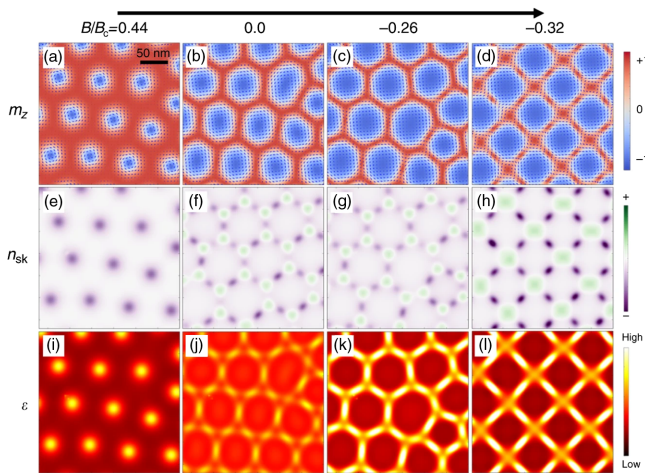


FIG. 11. Images from 2D micromagnetic simulations showing (a)–(d) local magnetization m_z , (e)–(h) topological charge density n_{sk} , and (i)–(l) energy density ε at magnetic fields of $B/B_c = 0.44, 0.0, -0.26,$ and -0.32 (from left to right), where B_c is the field at which a uniform ferromagnetic state emerges. These models reveal the size change and shape distortions of the skyrmions as well as the different types of textures that can arise. The size of the skyrmions increases as the lattice transitions from triangular to square. From Takagi *et al.*, 2020.

form a square lattice. Micromagnetic calculations can also capture the emergence of additional textured states beyond skyrmion lattices. Both particle-based simulations and micromagnetic simulations can become trapped in metastable states.

Micromagnetic models allow skyrmion distortions and breathing modes to occur along with skyrmion annihilation and creation. The internal dynamics of a single skyrmion can be studied in detail, and inclusion of additional terms can give rise to rich behaviors. Phase diagrams from micromagnetic simulations in the absence of drive under an applied field reveal the transition from a zero field helical state to skyrmion lattices of varied density followed by the emergence of a high field ferromagnetic state. When a driving force is applied, the range of magnetic fields that stabilize skyrmions can change even in the absence of pinning. Figure 12 shows a micromagnetic dynamic phase diagram as a function of current versus magnetic field for driven skyrmions in a pin-free system. At low fields, a pinned spiral state forms, and there are regions of flowing skyrmions, a ferromagnetic state, and a high drive chiral state. These simulations indicate that application of a current can cause skyrmions to emerge from ferromagnetic or spiral states, while strong driving can destroy the skyrmions (Lin *et al.*, 2013a). For weakly pinned systems, current-induced creation and annihilation of skyrmions was demonstrated experimentally (Yu *et al.*, 2017). Current-induced skyrmion nucleation was also observed in experiments in Co-based Heusler alloys (Akhtar *et al.*, 2019), where the nucleation current increases with increasing magnetic field. These samples were strongly pinned, suggesting that pinning in combination with a drive can create skyrmions.

Several magnetic codes are available that can be used to simulate skyrmions interacting with pinning, including MuMax (Leliaert *et al.*, 2018) and OOMMF. Micromagnetic simulations are generally limited in the number of skyrmions

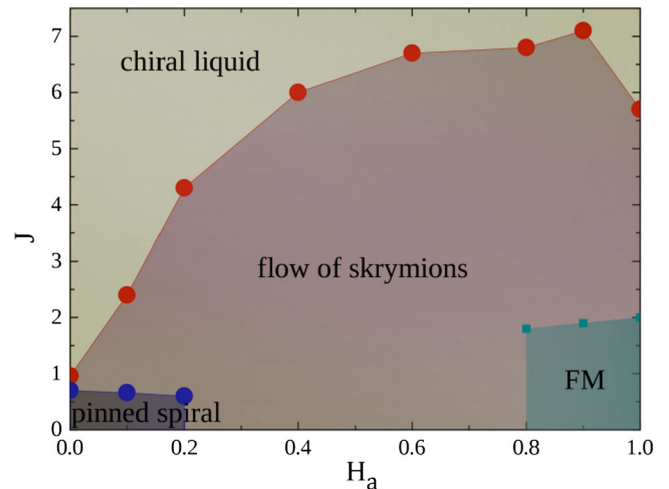


FIG. 12. Dynamic phase diagram as a function of current J vs magnetic field H_a from 2D micromagnetic simulations. In the absence of a current ($J = 0$), pinned spiral, skyrmion lattice, and ferromagnetic (FM) phases appear. At finite J , a moving skyrmion lattice and a chiral liquid phase form at high drives. This indicates that a drive can be used to nucleate skyrmions from a spiral or ferromagnetic state. From Lin *et al.*, 2013a.

and the timescales that can be accessed. Thus, such simulations are unsuitable for examining hundreds or thousands of skyrmions interacting with pinning sites under a drive due to the relatively long transient times that can occur before the system settles into a steady state. Other types of numerical models can also be applied to skyrmions or skyrmion-defect interactions. For example, density functional theory (Choi, Lin, and Zhu, 2016) or combined multiscale approaches using Heisenberg models mapped from first principles calculations (Fernandes *et al.*, 2018; Fernandes, Bouhassoune, and Lounis, 2020) can be particularly powerful for extracting the energies of skyrmion-pin interactions on the atomic scale.

A. Pinning mechanisms

In the experiments by Schulz *et al.* (2012), skyrmion motion was inferred from observations of changes in the THE. This technique provided evidence of a finite skyrmion-depinning threshold, and many subsequent imaging experiments revealed a wide range of depinning thresholds from 10^6 to 10^{11} A/m². In superconducting vortex systems, pinning arises at locations where the order parameter of the superconducting condensate is lowered. Placing a vortex at these locations minimizes the energy since the condensation energy is already suppressed to zero at the vortex core (Blatter *et al.*, 1994). Pinning of colloidal particles can be achieved via optical trapping (Brunner and Bechinger, 2002) or by providing a substrate on which the particles can be localized (Pertsinidis and Ling, 2008; Tierno, 2012), while in Wigner crystals pinning is produced by offset charges (Reichhardt *et al.*, 2001). For skyrmions, there are numerous possible pinning mechanisms, such as local changes in the DMI, missing spins, holes in thin-film samples, a local change in the anisotropy, sample thickness modulations, localized changes in the magnetic field, impurity atoms embedded in

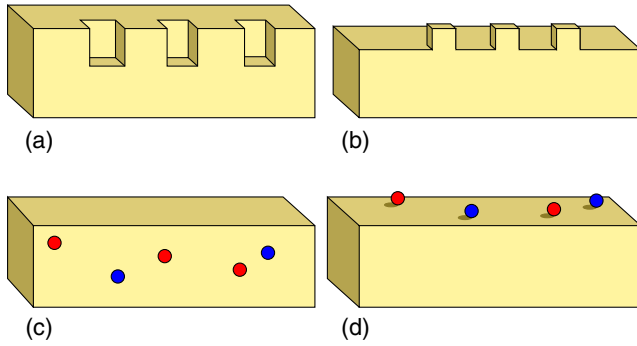


FIG. 13. Schematic illustrations of possible ways that pinning can arise in skyrmion systems. (a) Surface thickness modulations. (b) Addition of nanodots to the surface. (c) Naturally occurring atomic defects or substitutions in the bulk of the sample. (d) Adatoms on the surface of the sample.

the bulk, or adatoms adhering to the surface. Schematics of some possible pinning mechanisms appear in Fig. 13, including surface modulation by fabricated holes or antidots in Fig. 13(a) or by magnetic nanoparticles in Fig. 13(b); naturally occurring atomic defects in the bulk such as missing atoms or substitutions in Fig. 13(c) and surface adatom placement in Fig. 13(d). Grain boundaries, twin boundaries, or dislocations can also serve as pinning sites in thin-film systems.

There is no threshold current for skyrmion motion in micromagnetic simulations of uniform samples without defects (Lin *et al.*, 2013a). Iwasaki, Mochizuki, and Nagaosa (2013b) performed one of the first theoretical studies of skyrmion pinning using micromagnetic simulations with parameters appropriate for MnSi where pinning was modeled as small regions in which the local anisotropy A varied. In this system, where the ratio of the local anisotropy to the exchange term J is $A/J = 0.2$, the depinning threshold is $j_c \approx 10^{10} - 10^{11}$ A/m² and the skyrmion depins elastically. Lin *et al.* (2013b) used a combination of micromagnetic simulations and particle-based simulations for 2D skyrmions and also found finite depinning thresholds for both cases.

Liu and Li (2013) considered a local exchange mechanism for producing skyrmion pinning that was achieved by varying the local density of itinerant electrons. Using micromagnetics and a Thiele equation approach, they found that the skyrmion is pinned due to the lowering of the skyrmion core energy. They also showed that, under perturbation by a small drive, the skyrmion performs a spiraling trajectory as it returns to the pinning site, in contrast to an overdamped particle that moves linearly back to its equilibrium position. The spiraling motion is produced by the Magnus force. When the current is large, the skyrmion is able to escape the trap and depin.

Sampaio *et al.* (2013) used micromagnetic simulations to study the pinning of isolated skyrmions driven by a spin-polarized current through nanotracks containing notches, as illustrated in the insets of Fig. 14. As a function of the driving current j versus the notch depth, which is plotted in the main panel of Fig. 14, the skyrmion either is pinned by the notch or moves around it. Sampaio *et al.* found that the critical depinning current increases rapidly with notch depth, changing by 2 orders of magnitude as the notch depth increases from

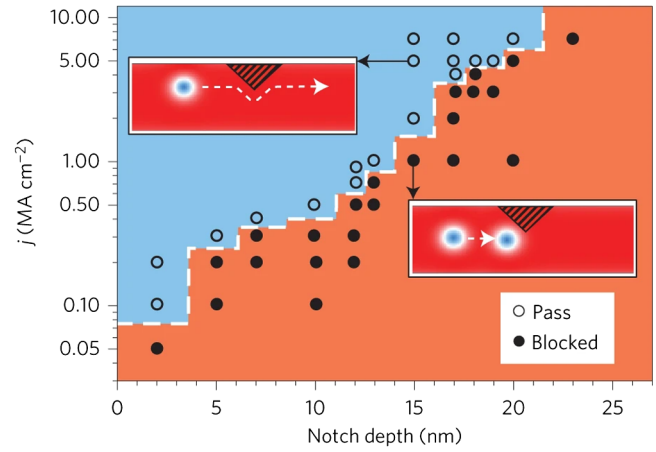


FIG. 14. Micromagnetic simulations of skyrmion pinning using a notch plotted as a function of the applied spin-polarized current j and the notch depth. The geometry appears in the insets, where a dashed white line indicates the skyrmion trajectory. A notch (hatched region) is introduced into a nanotrack (red). The skyrmion (blue circle) either flows past the notch (upper inset and open circles) or becomes pinned near the notch tip (lower inset and filled circles). The current required to prevent pinning increases with increasing notch depth. From Sampaio *et al.*, 2013.

3 to 25 nm. Here the notch serves as a barrier for skyrmion motion.

Müller and Rosch (2015) considered a skyrmion interacting with a hole or locally damaged region both analytically and numerically using continuum methods and the Thiele equation approach. They found that the potential generated by the hole has the interesting property of combining a longer-range repulsion with a short-range attraction. The resulting competition produces an unusual effect under an applied drive. The skyrmion moves around the pinning site at low drives due to the repulsion, but at high drives it jumps over the repulsive barrier and is captured by the short-range attraction. At even higher drives, a flow regime appears when the skyrmion escapes from the attractive part of the pinning site. The competing attractive and repulsive potential produced by the hole is illustrated in Fig. 15.

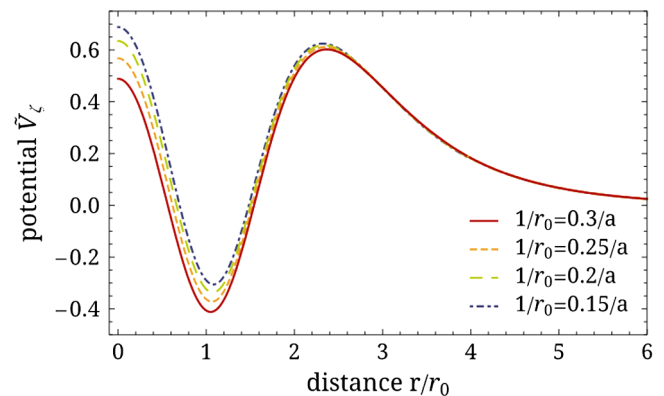


FIG. 15. Shape of the pinning potential produced by a hole in the sample, which has longer-range repulsion and a short-range attraction. From Müller and Rosch, 2015.

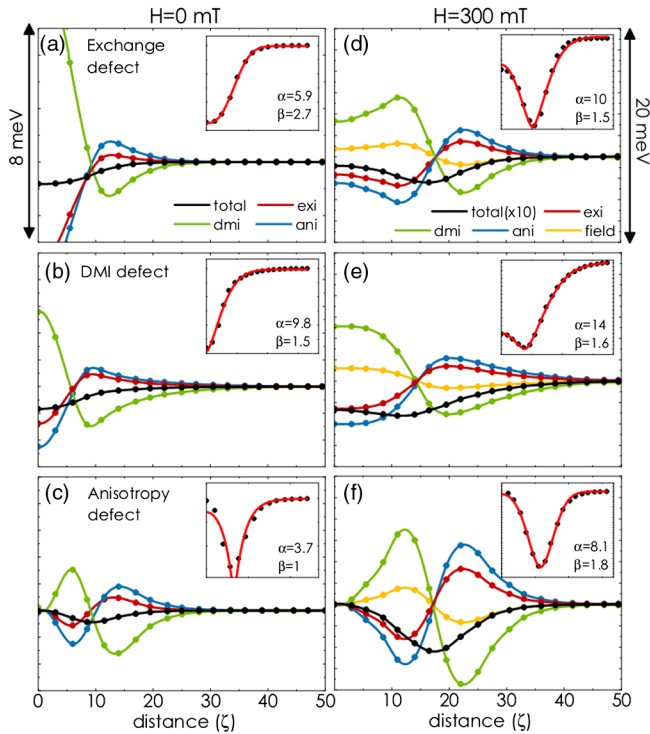


FIG. 16. The total, exchange (exi), Dzyaloshinskii-Moriya (DMI), anisotropy (ani), and Zeeman (field) energies plotted as a function of distance ζ along the minimum energy path for a skyrmion to escape from the defect for three different types of defects at external fields of (a)–(c) $H = 0$ mT and (d)–(f) $H = 300$ mT. Insets: total energy landscape or effective pinning potential fit to an exponential power function. From Stosic, Ludermir, and Milošević, 2017.

Choi, Lin, and Zhu (2016) used density functional theory to study the interaction of skyrmions in MnSi with atomic defects. They found that attractive sites form if Pb is substituted for Si or if Zn or Ir is substituted for Mn, while repulsive sites form if Co is substituted for Mn. For Co monolayers on Pt, Stosic, Ludermir, and Milošević (2017) studied the pinning potentials at different locations (including on or between domain walls). Figure 16 shows the total, exchange, DMI, anisotropy, and Zeeman energies as a function of the distance ζ along the minimum energy path for the skyrmion to escape from the pinning. The insets indicate that the total energy G can be fit to an exponential power function $G(\zeta) \propto -\exp[-(\zeta/\alpha)^\beta]$, where α and β are the scale and shape parameters. Stosic, Ludermir, and Milošević (2017) found that off-center pinning sites are well described using a similar energy expression with a radial shift. Navau, Del-Valle, and Sanchez (2018) used micromagnetic simulations to study skyrmion-defect interactions in thin films containing DMI modulations and obtained analytic expressions for the skyrmion-defect forces within a rigid skyrmion approximation. They found that the pinning is enhanced (weakened) when the defect increases (decreases) the DMI. Anisotropic defects can be attractive or repulsive or can have a combination of the two effects.

From first principles calculations for skyrmions interacting with single-atom impurities, Fernandes *et al.* (2018) found

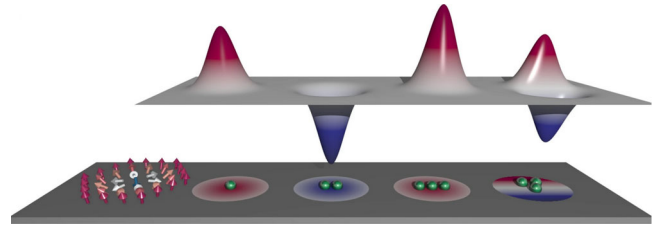


FIG. 17. Schematic of atom-by-atom construction of potential landscapes for skyrmions. The leftmost cluster of arrows illustrates the size of a typical skyrmion. Green spheres are atoms placed so as to construct, from left to right, a repulsive, attractive, strongly repulsive, or combined attractive and repulsive pinning potential. From Arjana *et al.*, 2020.

that defects can be both attractive and repulsive or purely attractive depending on the impurity type. They focused on PdFe bilayers on an Ir substrate and considered a range of defect transition metal atoms including $3d$ (Sc, Ti, V,...) and $4d$ (Y, Zr, Nb,...) atoms as well as Cu and Ag atoms, with the defects either located on the surface or embedded in the Pd surface layers. By determining whether the binding energy is positive or negative, they found that attractive and repulsive interactions of varying strength can appear, depending on the element used. A key feature of this system is that strongly magnetic defects locally stiffen the skyrmion, leading to a repulsive skyrmion-defect interaction, while weakly interacting defects produce attractive pinning due to the substrate contribution. Since the pinning originates from surface atoms, scanning tunneling microscopy could be employed to add atoms in prescribed patterns in order to create attractive and repulsive pinning sites that precisely control the skyrmion deviations. Arjana *et al.* (2020) pursued this idea by examining atom-by-atom crafting of skyrmion-defect landscapes using single-, double-, and triple-atom states to create repulsive, attractive, and combined repulsive and attractive pinning sites, as illustrated in Fig. 17. They also generated asymmetric landscapes and demonstrated that atomic clusters could be used to construct reservoir computing devices.

Larger-scale magnetic defects can be created using the following variety of nanoscale methods: changing local magnetic properties by irradiating particular regions of the sample (Fassbender *et al.*, 2009), changing the DMI with large-scale thickness modulations (Yang *et al.*, 2015), or adding magnetic dots to the surface in a manner similar to that used for introducing pinning in superconductors (Martín *et al.*, 1997; Marchiori *et al.*, 2017). In extensive micromagnetic simulations of skyrmion trapping by larger-scale magnetic defects, Toscano *et al.* (2019) found that the defects act either as attractive traps or as repulsive scatterers depending on the exchange stiffness, DMI, perpendicular anisotropy, and saturation magnetization. If the exchange stiffness is reduced at the defect, a skyrmion trap is formed, while if it is increased, a repulsive scattering site appears. Additionally, the strength of the pinning interaction increases when the skyrmion becomes smaller than the defect radius. In other micromagnetic simulations for skyrmions moving in nanostructured materials, a large region with altered local anisotropy acted as a repulsive area for the skyrmions (Ding, Yang, and Zhu, 2015; L. Wang *et al.*, 2018).

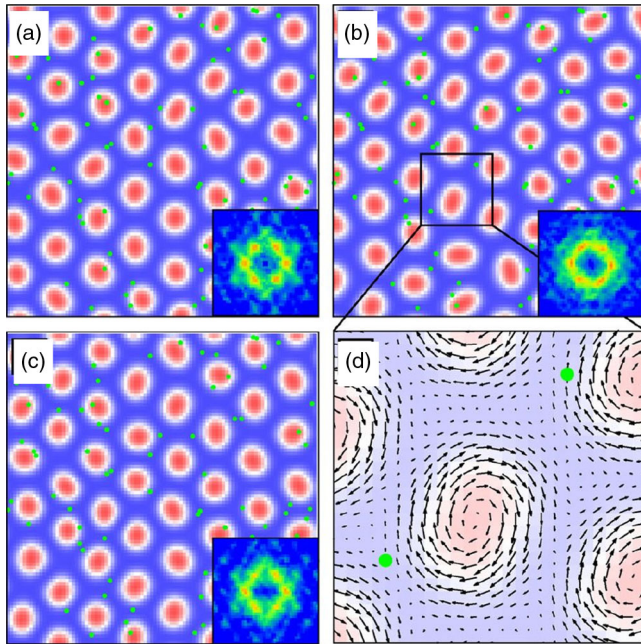


FIG. 18. Micromagnetic simulation images of the evolution of a skyrmion crystal and the skyrmion distortions for different times under an applied driving current. The times are (a) $t = 1.30 \times 10^{-8}$ s, (b) 2.60×10^{-8} s, and (c) 4.87×10^{-8} s. Green dots are the defect sites and red regions are the skyrmion centers. Insets: corresponding structure factor measurements. (d) Magnified view of the distorted skyrmions in (c). From Iwasaki, Mochizuki, and Nagaosa, 2013b.

Wang *et al.* (2017) introduced the concept of pinning skyrmions with magnetic field gradients and showed that the pinning strength depends on both the gradient intensity and the skyrmion size. They demonstrated that a skyrmion can be dragged and manipulated with a suitable magnetic field gradient, suggesting a new way to move skyrmions using a magnetic tip.

Beyond the evidence for skyrmion pinning obtained from transport studies, pinning effects can be deduced via manipulation of individual skyrmions. Hanneken *et al.* (2016) explored the interactions between nanometer-scale skyrmions and atomic-scale defects in PdFe by measuring the force needed to move a skyrmion, which revealed the presence of a range of pinning strengths. They also found that interlayer defects such as single Fe atoms interact strongly with a skyrmion, while single Co adatoms on the surface are weak pinning centers; however, clusters of such adatoms can serve as strong pinning sites.

B. Skyrmion pinning by individual versus extended defects and the role of the Magnus force

In many systems, such as vortices in type-II superconductors, it is known that extended or linelike defects can produce significantly different pinning than pointlike defects. Such extended defects can form naturally, as in the case of twin boundaries (Vlasko-Vlasov *et al.*, 1994), or they can be introduced with nanoscale techniques (Guillamón *et al.*, 2014). A line defect can produce increased pinning for

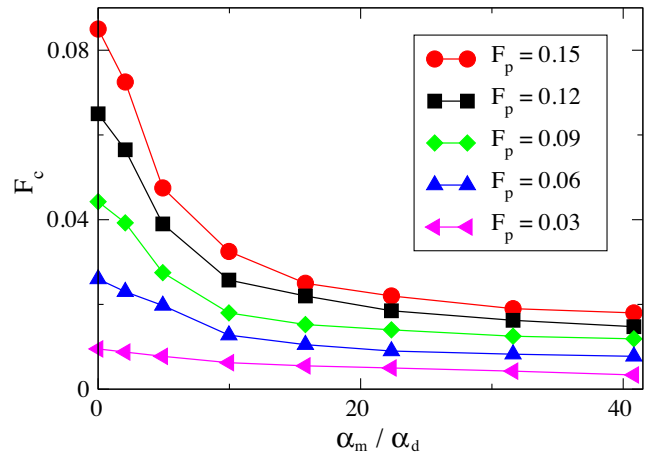


FIG. 19. The critical depinning force F_c vs the ratio α_m/α_d of the Magnus force to the dissipative term for 2D particle-based simulations of skyrmions moving over pointlike disorder sites for various pinning strengths F_p . The depinning threshold decreases with increasing Magnus force. From Reichhardt, Ray, and Reichhardt, 2015a.

superconducting vortex motion across the line (Vlasko-Vlasov *et al.*, 1994) while generating guided or easy flow for motion along the line (Durán *et al.*, 1992). In skyrmion systems, it was initially argued that a skyrmion can move around a point pinning site due to the Magnus effect (Nagaosa and Tokura, 2013). Micromagnetic simulations by Iwasaki, Mochizuki, and Nagaosa (2013b) showed that pinning was reduced not only by this avoidance motion but also by the ability of the skyrmions to change shape, as illustrated in Fig. 18.

Particle-based simulations of skyrmions interacting with pointlike random pinning (Reichhardt, Ray, and Reichhardt, 2015a) in 2D systems indicate that the depinning threshold decreases as the ratio α_m/α_d of the Magnus force to the dissipative term increases over a wide range of pinning strengths, as shown in Fig. 19. The schematic illustration in Fig. 20 shows how the Magnus force reduces the point pinning effectiveness. The velocity component induced by the attractive pinning force always points toward the pinning site, while the Magnus velocity component is perpendicular to the attractive force. The skyrmion moves in a direction defined by the resultant of these velocity components. The net effect is that, although the dissipative term favors the motion of the skyrmion toward the pinning site, the Magnus force causes the skyrmion to deflect around the pinning site. In contrast, a purely overdamped particle such as a superconducting vortex moves directly toward the center of the pinning site and is likely to be trapped. The deflection of the skyrmion around the pinning site depends strongly on the relative sizes of the skyrmion and the pinning site.

Experiments by Woo *et al.* (2016) on room-temperature ultrathin films unexpectedly showed that the skyrmions experience strong pinning. Owing to the nature of the films, which contain grain boundaries or extended defects, the intrinsic pinning in these samples may not be pointlike. Continuum-based simulations of skyrmions (Legrand *et al.*, 2017) confirmed that grain boundaries induce skyrmion

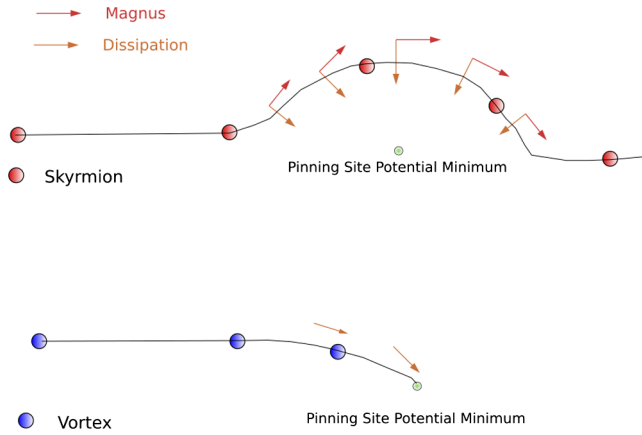


FIG. 20. Schematic of a skyrmion (upper red dots) with both Magnus and dissipative terms and a superconducting vortex (lower blue dots) with only a dissipative term interacting with an attractive point pinning site (green dot) to illustrate how the Magnus force decreases the pinning effectiveness. The skyrmion moves in a direction that is the resultant of two velocity components: dissipative (thin brown arrows) and Magnus force induced (thick red arrows). Since the Magnus-force velocity component is perpendicular to the attractive force around the pinning site, the skyrmion deflects around the pinning site. In contrast, the superconducting vortex moves directly toward the potential minimum and is more likely to be trapped by the pinning site.

pinning that increases in strength for smaller grain sizes; however, there is a minimum grain size below which pinning cannot occur. One explanation for the stronger pinning by extended defects is that it is not possible for the skyrmion to skirt an extended defect. In Fig. 21(a) we schematically illustrate the Magnus- and dissipation-induced velocity components of a skyrmion moving toward an attractive extended line defect. The dissipative velocity component points toward the defect, but the Magnus velocity component is oriented perpendicular to the line defect, bending the skyrmion trajectory sideways as the defect is approached. If the defect line extends across the sample, the skyrmion cannot avoid the defect but eventually reaches and crosses it while experiencing its full pinning potential. This is in contrast to the ability of a skyrmion to completely avoid a pointlike pin. If a driven skyrmion is inside an extended line defect such as a grain boundary, as shown schematically in Fig. 21(b), the Magnus force may bend the skyrmion trajectory upon approach to the boundary, but the skyrmion eventually must pass through the potential minimum in order to exit the grain boundary, as illustrated in the lower panel of Fig. 21(b). As a result, extended defects are always more effective than point defects at exerting pinning forces on skyrmions.

A numerical test of the effect of the Magnus force on skyrmions moving perpendicular to a line defect was performed by Reichhardt and Olson Reichhardt (2016) for a 2D skyrmion moving over a 1D pinning line. As shown in Fig. 22, for driving applied parallel to the pinning line, the critical current F_c is independent of the size of the Magnus term, in contrast to point pinning, where F_c decreases as the Magnus term increases. On the other hand, when the drive is applied

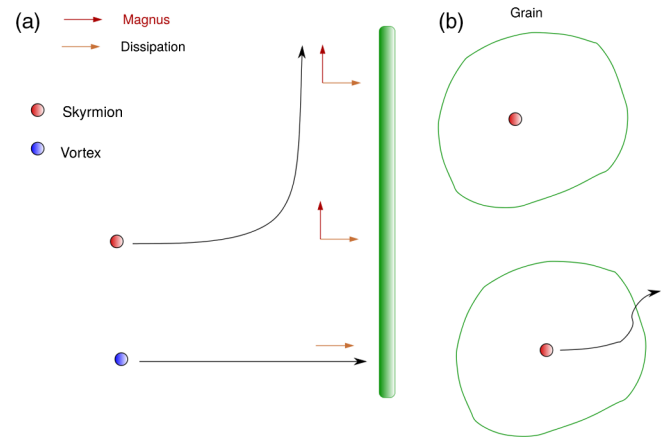


FIG. 21. (a) Schematic showing the dissipative (thin brown arrows) and Magnus (thick red arrows) velocity components for a skyrmion (upper red dot) or superconducting vortex (lower blue dot) moving toward an attractive extended line defect (green column). The overdamped superconducting vortex moves directly toward the line defect, while the skyrmion is deflected but gradually approaches the defect. Unlike the case for point pinning in Fig. 20, the skyrmion cannot simply move around the line defect but eventually reaches the defect and interacts with it. (b) Schematic of a skyrmion (red dot) located inside a closed grain boundary (green line). The skyrmion may be deflected as it moves toward the grain boundary; however, it must cross the pinning potential minimum in order to pass through the grain boundary.

perpendicular to the line defect, the depinning threshold decreases with increasing Magnus term. This effect would be most pronounced for skyrmions moving over 1D pinning features such as twin boundaries but would likely be absent in a sample filled with closed grain boundaries.

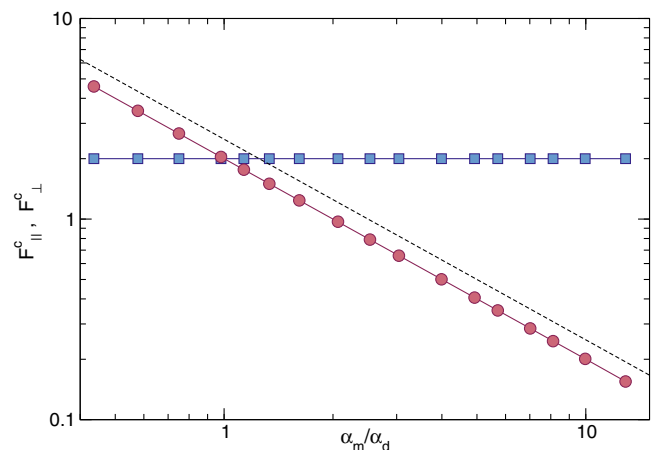


FIG. 22. Two-dimensional particle-based simulations of a skyrmion interacting with a 1D defect line showing the critical depinning force for driving applied parallel (F_{\parallel}^c ; blue squares) and perpendicular (F_{\perp}^c ; red circles) to the line vs the relative strength α_m/α_d of the Magnus force. F_{\parallel}^c is insensitive to the Magnus force, while F_{\perp}^c decreases with increasing Magnus force. From Reichhardt and Olson Reichhardt, 2016.

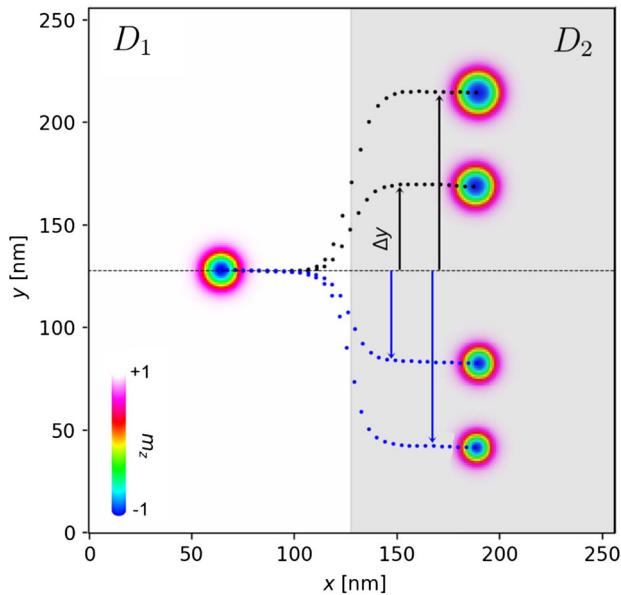


FIG. 23. Illustration of skyrmion motion through a heterochiral interface. The initial skyrmion position is on the left side of the interface. As the relative DMI strengths D_1 and D_2 are varied with respect to each other, the skyrmion trajectory is deflected by a distance δy in the positive (upper black arrows) or negative (lower blue arrows) y direction. From Menezes, Mulkers *et al.*, 2019.

The best model for the interaction between skyrmions and extended defects is dictated by the nature of the defects. For example, thickness modulation defects produce short-range attractive pinning, whereas magnetic stripe defects give longer-range pinning with a dipolar form A/r^3 that is either attractive or repulsive. In some cases the extended defect could have a competing potential that is repulsive at longer distances but becomes attractive close to the defect. The edges of the sample act as an extended repulsive potential, and the skyrmion Hall effect can push the skyrmion toward and out of the sample edge. Iwasaki, Mochizuki, and Nagaosa (2013a) studied skyrmion-sample edge interactions and identified a critical current below which the skyrmions are unable to overcome the repulsive edge barrier.

Navau, Del-Valle, and Sanchez (2016) simulated the Thiele model for a single skyrmion interacting with an extended defect representing an edge. The skyrmion is strongly deflected by the edge, which exerts a force of the form $\mathbf{f} = -f_0 e^{-d/d_0} \hat{\mathbf{n}}$, where d is the distance between the skyrmion center of mass and the edge, $\hat{\mathbf{n}}$ is a unit vector perpendicular to the edge, and d_0 is approximately equal to the skyrmion diameter. Other work (Navau, Del-Valle, and Sanchez, 2018) showed that extended defects can produce either repulsive or attractive forces on a skyrmion. The dynamics of a skyrmion interacting with an extended defect depends on both the form of the defect and the skyrmion type. Menezes, Mulkers *et al.* (2019) considered micromagnetic simulations of a skyrmion moving toward a heterochiral interface created with multilayers. They found that a ferromagnetic skyrmion is deflected by the interface with an amplitude that can be tuned by changing the applied current or by modifying the difference in the DMI across the interface,

as shown in Fig. 23. On the other hand, antiferromagnetic skyrmions experience no deflection at the interface.

C. Discussion

There are numerous theoretical, computational, and experimental directions for the further study of basic skyrmion-pinning mechanisms. Simulations and theory indicate that there are many ways to create attractive, repulsive, or both attractive and repulsive pinning sites, so one of the next steps is to consider how to combine different pin types to produce novel dynamical phenomena, control the skyrmion motion, and reduce or enhance pinning. In many other systems where pinning occurs, such as vortices in type-II superconductors, the natural or artificial defects producing the pinning reduce the superconducting condensation energy, so studies have focused on strictly attractive pinning sites. In colloidal systems, optical forces and most surface modifications also create attractive pinning sites. As a result, systems with repulsive defects represent a relatively unexplored regime of collective dynamics. Many skyrmions in thin films seem to show strong pinning effects from attractive pins; however, there may be a way to introduce additional repulsive defect sites that would effectively reduce the overall pinning by competing with the attractive pinning centers.

The pinning process for antiskyrmions or antiferromagnetic skyrmions is of interest since $\theta_{\text{SKH}}^{\text{int}} = 0$ in these systems (Woo *et al.*, 2018; Göbel, Mertig, and Tretiakov, 2021), so the dynamics and pinning effects should be modified and may resemble those found for superconducting vortices. Liang *et al.* (2019) considered antiferromagnetic (AFM) and ferromagnetic (FM) skyrmions interacting with a defect. They found that the critical depinning force increases with increasing defect strength, and that the FM skyrmions can bypass defects by moving around them due to the Magnus force while the AFM skyrmions become trapped. This suggests that AFM skyrmions may be much more susceptible to pinning effects than FM skyrmions are. The type of pinning matters, however, since the work of Menezes, Mulkers *et al.* (2019) on a line defect separating two regions with different DMI suggested that AFM skyrmions may not be susceptible to changes in the DMI. It would also be interesting to explore the pinning of biskyrmions, merons, and other related objects such as skyrmioniums (Kolesnikov *et al.*, 2018), as well as the role pinning plays in determining the direction of current flow. Stier *et al.* (2021) showed in simulations that, although magnetic impurities do not interfere with a uniform applied current, conducting impurities can change the current paths. If defects could be introduced that are able to move over time in response to a current, they would create a pinning landscape that can gradually be sculpted in a manner similar to electromigration. This could produce interesting memristorlike effects.

Most studies of pinning to date have focused on defects in 2D; however, for 3D linelike skyrmions (Milde *et al.*, 2013; Birch *et al.*, 2020; X. Yu *et al.*, 2020; Wolf *et al.*, 2022) entirely new types of pinning effects could arise along with an array of new methods for creating 3D pinning. In 3D superconducting vortex systems, columnar pinning enhances the critical depinning current (Civale, 1997) by trapping the

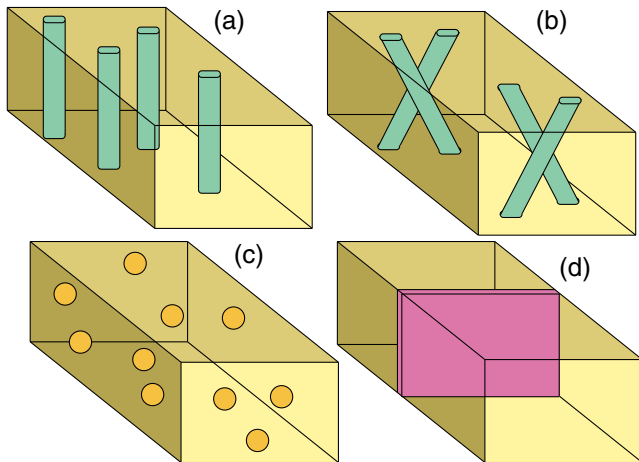


FIG. 24. Schematic of possible 3D defects that could be created for bulk skyrmions. (a) Columnar defect tracks, which could induce the formation of a skyrmion Bose glass. (b) Splayed columnar defects, which could create a splayed skyrmion glass or promote skyrmion entanglement. (c) Random point defects, which could generate a skyrmion glass. (d) 3D planar defects.

vortex line along the entire length of the pinning site, and a similar effect could occur for 3D skyrmions. Splayed columnar defects (Hwa *et al.*, 1993) could promote the entanglement of skyrmion lines, while proton irradiation could be used to create random point defects (Haberkorn *et al.*, 2012) or 3D line defects (Kafri, Nelson, and Polkovnikov, 2007). In the schematics in Fig. 24, we show possible 3D pinning arrangements for skyrmion systems, including columnar, splayed, 3D point-like, and 3D planar defects. It would be interesting to learn whether 3D pinning is more effective than 2D pinning or whether it can reduce skyrmion creep at finite temperatures. Some types of defects repel skyrmions rather than attracting them, and adding the 3D versions of such defects could increase the net skyrmion mobility. One possible experiment would be to irradiate bulk samples and determine whether the depinning threshold changes as measured by changes in the THE. If a sufficiently large density of 3D defects were added to the sample, percolation paths could emerge that serve as easy flow channels for skyrmion motion, leading to a net increase rather than net decrease in the skyrmion mobility. Recently Juge *et al.* (2021) used ion irradiation to create quasi-1D regions and showed that skyrmions could be guided along the irradiated channels.

In 3D samples it would be possible to place different types of pinning on the top and bottom surfaces of the sample, such as through nanopatterning or by adding adatoms. For example, if the top of the sample has antipinning sites and the bottom has pinning sites, a shear effect could arise under driving that would promote skyrmion cutting or the creation of monopoles along the skyrmion lines (Lin and Saxena, 2016). It may also be possible to create chiral bobbers.

V. COLLECTIVE STATES AND SKYRMION LATTICES WITH PINNING

We next consider the effect of pinning on the static configurations of collectively interacting skyrmions. The first

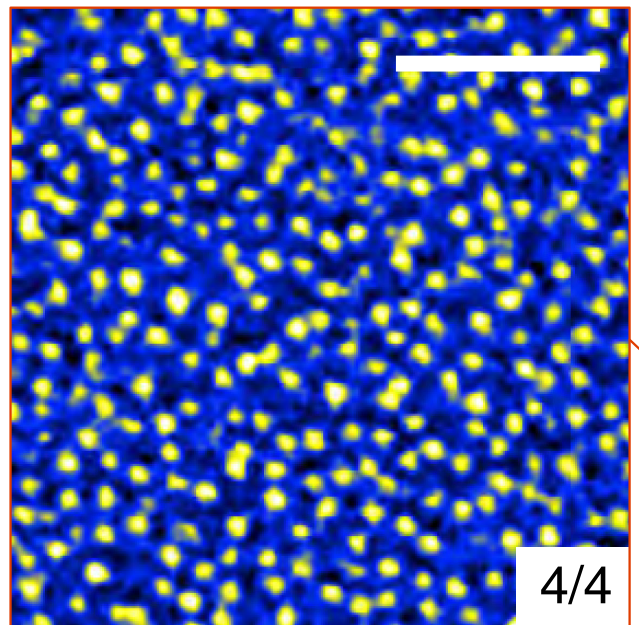


FIG. 25. Magnetic force microscope image of disordered skyrmions in Ir/Fe/Co/Pt multilayers. Black (blue) areas indicate low magnetic field and yellow (white) areas indicate high magnetic field. The scale bar is $0.5 \mu\text{m}$ long. From Soumyanarayanan *et al.*, 2017.

experimental observation of magnetic skyrmions was the imaging of a skyrmion lattice with neutron scattering (Mühlbauer *et al.*, 2009), followed by direct visualization of the skyrmion lattice with Lorentz microscopy (Yu *et al.*, 2010). The fact that the skyrmions formed a lattice suggests that, in these initial experiments, the pinning was relatively weak. There are now many examples of skyrmion systems, particularly in thin films, that form disordered states (Hsu *et al.*, 2018; Karube *et al.*, 2018; Zhang, Zhang *et al.*, 2018; Wang *et al.*, 2019). Figure 25 shows an image of disordered room-temperature skyrmions in Ir/Fe/Co/Pt multilayers (Soumyanarayanan *et al.*, 2017). The manner in which the system is prepared strongly impacts whether the skyrmions form a lattice. Consider a sample in which the skyrmion ground state at temperature T_1 is disordered. If the sample were prepared at another temperature T_2 where the ground state is ordered and the temperature is suddenly changed to T_1 , the skyrmions could remain in a metastable ordered lattice configuration. The metastable state could be destroyed by the application of a current or drive that allows the skyrmions to reach their disordered T_1 ground state configuration.

The structure of a skyrmion lattice can be measured using the structure factor as follows:

$$S(\mathbf{k}) = \frac{1}{N} \left| \sum_{j=1}^N e^{-i\mathbf{k}\cdot\mathbf{R}_j} \right|^2, \quad (8)$$

where \mathbf{R}_j is the position of skyrmion j and N is the total number of skyrmions sampled. For a glass state $S(\mathbf{k})$ has a ring structure, while for a triangular lattice $S(\mathbf{k})$ has sixfold peaks. The lattice structure can also be measured using a Voronoi or Delaunay construction to determine the fraction of

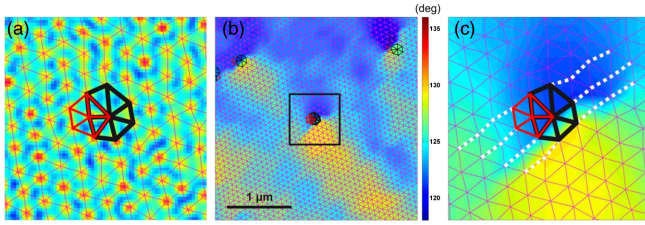


FIG. 26. Examples of Delaunay triangulations of skyrmion lattices. (a) Image of a lattice defect consisting of sevenfold-coordinated (left black) and fivefold-coordinated (right red) skyrmions adjacent to each other. (b) Map of the local spatial angle superimposed on top of the Delaunay triangulation with a defect at the center. (c) Enlarged view of the region marked with a square in (b) showing the presence of a dislocation line at the domain boundary. From Rajeswari *et al.*, 2015.

sixfold-coordinated skyrmions, as illustrated in Fig. 26 (Rajeswari *et al.*, 2015). Such measures permit the identification of different topological defects in the skyrmion lattice, such as adjacent fivefold- and sevenfold-coordinated skyrmions that form a dislocation pair as in Fig. 26(c). Dislocation pairs can glide or climb depending on the strength of the driving. Instead of completely disordering, the skyrmion lattice can form domains defined by grain boundaries, where the angular mismatch between skyrmion lattices in adjacent grains determines the spacing between the fivefold and sevenfold dislocation pairs decorating the boundaries (Lavergne *et al.*, 2018).

Disordered skyrmion arrangements can be produced by strong pinning, temperature, or polydispersity of the skyrmion sizes or types. For example, a disorder-free 2D system or collection of 3D lines with a triangular lattice ground state melts at a critical temperature T_c . The melting transition can be first or second order in the 3D system and second order in the 2D system according to the Kosterlitz-Thouless-Halperin-Nelson-Young (KTHNY) mechanism, in which a proliferation of dislocations is followed by the proliferation of free disclinations (Kosterlitz and Thouless, 1973; Nelson and Halperin, 1979; Young, 1979; Strandburg, 1988). There is evidence for 2D melting via intermediate hexatic phases in the absence of a substrate in numerous systems, including colloidal assemblies (Zahn, Lenke, and Maret, 1999), and a first order transition into a hexatic phase has been observed (Thorneywork *et al.*, 2017). The hexatic phase is detected via the density-density correlation function

$$g_G(|\mathbf{r} - \mathbf{r}'|) = \langle \exp\{i\mathbf{G} \cdot [\mathbf{u}(\mathbf{r}) - \mathbf{u}(\mathbf{r}')] \} \rangle \quad (9)$$

and the bond-angular correlation function

$$g_6(|\mathbf{r} - \mathbf{r}'|) = \langle \exp\{i6[\theta(\mathbf{r}) - \theta(\mathbf{r}')] \} \rangle. \quad (10)$$

In Eqs. (9) and (10) \mathbf{G} is the reciprocal lattice vector, $\mathbf{u}(\mathbf{r})$ is the particle displacement field, and $\theta(\mathbf{r})$ is the angle with respect to the x axis. For a 2D crystal, $g_6(\mathbf{r})$ is constant and $g_G(\mathbf{r})$ decays algebraically [$g_G(\mathbf{r}) \propto r^{-n(T)}$]. In the hexatic phase, $g_G(\mathbf{r})$ decreases exponentially while $g_6(\mathbf{r})$ decays algebraically as $g_6(\mathbf{r}) \propto r^{-n_6(T)}$, where n_6 approaches the

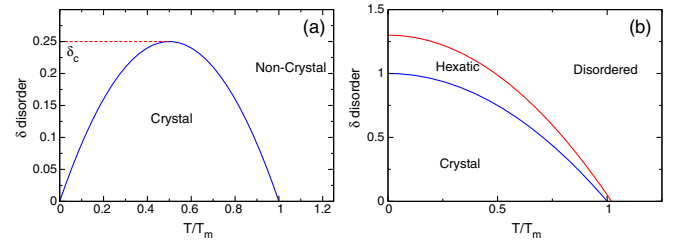


FIG. 27. (a) Schematic phase diagram as a function of quenched disorder δ vs temperature T/T_m for a 2D system, where T_m is the melting temperature. The solid line indicates the predicted transition from a crystal to a disordered noncrystalline state (Nelson, 1983). The disordered state becomes reentrant when the temperature overpowers the quenched disorder before the crystal lattice melts. The dashed red line is from the modified phase diagram proposed by Cha and Fertig (1995), where the system is ordered at $T = 0$ and a low temperature disordered state does not appear until a critical amount of disorder δ_c has been added. (b) The same for 2D colloidal experiments (Deutschländer *et al.*, 2013), where an intermediate hexatic phase appears between the crystal and disordered phases.

value $1/4$. In the fluid phase, both correlation functions decay exponentially. Several recent experiments provided evidence for a hexatic phase in skyrmion systems (Huang *et al.*, 2020; Zázvorka *et al.*, 2020).

Most skyrmion systems contain some quenched disorder. At $T = 0$ in a sample with random pinning, a lattice of interacting particles takes advantage of the pinning energy E_p at the cost of the elastic energy E_{el} . For weak pinning, a small amount of elastic distortion occurs but the triangular lattice symmetry is preserved. When the disorder is stronger, the elasticity breaks down and various topological defects appear. In 2D systems, a disordered KTHNY transition can occur in which the system passes from a lattice to a hexatic phase, while when the disorder is stronger a 2D glassy state appears. Nelson (1983) proposed the phase diagram illustrated in Fig. 27(a) as a function of disorder versus temperature. In the absence of quenched disorder, lattice ordering begins to disappear at the finite T transition to a hexatic or liquid state. Quenched disorder produces a disordered lattice even when $T = 0$; however, temperature can overwhelm the quenched disorder, producing a thermally induced transition to a floating crystalline state that melts into a liquid at a higher temperature. When the quenched disorder is strong enough, the system is always in a disordered state. Cha and Fertig (1995) argued that at $T = 0$ the system remains in a crystalline state until a critical amount of quenched disorder δ_c is added, at which point the system disorders, as indicated by the horizontal dashed line in Fig. 27(a). Thermal effects can wash out the pinning before the lattice melts only if the pinning sites are small. Experiments in 2D colloidal systems (Deutschländer *et al.*, 2013) support the phase diagram shown in Fig. 27(b), where an intermediate hexatic phase appears for zero quenched disorder and increases in extent as quenched disorder is added to the sample. In principle, a similar phase diagram could be constructed for 2D systems containing skyrmions of roughly uniform size.

Recent Monte Carlo simulations indicate that a 2D skyrmion lattice can melt without passing through a hexatic phase

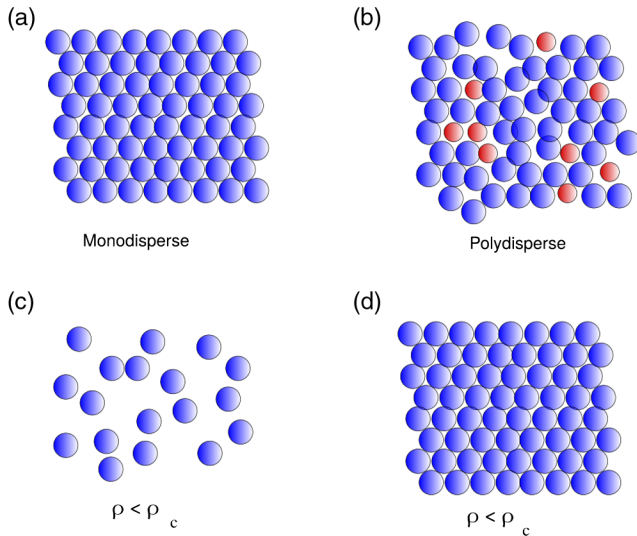


FIG. 28. Schematic illustrations of scenarios leading to disordered skyrmion structures without quenched disorder or temperature. (a),(b) Disorder induced by size polydispersity. (c), (d) Jamming mechanism for skyrmions with short-range contact forces. (c) Below a critical density $\rho < \rho_c$, the system is liquid-like, while (d) for $\rho > \rho_c$ the skyrmions are in contact and form a solid.

(Nishikawa, Hukushima, and Krauth, 2019); however, as suggested in Fig. 27, quenched disorder could enhance the hexatic phase in other types of skyrmion systems. Skyrmions in 2D are often already strongly disordered, but in a dense regime the skyrmion interactions could become strong enough to favor the formation of a hexatic phase. In addition to quenched disorder, two other mechanisms help determine whether the skyrmion arrangement is ordered or disordered. Polydispersity in the skyrmion sizes could induce the formation of a hexatic state even for weak quenched disorder. Simulations of 2D Lennard-Jones systems (Sadr-Lahijany, Ray, and Stanley, 1997) showed that, depending on the density, a dispersity in as few as 10% of the particles was sufficient to disorder the system. Numerical evidence given by Zhang, Xia, Zhou *et al.* (2017) for frustrated ferromagnetic films containing mixtures of different skyrmion sizes indicates that polydispersity can produce disordered skyrmion states. In Figs. 28(a) and 28(b) we schematically illustrate the disordering of a monodisperse triangular solid with the introduction of size dispersity. An open question for skyrmion systems is how much size dispersity is necessary to induce a transition from a triangular solid to a disordered state.

An effective jamming transition can also introduce disorder. In jamming, a fluidlike state of freely moving particles becomes a solid state with a finite shear response where the particles are in contact. Jamming is typically studied in systems with short-range or hard sphere interactions, such as grains and emulsions; however, the interaction between larger skyrmions can be described as a short-range repulsion, giving such skyrmions emulsionlike properties. Hard disks first come into contact at a jamming density or area coverage ϕ_J , where $\phi_J = 0.84$ for a 50:50 mixture of 2D bidisperse hard disks with a radius ratio of $R_1/R_2 = 1.4$ (O'Hern *et al.*, 2003).

There is a disordered fluid below ϕ_J and a jammed amorphous solid above it. Monodisperse disks form a jammed triangular solid at $\phi_c = 0.9$, suggesting that monodisperse skyrmions with short-range interactions can disorder below the jamming or solidification density ρ_c . Figure 28(c) illustrates particles such as skyrmions with short-range interactions in a disordered state at $\rho < \rho_c$, while at $\rho > \rho_c$ in Fig. 28(d) the particles are in contact and form a jammed crystalline solid. When skyrmion-skyrmion interactions extend beyond nearest neighbors, as with small skyrmions or 3D skyrmions, an ordered lattice forms, while for larger skyrmions or 2D skyrmions with a short interaction range a jamming transition to a disordered state can occur.

The skyrmion density is nonmonotonic as a function of the magnetic field, while the skyrmion size is affected by the out-of-plane magnetic field. As a result, at intermediate fields where the skyrmion density is high the skyrmions may form a triangular solid; however, when the skyrmion density decreases for higher or lower fields, the spacing between skyrmions could become large enough that the skyrmions no longer interact, causing the system to transition into a disordered state outside some critical window of magnetic fields. The skyrmions could exhibit two glassy states associated with the lower field low density limit, an intermediate field triangular lattice, and a higher field disordered state. In certain nonequilibrium cases the skyrmion number may remain fixed while the skyrmion radius changes.

For 3D systems containing quenched disorder, such as superconducting vortex lines, a Bragg glass can form in which both hexagonal order and glassy features appear (Giamarchi and Le Doussal, 1995; Klein *et al.*, 2001). If skyrmions in a bulk 3D sample form a Bragg glass, it could be detected through measurements of the in-plane correlation function $g(\mathbf{r})$ or by finding a power law divergence of the Bragg peaks in a scattering measurement (Giamarchi and Le Doussal, 1995). In analogy with the transitions observed in superconducting vortex systems, 3D skyrmions could undergo a first order transition from a Bragg glass to a liquid state or to a more disordered glass.

When columnar disorder is present, 3D superconducting vortices can form a disordered Bose glass, suggesting that skyrmions in linelike disorder could form a skyrmion Bose glass. Strong disorder in a 3D skyrmion system could also produce other glasses such as an entangled state in which skyrmion lines wrap around each other. These skyrmion glasses could have significantly different properties from superconducting vortex glasses since the skyrmions can in principle break or merge to form monopole states. In superconducting systems, glassy states can be detected through magnetization or voltage measurements, while for skyrmion systems, possible measurements that could reveal glassy features include magnetization, slow changes in the THE, or changes in the structure factor $S(k)$ as a function of time. The exploration of glassy states is an almost completely open field in skyrmions.

Samples with intermediate disorder contain only a few strong pinning sites, so a polydisperse state can form in which local ordering coexists with grain boundaries, or locally disordered regions could coexist with long-range order. In Fig. 29 we show an image of a weakly pinned

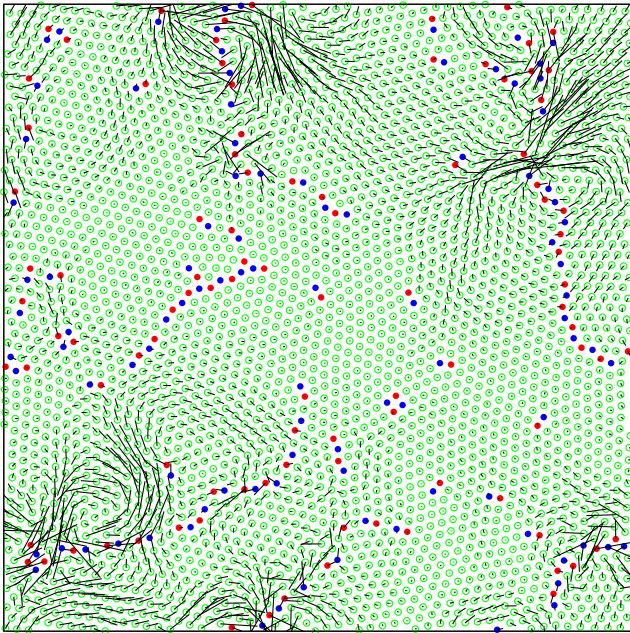


FIG. 29. Image of a superconducting vortex lattice with intermediate disorder showing regions of crystalline sixfold-coordinated vortices (hollow green circles) and grain boundaries composed of fivefold- and sevenfold-coordinated vortices (filled red and blue circles). Under a driving current, the trajectories (black lines) indicate that depinning occurs first along the grain boundaries. From Moretti and Miguel, 2009.

superconducting vortex lattice (Moretti and Miguel, 2009) that illustrates the initiation of motion at the grain boundaries under an applied drive. A similar initial depinning near grain boundaries should occur in moderately disordered skyrmion systems, where domains and grain boundaries have been experimentally observed (Rajeswari *et al.*, 2015; Matsumoto *et al.*, 2016a, 2016b; Zhang, Bauer *et al.*, 2016; Li *et al.*, 2017; Nakajima, Kotani *et al.*, 2017). The depinning could involve either grain boundary motion or grain rotation, with dynamics that may be significantly different from those of fully ordered skyrmion lattices or completely disordered skyrmion states. The ability of skyrmions to change shape modifies the grain boundary formation process compared to colloidal or atomic systems, and certain topological defects may be less costly in a skyrmion lattice than in a rigid particle assembly (Matsumoto *et al.*, 2016a).

In Monte Carlo simulations of skyrmion formation, Silva *et al.* (2014) found that a small number of pointlike non-magnetic defects could produce a disordered skyrmion structure. They also observed the emergence of bimerons for an increasing density of spin vacancies in both the spiral and the skyrmion state, as shown in Fig. 30. Although inclusion of even 1% of spin vacancies strongly disordered the system, it is unknown if there is a critical level of vacancies that triggers the skyrmion disordering transition. (Silva *et al.*, 2014). As has been done for other pinned systems (Giamarchi and Le Doussal, 1995), Hoshino and Nagaosa (2018) used theoretical methods such as replica theory from the glass literature to study a collective skyrmion glass phase. They found several scaling relations for the critical current and pinning

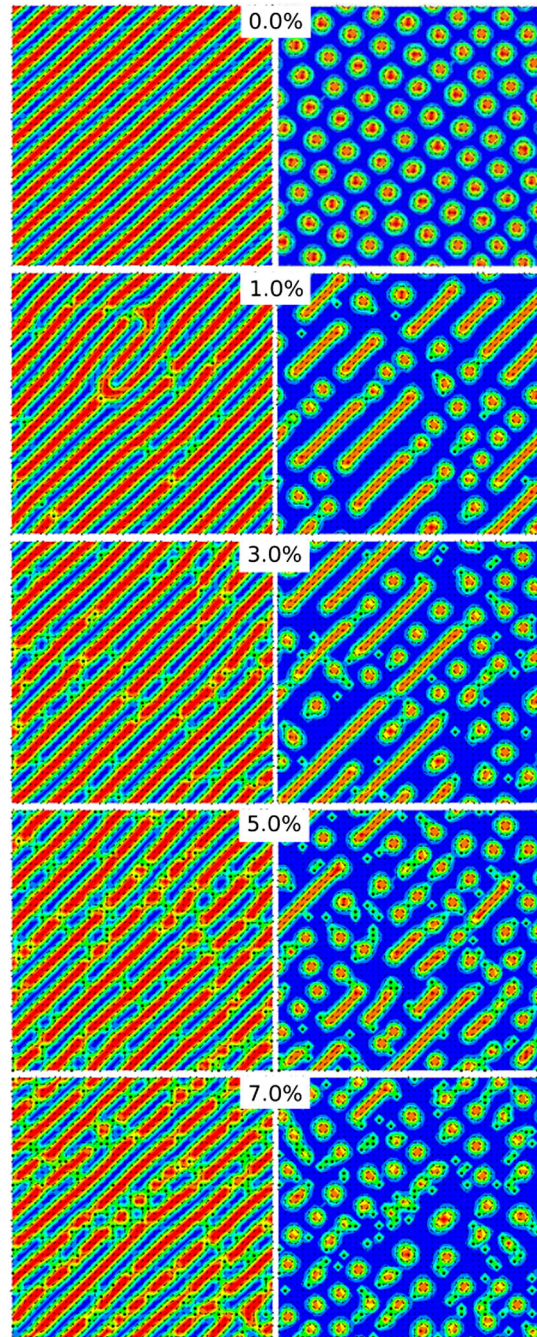


FIG. 30. Images from Monte Carlo simulations of spiral (left column) and skyrmion (right column) states with increasing magnetic spin vacancy densities ρ . At $\rho = 0$, an ordered spiral or triangular skyrmion lattice state forms. As ρ increases, skyrmions nucleate in the spiral state, the skyrmion lattice becomes disordered and bimerons appear. From Silva *et al.*, 2014.

frequencies, along with the key result that these quantities change sharply across the helical state to skyrmion state transition. Several other studies have demonstrated that quenched disorder can generate skyrmions (Chudnovsky and Garanin, 2018; Mirebeau *et al.*, 2018).

At transitions from square meron to hexagonal meron to hexagonal skyrmion states (Yu, Koshibae *et al.*, 2018), changes in the elastic constants can occur, and the system can disorder near the square to hexagonal transition if the

elastic constants drop below a certain level. Metastable glassy skyrmion states could be created by quenching rapidly from a higher temperature liquid state to a lower temperature at which the equilibrium state is an ordered solid. In the presence of pinning, the resulting metastable supercooled liquid or glassy state could be long-lived. Metastable and equilibrium disordered states can be distinguished from each other by applying perturbations such as a changing magnetic field. Experiments have shown that, even in systems with large intrinsic disorder, an ordered skyrmion lattice can be produced with a judicious selection of field application protocols (Gilbert *et al.*, 2019).

A. Future directions

Collective skyrmion states with disorder could form different types of glassy states, such as analogs to the vortex glass in type-II superconductors with point pinning, a Bose glass, a splay glass, or entirely new glassy phases not previously observed. For example, a Bragg glass could form for weak quenched disorder, while a skyrmion glass similar to a superconducting vortex glass could appear for stronger quenched disorder. At even stronger disorder, the skyrmion lines could break up to create something like a monopole glass or a skyrmion-bimeron glass. Other possible states include a skyrmion bobber glass or a state with chiral bobbars near the surface (Rybakov *et al.*, 2016) and a skyrmion glass in the bulk. In Fig. 31 we show a schematic of a possible phase diagram as a function of disorder strength δ versus magnetic field for a skyrmion system. At intermediate fields, where the skyrmion density is the highest, there is a skyrmion Bragg glass, while for larger δ the skyrmions positionally disorder and form a skyrmion glass. At the highest δ , the skyrmion lines break up into a disordered configuration of coexisting skyrmions and bimerons. Other arrangements are also possible. For example, with increasing field the skyrmions

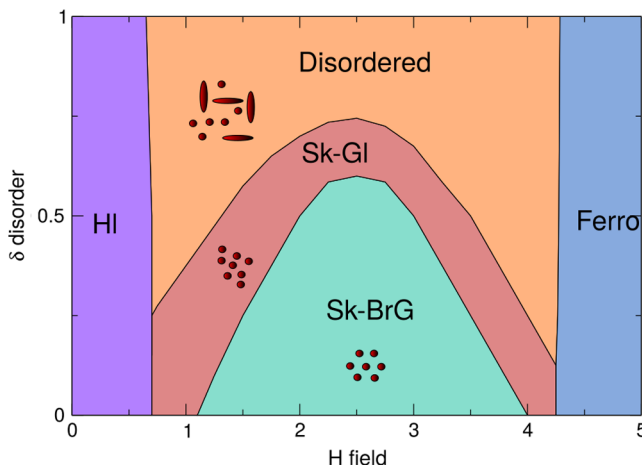


FIG. 31. Schematic of a possible phase diagram as a function of disorder strength δ vs magnetic field H for a skyrmion system. A helical state (HI) forms at low fields. At low δ and high skyrmion density there is a skyrmion Bragg glass (Sk-BrG), while at low skyrmion densities and intermediate δ a skyrmion glass (Sk-GI) appears. For large δ , a mixed skyrmion-meron state with skyrmion breaking (disordered) emerges. A ferromagnetic state (ferro) appears at the highest fields.

become smaller and more difficult to distort, so the disordered phase could shift to higher δ with increasing magnetic field. Each of these states could show unique responses to driving, ac perturbation, retardation effects, or creep. If a full phase diagram for static skyrmion states were measured as a function of quenched disorder, field, and temperature, it could contain skyrmion lattice, skyrmion glass, and skyrmion liquid states similar to the superconducting vortex phase diagram (Crabtree and Nelson, 1997). It is not known whether a 2D or 3D skyrmion liquid phase differs from a 2D or 3D skyrmion glass phase. Since many materials now support skyrmions at room temperature, some could have strong enough thermal fluctuations to create a diffusing skyrmion liquid. There is already evidence of skyrmion thermal motion (Nozaki *et al.*, 2019; Zázvorka *et al.*, 2019; Zhao *et al.*, 2020) and liquid phases (Chai *et al.*, 2021). The nature of the skyrmion liquid phase could depend strongly on the quenched disorder.

Differences between a pinned liquid and a pinned glass appear in correlation functions such as density fluctuations or $S(\mathbf{k})$. The same measures can detect the presence of disordered hyperuniformity, where, unlike in a completely random system, large-scale density fluctuations are suppressed (Torquato, 2016). Hyperuniformity can be used to distinguish jammed and liquid states (Dreyfus *et al.*, 2015), and it has been observed in simulations of interacting particles with pinning (Le Thien *et al.*, 2017). When the structure factor $S(\mathbf{k})$ in the limit $|\mathbf{k}| \rightarrow 0$ obeys a power law given by

$$S(\mathbf{k}) \propto |\mathbf{k}|^\alpha, \quad (11)$$

hyperuniformity is present when $\alpha > 0$, while in a random configuration $S(\mathbf{k})$ approaches a constant value at small \mathbf{k} . There are different hyperuniform scaling regimes with $\alpha > 1$, $\alpha = 1$, and $0 < \alpha < 1$. In general, larger values of α indicate larger amounts of short-range order. Hyperuniformity can also be characterized by measuring the number variance $\sigma^2(R) = \langle N^2(R) \rangle - \langle N(R) \rangle^2$, where $N(R)$ is the number of particles in a region of radius R . For a random system $\sigma^2(R) \propto R^2$, while for d -dimensional hyperuniform systems $\sigma^2(R) \propto R^{d-\alpha}$ when $\alpha < 1$, and $\sigma^2(R) \propto R^{d-1}$ when $\alpha > 1$ (Torquato, 2016). Skyrmion assemblies are an ideal system in which to test hyperuniformity concepts since skyrmions can easily be imaged over large scales.

It is an open question how all of the previously described disordered phases would change in different species of skyrmions such as an antiskyrmion lattice, antiferromagnetic skyrmions, or a 3D hedgehog lattice. Each variety of skyrmion could exhibit different collective interactions in the presence of disorder.

VI. DEPINNING DYNAMICS OF SKYRMIONS WITH PINNING

Skyrmions in the presence of pinning can be driven by various methods, depending on whether the host system is a metal or an insulator. A metallic system can be driven through the application of a current by means of the spin-torque effect (Schulz *et al.*, 2012; Iwasaki, Mochizuki, and Nagaosa, 2013a, 2013b; Nagaosa and Tokura, 2013; Liang *et al.*, 2015; Legrand *et al.*, 2017; Tolley, Montoya, and Fullerton,

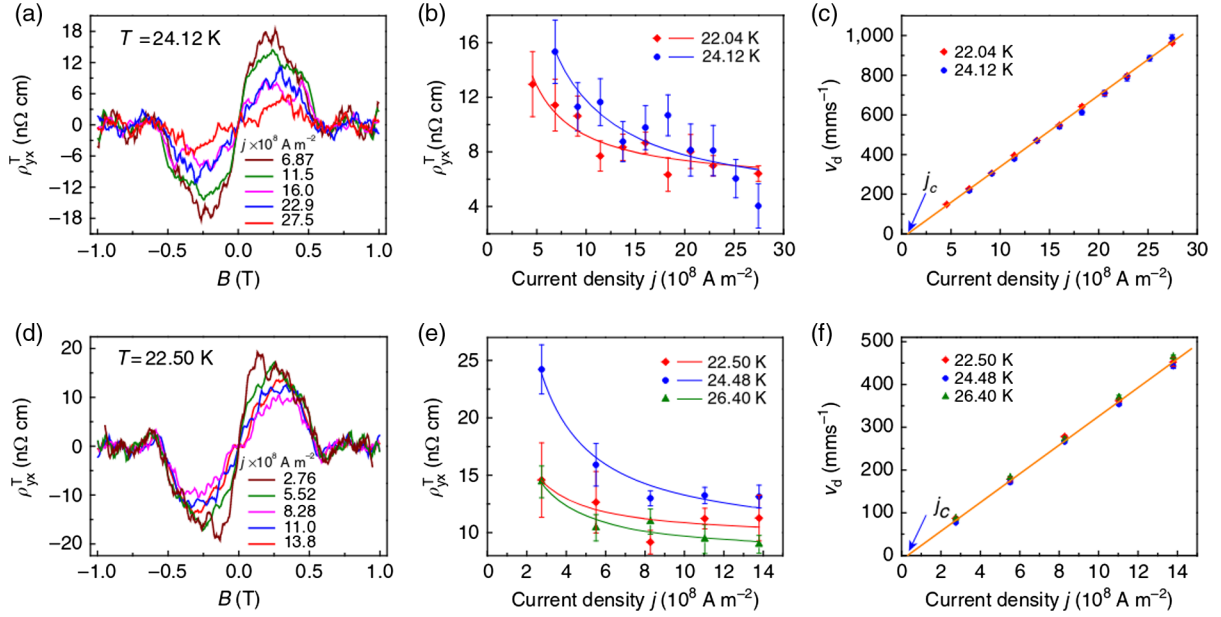


FIG. 32. Construction of skyrmion velocity-current curves based on measurements of the topological Hall effect ρ_{xy}^T . The results are from two different devices, one smaller (upper row) and one larger (lower row). (a),(d) ρ_{xy}^T vs magnetic field B for different applied current densities j . (b),(e) Average value of ρ_{xy}^T over the range $B = 0.2$ to 0.4 T vs j at different temperatures. (c),(f) Estimated skyrmion drift velocity v_d vs j . From Liang *et al.*, 2015.

2018). Other driving methods include thermal gradients (Kong and Zang, 2013; Kovalev, 2014; Lin *et al.*, 2014; Mochizuki *et al.*, 2014; Pöllath *et al.*, 2017; Z. Wang *et al.*, 2020), electric fields (White *et al.*, 2014; Ma *et al.*, 2019), spin waves (Zhang, Ezawa *et al.*, 2015; Zhang, Müller *et al.*, 2017; Shen, Zhang *et al.*, 2018; Yokouchi *et al.*, 2020), magnons (Psaroudaki and Loss, 2018), magnetic field gradients (Shen, Xia *et al.*, 2018; Zhang, Wang *et al.*, 2018), and acoustic waves (Nepal, Güngördü, and Kovalev, 2018; Yokouchi *et al.*, 2020), as well as skyrmioniums driven with spin waves (Li *et al.*, 2018). One of the first studies of skyrmion dynamics was performed by Zang *et al.* (2011), who showed that the skyrmion trajectories are deflected from the direction of the applied current and generate a THE that can be large. They also identified a weak pinning or collective pinning regime along with a strong pinning regime. Direct imaging of skyrmion dynamics has been achieved with a variety of experimental techniques, including Lorentz imaging (further described later).

Skyrmions produce the topological Hall effect (Neubauer *et al.*, 2009; Nagaosa and Tokura, 2013; Raju *et al.*, 2019), which combines additively with the other Hall effect terms to give a measured resistivity of

$$\rho_{xy}(H) = R_0 H + R_S M(H) + \rho_{TH}(H). \quad (12)$$

In Eq. (12) $R_0 H$ is the ordinary Hall effect and $R_S M(H)$ is the anomalous Hall effect, while ρ_{TH} is the THE, which is typically obtained by accurately accounting for the contribution of the first two terms and subtracting them from ρ_{xy} . The THE is linked to the skyrmion density according to $\rho_{TH} = P R_0 n_T \Phi_0$, where P is the density of mobile charges, R_0 is an unknown Hall resistivity from the effective charge

density that is often taken to be equal to the ordinary Hall coefficient, n_T is the density of the total topological charge from the skyrmions, and $\Phi_0 = h/e$ is the elementary flux quantum. According to this relation, ρ_{TH} is directly proportional to the number of skyrmions in the sample (Nagaosa and Tokura, 2013; Raju *et al.*, 2019). The skyrmion size affects ρ_{TH} , so smaller skyrmions produce a larger THE.

Schulz *et al.* (2012) constructed a skyrmion velocity-force curve based on changes in the THE. They argued that, for a constant H , ρ_{TH} remains constant at zero current ($j = 0$) when the skyrmions are stationary, but decreases when the skyrmions begin to move under an applied current. By measuring variations of ρ_{xy} in the skyrmion phase as a function of j , they observed a drop at a specific value of j that was argued to correspond to the critical depinning threshold and constructed an effective velocity-force curve. In Fig. 32, a similar approach was used to construct a skyrmion velocity-current curve for MnSi nanowires of different sizes (Liang *et al.*, 2015). The THE ρ_{xy}^T , which is nonzero only inside the skyrmion phase, is plotted versus B for different currents in Fig. 32(a). The average value of ρ_{xy}^T decreases with increasing j , as shown in Fig. 32(b). The skyrmion velocity v_d estimated from these data is plotted versus j in Fig. 32(c), and the critical current j_c is obtained from a linear fit of this curve. Figures 32(d)–32(f) indicates that similar trends appear in a larger device. This work established that $\rho_{xy}^T \propto 1/j$, implying a linear increase of the skyrmion velocity with drive for drives well above j_c . Near j_c , v varies nonlinearly with j . When the depinning is elastic, this nonlinear region extends only as high as currents below $1.1j_c$, but for plastic depinning the nonlinear regime can extend out to many multiples of j_c .

In principle, changes in the THE as a function of current could be measured carefully as a function of drive, temperature,

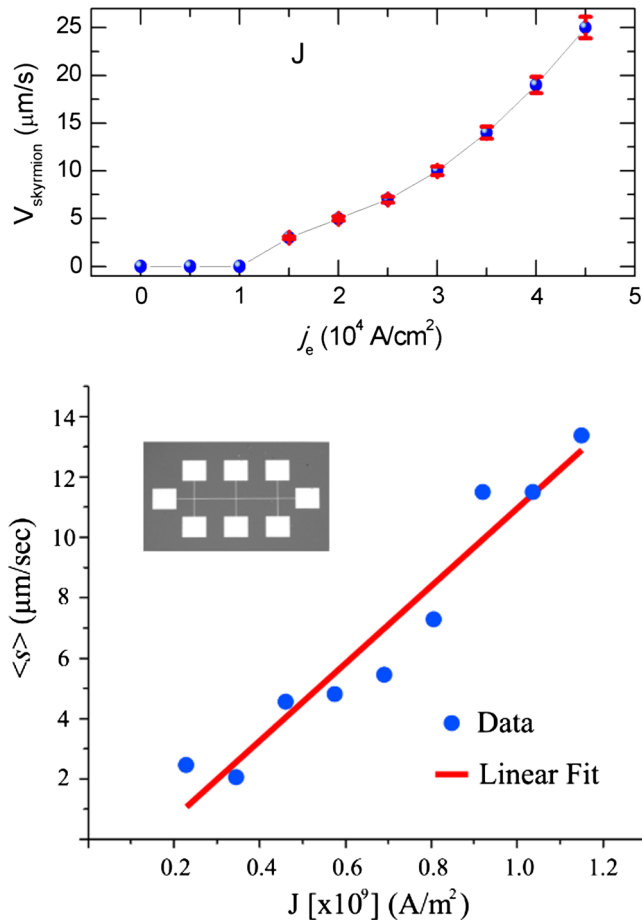


FIG. 33. Direct imaging measurements of skyrmion velocity. Top panel: skyrmion velocity V_{skyrmion} vs current j_e for room-temperature skyrmions. From Jiang *et al.*, 2015. Bottom panel: skyrmion velocity $\langle s \rangle$ vs current J for Pt/Co/Os/Pt thin films showing a linear fit. From Tolley, Montoya, and Fullerton, 2018.

and magnetic field in order to map the exact behavior of j_c . For example, a large increase in j_c could accompany an elastic to plastic depinning transition that is similar to the peak effect found in superconducting vortex systems (Reichhardt and Reichhardt, 2017a). Obtaining high precision ρ_{xy}^T measurements down to the single skyrmion level can be difficult since all other Hall contributions must be carefully accounted for (Maccariello *et al.*, 2018; Zeissler *et al.*, 2018). Therefore, only a few studies have used changes in ρ_{xy}^T to deduce j_c (Schulz *et al.*, 2012; Liang *et al.*, 2015). Other studies in systems known to support skyrmions have shown that ρ_{xy}^T is independent of j (Leroux *et al.*, 2018). Possible confounding factors include sign changes of the THE or the existence of nonskyrmionic THE sources (Denisov *et al.*, 2017, 2018; Maccariello *et al.*, 2018). Recent experiments have confirmed that ρ_{xy}^T increases as the number of skyrmions increases; however, there is not exact quantitative agreement with the theory, and the value of ρ_{xy}^T is actually higher than expected for the number of skyrmions counted (Raju *et al.*, 2019).

The most common method for generating skyrmion velocity-force or velocity-current curves and identifying j_c has been direct imaging (Yu *et al.*, 2012; Jiang *et al.*, 2015, 2017;

Woo *et al.*, 2016, 2018; Litzius *et al.*, 2017; Tolley, Montoya, and Fullerton, 2018). An example of results obtained with this technique appears in the top panel of Fig. 33 for room-temperature skyrmions with $j_c \approx 10^4 \text{ A/cm}^2$ (Jiang *et al.*, 2015). The bottom panel of Fig. 33 shows the skyrmion velocity versus the current in room-temperature Pt/Co/Os/Pt thin films obtained from magneto-optical Kerr effect (MOKE) microscopy images (Tolley, Montoya, and Fullerton, 2018). The amount of time required to image the skyrmion places a limitation on this technique. Images are often obtained after applying a current pulse rather than under a continuous current, and velocities must be deduced based on the skyrmion displacements rather than through direct visualization of the skyrmion motion, making it difficult to access high frequency dynamics or effects such as hysteresis that can appear under a continuous current sweep. Since MOKE microscopy has time resolution limitations, other methods could be considered, such as ultrafast photoemission electron microscopy.

A. Elastic and plastic depinning

Iwasaki, Mochizuki, and Nagaosa (2013b) performed micromagnetic simulations of driven skyrmions interacting with weak pinning sites that are much smaller than the skyrmion radius and found a triangular skyrmion lattice in both the pinned and moving states. The depinning threshold was zero in the absence of defects, but when pinning was added elastic depinning occurred in which each skyrmion maintained the same neighbors over time. As the ratio of the nonadiabatic portion of the interaction was decreased, j_c increased. The simulations revealed that the skyrmions not only moved around the defects due to the Magnus force but also changed shape. Figure 34 shows the longitudinal skyrmion velocity v_{\parallel} versus the current j from simulations for skyrmion and helical phases with and without disorder. The helical phases are strongly pinned when disorder is present, but the skyrmion phases are weakly pinned. Since the skyrmions form a triangular lattice, Iwasaki, Mochizuki, and Nagaosa (2013b) also analyzed the Bragg peaks and found weaker peaks with strong fluctuations at lower drives, while at higher drives the fluctuations were less pronounced and the Bragg peaks approached their pinning-free heights. This is similar to the dynamical ordering found in superconducting vortex systems (Koshelev and Vinokur, 1994; Olson, Reichhardt, and Nori, 1998b). Although no dislocations are generated at depinning, the skyrmion lattice interacts more strongly with the pinning at low drives and becomes less ordered. Iwasaki, Mochizuki, and Nagaosa argued that the particle-based Thiele equation approach can be applied to understand both the depinning and the skyrmion dynamics responsible for the behavior of the velocity-force curves.

The micromagnetic simulations of Iwasaki, Mochizuki, and Nagaosa (2013b) produced linear velocity-current curves with $v_{\parallel} \propto F_D$ but could not resolve the depinning threshold F_c in the skyrmion regime. Reichhardt, Ray, and Reichhardt (2015a) and Reichhardt and Reichhardt (2019a) examined a 2D particle-based model for skyrmions interacting with disordered pinning substrates of varied strength and found that the velocity-force curves are consistent with

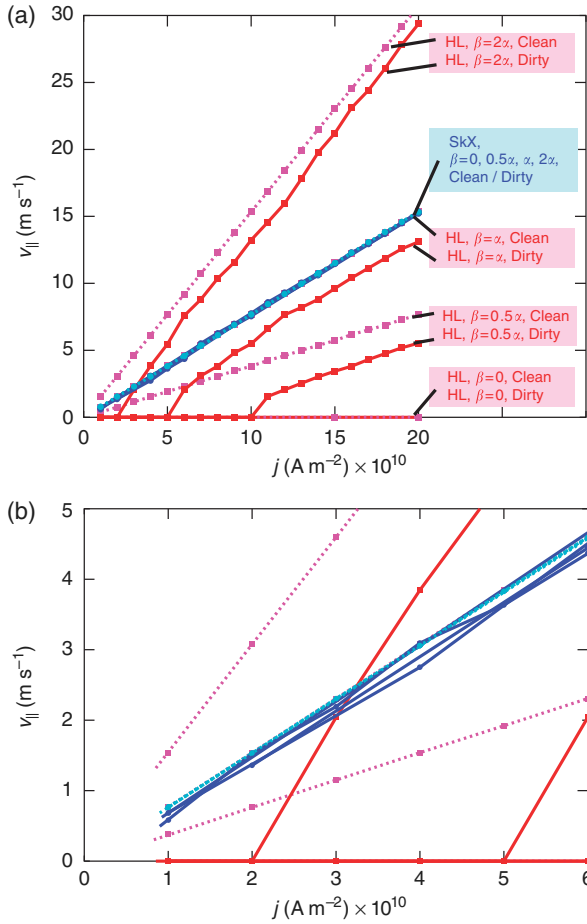


FIG. 34. Micromagnetic simulation measurements of the current-induced longitudinal velocities v_{\parallel} of the helical (HL) and skyrmion crystal (SkX) phases vs current density j in the clean (impurity-free) and dirty limits for different values of the nonadiabatic term β . Center blue lines, skyrmion phases; outer red and magenta lines, helical phases. The skyrmions are much more weakly pinned than the helical phases and show an elastic depinning transition. (b) Magnification of (a) in the region of low current density. From Iwasaki, Mochizuki, and Nagaosa, 2013b.

$v \propto (F_D - F_c)^\beta$, with $\beta < 1.0$. For elastic depinning $\beta < 1.0$, while for plastic depinning $\beta > 1.0$ (Fisher, 1998; Reichhardt and Reichhardt, 2017a); however, there has been no detailed finite size scaling to confirm the exact exponent values for either elastic or plastic depinning. The Magnus force might modify the scaling compared to what is found in overdamped systems. Reichhardt and Reichhardt (2019a) examined the magnitude $S(k_0)$ of one of the six Bragg peaks as a function of driving force F_D . Although the skyrmions retain sixfold ordering for all drives, a dip in $S(k_0)$ occurs at the depinning threshold, indicating that during depinning the lattice becomes more disordered, as also observed by Iwasaki, Mochizuki, and Nagaosa (2013b).

At stronger pinning, Reichhardt, Ray, and Reichhardt (2015a) and Reichhardt and Reichhardt (2019a) found a transition to a state in which, even for $F_D = 0$, dislocations proliferate and the skyrmions are in a glassy configuration, while at higher drives the skyrmions dynamically order into a

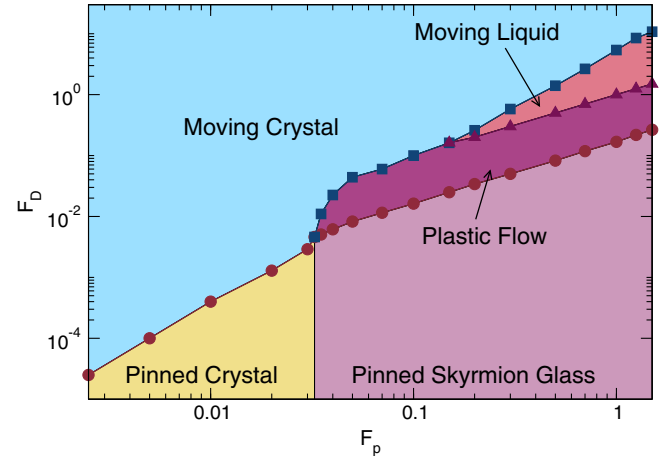


FIG. 35. Dynamic phase diagram as a function of the driving force F_D vs the pinning strength F_p from particle-based simulations, showing a pinned crystal to pinned glass transition. The pinned crystal depins elastically into a moving crystal, and the pinned glass depins plastically into a plastic flow regime that transitions into a moving liquid. At high drives, a moving crystal appears. The pinned to moving crystal transition follows $F_c \propto F_p^2$, while the pinned glass to plastic flow transition obeys $F_c \propto F_p$. From Reichhardt and Reichhardt, 2019a.

moving crystal phase. Figure 35 shows the dynamical phase diagram as a function of driving force versus pinning strength F_p , where there are two pinned phases: a pinned crystal for weak disorder and a pinned glass for stronger disorder. In the pinned crystal, the skyrmions form a defect-free lattice with sixfold peaks in $S(\mathbf{k})$ and the critical driving force $F_c \propto F_p^2$, as expected for elastic depinning from collective pinning theory (Blatter *et al.*, 1994), while in the pinned glass, which has a ringlike $S(\mathbf{k})$, $F_c \propto F_p$, as expected for plastic depinning. Although a transition from an ordered to a disordered state at $T = 0$ occurs as a function of increasing quenched disorder strength, in agreement with the predictions of Cha and Fertig (1995), it is not known if the pinned skyrmion crystal to pinned skyrmion glass transition is of the KTHNY type. A sudden increase in F_c appears at the crystal to glass transition. This is similar to the peak effect found for superconducting vortices, where particles in the plastic or disordered phase can better adjust their positions to optimize their interactions with randomly located pinning sites, increasing F_c (Bhattacharya and Higgins, 1993; Banerjee *et al.*, 2000; Reichhardt *et al.*, 2001; Toft-Petersen *et al.*, 2018). When the pinning is weaker, the relative magnitude of the jump in F_c at the elastic to plastic depinning transition increases (Reichhardt and Reichhardt, 2017a). At the elastic depinning transition, the motion can be jerky or intermittent but particles maintain the same neighbors. On the other hand, for plastic depinning numerous dislocations and topological objects appear and there is a coexistence of pinned and flowing skyrmions, as illustrated in Fig. 36 (Reichhardt and Reichhardt, 2016). The moving liquid state is distinct from the plastic flow state since all of the skyrmions are moving simultaneously but remain disordered. At higher drives, within the particle model the skyrmions dynamically reorder into a moving crystal and

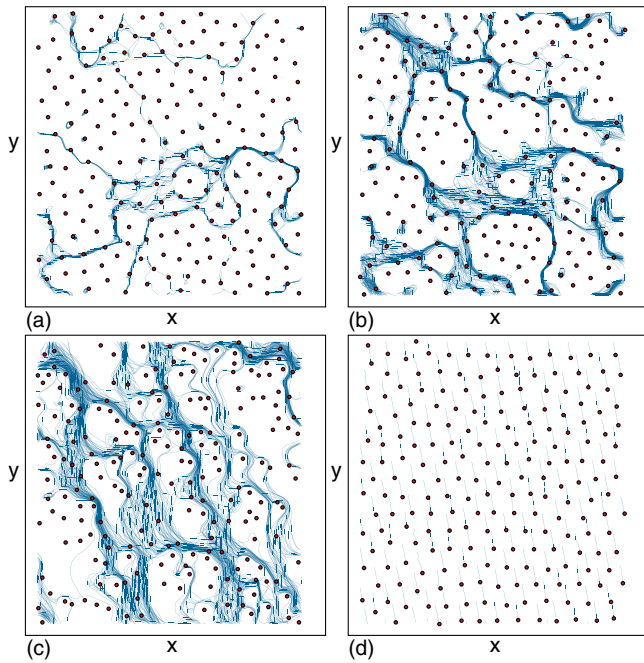


FIG. 36. Plastic flow phase just above depinning from particle-based simulations of skyrmions in strong random pinning. Skyrmion positions (dots) and trajectories (lines) are obtained for a fixed time interval, and the drive is in the $+x$ direction. (a) Near depinning, channels of flow coexist with pinned skyrmions. (b) The number of pinned skyrmions decreases with increasing drive. (c) At higher drives, plastic flow persists and the direction of motion rotates away from the driving direction. (d) Trajectories obtained over a shorter time period in a high drive dynamically ordered state where the skyrmions move at an angle of -79.8° to the drive. From Reichhardt and Reichhardt, 2016.

regain their mostly sixfold ordering (Reichhardt, Ray, and Reichhardt, 2015a; Reichhardt and Reichhardt, 2016, 2019a).

Evidence for collective plastic flow was obtained with direct imaging of room-temperature skyrmions in thin films. The skyrmion trajectories show coexisting moving and pinned regions along with channels or rivers of flow, as illustrated in Fig. 37 (Montoya *et al.*, 2018). The images closely resemble the motion observed experimentally near depinning transitions of superconducting vortices (Matsuda *et al.*, 1996; Fisher, 1998; Reichhardt and Reichhardt, 2017a) and colloidal particles (Pertsinidis and Ling, 2008; Tierno, 2012) on random substrates. Small-angle neutron scattering experiments on MnSi under an applied current showed a broadening of the peaks close to depinning, which could be evidence of dynamical disordering; however, it was also argued that the broadening could arise from edge effects that produce counter-rotating domains (Okuyama *et al.*, 2019).

Unlike particle-based models, actual skyrmions have internal degrees of freedom that can become excited. For example, one end of a skyrmion (a meron) could be pinned while the meron in the other half of the skyrmion continues to move. This could be viewed as the motion of an elongated skyrmion or as the emergence of a helical stripe phase. Dynamics of this type have been studied both theoretically (Lin, 2016) and experimentally (Hirata *et al.*, 2019; S. Zhang *et al.*, 2020).

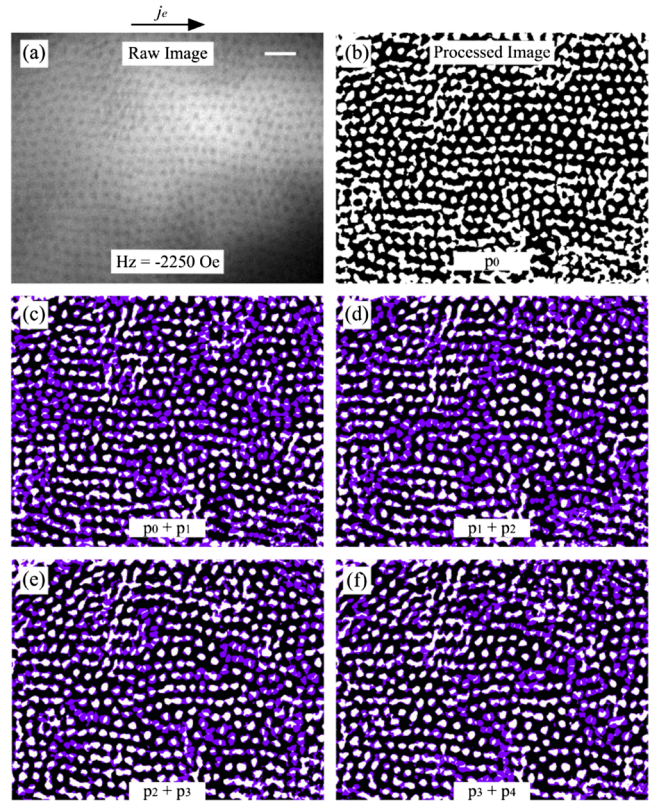


FIG. 37. Images showing current-induced plastic motion of dipole skyrmions from room-temperature experiments on Ta (5 nm)/[Fe (0.34 nm)/Gd(0.4 nm)] \times 100/Pt(3 nm). (a) Original soft x-ray microscopy image of a close-packed skyrmion lattice. (b) Postprocessed binary image of (a) where the background has been subtracted. (c)–(f) Skyrmion dynamics obtained by summing images of the domain morphology before and after a current pulse is injected, where purple indicates places where the domain morphology has changed. From Montoya *et al.*, 2018.

The dynamical ordering from a plastic flow state to an ordered state illustrated in Fig. 35 is similar to that found for superconducting vortices (Koshelev and Vinokur, 1994; Olson, Reichhardt, and Nori, 1998b; Reichhardt and Reichhardt, 2017a), Wigner crystals (Reichhardt *et al.*, 2001), pattern forming systems (Xu *et al.*, 2011; Zhao, Misko, and Peeters, 2013), and driven charge density waves (Danneau *et al.*, 2002; Du *et al.*, 2006; Pinsolle *et al.*, 2012). There are, however, several differences in the moving states of skyrmions with a Magnus force compared to the previously studied overdamped systems. In 2D superconducting vortices and overdamped systems in general, the moving state is typically a moving smectic in which particles form rows that slide past one another. Figures 38(a)–38(c) show $S(\mathbf{k})$ at fixed drives for an overdamped particle system that could represent superconducting vortices moving over random disorder (Díaz *et al.*, 2017). At lower drives in Fig. 38(a), the structure factor has a ring shape indicative of a liquid or glass and the particle configuration is disordered. At higher drives in Fig. 38(b), the system begins to dynamically reorder into a moving smectic state containing well-defined particle chains moving past each other. This creates a series of aligned dislocations and the structure factor contains two dominant peaks. For even higher

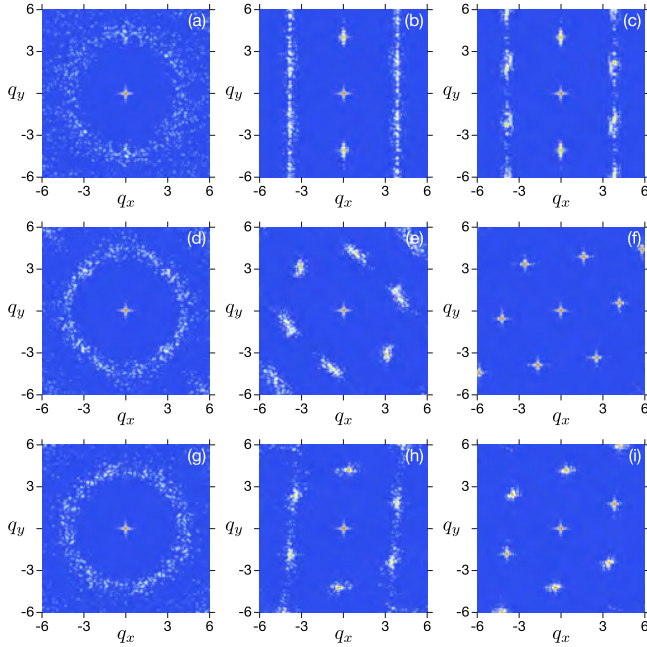


FIG. 38. Static structure factor $S(\mathbf{q})$ from particle-based skyrmion simulations. The driving force increases from left to right in each row. An overdamped system with an intrinsic Hall angle of $\theta_{\text{SKH}}^{\text{int}} = 0$ is displayed in (a) the plastic flow state, (b) the moving smectic state, and (c) the moving anisotropic crystal state. A system with $\theta_{\text{SKH}}^{\text{int}} = 45^\circ$ is shown in (d) the moving liquid state, (e) a slightly anisotropic moving crystal state, and (f) the moving crystal state. A system with $\theta_{\text{SKH}}^{\text{int}} = 70^\circ$ is displayed in (g) the moving liquid state, (h) a slightly anisotropic moving crystal state, and (i) the moving crystal state. From *Díaz et al., 2017*.

drives in Fig. 38(c), the moving smectic develops additional sixfold ordering, visible as additional smeared peaks in $S(\mathbf{k})$. At still higher drives, the structure factor ceases to evolve since the dislocations are dynamically trapped. The approach to a moving crystal state for overdamped particles such as superconducting vortices moving over random disorder was predicted theoretically (*Giamarchi and Le Doussal, 1996; Balents, Marchetti, and Radzihovsky, 1998*) and observed in numerous simulations (*Giamarchi and Le Doussal, 1996; Moon, Scalettar, and Zimányi, 1996; Olson, Reichhardt, and Nori, 1998b; Kolton, Domínguez, and Grønbech-Jensen, 1999; Fangohr, Cox, and de Groot, 2001; Gotcheva, Wang, and Teitel, 2004*) and experiments (*Pardo et al., 1998*).

When the Magnus force is present, as in driven skyrmions, simulations show that the dynamically reordered state has six strong peaks, indicating a higher degree of isotropic order compared to overdamped systems (*Díaz et al., 2017*). This effect is attributed specifically to the Magnus force. Viewed from a comoving frame, overdamped particles experience force perturbations from the substrate that are strongest in the direction of motion. The resulting fluctuations can be represented as a shaking temperature $T_{\text{sh}} \propto 1/F_D$ (*Koshelev and Vinokur, 1994*). For sufficiently large drives, the system freezes into a solid, but because the shaking temperature is anisotropic with $T_{\text{sh}}^{\parallel} > T_{\text{sh}}^{\perp}$ (*Giamarchi and Le Doussal, 1996; Balents, Marchetti, and Radzihovsky, 1998*), the direction perpendicular to the drive freezes first, locking dislocations

into the sample, while the direction parallel to the drive remains liquidlike. In the case of skyrmions, the Magnus force mixes the fluctuations from the driving direction into the perpendicular direction, resulting in a more isotropic shaking temperature that prevents the trapping of smectic defects and allows the system to freeze in both directions simultaneously. The isotropic nature of T_{sh} was confirmed in simulations through direct measurements of the fluctuations in both the transverse and longitudinal directions for skyrmions moving through random pinning (*Díaz et al., 2017*). For large Magnus forces, it is possible that the system would form a moving smectic structure aligned perpendicular, rather than parallel, to the drive.

Figures 38(d)–38(f) show $S(\mathbf{k})$ for three different drives in simulations of a 2D driven skyrmion system with random pinning where the intrinsic skyrmion Hall angle is $\theta_{\text{SKH}}^{\text{int}} = 45^\circ$ (*Díaz et al., 2017*). At a low drive in Fig. 38(d), the skyrmions are disordered and $S(\mathbf{k})$ has a ringlike structure. At a higher drive in Fig. 38(e), sixfold peaks begin to emerge that are much more isotropic than the peaks in Fig. 38(b) for the overdamped system, although the four side peaks are still somewhat smeared. For high drives, illustrated in Fig. 38(f), there are six sharp peaks of equal size and the skyrmions have organized into a crystal. A similar evolution of the structure factor with drive for skyrmions with $\theta_{\text{SKH}}^{\text{int}} = 70^\circ$ appears in Figs. 38(g)–38(i). Compared to the overdamped system, where a weakly disordered crystal aligned with the driving direction appears, the skyrmion crystal is well ordered and is not aligned with the driving direction. Instead, the crystal orientation rotates slightly with increasing drive. This is another consequence of the Magnus force, which aligns the lattice with the direction of motion rather than the driving direction. In an overdamped system, these two directions are the same, but in the skyrmion system, they are separated by the intrinsic skyrmion Hall angle.

The moving smectic state can also be distinguished from the moving crystal by measuring the relative motion of the particles in the comoving frame, where the center of mass motion has been subtracted. Skyrmions exhibit a long-time diffusive motion in the driving direction but have subdiffusive motion or no diffusion perpendicular to the driving direction (*Díaz et al., 2017*). The displacements in the moving frame are given by $\Delta_{\parallel}(t) = N^{-1} \sum_{i=1}^N [\tilde{r}_{i,\parallel}(t) - \tilde{r}_{i,\parallel}(0)]^2$, where $\tilde{r}_{i,\parallel} = r_{i,\parallel}(t) - R_{\parallel}^{\text{CM}}(t)$ and $\Delta_{\perp}(t) = N^{-1} \sum_{i=1}^N [\tilde{r}_{i,\perp}(t) - \tilde{r}_{i,\perp}(0)]^2$, with $\tilde{r}_{i,\perp} = r_{i,\perp}(t) - R_{\perp}^{\text{CM}}(t)$. Here R^{CM} is the center of mass in the moving frame and N is the number of skyrmions. The different phases can be identified through the power law behavior

$$\Delta(t)_{\parallel,\perp} \propto t^{\alpha_{\parallel,\perp}}. \quad (13)$$

For isotropic regular diffusion, $\alpha_{\parallel} = \alpha_{\perp} = 1$; for a smectic state, $\alpha_{\parallel} \geq 1$ and $\alpha_{\perp} = 0$; for a moving crystal, $\alpha_{\parallel} = \alpha_{\perp} = 0$; and for a moving liquid, $\alpha_{\parallel} \geq 1$ and $\alpha_{\perp} \geq 1$. Other regimes are also possible. For example, at short times there can be subdiffusive behavior with $0 < \alpha < 1$ in either direction, but at long times a crossover to regular diffusion occurs. Within the smectic phase, $\alpha_{\parallel} = 2$, indicating superdiffusive or

ballistic motion in the driving direction, while $\alpha_{\perp} = 0$. The ballistic behavior that appears even after the center of mass motion has been removed arises because the different rows in the smectic state are moving at different speeds relative to one another. In general, the moving smectic state in overdamped 2D systems always shows regular diffusion or superdiffusion in the direction parallel to the drive but no diffusion in the direction perpendicular to the drive. This is in contrast to the skyrmion moving crystal state that exhibits no diffusion in either direction, indicating the emergence of a truly crystalline state as a function of drive.

B. Noise

Noise fluctuations are a useful method for characterizing condensed matter (Weissman, 1988; Sethna, Dahmen, and Myers, 2001). For skyrmion systems, transitions between plastic flow and moving crystalline regimes can be distinguished with the power spectrum

$$S(\omega) = \left| \int \sigma(t) e^{-i2\pi\omega t} dt \right|^2 \quad (14)$$

of various time-dependent quantities $\sigma(t)$, such as the topological Hall resistance ρ_{xy}^T , the local magnetization, or the fluctuations in $S(\mathbf{k})$ at a particular value of \mathbf{k} . Separate time series $\sigma(t)$ can be obtained for different values of an applied drive in order to detect changes in the spectral response. Such measures have been used to study superconducting vortices (D'Anna *et al.*, 1995; Marley, Higgins, and Bhattacharya, 1995; Merithew *et al.*, 1996; Olson, Reichhardt, and Nori, 1998b; Kolton, Domínguez, and Grønbech-Jensen, 1999; Kolton *et al.*, 2002), sliding charge density waves (Grüner, Zawadowski, and Chaikin, 1981; Bloom, Marley, and Weissman, 1993), and the motion of magnetic domain walls (Sethna, Dahmen, and Myers, 2001), and they could prove to be a similarly powerful technique for skyrmion systems. Particle-based simulations of superconducting vortices showed that in the plastic flow phase the velocity noise has a broadband $1/f^{\alpha}$ signature, where $f = \omega/2\pi$ (Marley, Higgins, and Bhattacharya, 1995; Olson, Reichhardt, and Nori, 1998b). The value of the exponent α determines the type of noise. When $\alpha = 0$, the noise is white and has equal power in all frequencies, while $\alpha = 1$ or a $1/f$ signature is called pink noise and $\alpha = 2$ or a $1/f^2$ signature is known as brown or Brownian noise. Brownian noise can be produced by the trajectories of a random walk, whereas white noise has no correlations. In overdamped systems that undergo depinning, values of $0.75 < \alpha < 1.8$ are associated with collective dynamics, and in some cases the presence of a critical point produces a distinct spectral response (Travesset, White, and Dahmen, 2002). This implies that if depinning is a critical phenomenon, it may be possible to use the noise power to determine its universality class. In addition to broadband noise, there may be a knee at a specific frequency of the form $S(f) \propto \tau/[1 + (2\pi\tau f)^2]$, which approaches a constant value as f goes to zero. Such a response is often associated with telegraph noise, where τ is the characteristic time of jumps between the two states of the signal. A narrowband

noise signal produces one or more peaks at characteristic frequencies that are related to a length scale in the system. For example, a random arrangement of particles moving over random disorder can have a time-of-flight narrowband noise peak in which the characteristic frequency is the inverse of the time required to traverse the sample (D'Anna *et al.*, 1995; Olson, Reichhardt, and Nori, 1998a). Alternatively, a moving lattice can produce a washboard signal corresponding to the time required for a particle to move one lattice constant (Harris *et al.*, 1995; Olson, Reichhardt, and Nori, 1998b; Togawa *et al.*, 2000; Okuma, Inoue, and Kokubo, 2007; Klongcheongsan, Bullard, and Täuber, 2010).

In simulations, a time-of-flight signal can arise from the motion of a large-scale structure, such as a grain boundary in a skyrmion lattice, through the periodic boundary conditions. A signal of this type typically appears at relatively low frequencies. In skyrmion experiments, narrowband noise could be produced by the periodic nucleation of skyrmions at the edge of the sample, where the time of flight would correspond to the time required for the skyrmion to cross to the other side of the sample and be annihilated. The washboard frequency of an elastic lattice moving over disorder is given by $\omega = \langle v \rangle / a$ (Harris *et al.*, 1995), where $\langle v \rangle$ is the time-averaged dc velocity and a is the lattice constant. A measurement of the washboard frequency can thus be used to determine the lattice constant. Both the time-of-flight and washboard signals are generated when the particles are in steady, continuous motion, rather than intermittently alternating between pinned and moving. For a moving liquid, the sharp narrowband peaks are lost, but a smoother peak can still appear that is associated with the average time between collisions of a particle with a pinning site. Figure 39 shows the power spectra S_{\parallel} and S_{\perp} of the longitudinal and transverse velocity signals from a particle-based simulation of skyrmions moving over random disorder at various drives (Díaz *et al.*, 2017). In Fig. 39(a), an overdamped system in the plastic flow regime has higher noise power parallel to the drive than perpendicular to the drive, which is consistent with the idea that the shaking temperature is largest in the driving direction for overdamped systems moving over quenched disorder. There is also a $1/f^{\alpha}$ tail with $\alpha \approx 1.5$, which is similar to the noise observed in simulations of other overdamped systems. At higher drives in Figs. 39(b) and 39(c), the broadband signal disappears and high frequency peaks emerge at multiples of the washboard frequency. At much lower frequencies, the time-of-flight signal produces a second series of peaks that are the most pronounced in Fig. 39(c). Figures 39(d) and 39(g) show the plastic flow regime for skyrmion systems with $\theta_{\text{SkH}}^{\text{int}} = 45^{\circ}$ and 70° , respectively. The magnitude of the higher frequency noise is nearly identical in the two directions, which is in agreement with the argument that skyrmions have a more isotropic shaking temperature. At higher drives in Figs. 39(e), 39(f), 39(h), and 39(i), peaks once again appear at both the time-of-flight and washboard frequencies. The evolution of these peaks as a function of current provides additional dynamical information. For example, a sudden switch in the peak frequency would indicate the reorientation of the lattice or the annihilation of dislocations.

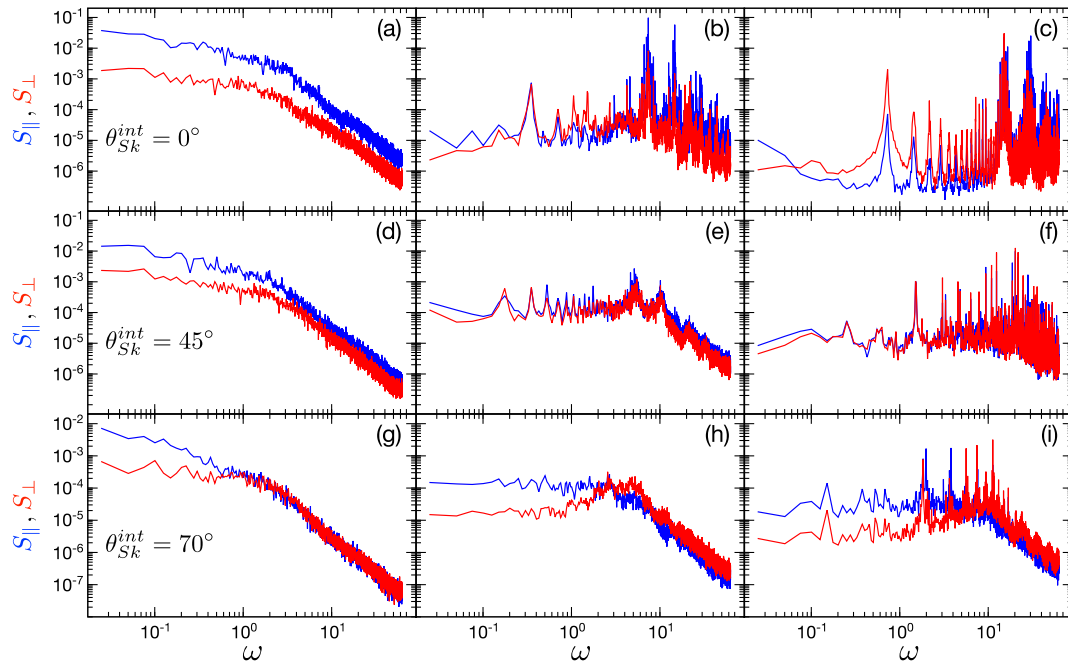


FIG. 39. Spectral density plots from particle-based skyrmion simulations showing $S_{\parallel}(\omega)$ (upper blue lines) and $S_{\perp}(\omega)$ (lower red lines) for velocity fluctuations parallel and perpendicular, respectively, to θ_{SKH} . The driving force increases from left to right. An overdamped sample with $\theta_{\text{SKH}}^{\text{int}} = 0^\circ$ is displayed in (a) the disordered flow state and (b),(c) two drives in the moving smectic phase. A sample with $\theta_{\text{SKH}}^{\text{int}} = 45^\circ$ is shown in (d) the disordered flow state, (e) the moving liquid phase, and (f) the moving crystal phase. A sample with $\theta_{\text{SKH}}^{\text{int}} = 70^\circ$ is displayed in (g) the disordered flow state, (h) the moving liquid phase, and (i) the moving crystal phase. From Díaz *et al.*, 2017.

Although skyrmions exhibit a number of dynamical features similar to those found in overdamped superconducting vortex systems, they also have some unique behaviors. For example, if a current were used to create skyrmions, this process could be detected via changes in the narrowband noise signature. In a sample where skyrmions coexist with different species of topological defects such as large ferromagnetic domains, the low frequency noise generated by density fluctuations could be used to determine the size of the domains (Mohan *et al.*, 2009). The noise power could increase as a function of increasing temperature near a 2D melting transition, where fluctuations are expected to increase strongly (Koushik *et al.*, 2013). In addition to the power spectrum, higher order measures such as the second spectrum or the noise of the noise can be analyzed to examine the persistence times of metastable processes (Merithew *et al.*, 1996). Noise has been used to measure various nonequilibrium effects, such as negative velocity fluctuations (Bag *et al.*, 2017), and similar studies could be performed for driven skyrmions, where the nonconservative Magnus force could produce novel effects. Skyrmion systems in which the dynamics of small numbers of skyrmions can be accessed could be ideal for studying routes to chaos using techniques similar to previous work performed on noise in charge density waves (Levy and Sherwin, 1991) and superconducting vortex systems (Olive and Soret, 2006).

Sato *et al.* (2019) experimentally examined noise fluctuations for current-induced skyrmions in micrometer-size MnSi samples and found a transition from broadband to narrowband noise above a threshold current. A narrowband noise peak in

the range $10 - 10^4$ Hz that appears for a current density of 10^9 A/m² was interpreted as originating from steady state skyrmion flow. The peak frequency increases with increasing current, which is consistent with behavior expected from a more rapidly moving skyrmion lattice. Figures 40(b)–40(d) show the voltage noise power spectrum for three different current densities, while Fig. 40(a) illustrates the spectral voltage noise power versus the applied current. At low currents, the noise power increases slowly with increasing current, while for intermediate currents there is a rapid increase in the low frequency noise power. At larger currents, two peaks appear in the power spectrum, thus indicating the emergence of narrowband noise, and the low frequency noise diminishes in magnitude. This result is similar to voltage noise spectra observations for the depinning of vortices in type-II superconductors.

To date numerical studies of skyrmion noise have been limited to particle-based models (Reichhardt and Reichhardt, 2016; Díaz *et al.*, 2017); however, continuum-based approaches could permit the exploration of additional contributions to noise from shape fluctuations or skyrmion breathing modes. For example, a moving skyrmion lattice has a washboard frequency associated with the lattice spacing, but a second, much higher frequency signal could appear as a result of collective breathing modes excited by the motion over random disorder. Other noise signatures could arise due to coupling of the internal modes with the skyrmion lattice. Experimental noise measurements in skyrmion systems are just beginning, with a recent experiment on skyrmion motion in a narrow channel showing a transition from $1/f$ noise to

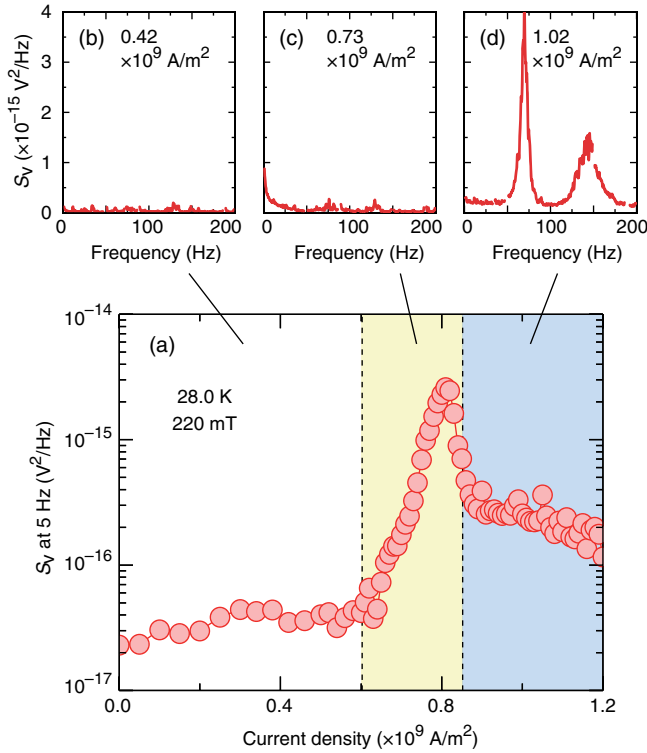


FIG. 40. (a) Spectral voltage noise power vs applied current density obtained from micrometer-size MnSi samples in the skyrmion lattice phase. Representative power spectra as a function of S_v vs frequency are displayed in (b) the white noise regime (left white region), (c) the broadband noise regime (center yellow area), and (d) the narrowband noise regime (right blue region). From Sato *et al.*, 2019.

narrowband noise similar to what has been seen in simulations (Sato *et al.*, 2019).

C. Avalanches

In intermittent systems, time windows of little or no activity are interspersed with windows of large activity or avalanches. Avalanchelike behavior is a ubiquitous phenomenon in driven systems with quenched disorder (Bak, Tang, and Wiesenfeld, 1988; Carlson, Langer, and Shaw, 1994; Fisher, 1998; Sethna, Dahmen, and Myers, 2001; Reichhardt and Reichhardt, 2017a), and one of the best-known examples is Barkhausen noise in magnetic systems (Barkhausen, 1919; Cote and Meisel, 1991; Bertotti, Durin, and Magni, 1994; Zapperi *et al.*, 1998). Avalanches are often most clearly resolvable at low driving, where distinct jumps can be distinguished from one another.

Numerous methods exist for analyzing avalanches. Construction of the probability distribution function of the magnitude of the velocity or other signal as a function of time can show whether the avalanches are all close to the same size, are exponentially distributed, have a specific range of sizes, or are power law distributed. A power law distribution of avalanche events is often associated with critical behavior (Bak, Tang, and Wiesenfeld, 1988; Perković, Dahmen, and Sethna, 1995). For example, if depinning in systems driven over quenched disorder is a critical phenomenon, then

avalanche behavior could appear close to the depinning transition. It has been argued theoretically that avalanches are critical only for a critical disorder strength R_c , with large avalanches that are close to the same size occurring for disorder strengths $R < R_c$ and exponentially distributed avalanches appearing for $R > R_c$; however, it is possible to be fairly far from R_c and still observe a regime of power law distributed avalanche sizes (Sethna *et al.*, 1993; Perković, Dahmen, and Sethna, 1995; Sethna, Dahmen, and Myers, 2001). Avalanches can occur in driven systems without thermal fluctuations; however, there are cases in which thermal effects can trigger avalanches. Both elastic and plastic systems exhibit avalanches, and in principle the avalanche distributions would change across an elastic-plastic transition. Since avalanches occur so routinely in magnetic systems, the skyrmion system is ideal for examining avalanche effects.

Skyrmion avalanches remain largely unexplored but were studied by Díaz *et al.* (2018) using a 2D particle-based model in which skyrmions entered the edge of the sample under a low driving force through a series of jumps. For zero or weak Magnus forces, the avalanche sizes S and durations T are power law distributed as $P(T) \propto T^\alpha$ and $P(S) \propto S^\tau$, with $\alpha = 1.5$ and $\tau = 1.33$. Near a critical point there should be an additional scaling relation $\langle S \rangle \propto T^{1/\sigma\nu z}$ between the avalanche sizes and durations (Sethna, Dahmen, and Myers, 2001) so that, in this case, $1/\sigma\nu z = 1.63$. The exponents should also obey

$$\frac{\alpha - 1}{\tau - 1} = \frac{1}{\sigma\nu z} \quad (15)$$

near the critical point. In the work of Díaz *et al.*, this equality was satisfied, indicating that near depinning the system is critical. For large values of $\theta_{\text{SKH}}^{\text{int}}$, the scaling exponents for the avalanches change but Eq. (15) still holds, suggesting that the nature of the criticality changes with increasing Magnus force. The avalanches can also be characterized by scaling the shape of avalanches that have the same duration. In certain universality classes, such as the random field Ising model, such scaling will produce a symmetric curve (Sethna, Dahmen, and Myers, 2001; Mehta *et al.*, 2002). Díaz *et al.* found that avalanches in the overdamped system and in samples with weaker Magnus forces were symmetric in shape, while those for strong Magnus forces were strongly skewed. This is also correlated with the change in the avalanche exponents at strong Magnus forces. Skewed avalanche shapes can result from nondissipative effects such as inertia, which tends to speed up the avalanche at later times and produce a leftward skew, or negative mass effects, which have the opposite effect and give a rightward skew (Zapperi *et al.*, 2005). Skyrmions have a tendency to be more strongly deflected at later times, which is similar to a negative mass effect. In Fig. 41 we show images of skyrmion avalanches for different $\theta_{\text{SKH}}^{\text{int}}$ (Díaz *et al.*, 2018). At $\theta_{\text{SKH}}^{\text{int}} = 0^\circ$ in Fig. 41(a), the avalanche motion proceeds directly down the skyrmion density gradient along the $+x$ direction. As $\theta_{\text{SKH}}^{\text{int}}$ increases, the motion curves increasingly into the $+y$ direction, as shown in Figs. 41(b)–41(d); however, the angle of the avalanche motion is always much smaller than $\theta_{\text{SKH}}^{\text{int}}$.

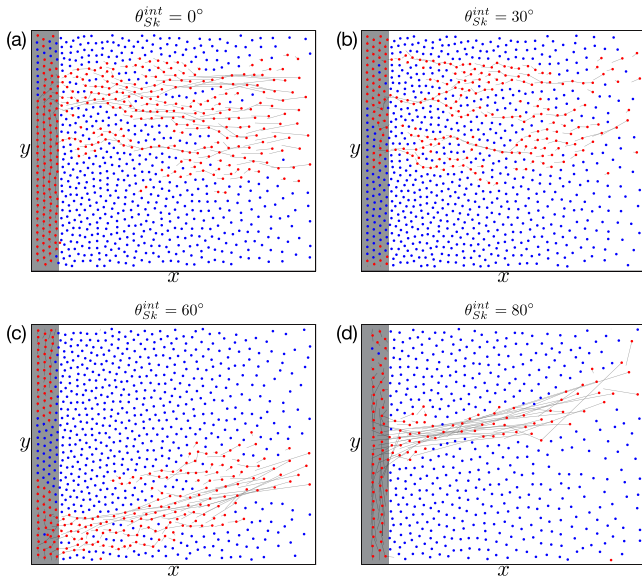


FIG. 41. Images from particle-based simulations of skyrmion avalanches where skyrmions are added slowly to the pin-free region (left gray regions) and move into the pinned region (right white areas) under their own gradient-induced repulsion. In each avalanche event, light red dots indicate skyrmions that translated a distance greater than a pinning site radius, dark blue dots are stationary skyrmions, and lines show the skyrmion trajectories. Here (a) $\theta_{\text{SkH}}^{\text{int}} = 0^\circ$, (b) 30° , (c) 60° , and (d) 80° . The avalanche motion curves increasingly into the $+y$ direction as the magnitude of the Magnus term increases. From [Díaz *et al.*, 2018](#).

Experimental studies of avalanches or cascades in stripe and skyrmion phases that focused on jumps or changes in the pairwise correlation functions have provided evidence for power law distributions of jump sizes in the skyrmion regime, as well as different avalanche exponents in the skyrmion and stripe phases ([Singh *et al.*, 2019](#)).

D. Continuum-based simulations of the dynamic phase diagram

A variety of continuum- and lattice-based simulation studies have explored the dynamical ordering of driven skyrmions in the presence of quenched disorder. [Koshibae and Nagaosa \(2018\)](#) used a 2D continuum model for skyrmions interacting with random point pinning to construct a driving force versus disorder strength phase diagram. They initialized the system in a skyrmion lattice at a drive of $j = 0$. When a finite drive is applied, the skyrmions move plastically and disorder, while for higher drives a transition to a moving skyrmion lattice occurs. A phase diagram as a function of j versus impurity strength K_{imp} appears in [Figs. 42\(a\) and 42\(b\)](#) for magnetic field strengths of $h = 0.025$ and 0.04 . At $h = 0.025$, the pinned phase grows in extent with increasing impurity strength, and there are large regions of moving skyrmion glass or disordered moving phases. For $K_{\text{imp}} < 0.1$, the moving skyrmion glass orders into a moving crystal. The first of two new phases that appear is a multiplication phase in which skyrmions are dynamically created by the combination of current and pinning. The second is a segregated or clustered state. For $h = 0.04$, the multiplying phase is replaced by a

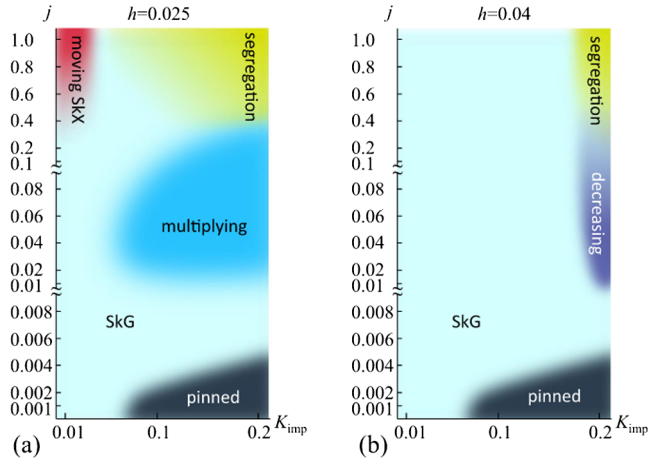


FIG. 42. Dynamic phase diagrams as a function of applied current j vs impurity strength K_{imp} from continuum simulations. The applied magnetic field is (a) $h = 0.025$ and (b) 0.04 . The dynamic phases include the skyrmion glass (SkG) and moving skyrmion crystal (SKX) states. From [Koshibae and Nagaosa, 2018](#).

decreasing phase in which skyrmions are annihilated. The segregated phase was argued to result from the modification of skyrmion-skyrmion interactions by the emission of spin excitations, which produce an effective attractive interaction between the skyrmions. In subsequent 2D particle-based simulations of skyrmions moving over strong disorder, a segregated phase was also observed that was argued to be due to a Magnus-force-induced effective attraction between skyrmions that are moving at different skyrmion Hall angles ([Reichhardt and Reichhardt, 2019a](#)).

The different phases in [Fig. 42](#) could be detected using imaging and neutron scattering techniques. They could also be identified in principle by analyzing the noise fluctuations since, as previously shown, a change in the noise power occurs across the transition from the moving glass to the moving lattice state. The multiplying, decreasing, and segregated phases shown in [Fig. 42](#) could each have their own distinct noise signatures or changes in the THE.

E. Three-dimensional skyrmion dynamics

Although stiff 3D skyrmions can be treated with 2D models, a fully 3D system can have numerous new effects, such as skyrmion line wandering, skyrmion breaking, and skyrmion cutting or entanglement. In 3D driven superconducting vortex systems with random disorder, a variety of phases distinct from those found in 2D systems arise depending on the material anisotropy and the pinning strength ([Olson *et al.*, 2000](#); [Chen and Hu, 2003](#); [Zhao *et al.*, 2016](#); [Reichhardt and Reichhardt, 2017a](#)). In particular, the 3D vortex system often shows signatures of dynamical first order phase transitions ([Olson *et al.*, 2000](#); [Chen and Hu, 2003](#); [Reichhardt and Reichhardt, 2017a](#)) in the form of sharp jumps and hysteresis in the velocity-force curves. Similar effects could occur in skyrmion systems. Driven 3D skyrmions moving over quenched disorder could also exhibit unusual behavior such as the proliferation of monopoles in driven phases when

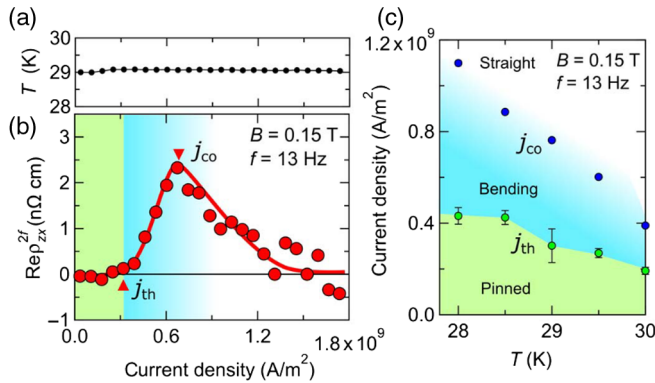


FIG. 43. Results from Hall measurements of 3D skyrmions in MnSi thin-plate samples. (a) Sample temperature T and (b) the real part of the second-harmonic Hall resistivity $\text{Re} \rho_{zx}^{2f}$ vs the driving current density measured at a frequency of $f = 13$ Hz. (c) Dynamic phase diagram as a function of the current density vs the temperature T showing regions where the skyrmions are pinned (left green band), bending (center blue area), and straight (right white region). From Yokouchi *et al.*, 2018.

the skyrmions break or cut (Milde *et al.*, 2013; Schütte and Rosch, 2014; Lin and Saxena, 2016; Zhang, Mishchenko *et al.*, 2016).

In transport experiments, Yokouchi *et al.* (2018) examined the current-induced skyrmion motion in MnSi and found strong nonlinear signatures above the threshold current. These effects are reduced at higher drives. Figure 43(b) shows the real part of the second-harmonic Hall resistivity $\text{Re} \rho_{zx}^{2f}$ versus the current density at a fixed magnetic field. It was argued that the peak in $\text{Re} \rho_{zx}^{2f}$ arises from the bending of the skyrmion strings just above the depinning threshold. Such bending occurs in an asymmetric manner due to the creation of a nonequilibrium or nonlinear Hall response by the DMI. At higher drives, the skyrmions become straighter and the effect is reduced. The features in $\text{Re} \rho_{zx}^{2f}$ can be used to construct the dynamical phase diagram shown in Fig. 43(c). A pinned phase appears below the threshold current j_{th} , while the bent to straight skyrmion string transition is labeled j_{co} . As the temperature increases j_{th} decreases since thermal activation makes it easier for the skyrmions to jump out of the pinning sites. There is also some experimental evidence for the unwinding of skyrmion strings in 3D systems under repeated drive pulses (Kagawa *et al.*, 2017). Pinning could play a role in this process since a partially unwound string can become trapped by the disorder during the intervals between driving pulses.

Koshibae and Nagaosa (2019) numerically studied a skyrmion string driven through random disorder in a 3D system for varying sample thicknesses and identified a pinned regime, a moving skyrmion regime, and regions of skyrmion string annihilation. They found that current-induced skyrmion annihilation occurs at a finite current for thin and thick samples, but not for samples of intermediate thicknesses, indicating that there is an optimal sample length for skyrmion stability. Figure 44 shows a dynamic phase diagram for the skyrmion string as a function of the sample thickness L_z versus the applied current. The extent of the pinned regime decreases

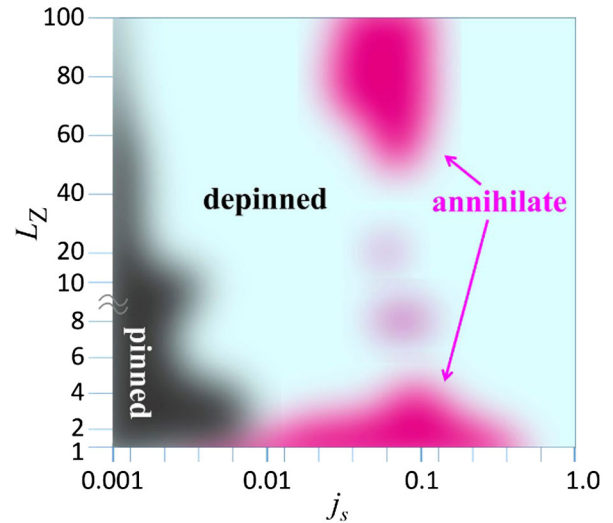


FIG. 44. Dynamic phase diagram from numerical simulations of skyrmion strings as a function of L_z , the thickness of the 3D system, vs j_s , the applied current density. From Koshibae and Nagaosa, 2019.

with increasing L_z , indicating that it is more difficult to pin long 3D skyrmion strings than 2D skyrmions. This is in agreement with experimental observations in which the depinning threshold is low in bulk samples (Schulz *et al.*, 2012) but high in thin films (Woo *et al.*, 2016). Such behavior could be due to the fact that bulk samples are single crystal structures, whereas thin films produced by sputtering are amorphous. In the regime where skyrmion annihilation does not occur, the skyrmions show pronounced roughening at low currents but become straighter at higher drives, similar to the dynamic ordering transition observed in 2D driven skyrmion assemblies with disorder (Koshibae and Nagaosa, 2018).

F. Further directions for dynamic skyrmion phases with random disorder

There are many future directions for studying the collective dynamics of skyrmions with random disorder, including noise analysis, imaging, neutron scattering, and other experimental probes. Of highest priority is developing a method using THE or another signal to obtain clear transport measures on size scales and timescales beyond those of imaging measurements in order to detect depinning, elastic or plastic flow, and drive-induced transitions such as dynamical reordering and skyrmion annihilation or creation, similar to the way in which dynamic phase boundaries are deduced from superconducting vortex transport measurements. The relaxation time of a skyrmion system subjected to a driving pulse is also of interest. For example, skyrmions under a small ac drive perform spiraling motion, and a crossover in the response or dc depinning threshold could occur when the spiral radius matches the effective dimension of the pinning or disorder sites in the sample. For antiferromagnetic skyrmions, Jin *et al.* (2020) found numerical evidence that an ac drive substantially lowers the dc threshold.

Boundaries such as sample edges can be associated with nonuniform edge currents or the injection or annihilation of

skyrmions. These effects are minimized in a Corbino geometry, where skyrmions circulate around the sample rather than entering from the edges. For superconducting vortices, the Corbino geometry successfully eliminated edge contamination of the dynamics. Skyrmions subjected to ac driving should also experience reduced sample edge effects. For example, if there is a transient time associated with a skyrmion that has a velocity-dependent skyrmion Hall angle, time asymmetry from the ac driving would cause the skyrmion to move away from the sample edge periodically while still undergoing a net translation in the driving direction. Measurements of the ac susceptibility could detect dynamical responses associated with specific frequencies, such as a pinning frequency from trapped skyrmions that oscillate within a pinning site, or a characteristic washboard frequency excited when the skyrmions flow elastically. Distinct types of skyrmion avalanche behavior should also be observable. For example, under an applied magnetic field of changing direction, the reorientation of 3D skyrmion lines to follow the field could occur in a series of jumps, and not smoothly if pinning is present. When temperature is relevant, thermally activated avalanches could appear for a finite drive below the depinning threshold. If a global current is applied simultaneously with local excitations such as local heating or a local probe, large-scale rearrangements of the skyrmions could be induced by the local perturbation.

Beyond 2D and 3D linelike skyrmions, unique dynamics should appear for 3D skyrmion hedgehog lattices (Lin and Batista, 2018; Fujishiro *et al.*, 2019), which could provide one of the first realizations of the depinning of a 3D particlelike lattice. In such a system, a transformer geometry in a uniform field could be created using inhomogeneous pinning that is present at the top but absent at the bottom of the sample. Under a finite temperature near the skyrmion melting transition, a divergence could occur in the amplitude of the drive required to dynamically order the skyrmion lattice, similar to what is found in superconducting vortex systems (Koshelev and Vinokur, 1994). Both 3D skyrmion lines and point skyrmions could exhibit a peak effect (Bhattacharya and Higgins, 1993; Cha and Fertig, 1998; Banerjee *et al.*, 2000; Toft-Petersen *et al.*, 2018) in which the depinning current strongly increases when the skyrmions transition from 3D lines to broken lines or from a 3D point particle lattice to a 3D glass. A peak effect as a function of drive could be associated with reentrant pinning, where the skyrmions form mobile straight lines at low drives but break apart or disorder at higher drives and become pinned again.

Metastability and memory effects associated with dynamical phases commonly appear in other systems that exhibit depinning (Henderson *et al.*, 1996; Xiao, Andrei, and Higgins, 1999; Paltiel *et al.*, 2000) and can produce hysteresis in the velocity-force curves or persistent memory between driving pulses that generates an increasing or decreasing response depending on the pulse duration. Memory effects could be observed by initializing skyrmions in a metastable ordered or disordered state, applying a series of drive pulses, and determining whether a gradual transition to a stable state occurs, similar to what has been observed for metastable states in type-II superconducting vortices (Paltiel *et al.*, 2000; Olson *et al.*, 2003; Pasquini *et al.*, 2008). The presence of pinning

can trap the skyrmions in a metastable phase, while application of a current that is large enough to destabilize the metastable state gives the skyrmions access to the dynamics that permit them to reach a stable low energy state.

VII. PINNING AND THE SKYRMION HALL ANGLE

A skyrmion under an applied drive moves at an angle called the skyrmion Hall angle (θ_{SKH}) with respect to the drive. This angle is proportional to the Magnus force, and in the absence of pinning it is independent of the driving force magnitude (Zang *et al.*, 2011; Nagaosa and Tokura, 2013) but is affected by the manner in which the skyrmion is driven. For example, under combined adiabatic and nonadiabatic spin-transfer torques, the skyrmion moves in the direction of driving when the nonadiabatic torque is equal to the damping (Zhang, Xia, Zhou *et al.*, 2017). Skyrmions in antiferromagnetic materials (Barker and Tretiakov, 2016; Zhang, Zhou, and Ezawa, 2016a) and in compensated synthetic antiferromagnetic structures (Zhang, Zhou, and Ezawa, 2016b; Zhang, Ezawa, and Zhou, 2016) also do not exhibit a skyrmion Hall effect. In frustrated spin systems, the skyrmions can move in circular trajectories, generating a time-dependent skyrmion Hall angle (Lin and Hayami, 2016; Zhang, Xia, Zhou *et al.*, 2017).

Particle-based simulations for skyrmions moving over random and periodic pinning showed that θ_{SKH} is not constant but is nearly zero at depinning and increases with increasing drive before saturating close to the intrinsic or pin-free value $\theta_{\text{SKH}}^{\text{int}}$ at higher drives (Reichhardt, Ray, and Reichhardt, 2015a, 2015b; Reichhardt and Reichhardt, 2016; Díaz *et al.*, 2017). The average velocity in the directions parallel ($|V_{\parallel}|$) and perpendicular ($|V_{\perp}|$) to the drive versus the driving force F_D for a collection of skyrmions driven over random pinning with values of α_m and α_d that give $\theta_{\text{SKH}}^{\text{int}} = 80.06^\circ$ appears in Fig. 45(a) (Reichhardt and Reichhardt, 2016). The corresponding ratio $R = |V_{\perp}|/|V_{\parallel}|$ along with $\theta_{\text{SKH}} = \tan^{-1}(R)$ are shown in Fig. 45(b), where the dashed lines are the expected values of each quantity in the pin-free limit. The inset of Fig. 45(a) indicates that there is a finite depinning threshold as well as a range of drives for which $|V_{\parallel}| > |V_{\perp}|$; however, as the drive increases $|V_{\perp}|$ grows more rapidly than $|V_{\parallel}|$ since $\theta_{\text{SKH}}^{\text{int}}$ in the clean limit would give $R^{\text{int}} = |V_{\perp}|/|V_{\parallel}| \approx 6$. Figure 45(b) shows that over a wide range of drives R increases roughly linearly with F_D up to $F_D = 0.75$, then saturates close to R^{int} . The skyrmions move in the driving direction for small drives, gradually develop a greater perpendicular motion as the drive increases, and move along $\theta_{\text{SKH}}^{\text{int}}$ at large drives. In the regime where $R \propto F_D$, the skyrmions are moving plastically, while, at higher drives when the skyrmions begin to move in a more coherent fashion, R starts to saturate. These behaviors are robust over a range of $\theta_{\text{SKH}}^{\text{int}}$, disorder strength, and pinning densities, while when the Magnus force is zero, $|V_{\perp}| = 0$ and $\theta_{\text{SKH}} = 0$ for all F_D (Reichhardt and Reichhardt, 2016). For $\theta_{\text{SKH}}^{\text{int}} < 50^\circ$, the skyrmion Hall angle generally increases linearly with F_D since $\tan^{-1}(x)$ can be expanded as $\tan^{-1}(x) = x - x^3/3 + x^5/5 \dots$. For small R the first term dominates, while for $\theta_{\text{SKH}}^{\text{int}} > 50^\circ$, nonlinear effects appear in θ_{SKH} with increasing F_D .

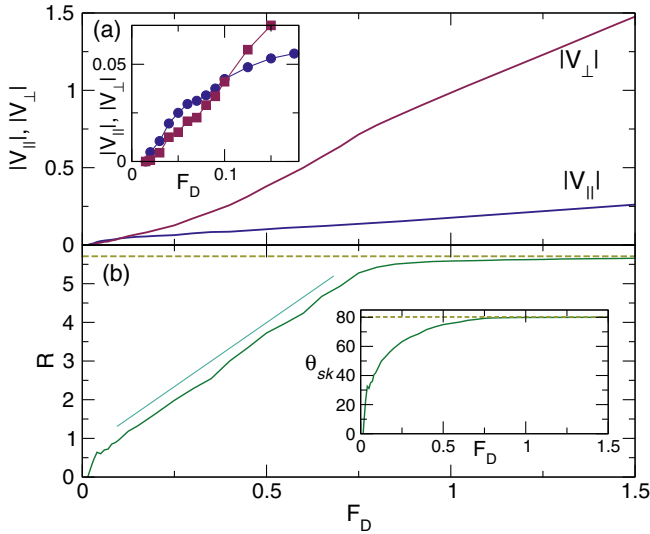


FIG. 45. Particle-based simulation measurements of the behavior of the skyrmion Hall angle θ_{sk} for skyrmions driven over random disorder. (a) Skyrmion velocities in the directions parallel ($|V_{\parallel}|$, lower blue line) and perpendicular ($|V_{\perp}|$, upper red line) to the driving force vs F_D . Inset: enlargement of the main panel in the region just above depinning where there is a crossing of the velocity-force curves. (b) Corresponding $R = |V_{\perp}|/|V_{\parallel}|$ vs F_D . The solid straight line is a linear fit and the dashed line is the clean limit value of $R \approx 6.0$. Inset: $\theta_{sk} = \tan^{-1}(R)$ vs F_D . The dashed line is the clean limit value of θ_{sk} . From Reichhardt and Reichhardt, 2016.

A drive-dependent θ_{skH} was partially observed in continuum and Thiele equation work by Müller and Rosch (2015) for a single skyrmion interacting with a single defect. A more extensive study of the evolution of θ_{skH} with drive was subsequently conducted using particle-based simulations of skyrmion motion through periodic (Reichhardt, Ray, and Reichhardt, 2015b) and random (Reichhardt, Ray, and Reichhardt, 2015a) pinning. Both Müller and Rosch (2015) and Reichhardt, Ray, and Reichhardt (2015a) argued that the microscopic origin of the drive dependence of θ_{skH} is a side jump effect (illustrated in Fig. 46). Upon moving through the pinning site, the skyrmion executes a Magnus-induced orbit that causes it to jump in the direction of the applied drive. Repeated jumps lower the effective skyrmion Hall angle compared to θ_{skH}^{int} . The skyrmion motion resembles that of a charged particle in a magnetic field (Nagaosa and Tokura, 2013), and the skewed scattering of the skyrmion by a pinning site is similar to what is known as a side jump effect for electron scattering off magnetic defects, where an electron undergoes a sideways displacement when interacting with a potential as a result of spin-orbit interactions (Berger, 1970). As illustrated in Fig. 46(a), a more slowly moving skyrmion spends more time in the pinning site, resulting in a larger jump. At higher drives, when the skyrmion is moving faster, the jump is smaller and θ_{skH} is closer to the defect-free value, while at the highest drives, the skyrmions move so rapidly through the pinning sites that there is hardly any jump. This is illustrated in Fig. 46(b), which corresponds to the saturation of θ_{skH} at higher drives as observed in simulation (Reichhardt,

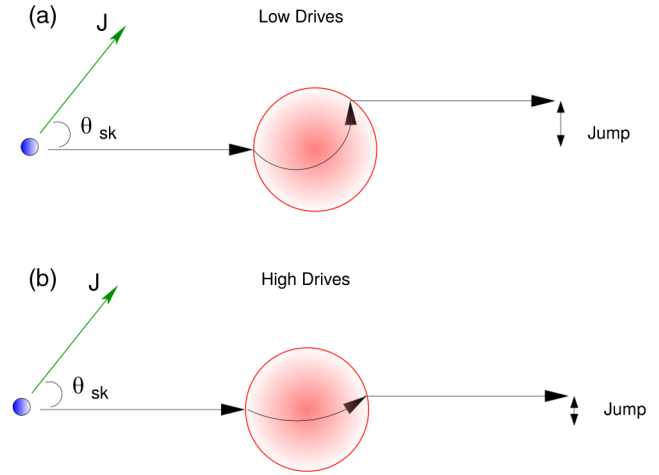


FIG. 46. Schematic illustration of how pinning changes the effective skyrmion Hall angle. The left blue dot is the skyrmion and the right red circle is the pinning site, while J is the direction of the applied current and θ_{sk} is the intrinsic skyrmion Hall angle. (a) At low drives, the skyrmion executes a Magnus-induced orbital motion as it traverses the pinning site, leading to a side jump in the direction of the current that reduces the effective skyrmion Hall angle. (b) At higher drives, the skyrmion moves rapidly through the pinning site and the magnitude of the side jump is strongly reduced.

Ray, and Reichhardt, 2015a, 2015b; Reichhardt and Reichhardt, 2016; Díaz *et al.*, 2017). The jump varies depending on whether the skyrmion approaches the top or the bottom of the pinning site, so strongly asymmetric jumps appear for an ensemble of different impact parameters (Reichhardt, Ray, and Reichhardt, 2015b). Reichhardt, Ray, and Reichhardt showed that for zero Magnus force the pinning site still produces a jump, but the jump is symmetric as a function of impact parameter, so no net jump appears in the ensemble average.

In multiscale simulations, Fernandes, Chico, and Lounis (2020) examined deflections of skyrmions interacting with single-atom defects consisting of a Pd layer deposited on an Fe/Ir(111) surface. The trajectories in Fig. 47(a) indicate that at low driving currents skyrmions become trapped at the defect, while at higher currents in Fig. 47(b) the skyrmions escape from the defect but experience a trajectory deflection that decreases as the skyrmion velocity increases. An attractive disorder site deflects the skyrmions in the opposite direction. Fernandes, Chico, and Lounis also showed that the Thiele equation approach is a reasonable approximation for capturing the skyrmion dynamics.

Jiang *et al.* (2017) experimentally imaged current-driven skyrmions to obtain the drive dependence of θ_{skH} . The skyrmion motion produced no THE signature but was instead deduced from the images. Figure 48 shows four dynamical regimes: a low drive pinned state, a $\theta_{skH} = 0^\circ$ state with finite skyrmion velocity, a region where θ_{skH} increases linearly with drive, and a high drive regime in which θ_{skH} saturates to the clean limit of $\theta_{skH}^{int} = 30^\circ$. This is similar to the trend observed in particle-based simulations (Reichhardt, Ray, and Reichhardt, 2015a, 2015b; Reichhardt and Reichhardt, 2016). It would be interesting to identify a system in which a

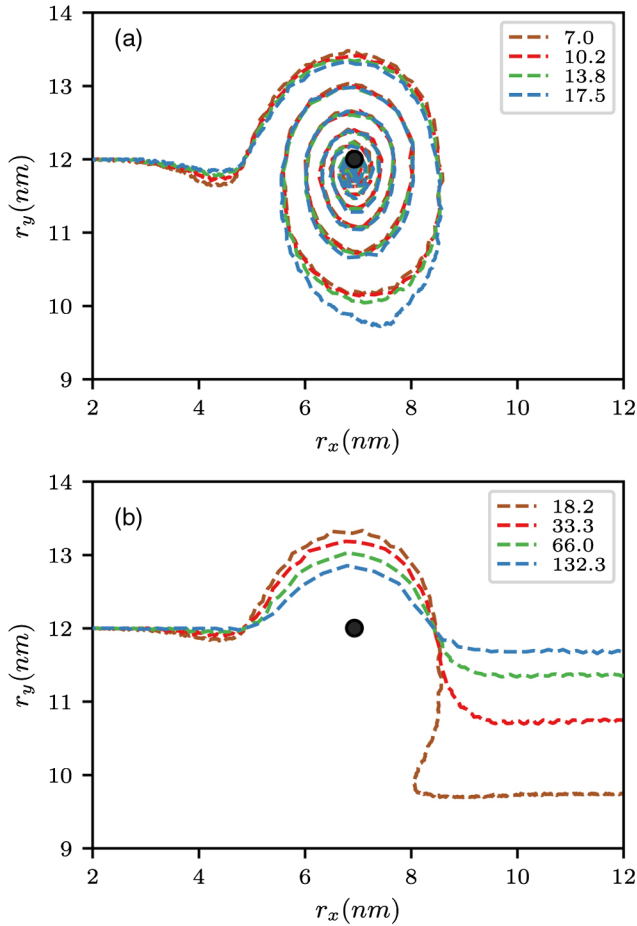


FIG. 47. Multiscale simulations of the trajectories of skyrmions scattering from a defect site (black dot) consisting of a single atom. (a) Skyrmions are pinned at low currents. (b) For higher currents, the skyrmions escape but the trajectories are deflected by an amount that decreases with increasing current. From Fernandes, Chico, and Lounis, 2020.

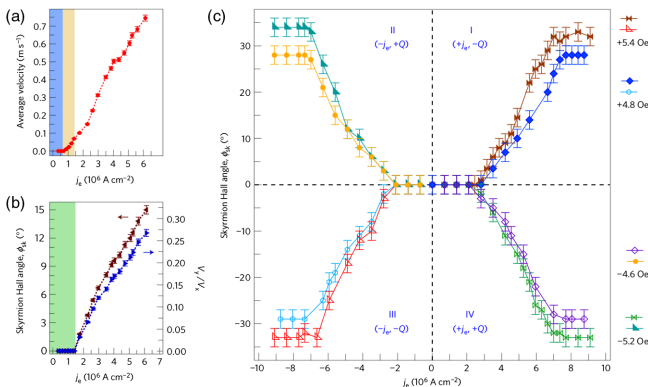


FIG. 48. Skyrmion velocity and skyrmion Hall angle obtained from direct imaging of the skyrmion motion. (a) Average skyrmion velocity vs current density j_e showing a pinned regime (left blue band) and a $\theta_{\text{SkH}} = 0^\circ$ region (center orange band). (b) The corresponding θ_{SkH} vs j_e . (c) θ_{SkH} for positive and negative driving currents j_e under positive and negative applied magnetic fields. In each case, θ_{SkH} saturates for sufficiently large magnitudes of j_e . From Jiang *et al.*, 2017.

directly measured θ_{SkH} could be compared to a changing THE since both the skyrmion velocity and the direction of motion need to be considered when the magnitude of the THE is measured as a function of drive.

Litzius *et al.* (2017) studied skyrmions under forward and backward pulsed drives of varied amplitude and used imaging to construct the θ_{SkH} versus the current curve shown in Fig. 49. The initially small θ_{SkH} increases with increasing drive and reaches a value close to $\theta_{\text{SkH}} = 40^\circ$. Imaging experiments and micromagnetic simulations of skyrmion motion in ferrimagnetic systems (Woo *et al.*, 2018) show a similar increase in θ_{SkH} with drive. Litzius *et al.* (2017) argued that the change of θ_{SkH} is produced by changes in the skyrmion shape or size under an applied current, rather than the side jump effect observed in the particle-based models. Using micromagnetic simulations, Tomasello *et al.* (2018) found that breathing modes of moving skyrmions excited by a current could modify θ_{SkH} as a function of drive in the absence of pinning. Litzius *et al.* (2020) recently provided evidence for a high current pinning-dominated regime as well as another regime in which excitations change θ_{SkH} , so the scaling is not constant as a function of drive. Current-driven studies of thin-film skyrmions in the 100 nm size range at speeds of up to 100 m/s reveal a strong dependence of θ_{SkH} on drive, with an increase to a high velocity saturation value of $\theta_{\text{SkH}} = 55^\circ$ (Juge *et al.*, 2019). Both the experimental observations and the continuum modeling show that θ_{SkH} is constant in the absence of quenched disorder, and that the addition of pinning produces a finite depinning threshold and an increase of θ_{SkH} up to a saturation value. Although the work of Litzius *et al.* (2020) showed that the current produced strong skyrmion shape changes in the absence of disorder, the authors argued that the changes in θ_{SkH} were due to the pinning rather than the shape fluctuations.

Within the particle-based model, $\theta_{\text{SkH}}^{\text{int}}$ is controlled by the values of α_d and α_m according to $\theta_{\text{SkH}}^{\text{int}} = \tan^{-1}(\alpha_m/\alpha_d)$ and is not influenced by the skyrmion size. When simulation values of α_d and α_m are selected to match experimentally measured values of θ_{SkH} , it can be argued that changing the α_m -to- α_d ratio is related to changing the skyrmion size. In other work, varied $\theta_{\text{SkH}}^{\text{int}}$ in a particle-based model produced a robust velocity dependence of θ_{SkH} , and some of the simulated skyrmion Hall angles were within the range measured by experiments (Reichhardt and Reichhardt, 2016).

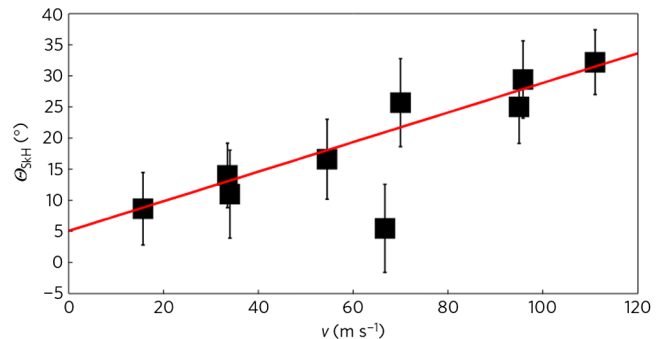


FIG. 49. Image-based experimental measurements of θ_{SkH} vs skyrmion velocity v showing a linear dependence. From Litzius *et al.*, 2017.

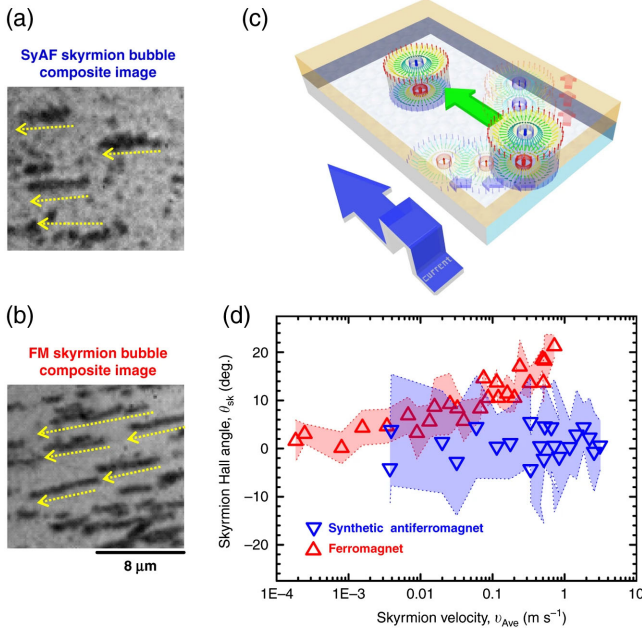


FIG. 50. Composite magneto-optical polar Kerr effect images showing the current-induced motion (yellow arrows) of (a) synthetic antiferromagnetic skyrmion bubbles and (b) ferromagnetic skyrmion bubbles under a pulsed current. (c) Schematic of the experiment in which each bubble moves during the current pulse. (d) Skyrmion Hall angle as a function of skyrmion velocity in the two systems indicating that the skyrmion Hall angle in the ferromagnet is more sensitive to skyrmion velocity than that of the synthetic antiferromagnet. From [Dohi et al., 2019](#).

[X. Z. Yu et al. \(2020\)](#) investigated the motion of individual and small clusters of 80 nm skyrmions in FeGe systems with low currents of 0.96×10^9 to 1.92×10^9 A m⁻² and found that a skyrmion cluster can undergo rotation as it translates. This suggests that the Magnus force can induce unusual dynamics in clusters of moving skyrmions. [S. Zhang et al. \(2020\)](#) imaged the motion of half skyrmions, which have θ_{SKH} that is half as large as that of a full skyrmion. [Hirata et al. \(2019\)](#) analyzed the elongation of pinned ferrimagnetic bubbles or half skyrmion propagation and found that θ_{SKH} vanishes at the momentum compensation temperature. Other experiments found that shape distortions of half skyrmions could further reduce θ_{SKH} ([Yang et al., 2021](#)).

Antiferromagnetic and synthetic antiferromagnetic skyrmion systems are of interest since θ_{SKH} is small or zero in such materials. [Dohi et al. \(2019\)](#) examined the formation and current-driven motion of skyrmion bubbles in synthetic antiferromagnets. Using magneto-optical polar Kerr effect imaging in the geometry illustrated in Fig. 50(c), they compared the pulsed drive motion of elongated skyrmions or a half skyrmion in a synthetic antiferromagnet and in a ferromagnet, as shown in Figs. 50(a) and 50(b). Figure 50(d) indicates that θ_{SKH} for the ferromagnet increases with increasing skyrmion velocity from 0° up to 20°, while in the synthetic antiferromagnet θ_{SKH} remains close to zero as the skyrmion velocity increases.

Most experiments performed thus far have been in the single or few skyrmion limit, so it would be interesting to

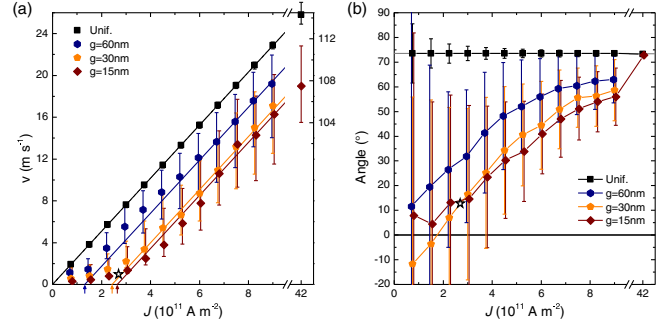


FIG. 51. Continuum simulations of skyrmion motion through a disordered landscape composed of grains of different sizes g . (a) Mean skyrmion velocity v vs the driving current J showing a finite depinning threshold. (b) Skyrmion Hall angle vs J showing that the angle increases with an increasing J from a value near zero at zero current. From [Legrand et al., 2017](#).

understand what happens in the collective or lattice limit. Beyond side jump effects, it may be possible that the pinning effectively increases the skyrmion damping through some other mechanism. Since $\theta_{\text{SKH}} \propto \tan^{-1}(\alpha_m/\alpha_d)$, if α_d is itself drive dependent, this could produce a drive dependence of θ_{SKH} .

Several continuum-based simulations have shown a drive dependence of θ_{SKH} as a function of pinning ([Kim and Yoo, 2017](#); [Legrand et al., 2017](#); [Juge et al., 2019](#)). [Legrand et al. \(2017\)](#) considered pinning produced by grain boundaries, where small dense grains corresponded to strong pinning. In this study, a clean system has no depinning threshold and θ_{SKH} is constant, while when pinning is present there is a finite depinning threshold and θ_{SKH} increases from an initially small level to a saturation value, as shown in Fig. 51. Since there is an optimal grain size for pinning, the relative size of the skyrmions and the pinning sites is important, which merits further study. Optimal pinning could be due to a resonance or commensuration effect arising when the pinning and skyrmion sizes match. Owing to the limited number of skyrmions simulated, the θ_{SKH} versus drive curves contain considerable scattering, and there could be multiple regimes for θ_{SKH} rather than only a linearly increasing regime and a saturation regime, which offers another avenue for future study. Numerical work by [Juge et al. \(2019\)](#) produced results similar to those of [Legrand et al. \(2017\)](#), but the scattering in the data was much smaller. In these works, the skyrmion trajectories in regimes with an increasing θ_{SKH} show coexisting pinned and moving skyrmions, similar to what is observed in particle-based simulations ([Reichhardt and Reichhardt, 2016](#)). Similar dynamics appeared in the imaging experiments of [Montoya et al. \(2018\)](#). In the continuum simulations, the skyrmions at higher drives moved in fairly straight trajectories along a direction close to $\theta_{\text{SKH}}^{\text{int}}$ ([Legrand et al., 2017](#)). [Kim and Yoo \(2017\)](#) performed continuum simulations that showed a similar drive dependence of $\theta_{\text{SKH}}^{\text{int}}$.

Another question is the role of the skyrmion diameter in determining θ_{SKH} . [Zeissler et al. \(2020\)](#) examined skyrmions in a magnetic multilayer under a pulsed drive and found $\theta_{\text{SKH}} \approx 10^\circ$ regardless of the skyrmion diameter. In the skyrmion trajectory images of Fig. 52, the skyrmion diameter

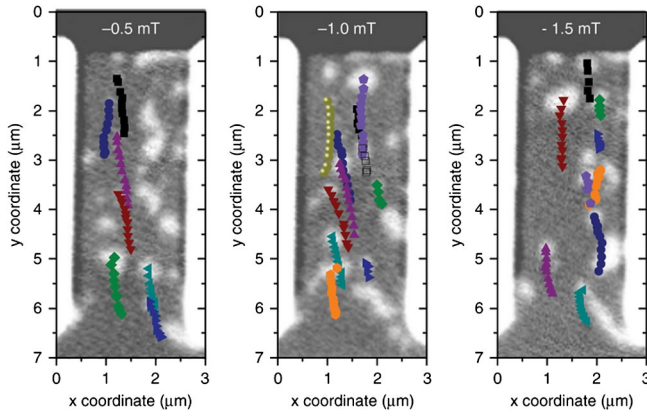


FIG. 52. Images of skyrmion motion in a multilayer system at varied magnetic fields. In each case, $\theta_{\text{SKH}} = 10^\circ$. The skyrmion size changes as the field varies, so this result indicates that θ_{SKH} is independent of the skyrmion diameter. From Zeissler *et al.*, 2020.

increases with an increasing magnetic field magnitude but the direction of motion does not change. They also revealed that the skyrmion trajectories are deflected by disorder sites. The disorder length scale or pinning radius might be much larger than the skyrmion diameters, or collective interactions between skyrmions could increase the effective pinning radius, placing the system in a pinning-dominated regime (Zeissler *et al.*, 2020). It would be interesting to perform a separate study of θ_{SKH} for varied disorder sizes to see whether a change occurs when the effective pinning diameter becomes smaller rather than larger than the skyrmion size.

Studies of skyrmions moving in samples with magnetic grain boundaries have shown that in some cases disorder can enhance θ_{SKH} (Salimath *et al.*, 2019). A guidance effect in the direction of $\theta_{\text{SKH}}^{\text{int}}$ occurs when the grains are magnetically aligned in the direction in which the skyrmions would move in the absence of disorder. This effect depends on the magnitude of the drive and the orientation of the grains, but it suggests that θ_{SKH} could be controlled through the proper orientation of extended defects.

The drive dependence of θ_{SKH} can generate a wealth of new dynamical effects distinct from those found in previously studied overdamped systems. For example, θ_{SKH} for a skyrmion driven over a periodic pinning array increases with drive but becomes quantized due to locking with substrate symmetry directions (Reichhardt, Ray, and Reichhardt, 2015b). To date the modification of θ_{SKH} by pinning has been considered only for ferromagnetic skyrmions, but studies of antiferromagnetic skyrmions, polar skyrmions, skyrmioniums, antiskyrmions, and merons would reveal whether the effect of pinning differs depending on the nature of the skyrmion.

Antiferromagnetic skyrmions with $\theta_{\text{SKH}} = 0^\circ$ are of particular interest and in principle have dynamics similar to those of superconducting vortices. The lack of a Magnus force could produce stronger pinning effects than with ferromagnetic skyrmions. For example, numerical work by Liang *et al.* (2019) indicated that pinning is enhanced for ferromagnetic skyrmions. Other methods of controlling θ_{SKH} include the use of internal modes (Tomasello *et al.*, 2018; Chen *et al.*, 2019)

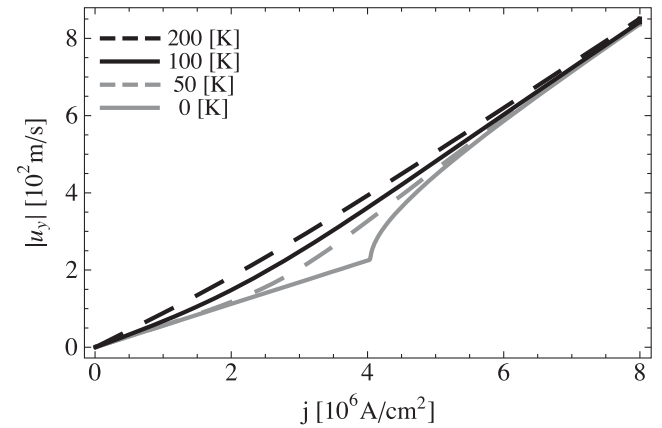
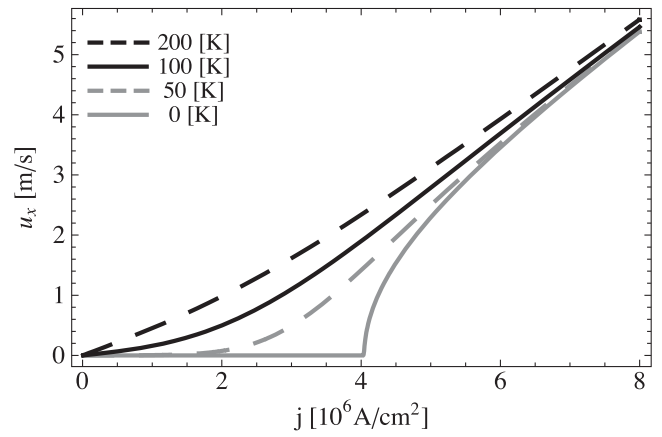


FIG. 53. Theoretical predictions for skyrmion velocity response at different temperatures, showing a creep regime below the zero-temperature depinning threshold. Top panel: longitudinal velocity u_x vs driving current j . Bottom panel: transverse velocity u_y vs j . From Troncoso and Núñez, 2014.

that can change and even vanish at the angular momentum compensation temperature (Woo *et al.*, 2018; Hirata *et al.*, 2019), the application of particular gate voltage configurations (Plettenberg, Stier, and Thorwart, 2020), or changing the skyrmion number in a multilayer system where the skyrmion number can depend on the number of layers (Zhang, Ezawa, and Zhou, 2016; Xia *et al.*, 2021). The role of pinning in such scenarios remains open for further investigation.

A. Thermal effects

Most experimental observations of the skyrmion Hall effect are performed at room temperature, and there are numerous indications that skyrmions exhibit thermal effects such as Brownian motion (Nozaki *et al.*, 2019; Zázvorka *et al.*, 2019; Zhao *et al.*, 2020) that could induce creep or thermally activated hopping between pinning sites. To address the question of how the depinning threshold and θ_{SKH} behave under the combination of pinning and temperature, Troncoso and Núñez (2014) theoretically studied thermally assisted current-driven skyrmion motion in the presence of pinning and found that the Brownian motion could be described by a stochastic Thiele equation. They observed a finite depinning threshold at zero temperature as well as a creep regime for increasing drive, as shown in Fig. 53. Reichhardt and

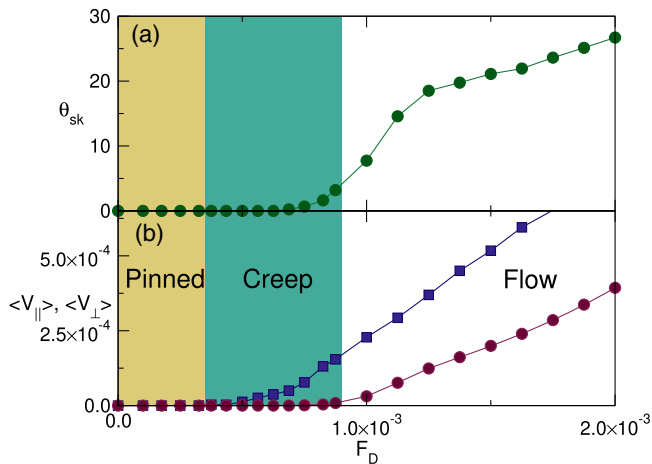


FIG. 54. Particle-based simulations of skyrmion motion with finite thermal fluctuations. (a) Skyrmion Hall angle θ_{sk} vs the driving force F_D . (b) Corresponding skyrmion velocity parallel $\langle V_{\parallel} \rangle$ (blue squares) and perpendicular $\langle V_{\perp} \rangle$ (red circles) to the drive vs F_D . There is a pinned phase (left yellow band), a creep phase with $\theta_{\text{sk}} \approx 0^\circ$ (center green band), and a flowing phase. From Reichhardt and Reichhardt, 2019b.

Reichhardt (2019b) studied the elastic depinning of skyrmions with random disorder and thermal fluctuations. The depinning threshold is well defined at $T = 0$ but decreases and becomes more rounded as T increases. Figure 54(a) illustrates θ_{SKH} versus drive for a finite temperature system with appreciable creep, and Fig. 54(b) shows $\langle V_{\parallel} \rangle$ and $\langle V_{\perp} \rangle$ versus F_D . There is a pinned phase with $\langle V_{\parallel} \rangle = \langle V_{\perp} \rangle = 0$, an intermittent creep or thermally activated avalanche phase with finite $\langle V_{\parallel} \rangle$, $\langle V_{\perp} \rangle = 0$, and $\theta_{\text{SKH}} = 0^\circ$, and a high drive continuously moving phase with finite velocity in both directions. In the last region, θ_{SKH} increases with drive and saturates at the high drive limit. The appearance of a regime with finite longitudinal velocity but zero perpendicular velocity is consistent with the observations of Jiang *et al.* (2017) just above depinning. Using resonant ultrasound spectroscopy in MnSi, Luo *et al.* (2020) found evidence that thermal fluctuations reduce the critical current to 4% of its nonthermal value, which is in agreement with the Anderson-Kim theory for flux creep in superconductors (Anderson and Kim, 1964).

There could be multiple regimes for the evolution of θ_{SKH} with current and velocity. Litzius *et al.* (2020) studied the impact of thermal fluctuations on θ_{SKH} in both experiment and simulations and found distinct behaviors in the low and high current regimes. The increase of θ_{SKH} with current is rapid for lower currents but crosses over to a slower increase at higher currents. It was argued that at low drives the skyrmion behaves like a particle and θ_{SKH} is dominated by thermal disorder, whereas at higher drives the internal degrees of freedom become important and θ_{SKH} is controlled by skyrmion distortions or shape changes. As shown in Fig. 55, where θ_{SKH} is plotted versus skyrmion velocity v (Litzius *et al.*, 2020), continuum-based simulations are consistent with experiment. In the absence of thermal disorder, θ_{SKH} changes little with velocity except at the highest values of v . When thermal disorder is present, there is a sharp increase in θ_{SKH} at low

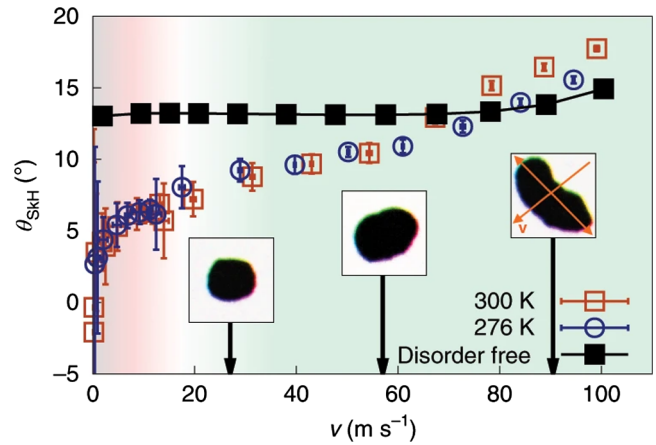


FIG. 55. Continuum simulations of θ_{SKH} vs skyrmion velocity v in a sample with no thermal disorder (black squares) and at two different finite temperatures (open symbols). θ_{SKH} is nearly independent of velocity in the absence of temperature, but when thermal fluctuations are present θ_{SKH} increases with increasing velocity. Insets: display of change in skyrmion shape from nearly circular at low velocities to strongly distorted at high velocities. From Litzius *et al.*, 2020.

velocities and a more gradual increase at higher velocities. The images in the insets of Fig. 55 indicate that the skyrmion shape becomes more distorted with increasing velocity. MacKinnon *et al.* (2020) showed that additional interfacial spin-transfer torques can strongly reduce θ_{SKH} for driven skyrmions less than 100 nm in diameter. They also observed that when disorder is present θ_{SKH} increases rapidly at low velocities, then increases more slowly or saturates at high velocities.

At higher drives, numerical work indicates that skyrmions can develop a noncircular shape with a tail (Masell *et al.*, 2020) and can become unstable above a critical current (Liu, Chen, and Zheng, 2020; Masell *et al.*, 2020). For dense skyrmion lattices, if skyrmion shape changes at higher currents cause the skyrmion-skyrmion interactions to become more anisotropic, lattice transitions could occur.

B. Future directions

Future studies could examine the evolution of θ_{SKH} for different types of pinning, such as short versus long range, repulsive versus attractive, or grain boundary and extended pinning versus point pinning. For applications that require $\theta_{\text{SKH}} = 0^\circ$, pinning or defect arrangements that reduce θ_{SKH} are desirable, while new devices might be created that exploit the behavior of θ_{SKH} . The skyrmion type or symmetries in the system (Güngördü *et al.*, 2016) can also strongly modify θ_{SKH} . For example, when the skyrmion itself contains an anisotropy direction, in certain regimes θ_{SKH} is affected by the applied current orientation with respect to this anisotropy, which could produce rich behavior of objects such as antiskyrmions under a drive in the presence of pinning (Kovalev and Sandhoefer, 2018). Most studies have been performed using dc drives, but adding a high frequency ac drive component could create breathing modes that might reduce the pinning, increase the creep, or change θ_{SKH} . The interplay between skyrmion motion, pinning, and θ_{SKH} could be explored for other textures

such as biskyrmions, half skyrmions, merons, and antiskyrmions. The skyrmion Hall effect was already studied in a disorder-free system for elliptical skyrmions (Xia *et al.*, 2020), so a natural next step would be to add disorder.

Existing studies of pinning effects and dynamics of 2D skyrmions could be extended to 3D systems, where a variety of interesting new effects should appear. Linelike skyrmions could undergo elastic depinning of the type found for stringlike objects but could have distinct modes of motion along the length of the line. There have already been several studies of the scaling of certain 3D skyrmion modes (Lin, Zhu, and Saxena, 2019; Seki *et al.*, 2020). The roughening transition of skyrmion lines near depinning could be analyzed to see whether the skyrmions become more stringlike at higher drives based on changes in the fractal dimension. Like entangled superconducting vortex states, the linelike skyrmions might become entangled and could be unable to cut themselves free.

Studies of skyrmion dynamic phases and the evolution of θ_{SKH} have employed drives arising from an applied current, but alternative forms of driving such as thermal gradients or magnetic gradients could generate new behavior. Existing studies also focused on uniform drives; however, the introduction of nonuniform drives could produce interesting effects due to the velocity dependence of θ_{SKH} . A system with a nonuniform current could exhibit clustering or other effects not found in overdamped systems.

VIII. NANOSTRUCTURED AND PERIODIC LANDSCAPES

There are already a number of proposals for using skyrmions in highly confined racetrack geometry devices. Skyrmion motion can also be controlled by fabricating nanostructured pinning arrays, similar to those employed for vortices in type-II superconductors (Baert *et al.*, 1995; Harada *et al.*, 1996; Martín *et al.*, 1997; Reichhardt, Olson, and Nori, 1998; Berdiyrov, Milošević, and Peeters, 2006; Reichhardt and Reichhardt, 2017a), vortices in Bose-Einstein condensates with optical traps (Reijnders and Duine, 2004; Tung, Schweikhard, and Cornell, 2006), cold atoms (Büchler, Blatter, and Zwerger, 2003; Benassi, Vanossi, and Tosatti, 2011), and colloidal particles (Wei *et al.*, 1998; Brunner and Bechinger, 2002). In these systems, the particles can interact with 1D periodic substrates (Martinoli *et al.*, 1975; Wei *et al.*, 1998; Reichhardt *et al.*, 2001; Reijnders and Duine, 2004; Dobrovolskiy and Huth, 2015), 2D square (Baert *et al.*, 1995; Harada *et al.*, 1996; Reichhardt, Olson, and Nori, 1998; Berdiyrov, Milošević, and Peeters, 2006; Tung, Schweikhard, and Cornell, 2006; Bohlein, Mikhael, and Bechinger, 2012), triangular (Reichhardt, Olson, and Nori, 1998; Brunner and Bechinger, 2002), or quasicrystalline (Kemmler *et al.*, 2006; Villegas *et al.*, 2006; Mikhael *et al.*, 2008) substrates, or arrangements with geometric frustration (Libál, Olson Reichhardt, and Reichhardt, 2009; Latimer *et al.*, 2013; Ortiz-Ambríz and Tierno, 2016; Y.-L. Wang *et al.*, 2018). Figure 56 illustrates three possible pinning geometries: a 2D periodic array of trapping sites, a periodic 1D array, and an asymmetric 2D array that can generate diode or ratchet effects. Nanostructures of this type could be created using controlled irradiation, which has been used to construct

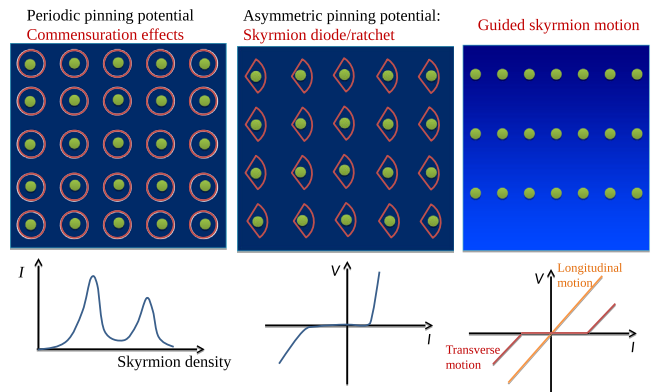


FIG. 56. Examples of skyrmions interacting with nanostructured pinning. Left panels: 2D periodic pinning, where commensuration can occur between the number of skyrmions and the number of pinning sites. Center panels: asymmetric 2D periodic pinning capable of generating ratchet and diode effects. Right panels: 1D periodic pinning. The lower panels show schematic transport curves that could be observed with each pinning geometry.

1D channels in which skyrmions nucleate and undergo channeling flow with an applied drive (Juge *et al.*, 2021).

For assemblies of particles interacting with either 1D or 2D periodic substrates, commensuration effects (Bak, 1982) can occur when the particle lattice and substrate periodicities match. Strong pinning appears under commensurate conditions since the particle-particle interaction forces cancel via symmetry and the entire ensemble behaves similarly to an isolated particle. If, however, there is some lattice mismatch or an incommensuration, collective interactions between the particles become important. For example, at a particle density slightly above commensuration, most particles remain at their commensurate positions in the substrate potential energy minima, but a small number of particles are located at higher energy portions of the substrate. Under an applied drive, these extra particles or kinks depin first at F_{c1} , while the remaining particles depin at a higher drive F_{c2} , producing a two step or even multiple step depinning phenomenon (Bak, 1982; Reichhardt, Olson, and Nori, 1997; Gutierrez *et al.*, 2009; Avci *et al.*, 2010; Benassi, Vanossi, and Tosatti, 2011; Bohlein, Mikhael, and Bechinger, 2012). A similar effect occurs just below commensuration, where the vacancies or antikinks depin before the other particles (Bohlein, Mikhael, and Bechinger, 2012). Commensuration appears whenever the number of particles p is an integer multiple of the number of substrate potential minima q , $p/q = 1, 2, \dots, N$. At these integer matching fillings, the depinning threshold F_c has a local maximum (Baert *et al.*, 1995; Reichhardt, Olson, and Nori, 1997, 1998; Berdiyrov, Milošević, and Peeters, 2006). There can also be fractional commensuration effects at fillings such as $p/q = 1/2$ or $1/3$ depending on the substrate lattice symmetry (Bak, 1982; Grigorenko *et al.*, 2003). In quasi-periodic or frustrated substrates, other types of commensuration effects can arise at integer and noninteger matchings (Kemmler *et al.*, 2006; Villegas *et al.*, 2006; Latimer *et al.*, 2013; Y.-L. Wang *et al.*, 2018). Under an applied drive, a rich variety of dynamical behaviors appear with well-defined

transitions between different kinds of plastic flow, turbulent flow, and ordered flow, and the extent and number of phases depends on the commensurability, pinning strength, and direction of drive with respect to the substrate periodicity (Martinoli *et al.*, 1975; Harada *et al.*, 1996; Reichhardt, Olson, and Nori, 1997; Gutierrez *et al.*, 2009; Avci *et al.*, 2010; Benassi, Vanossi, and Tosatti, 2011; Bohlein and Bechinger, 2012; Bohlein, Mikhael, and Bechinger, 2012; Dobrovolskiy and Huth, 2015; Juniper *et al.*, 2015; Y.-L. Wang *et al.*, 2018).

The particlelike nature of skyrmions makes them ideal for studying commensurate and incommensurate effects on a range of substrate geometries and could be exploited to create new types of devices. For example, certain skyrmion configurations in pinning site clusters could represent a memory bit. If a periodic substrate were combined with a racetrack, a skyrmion subjected to a current pulse would always move a fixed number of substrate lattice constants even under slightly varying pulse duration or direction, thereby giving a more robust device. Periodic pinning could also stabilize skyrmions against thermal wandering over relatively long periods of time, allowing for the precise control of skyrmion motion in repeatable patterns. A variety of superconducting vortex logic devices such as vortex cellular automata have been proposed for vortices interacting with periodic substrates (Milošević, Berdiyrov, and Peeters, 2007), and similar approaches could be used for skyrmions. Additionally, the Magnus force and internal degrees of freedom could cause skyrmions to exhibit a variety of new types of static and dynamic commensurate phases distinct from those found for overdamped systems.

A. One-dimensional periodic substrates and speedup effects

We first consider the simplest example of a skyrmion interacting with the 1D pinning array illustrated in Fig. 57. Significantly different dynamical responses appear depending on whether the external driving is applied parallel or perpendicular to the substrate periodicity. An overdamped system has a finite depinning threshold F_c only for parallel driving, while perpendicular driving simply causes the particles to slide along the potential minima. For skyrmions with a finite Magnus force, which move at an angle with respect to the drive, there is a finite parallel depinning threshold even for perpendicular driving. Reichhardt and Olson Reichhardt (2016) used a 2D particle-based simulation to study skyrmions interacting with a periodic 1D substrate and found that, for parallel driving, the critical depinning force F_c is independent of the ratio of the Magnus force to the damping strength. This is in contrast to the case of random point pinning, where F_c decreases with increasing Magnus force. Although skyrmions can skirt around pointlike pinning sites, they cannot avoid passing through a 1D extended pinning site. For perpendicular driving, there is no finite depinning threshold and the skyrmions initially move only in the perpendicular direction with $\theta_{\text{SkH}} = 0^\circ$. As the drive increases, the Magnus force parallel to the substrate periodicity increases until, above a critical drive, the skyrmions begin to jump over the barriers and move in both the parallel and perpendicular directions. A perpendicular drive produces a situation similar to that of a skyrmion in a thin racetrack, which moves toward the edge of the track due to the Magnus force and leaves the track

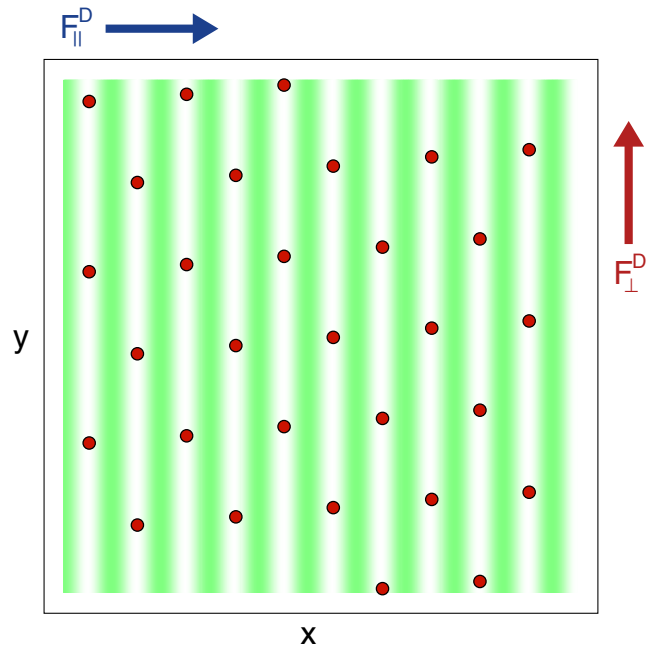


FIG. 57. An example of a periodic quasi-one-dimensional substrate for skyrmions. The substrate is sinusoidal along the x direction with regular minima (white bands) and maxima (green bands). The skyrmions (red dots) are driven parallel to the substrate periodicity by F_{\parallel}^D (blue arrow), or perpendicular by F_{\perp}^D (red arrow). From Reichhardt and Olson Reichhardt, 2016.

completely above a critical velocity. In the case of the 1D periodic substrate in a 2D sample, the skyrmion hops into the next potential minimum when the critical velocity is exceeded.

Figure 58 shows the skyrmion velocity-force curves for perpendicular driving in the system from Fig. 57 (Reichhardt and Olson Reichhardt, 2016). In Fig. 58(a) at $\theta_{\text{SkH}}^{\text{int}} = 30^\circ$, there is a finite depinning threshold F_c^{\parallel} for motion in the parallel direction, and for $0 < F_D < F_c^{\parallel}$ the skyrmion motion is locked along the perpendicular direction with $\theta_{\text{SkH}} = 0^\circ$. For $F_D > F_c^{\parallel}$, the skyrmion begins to move in both directions, and the onset of finite $\langle V_{\parallel} \rangle$ is accompanied by a decrease in $\langle V_{\perp} \rangle$. In Figs. 58(b) and 58(c), systems with $\theta_{\text{SkH}}^{\text{int}} = 64^\circ$ and 84.3° show that F_c^{\parallel} shifts to lower drives with an increasing $\theta_{\text{SkH}}^{\text{int}}$, while the drop in $\langle V_{\perp} \rangle$ at F_c^{\parallel} becomes more pronounced. For a sample with $\theta_{\text{SkH}}^{\text{int}} = 84.3^\circ$, Fig. 58(d) illustrates the net skyrmion velocity $\langle V \rangle = (\langle V_{\perp} \rangle^2 + \langle V_{\parallel} \rangle^2)^{1/2}$ versus F_{\perp}^D along with the velocity $\langle V_0 \rangle$ expected in the absence of a substrate. A pinning-induced speedup effect appears near F_c^{\parallel} in which $\langle V \rangle > \langle V_0 \rangle$, meaning that the skyrmion is moving faster than it would if the substrate were not present. This speedup effect, which does not occur in overdamped systems, is produced by a combination of the Magnus force and the pinning potential. When the skyrmion is constrained by the pinning potential to move in the direction of the drive, the Magnus-force-induced velocity component from the pinning $\alpha_m F_p$ is aligned with the drive. This is added to the velocity component $\alpha_d F_D$ produced by the drive, giving a total velocity of $\langle V \rangle = \alpha_d F_D + \alpha_m F_p$. The nonconservative

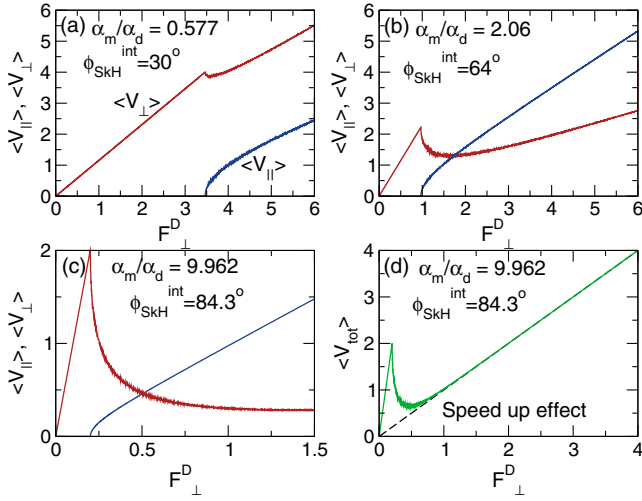


FIG. 58. Illustration of the speedup effect from particle-based simulations of skyrmion velocities parallel ($\langle V_{\parallel} \rangle$; lower blue lines) and perpendicular ($\langle V_{\perp} \rangle$; upper red lines) to the substrate periodicity direction for perpendicular driving F_{\perp}^D in the quasi-1D potential illustrated in Fig. 57. (a) At $\theta_{\text{SkH}}^{\text{int}} = 30^{\circ}$, the initial skyrmion motion is locked in the perpendicular direction. There is a drop in $\langle V_{\perp} \rangle$ at the critical drive F_c^{\parallel} for the onset of motion in the parallel direction. At (b) $\theta_{\text{SkH}}^{\text{int}} = 64^{\circ}$ and (c) $\theta_{\text{SkH}}^{\text{int}} = 84.3^{\circ}$, F_c^{\parallel} shifts to lower drives and the drop in $\langle V_{\perp} \rangle$ becomes more pronounced. (d) Total velocity $\langle V_{\text{tot}} \rangle$ vs F_{\perp}^D at $\theta_{\text{SkH}}^{\text{int}} = 84.3^{\circ}$. The dashed line indicates the response $\langle V_0 \rangle$ expected in a system with no substrate. In the speedup effect, $\langle V_{\text{tot}} \rangle > \langle V_0 \rangle$. From Reichhardt and Olson Reichhardt, 2016.

Magnus force turns the pinning force into an effective additional driving force. Speedup effects are most prominent on 1D substrates and have been studied numerically for a single skyrmion moving along domain walls (Xing, Åkerman, and Zhou, 2020). They can also occur for random and 2D periodic pinning arrays. Gong, Yuan, and Wang (2020) numerically studied skyrmion motion in random disorder and found that the skyrmion velocity can be boosted in regimes where motion in the transverse or skyrmion Hall angle direction is suppressed. This indicates that whenever the skyrmion motion along $\theta_{\text{SkH}}^{\text{int}}$ is impeded, the Magnus force can transfer part or all of that component of motion to the direction along which the skyrmion is constrained to move.

Skyrmion speedup effects have been observed in micromagnetic simulations of racetracks (Sampaio *et al.*, 2013) and for scattering off a single pinning site in both continuum and Thiele-based approaches (Müller and Rosch, 2015). Iwasaki, Koshibae, and Nagaosa (2014) used a Thiele approach and micromagnetic simulations to examine the large velocity enhancement near a boundary and showed that it is related to a colossal spin-transfer-torque effect. The velocity is enhanced by a factor of $1/\alpha$, where α is the Gilbert damping, and the maximum velocity is determined by the magnitude of the confining force produced by the sample edge. Multiple other works have also described the acceleration of skyrmions along sample edges (Martinez *et al.*, 2018; Castell-Queralt *et al.*, 2019). Castell-Queralt *et al.* (2019) examined the dynamics of a skyrmion moving across a rail where, in

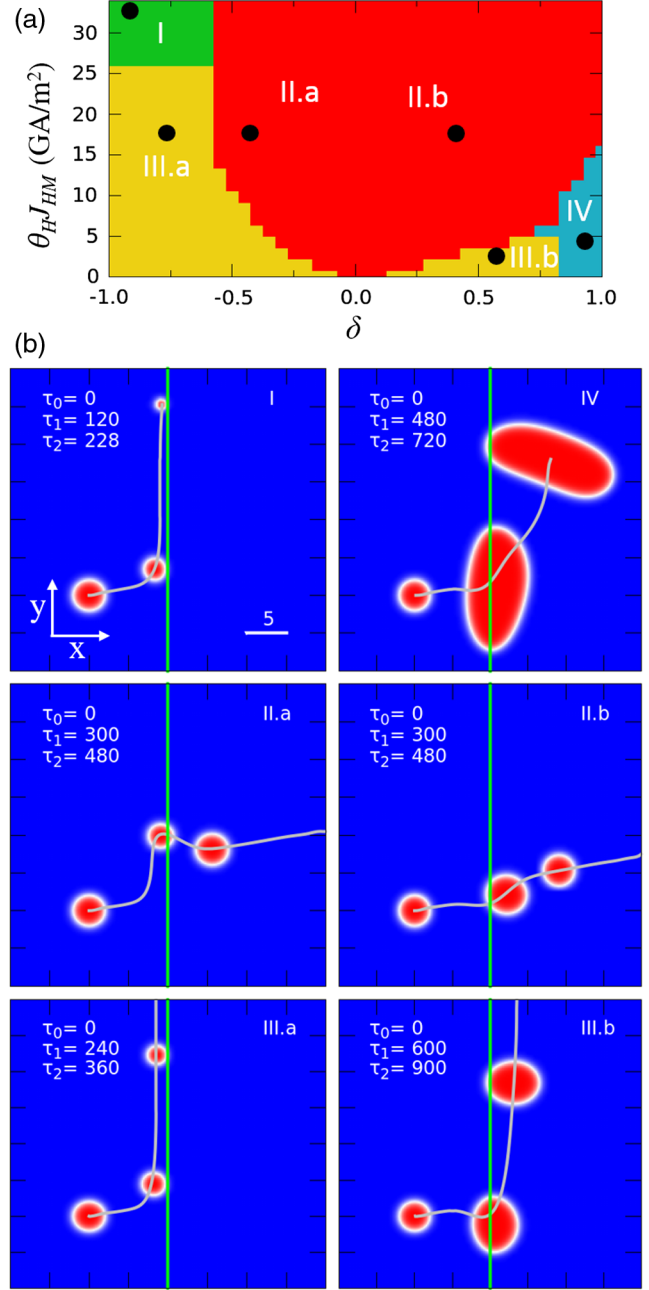


FIG. 59. Results from continuum simulations of a skyrmion interacting with a line along which the DMI has been changed by an amount δ compared to the rest of the sample. (a) Phase diagram as a function of the product of the skyrmion Hall angle θ_H and current J_{HM} vs δ . (b) Illustration of motion in the six different regimes. The green vertical line is the defect and the curved gray line is the skyrmion trajectory. From Castell-Queralt *et al.*, 2019.

addition to skyrmion acceleration along the edge, they observed guiding and compressing effects. They found that speedups of as much as an order of magnitude are possible compared to motion in a system without defects. Figure 59 shows the results from micromagnetic simulations (Castell-Queralt *et al.*, 2019) of a skyrmion approaching a defect line with a modified DMI. Here $\delta = -1$ indicates complete DMI suppression and $\delta = 1$ is unaltered DMI, so $\delta < 0$ produces

skyrmion repulsion and $\delta > 0$ causes the line to attract the skyrmion. The dynamic phase diagram in Fig. 59(a) shows the behavior as a function of the product of θ_{SKH} and the current versus δ , while Fig. 59(b) illustrates the six different phases of motion. In phases I and III.a, the skyrmion is guided along the line and shrinks, while in the other phases the skyrmion crosses the line. The skyrmion experiences strong distortion in phase IV, is weakly deflected in phases II.a and II.b, and is strongly deflected in phase III.b. Castell-Queralt *et al.* also demonstrated skyrmion guidance with a strong acceleration effect using a combination of two line defects, one repulsive and the other attractive.

Reichhardt and Olson Reichhardt (2016) also considered collective effects for skyrmions moving over 1D periodic arrays. A number of dynamical phases arise for perpendicular driving, including a pinned smectic state similar to that observed for colloidal particles and superconducting vortices in periodic 1D substrates, a disordered plastic flow state just above depinning, a moving hexatic state, and a moving crystal state. All these phases produce signatures in the velocity components and θ_{SKH} , and they can be detected experimentally via neutron scattering, changes in the THE, or noise measurements.

Various interference effects can arise for a skyrmion moving over a 1D or 2D substrate. A dc-driven particle moving over a periodic substrate experiences a time-dependent velocity modulation at a washboard frequency ω_d that increases with an increasing drive F_D or current J . When an ac drive $F_{\text{ac}} = A \sin(\omega_{\text{ac}} t)$ is added to the dc drive, there is a resonance between ω_{ac} and ω_d at certain values of F_{ac} . Resonance effects have been observed experimentally for superconducting vortex lattices moving over random disorder (Fiory, 1971; Harris *et al.*, 1995; Okuma, Inoue, and Kokubo, 2007; Okuma *et al.*, 2011). Since the resonance condition is met at a specific dc velocity for a fixed ω_{ac} , a region of constant or locked velocity appears over an interval of F_D values close to resonance. When the difference between ω_{ac} and ω_d becomes too large, the system jumps out of the velocity locked step; however, additional velocity locking steps appear whenever $\omega_d/\omega_{\text{ac}}$ is an integer. The velocity steps at the resonant condition and its higher harmonics are known as Shapiro steps (Shapiro, 1963; Benz *et al.*, 1990). If the ac amplitude A is large, nonlinear effects produce fractional steps and strongly fluctuating regions. Shapiro steps have been observed in a wide variety of systems that exhibit depinning on periodic substrates, such as sliding charge density waves (Coppersmith and Littlewood, 1986) and vortices in type-II superconductors with 1D and 2D periodic substrates (Martinoli *et al.*, 1975; Van Look *et al.*, 1999). All of these systems either are overdamped or have inertial effects, but none of them include Magnus forces.

In skyrmion systems, the Magnus force should produce new phase locking phenomena. For example, the mixing of the velocity components by the Magnus force permits locking steps to occur for any driving direction, as demonstrated in a particle-based model for skyrmions moving over a periodic 1D potential with a parallel dc drive and a parallel or perpendicular ac drive (Reichhardt and Olson Reichhardt, 2015). Here Magnus-induced steps appear in the velocity-force curves with step widths ΔF_{ac} that oscillate according to

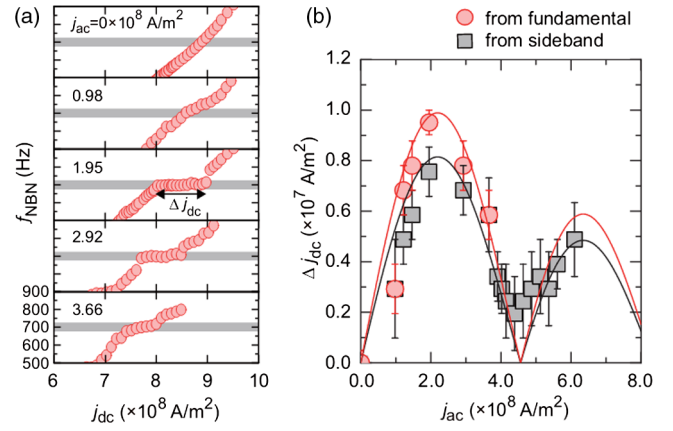


FIG. 60. Phase locking and Shapiro steps for current-driven skyrmions in MnSi under combined dc and ac driving. (a) Magnitude of the narrowband noise f_{NBN} as a function of dc driving current j_{dc} for different values of the ac current j_{ac} , showing the emergence of a locking step when $j_{\text{ac}} = 1.95 \times 10^8 \text{ A/m}^2$. (b) Dependence of the locking step width Δj_{dc} on ac current amplitude j_{ac} showing Bessel function oscillations consistent with Shapiro steps. From Sato *et al.*, 2020.

the Bessel function $\Delta F_{\text{ac}} = |J_n(F_x^{\text{ac}})|$, which is consistent with Shapiro steps. The locking step orbits are considerably more complex for skyrmions than for overdamped particles. Sato *et al.* (2020) measured voltage fluctuations for current-induced skyrmion lattice motion in MnSi. They found a narrowband noise (NBN) signal that shifted to higher frequency with increasing current, indicating increasing skyrmion velocity. When they added an ac driving current, a clear mode locking signal emerged with strongly enhanced NBN. The plots of NBN magnitude versus dc current density in Fig. 60(a) contain a steplike regime where the narrowband signal is locked to the washboard frequency. For zero applied ac current no step is present, but as the amplitude of the ac current increases the width of the narrowband step Δj_{dc} in Fig. 60(b) follows the Bessel function behavior of Shapiro steps.

Other combinations of drives for skyrmions on 1D periodic arrays produce unusual collective effects. For example, in an overdamped system, a perpendicular dc drive combined with a parallel or perpendicular ac drive does not produce any interference effects; however, in the skyrmion system phase locking effects appear, including a new phenomenon in which the velocity-force curves contain spikes rather than steps. This Shapiro spike structure occurs when the ac and dc drives are both perpendicular to the substrate periodicity (Reichhardt and Reichhardt, 2017b). Here phase locking can cause the skyrmion to move at 90° with respect to the dc drive. There can also be regions of negative V_{\perp} , which is indicative of absolute negative mobility (Eichhorn, Reimann, and Hänggi, 2002; Ros *et al.*, 2005), where the skyrmion is actually moving against the direction of the external drive.

Since skyrmions have internal modes with their own intrinsic frequencies, there should be a wealth of possible resonances involving the coupling of these modes to an external ac frequency, a substrate frequency produced by dc motion over periodic pinning, or the intrinsic washboard

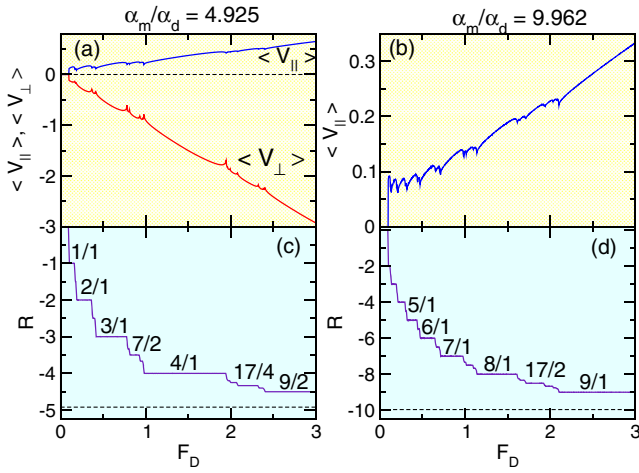


FIG. 61. Particle-based simulations of skyrmions moving over a square array of pinning sites showing the quantization of θ_{SKH} . (a) The velocity parallel ($\langle V_{\parallel} \rangle$; upper blue line) and perpendicular ($\langle V_{\perp} \rangle$; lower red line) to the driving direction vs the dc drive amplitude F_D at a Magnus-to-damping ratio of $\alpha_m/\alpha_d = 4.925$. (b) $\langle V_{\parallel} \rangle$ vs F_D for a larger ratio $\alpha_m/\alpha_d = 9.962$. (c) The ratio $R = \langle V_{\perp} \rangle / \langle V_{\parallel} \rangle = \tan(\theta_{\text{SKH}})$ vs F_D for the sample in (a), where steps appear at rational fractions. (d) R vs F_D for the sample in (b) also exhibits a series of steps. From Reichhardt, Ray, and Reichhardt, 2015b.

frequency of the skyrmion lattice. These dynamics would be much different from those typically found for overdamped or rigid particles. There was already some work done along these lines by Leliaert *et al.* (2019), who performed micromagnetic simulations of skyrmions moving through a wire with a periodic modulation of notches produced by varying the DMI. The notches induce a periodic modulation of the skyrmion motion that couples to the skyrmion breathing mode, producing a series of resonances in the velocity-force curves.

B. Skyrmions with 2D periodic pinning

Reichhardt, Ray, and Reichhardt (2015b) used a particle-based model to study a single skyrmion moving over a 2D square periodic potential. This system has a finite depinning threshold and a drive-dependent θ_{SKH} similar to what is observed for random pinning, as previously discussed (Reichhardt, Ray, and Reichhardt, 2015a; Reichhardt and Reichhardt, 2016; Jiang *et al.*, 2017; Kim and Yoo, 2017; Legrand *et al.*, 2017; Litzius *et al.*, 2017); however, owing to the square substrate symmetry, the skyrmion motion preferentially locks to certain directions $\theta_{\text{SKH}} = \tan^{-1}(n/m)$ with integer m and n . For a substrate with lattice constant a , these integers indicate that the skyrmion moves a distance na in the y direction during the time required to translate a distance ma in the x direction. For example, locking at $\theta_{\text{SKH}} = 45^\circ$ occurs when $n = 1$ and $m = 1$ while locking at $\theta_{\text{SKH}} = 23^\circ$ corresponds to $n = 1$ and $m = 2$. For increasing drive, the skyrmion can remain locked in its direction of motion only if its net velocity $\langle V \rangle$ decreases, so each locking step is associated with a window of negative differential mobility in which $d\langle V \rangle / dF_D < 0$. Cusps in both the parallel and perpendicular

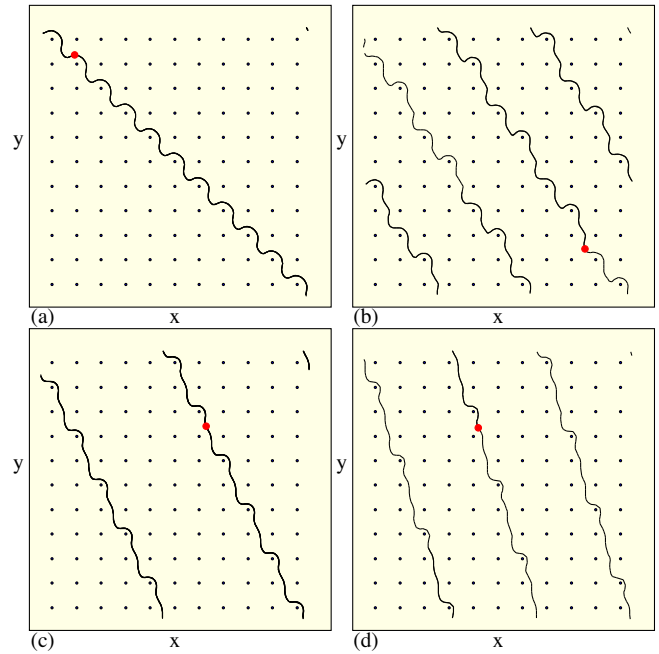


FIG. 62. Skyrmion trajectories (lines) for particle-based simulations of the system in Fig. 61 with a skyrmion (red circle) moving through a periodic array of pinning sites (black dots) at (a) $|R| = 1$, (b) $|R| = 5/3$, (c) $|R| = 2$, and (d) $|R| = 3$. From Reichhardt, Ray, and Reichhardt, 2015b.

velocities ($\langle V_{\parallel} \rangle$ and $\langle V_{\perp} \rangle$) appear at the transition from one directional locking step to the next, as shown in Figs. 61(a) and 61(b). Figures 61(c) and 61(d) illustrate the ratio $R = \langle V_{\perp} \rangle / \langle V_{\parallel} \rangle = \tan(\theta_{\text{SKH}})$, indicating that θ_{SKH} is quantized. On the $|R| = 1$ step, the skyrmion is constrained to move along $\theta_{\text{SKH}} = 45^\circ$, as illustrated in Fig. 62(a). The skyrmion trajectories for motion on the $|R| = 5/3$, 2, and 3 steps appear in Figs. 62(b), 62(c), and 62(d), respectively. In general, the integer steps are more pronounced than the fractional steps. Such directional locking should be a generic feature of ferromagnetic skyrmions moving over periodic pinning arrays. A similar directional locking effect with steps in the velocity-force curves was studied for superconducting vortices (Reichhardt and Nori, 1999) and colloidal particles (Korda, Taylor, and Grier, 2002; MacDonald, Spalding, and Dholakia, 2003; Risbud and Drazer, 2014) moving over 2D periodic substrates, but in these overdamped systems the external drive must change direction in order to generate the locking steps, whereas in the skyrmion system the driving direction remains fixed.

Feilhauer *et al.* (2020) employed a combined micromagnetic and Thiele equation approach to study skyrmion motion in a magnetic antidot array. They found that the skyrmion motion locks to the symmetry angles of the array and that θ_{SKH} can be controlled by varying the damping, as shown in Fig. 63. By careful choice of the current pulse direction, a skyrmion can be steered to move into almost any plaquette position, suggesting that this drive protocol could be useful for applications. There have already been some experimental efforts to create a similar type of substrate using antidot lattices (Saha *et al.*, 2019).

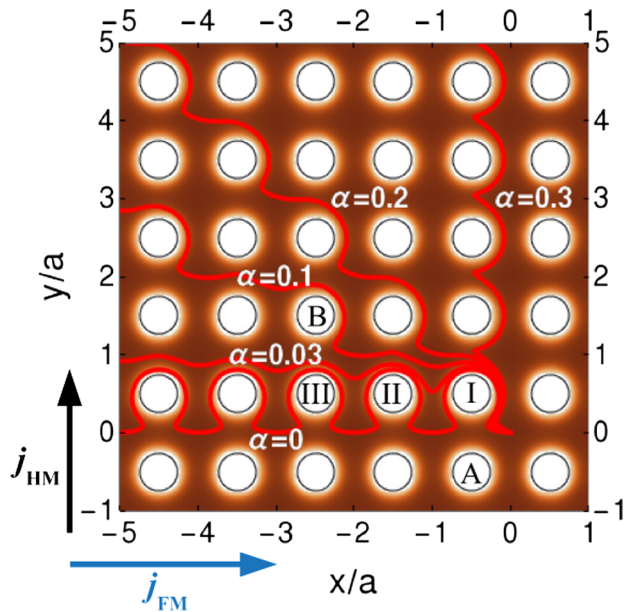


FIG. 63. Combined micromagnetic and analytic calculations of skyrmion trajectories (red lines) in a square array of magnetic dots for different values of the damping coefficient α . By varying the direction of the applied current pulse, the skyrmion can be steered to any position in the array. From Feilhauer *et al.*, 2020.

Locking of the skyrmion motion to particular symmetry directions of 2D periodic arrays could be harnessed to create a topological sorting device for different skyrmion species with slightly different values of $\theta_{\text{SKH}}^{\text{int}}$. When one species locks to a substrate symmetry direction while the other does not, the species can be separated laterally over time. A demonstration of this separation effect was achieved in simulations by Vizir, Reichhardt, Reichhardt, and Venegas (2020) for a bidisperse assembly of skyrmions driven through a square obstacle array. This procedure is similar to that used in microfluidic systems and suggests that skyrmion bubbles with a carefully selected size could be separated from skyrmion bubbles of other sizes. Micromagnetic simulations of skyrmions of different sizes in a branching nanostructure showed that each skyrmion size could be controlled to move at a different angle than the other skyrmion sizes (Chen *et al.*, 2020), thus forming a skyrmion interconnect device.

Using particle-based simulations, Vizir, Reichhardt, Venegas, and Reichhardt (2020) also showed that a skyrmion interacting with a 2D periodic array under a dc drive and one or more ac drives can undergo a variety of controlled motions and can exhibit nonmonotonic behaviors. Skyrmions driven over periodic arrays can also exhibit clustering or segregation. This is similar to the segregated states found for strong random pinning in both lattice-based (Koshibae and Nagaosa, 2018) and particle-based simulations (Reichhardt and Reichhardt, 2019a).

Reichhardt, Ray, and Reichhardt (2018) studied collective static arrangements of skyrmions interacting with square pinning arrays as a function of skyrmion density using a particle-based model. When the number of skyrmions N_{sk} is an integer multiple of the number of pinning sites N_p , a series of commensurate states appear in which different types of

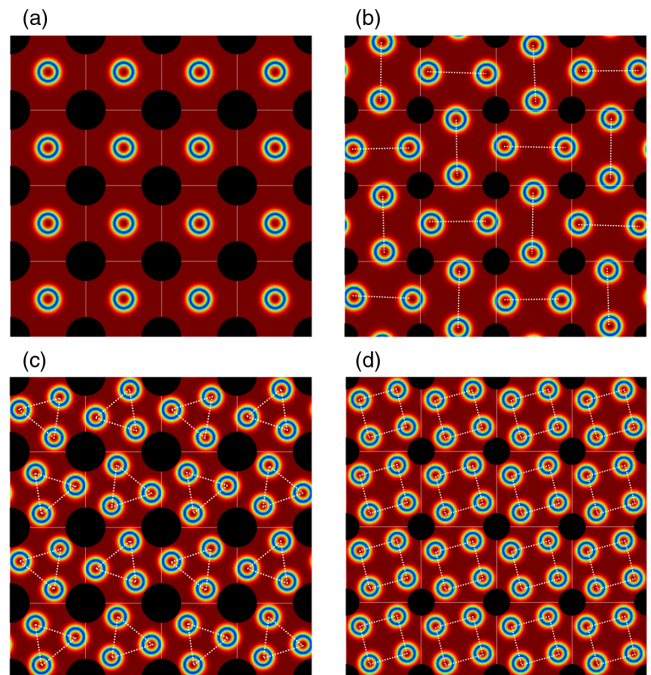


FIG. 64. Continuum simulations of chiral liquid-crystal skyrmions (blue rings) interacting with a periodic array of obstacles (black circles). (a) Filling ratio of $f = 1$, where the skyrmions form a square lattice. (b) Alternating dimer ordering for $f = 2$. (c) Trimer arrangement at $f = 3$. (d) Ordered quadrimer state at $f = 4$. From Duzgun *et al.*, 2020.

skyrmion crystals can be stabilized, including square or triangular lattices. Ordered skyrmion lattices can also form at rational filling fractions $f \equiv N_{\text{sk}}/N_p$ such as $f = 1/2$, where the skyrmions adopt a checkerboard pattern. The $f = 1.65$ and 2.0 configurations were also observed in continuum-based simulations for a square array of pinning sites produced by local changes in the anisotropy (Koshibae and Nagaosa, 2018).

Duzgun *et al.* (2020) explored the ordering of liquid-crystal skyrmions interacting with a square array of defects using continuum-based simulations. At a one-to-one matching of $f = 1$, the skyrmions form a square lattice, as illustrated in Fig. 64(a). Fillings of $f = 2, 3$, and 4 produce dimer, trimer, and quadrimer states, as shown in Figs. 64(b)–64(d). At some filling fractions, such as $f = 2$, the skyrmions deform into elongated states in order to better match the substrate symmetry.

Observation of skyrmion motion in systems with two periodic surfaces can be achieved using moiré patterns in van der Waals 2D magnets (Tong *et al.*, 2018). The moiré patterns are generated by introducing a lateral modulation of the interlayer magnetic coupling for different atomic angles. In the case of weak interlayer coupling, a skyrmion can be viewed as moving over a periodic substrate composed of trapping sites formed by the moiré pattern. Figure 65(a) shows the periodic motion that can be induced by the pattern. In Fig. 65(b), application of a current pulse can cause the skyrmion to jump from one side of a trapping barrier to the other. Tong *et al.* (2018) proposed that the 2D moiré trapping array could be used to create a stable background

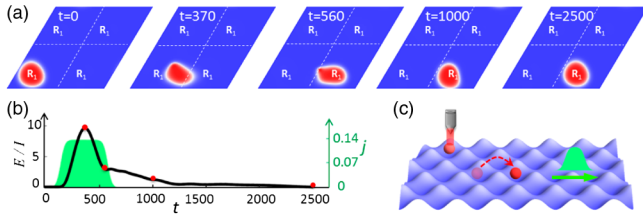


FIG. 65. Numerical model for the motion of a skyrmion over a moiré pattern formed by a van der Waals 2D magnet. (a) The localized region (red) indicates the location of the skyrmion as a function of time. (b) The time profile of the applied current j (green profile) and the energy of the skyrmion E/I during the motion illustrated in (a). (c) Schematic of the use of a spin-polarized scanning tunneling microscopy tip (upper left gray area) to write a skyrmion, which is then moved from one substrate minimum to another with a current pulse (green profile). From Tong *et al.*, 2018.

substrate for controlled skyrmion motion for various applications.

Skyrmions have also been studied in 2D arrays of artificial spin ice geometries, where the position of a skyrmion on either end of a double well potential can be mapped onto an effective spin direction. Figure 66 shows schematically how such structures could be made via thickness modulation (Ma *et al.*, 2016). The skyrmions form a spin ice ordering similar to that observed for superconducting vortices (Libál, Olson Reichhardt, and Reichhardt, 2009) on square and hexagonal double well artificial ice arrays. Since the skyrmions can change size or deform, a transition can occur from a frustrated state in which each skyrmion occupies only one side of the

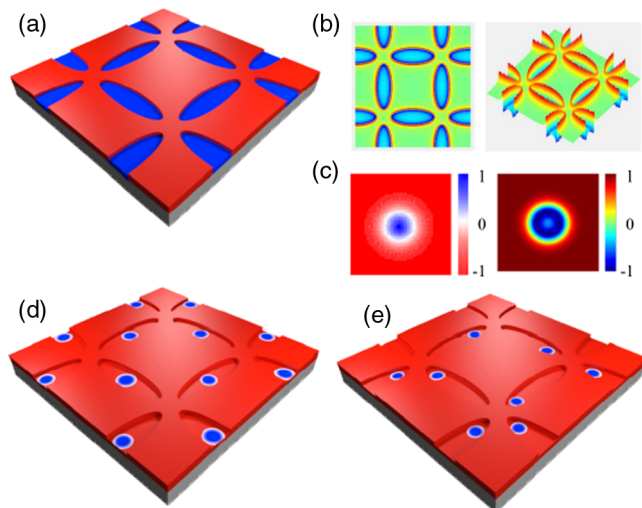


FIG. 66. Artificial ice geometry for skyrmions. (a) Geometry constructed using elliptical blind holes with opposing magnetization directions inside and outside the holes. (b) Perpendicular or z component of the resulting stray field. (c) Images of the spin configuration (left panel) and the topological density distribution (right panel) of an isolated individual skyrmion. (d) Large skyrmions sit at the center of each blind hole to form a nonfrustrated configuration. (e) Small skyrmions sit at one end of each blind hole and form a frustrated state. From Ma *et al.*, 2016.

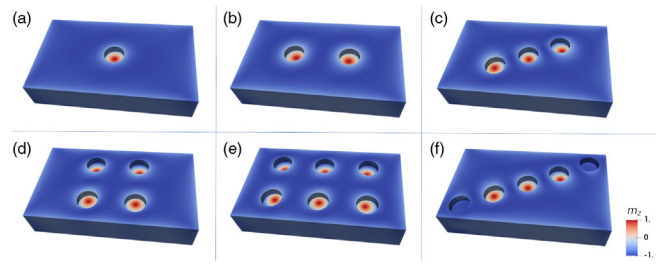


FIG. 67. Micromagnetic simulations of skyrmion localization in a sample with blind holes etched on the top and bottom faces. In (a)–(e), each blind hole is able to capture a single skyrmion, but if the spacing between etched regions or the distance to the sample edge becomes too small, only some blind holes capture a skyrmion, as shown in (f). From Pathak and Hertel, 2021.

double well to an unfrustrated state in which a single skyrmion stretches out and occupies the center of the well, as shown in Figs. 66(d) and 66(e). There have also been studies of so-called artificial skyrmion lattices in a 2D array of magnetic dots (Sun *et al.*, 2013; Gilbert *et al.*, 2015; Zhang, Petford-Long, and Phatak, 2016). The next step in such work would be to see whether skyrmions in adjacent dots could be coupled or the entire system could be placed on a ferromagnetic substrate that would permit the skyrmions to hop directly from one dot to the next. Sun *et al.* (2018) performed numerical work along these lines for coupled magnetic disks. Pathak and Hertel (2021) used micromagnetic simulations to study geometrically constrained 3D skyrmions in a sample with etched blind holes, as illustrated in Fig. 67. When the constraints are not too restrictive, each blind hole can capture a skyrmion to form a range of patterns, as shown in Figs. 67(a)–67(e). If the spacing between adjacent etched sites becomes too small or the sample edge is too close, not all of the blind holes are able to capture skyrmions, as indicated in Fig. 67(f).

C. Further directions for 1D and 2D periodic substrates

There are a variety of potential racetrack memory applications of 1D periodic substrates for both bulk and thin films, including situations in which multiple interacting skyrmions could be coupled inside a nanowire with a periodic modulation. In this case, mobile kinks in the 1D skyrmion chain could reduce θ_{SKH} . An example is shown schematically in Fig. 68(a), where a constriction with a periodic modulation is filled with skyrmions just above 1:1 matching. The extra skyrmion forms a kink that travels in the driving direction. In Fig. 68(b), just below 1:1 matching a vacancy appears that moves in the opposite direction. Here the skyrmion to the left of the kink experiences a repulsion from its left neighbor that is uncompensated due to the vacancy inside the kink, causing the skyrmion to hop to the right into the kink and resulting in a leftward-moving kink. The kinks could serve as information carriers instead of the actual skyrmions. At higher drives there is a second depinning transition from kink to bulk flow in which all of the skyrmions move simultaneously. The periodic modulation could be created using a periodic array of notches (Marchiori *et al.*, 2017), variations of the DMI, spatially

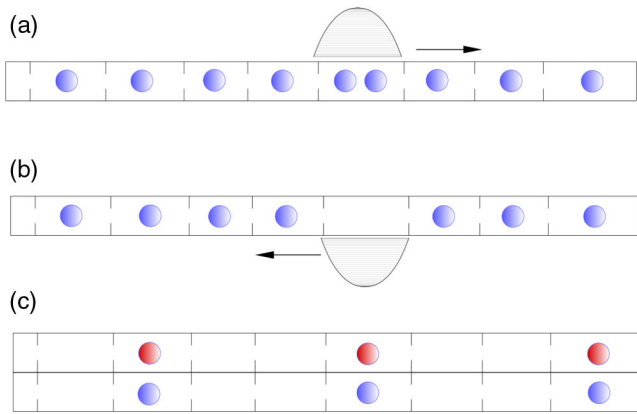


FIG. 68. (a) Schematic of skyrmions in a nanowire interacting with a 1D periodic substrate at a filling just above 1:1 matching. The additional skyrmion forms a mobile kink that moves in the driving direction. Every time the kink moves through the system, the skyrmion translates by one lattice constant. (b) The same for an antikink just below 1:1 matching that moves in the opposite direction. (c) Two coupled wires with different skyrmion species that could bind together into skyrmion excitons.

varying damping (Zhang, Xia, Zhau *et al.*, 2017; Zhou *et al.*, 2019), or periodic thickness modulations (Loreto *et al.*, 2019).

For coupled colloidal particles on 1D periodic substrates, it was shown that kinks can act like emergent particles with their own internal frequency, making it possible to observe kink phase locking under combined dc and ac driving (Juniper *et al.*, 2015). The 1D substrate need not be static: a dynamic substrate can be created using arrays with different gate voltages (Zhang, Zhou *et al.*, 2015; Kang *et al.*, 2016; Liu *et al.*, 2019) that can be turned on and off to create a flashing potential for the skyrmions. The periodic flashing introduces an additional frequency that could couple with the internal skyrmion frequencies. In most overdamped systems, Shapiro steps appear when a dc drive is combined with a single ac driving frequency; however, for skyrmions it was shown that biharmonic ac forces (Chen *et al.*, 2019) can produce directed skyrmion motion even in the absence of a dc drive. Thus, new phenomena could arise for skyrmions under both dc and biharmonic ac driving over a 1D substrate. It would also be possible to couple nanowires of different materials such that the skyrmions interact between the nanowires, leading to skyrmion drag effects, as shown schematically in Fig. 68(c). For example, a nanowire containing antiskyrmions that couples to another nanowire containing regular skyrmions could produce an effective skyrmion exciton. Driving one magnetic object by coupling it to another magnetic object has been proposed for magnetic domain walls (Purnama *et al.*, 2014), and there is also some work on draglike effects for skyrmions in 1D channels (Bhatti and Piramanayagam, 2019).

A wide variety of avenues of study are available for skyrmions on 2D periodic substrates created using a range of methods. New types of skyrmion-based memory devices could be produced by storing information in certain skyrmion configurations that could be changed by applying a current. At fillings slightly away from commensuration, a well-defined number of kinks or antikinks are present that act like emergent particles with their own dynamics. It would be interesting to

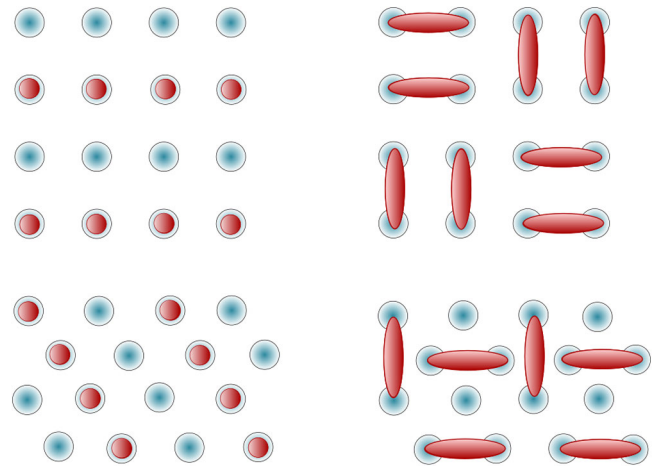


FIG. 69. Schematic of possible orderings on square and triangular pinning arrays (large blue circles) at half filling. Left side: skyrmion (small red circles) orderings. Right side: skyrmions elongate into meron pairs (red lozenges) to create a 1:1 filling for the square pinning array but still leave unoccupied pins in the triangular pinning array.

explore whether the Magnus force or the internal skyrmion degrees of freedom would change the dynamics of kinks and antikinks compared to what is observed in overdamped or rigid particle systems. When thermal fluctuations become relevant, the kinks or antikinks could form their own lattice and exhibit melting phenomena. To date numerical work on incommensurate states has employed particle-based models, so new studies based on micromagnetic calculations could reveal many additional effects related to the ability of the skyrmion to change its shape, such as new types of commensuration and dynamical effects. For example, a system containing twice as many pinning sites as particles normally forms a square or striped sublattice, as illustrated in Fig. 69. If the pinning is strong enough, however, the skyrmions can elongate to form pairs of merons that cover each lattice site, representing an effective dimer covering model that has numerous possible ordered states. Triangular substrates at half filling would form strongly frustrated states if the skyrmions elongate into meron pairs.

The strong gyrotropic motion of skyrmions makes it possible to explore coupled skyrmions oscillating in dense 2D arrays of dots where each dot can have different material properties. The coupled oscillations could pass through a series of locking transitions as a function of some form of ac driving. The sliding dynamics of skyrmions over a periodic array would also be an interesting avenue of study. Koshibae and Nagaosa (2018) showed that skyrmion creation and annihilation occurs at certain drives and pinning strengths when skyrmions move through random arrays. On periodic arrays, such events may be much better controlled. For instance, a skyrmion could move a specific number of lattice sites before an annihilation or creation event occurs. This would allow skyrmions to be moved a precise distance and confer robustness against disorder, suggesting that a racetrack combined with periodic pinning could be one of the next steps for realizing memory devices. Under superimposed ac and dc driving, a resonance could arise between the ac drive and the

motion of the skyrmions over the substrate or the skyrmion breathing modes. Similar effects could be studied for other systems, such as merons, combined meron-skyrmion lattices, antiskyrmions, bimerons (Zhang *et al.*, 2021), and antiferromagnetic skyrmions (Göbel, Mertig, and Tretiakov, 2021). In bulk systems, periodic pinning arrays could be present only on the surface or could pass through the bulk in the form of columnar defects generated using patterned irradiation, as has been done in superconducting systems (Civale, 1997).

D. Asymmetric arrays, diodes, and ratchets

In a ratchet device, an applied ac drive leads to the net dc motion of a particle. Ratcheting motion in overdamped systems is typically achieved using an asymmetric pinning potential (Reimann, 2002; Hänggi and Marchesoni, 2009). The flashing of an asymmetric substrate in a thermal system can generate stochastic ratchet transport, while higher-dimensional ratchet effects can occur on symmetric substrates if time symmetry is broken by a chiral ac drive. Ratchet effects have been studied extensively in particle-based systems such as colloidal particles (Rousselet *et al.*, 1994; Xiao, Roichman, and Grier, 2011), vortices in type-II superconductors (Lee *et al.*, 1999; Villegas *et al.*, 2003; Lin *et al.*, 2011; Shklovskij, Sosedkin, and Dobrovolskiy, 2014), and cold atoms (Salger *et al.*, 2009). In magnetic systems, domain walls interacting with asymmetric dot arrays undergo ratcheting motion under various types of external ac driving (Marconi *et al.*, 2011; Franken, Swagten, and Koopmans, 2012; Herrero-Albillos *et al.*, 2018). Ratchet effects have generally been studied in overdamped systems; however, additional effects appear when inertial terms are included in the equation of motion (Reimann, 2002; Hänggi and Marchesoni, 2009). Skyrmions, as particle-like objects, represent a natural system in which to study ratchet effects, and their strong nondissipative Magnus force can produce new effects distinct from what was previously observed in other ratchet systems.

The first proposal for a skyrmion ratchet involved a 1D asymmetric substrate studied by Reichhardt, Ray, and Olson Reichhardt (2015) using a particle-based approach. The skyrmions move in two dimensions on the substrate potential illustrated in Fig. 70, which has the form

$$U(x) = U_0[\sin(2\pi x/a) + 0.25 \sin(4\pi x/a)], \quad (16)$$

where a is the substrate periodicity. In the overdamped limit, if an ac drive is applied in the substrate periodicity or x direction, a standard ratchet effect arises in which the particle translates by one or more substrate periods in the easy ($+x$) direction under each ac drive cycle. The depinning threshold is finite for both the easy ($+x$) and hard ($-x$) directions but is larger in the hard direction, so the system acts as a diode in the dc limit. If the ac drive is applied in the perpendicular or y direction in an overdamped system, there is no ratchet effect, since no symmetry is broken. In the case of skyrmions with a finite Magnus force, which move at an angle θ_{SKH} with respect to the driving direction, a ratchet effect can occur even for purely perpendicular ac driving. This is termed a Magnus ratchet effect. Figure 71 shows the velocity component in both the parallel and perpendicular directions for the system in Fig. 70

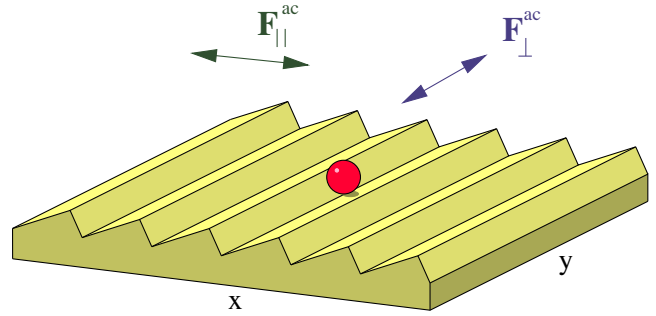


FIG. 70. Schematic of a quasi-one-dimensional asymmetric ratchet potential. A skyrmion (red circle) can be driven by an ac current applied parallel ($F_{\parallel}^{\text{ac}}$; left green arrow) or perpendicular (F_{\perp}^{ac} ; right blue arrow) to the substrate periodicity direction. An overdamped particle would exhibit no ratcheting effect under F_{\perp}^{ac} , but due to the Magnus effect a skyrmion can undergo ratcheting motion under either ac driving direction. From Reichhardt, Ray, and Olson Reichhardt, 2015.

under perpendicular ac driving F_{\perp}^{ac} . The inset of Fig. 71(a) indicates that an overdamped system produces no ratchet effect, while Figs. 71(a)–71(c) illustrate ratcheting motion in samples with various values of $\theta_{\text{SKH}}^{\text{int}}$. The ratchet velocities have well-defined quantized values, and there are regions of ac amplitude over which no ratchet effect occurs. The inset in Fig. 71(c) shows an enlargement of a single step where there

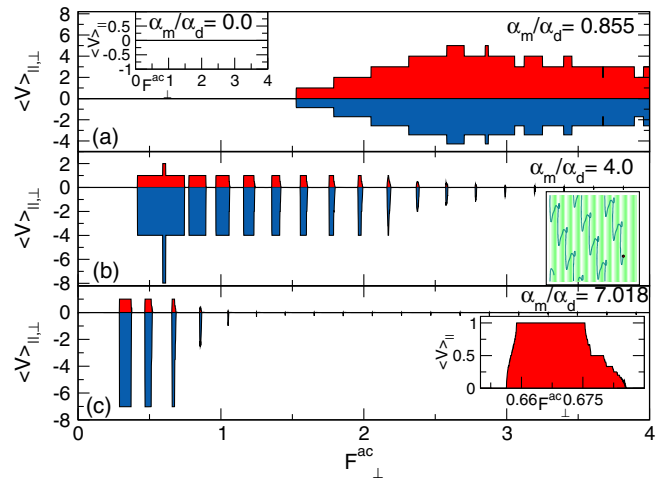


FIG. 71. Particle-based simulations of skyrmion ratchet motion under perpendicular driving F_{\perp}^{ac} on the asymmetric substrate illustrated in Fig. 70. (a)–(c) Velocities parallel ($\langle V_{\parallel} \rangle$; upper red area) and perpendicular ($\langle V_{\perp} \rangle$; lower blue region) to the substrate asymmetry as a function of the ac driving force magnitude F_{\perp}^{ac} for different values of the Magnus-force-to-damping-force ratio α_m/α_d . Ratcheting with quantized velocity values occurs in both the parallel and perpendicular directions above a threshold value of F_{\perp}^{ac} , and there can be drive windows in which no ratcheting motion occurs. Inset of (a): In an overdamped system, no ratcheting occurs in either direction at any value of F_{\perp}^{ac} . Inset of (b): Illustration of the skyrmion trajectory on the $n = 2$ ratcheting step from the main panel. Inset of (c): enlargement of (c) highlighting the presence of fractional velocity steps. From Reichhardt, Ray, and Olson Reichhardt, 2015.

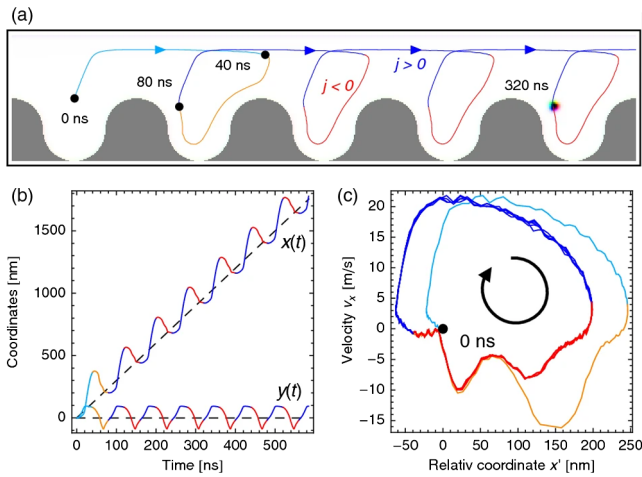


FIG. 72. Thiele-based simulations showing the operation of a ratchet mechanism in a skyrmion racetrack. (a) An asymmetry in the racetrack edge combining with the Magnus force to produce a 2D orbit that translates over time. (b) Plot of the skyrmion position vs time showing deterministic ratcheting motion in the $+x$ direction. (c) Shape of the skyrmion orbit as a function of the x direction velocity v_x vs the relative displacement in x from the average position. From Göbel and Mertig, 2021.

are also fractional ratchet steps. The skyrmions execute complex 2D orbits while ratcheting, as indicated in the inset of Fig. 71(b).

Ma, Olson Reichhardt, and Reichhardt (2017) used particle-based simulations to consider skyrmions interacting with 2D asymmetric arrays in which the pinning sites have a density gradient. They found that, depending on whether the ac drive is applied parallel or perpendicular to the substrate periodicity direction, an entirely new type of ratchet effect called a vector ratchet can appear, in which the direction of skyrmion motion can be tuned by up to 360° by varying the ac drive amplitude.

Göbel and Mertig (2021) performed numerical continuum modeling of skyrmions interacting with a patterned racetrack to show that θ_{SKH} can be used to create a skyrmion ratchet. Figure 72(a) illustrates the racetrack geometry with a ratcheting skyrmion orbit appearing as a function of time under an oscillating drive. The Magnus force is responsible for creating the 2D orbit that is necessary to induce the ratchet effect. Figure 72(b) shows that the skyrmion propagates deterministically as a function of time, while Fig. 72(c) illustrates the skyrmion velocity versus the relative position. Göbel and Mertig explained that the skyrmion ratchet differs from a standard overdamped ratchet due to the fact that the Magnus force allows velocity components to be created perpendicular to the confining force produced by the sample edges. In continuum simulations of skyrmions in asymmetric constricted geometries under an oscillating magnetic field, Migita, Yamada, and Nakatani (2020) showed that the diameter of the skyrmion oscillates as a function of time, thereby producing a unidirectional translation of the skyrmion.

Skyrmion ratchet effects can emerge even in the absence of a substrate. Chen *et al.* (2019) used continuum-based modeling to obtain a skyrmion ratchet effect from biharmonic ac driving. The directed motion appears when the internal

skyrmion modes induce an asymmetric shape oscillation, and it can be controlled by varying the ac drive parameters. Further studies by Chen, Liu, and Zheng (2020) extended this mechanism by coupling the skyrmion to a linear defect in order to take advantage of the speedup effect and create an ultrafast ratchet.

Wang *et al.* (2015) found that under an oscillating field, the changing skyrmion shape can produce directional motion in the absence of a substrate. A similar wiggling skyrmion propagation mechanism based on parametric pumping in an oscillating electric field was studied by Yuan *et al.* (2019). There have also been proposals to drive gyrotropic skyrmion motion by means of steps in the magnetic anisotropy (Liu *et al.*, 2019; Zhou, Mansell, and van Dijken, 2019). These results indicate that in skyrmion systems there are many possible ways in which to achieve the temporal or spatial symmetry breaking required for a ratchet effect. If the skyrmion breathing modes produced by biharmonic drives were coupled to 1D, 2D periodic, or asymmetric periodic substrates, the breathing might strongly enhance the directed motion or make it easier to control.

The rich Magnus-force and internal mode dynamics of skyrmions could produce many other types of ratchets. One effect that has been considered only briefly is collective ratchets. In overdamped systems, collective interactions between particles can produce incommensurate states in which solitons undergo ratcheting motion with a reversible direction (Hänggi and Marchesoni, 2009). If skyrmions of different sizes or species are present, a ratchet could be realized in which one skyrmion size or species is ratcheted more effectively or in a different direction than the other sizes or species. It may be possible to use the internal skyrmion modes to realize propagating skyrmion breathing modes, which would have low dissipation and could be used as another method for transmitting information. The skyrmion Hall angle could be alleviated by creating a propagating breathing mode that can excite neighboring skyrmions and travel over some distance before becoming localized. Experimentally, asymmetric substrates could be created using periodic gradients in the sample thickness, DMI, doping, irradiation, or magnetic field.

E. Coupling skyrmions to other quasiperiodic lattice structures

Periodic pinning can also be created by causing the skyrmions to interact with other topological objects, such as vortices in a type-II superconductor. More generally, there is interest in coupling skyrmions to superconductors in order to control certain topological aspects of the superconductor (Mascot *et al.*, 2021). Several studies have already examined interactions between superconducting vortices and skyrmions (Hals, Schecter, and Rudner, 2016; Baumard *et al.*, 2019; Dahir, Volkov, and Eremin, 2019; Petrović *et al.*, 2021). Figure 73 shows a schematic from Dahir, Volkov, and Eremin (2019) of a chiral ferromagnet coupled to a superconducting thin film through an insulating layer, where the skyrmions produce a vortex-antivortex lattice in the superconductor. Baumard *et al.* (2019) considered a thin-film superconductor in which the skyrmions induce Pearl vortices. The ratio of the number of skyrmions to the number of superconducting

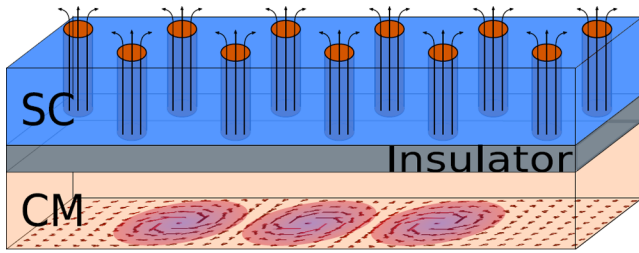


FIG. 73. Schematic of the coupling between a chiral ferromagnet (CM) (lower tan region) containing a skyrmion crystal (lower purple circles) and a superconducting film (SC) (upper blue area). The materials are separated by a thin insulating barrier (center gray section) to ensure that only the magnetic fields from the skyrmion lattice pass into the superconductor. The attractive interaction between vortices and skyrmions generates vortices (upper orange circles) in the superconductor. From Dahir, Volkov, and Eremin, 2019.

vortices can be tuned with a magnetic field, and the superconducting vortex lattice serves as an effective periodic substrate for the skyrmions. If a driving current is applied, the voltage response in the superconductor could be used to detect the skyrmion motion. The effects of either naturally occurring or artificially nanostructured pinning could also be explored. Menezes, Neto *et al.* (2019) calculated the dynamics of skyrmions interacting with a moving superconducting vortex using both micromagnetic simulations and the Thiele equation. In Fig. 74, the skyrmion trajectories in the moving frame exhibit gyrotropic spiraling motion, and in some cases skyrmions are captured by the superconducting vortex core. Recently Palermo *et al.* (2020) demonstrated experimentally that skyrmions could be used to tailor a pinning potential for vortices in a type-II superconductor. Petrović *et al.* (2021) experimentally examined the coupling between chiral magnets and superconductors and found that the stray field of skyrmions can nucleate antivortices in the superconductor. The coupling to the skyrmions generated features in the superconducting vortex critical current. Future directions include analyzing different types of skyrmions

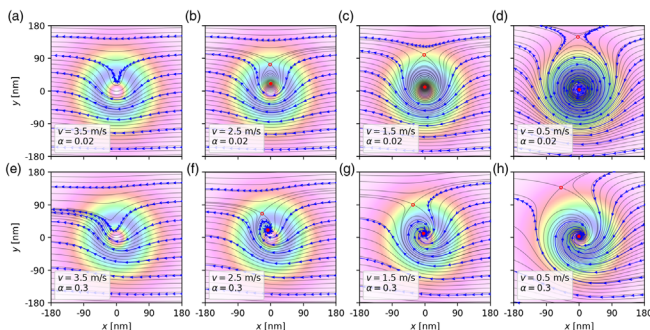


FIG. 74. Micromagnetic calculations (arrows) and Thiele equation calculations (thin lines) of skyrmion trajectories in the moving frame produced by interactions with a moving superconducting vortex. The background coloring represents the z component of the magnetization from the vortex that would appear in the absence of the skyrmion. Open dots represent fixed saddle points and filled dots indicate stable spiral points. From Menezes, Neto *et al.*, 2019.

interacting with superconducting vortices and considering bulk rather than thin-film superconducting vortices.

F. Single skyrmion manipulation

A single particle dragged through a random disordered bath of other particles acts as a local probe of colloidal assemblies (Puertas and Voigtmann, 2014) or superconducting vortices (Kafri, Nelson, and Polkovnikov, 2007; Straver *et al.*, 2008; Auslaender *et al.*, 2009). The velocity-force curves of the probe particle provide information about the behavior of the bulk system, such as changes in the viscosity and pinning force as well as the existence of cutting or entanglement. A similar local probe technique could be applied to a skyrmion system by dragging individual skyrmions with some form of tip or by coupling an individual skyrmion to a driven object. In experimental work along these lines, Ogawa *et al.* (2015) showed that a local optical tip could be used to manipulate magnetic bubbles. X.-G. Wang *et al.* (2020) proposed using an optical tweezer to manipulate skyrmions by optically trapping and dragging the skyrmion. If the tip speed is too fast, the skyrmion could break away from the tip. Other possible local probes include dragging a skyrmion with a magnetic tip or dragging a group of skyrmions with an array of optical traps or magnetic tips.

It is possible that skyrmions could host Majorana fermion states (Yang *et al.*, 2016; Rex, Gornyi, and Mirlin, 2019), so dragging Majorana-containing skyrmions around one another on a patterned substrate could provide a method for creating braided Majorana states for qubit operations. Operations of this type were proposed for superconducting vortex systems with Majorana states in the vortex core (Ma, Reichhardt, and Reichhardt, 2020). The vortices are coupled to a periodic pinning array and a magnetic tip is used to perform a representative set of braiding moves that contain all of the necessary operations for quantum logic gates. A similar approach could be used for skyrmions.

IX. FUTURE DIRECTIONS

One of the major goals for future work on skyrmions interacting with pinning is to develop a comprehensive understanding of the type of pinning produced by different types of defects, such as atoms, groups of atoms, inclusions, missing atoms, or doping. For example, localized or etched defects could repel, attract, or provide a combination of repulsion and attraction for skyrmions. Possible next steps include the creation of detailed substrate patterns for skyrmions that could be used for devices or for studying commensuration effects, skyrmion lattice transitions, and the stability of a wide range of magnetic textures. Nanostructured pinning substrates are known to produce a wealth of phenomena in superconducting vortex systems, and similar effects along with new behaviors could arise for skyrmions coupled to nanostructured arrays. Issues to explore include the use of dynamical substrates that vary over time, created using applied voltages, optical trapping, local temperature gradients, acoustic trapping, or magnetic manipulation. It will also be important to understand how to tailor artificial or quenched disorder to guide skyrmions and create ratchets,

diodes, or transistors for applications. Another question is whether quenched disorder has different effects on different skyrmionlike textures. Studies could address whether anti-ferromagnetic skyrmions or hedgehog states have different pinning and dynamics from skyrmions, as well as the nature of the pinning and dynamics of antiskyrmions, skyrmioniums, or chiral bobbbers. The question of defect dimensionality is also of interest, such as the creation of effectively 3D defects in the form of columnar defects, which could produce novel skyrmion behaviors.

On a more basic science level, the collective dynamics of large assemblies of interacting skyrmions moving under driving or shearing is of interest. Here skyrmions are approached as a new class of system with collective dynamics interacting with quenched disorder that can produce effects not found in other systems. Such behavior could include skyrmion creation and annihilation, structural transitions among different textures, collective gyrotropic modes of motion, and collective internal modes. This is a relatively unexplored field of study. Beyond magnetic skyrmions, many of the same effects could arise for other skyrmionlike textures, such as liquid crystals, 2D electron gases, Bose-Einstein condensates, superconductors, optical systems, and soft matter systems.

X. CONCLUSION

Skyrmions are attracting increasing interest as new materials continue to be identified that support different skyrmion species as well as related topological objects. Since skyrmions can be manipulated or driven by a variety of techniques, the role of pinning or quenched disorder will become a more important aspect of future skyrmion studies. There is already considerable evidence that skyrmions can experience both weak and strong pinning effects depending on the sample thickness or material type, and it has been demonstrated that skyrmions exhibit a rich phenomenology of dynamics, including gyrotropic motion and the skyrmion Hall angle, all of which appear to depend on the nature of the disorder as well as the drive. Owing to the presence of the Magnus force, both individual and collective skyrmion states undergo new types of pinning and depinning phenomena that are distinct from those previously studied in overdamped systems. Pinning and dynamic effects of skyrmions interacting with disordered or ordered substrates are of technological importance for skyrmion applications, and the Magnus effects in the skyrmion system open a new field in equilibrium and nonequilibrium statistical mechanics.

ACKNOWLEDGMENTS

We acknowledge useful comments from Karin Everschor-Sitte, Peter Fischer, Laura Heyderman, Axel Hoffmann, Marc Janoschek, Mathias Kläui, Alexey Kovalev, Shizeng Lin, Samir Lounis, Boris Maiorov, Jan Masell, Achim Rosch, Avadh Saxena, Robert Stamps, Nicolas Porto Vizarrim, and the two anonymous referees. We gratefully acknowledge the support of the U.S. Department of Energy through the LANL/LDRD program for this work. This work was supported by the U.S. Department of Energy through the Los Alamos National

Laboratory. Los Alamos National Laboratory is operated by Triad National Security, LLC, for the National Nuclear Security Administration of the U.S. Department of Energy (Contract No. 892333218NCA000001).

REFERENCES

- Ackerman, P. J., R. P. Trivedi, B. Senyuk, J. van de Lagemaat, and I. I. Smalyukh, 2014, “Two-dimensional skyrmions and other solitonic structures in confinement-frustrated chiral nematics,” *Phys. Rev. E* **90**, 012505.
- Akhtar, W., *et al.*, 2019, “Current-Induced Nucleation and Dynamics of Skyrmions in a Co-Based Heusler Alloy,” *Phys. Rev. Applied* **11**, 034066.
- Akosa, C. A., O. A. Tretiakov, G. Tatara, and A. Manchon, 2018, “Theory of the Topological Spin Hall Effect in Antiferromagnetic Skyrmions: Impact on Current-Induced Motion,” *Phys. Rev. Lett.* **121**, 097204.
- Al Khawaja, U., and H. Stoof, 2001, “Skyrmions in a ferromagnetic Bose-Einstein condensate,” *Nature (London)* **411**, 918.
- Anderson, P. W., and Y. B. Kim, 1964, “Hard superconductivity: Theory of the motion of Abrikosov flux lines,” *Rev. Mod. Phys.* **36**, 39–43.
- Arjana, I. G., I. L. Fernandes, J. Chico, and S. Lounis, 2020, “Subnanoscale atom-by-atom crafting of skyrmion-defect interaction profiles,” *Sci. Rep.* **10**, 14655.
- Auslaender, O. M., L. Luan, E. W. J. Straver, J. E. Hoffman, N. C. Koshnick, E. Zeldov, D. A. Bonn, R. Liang, W. N. Hardy, and K. A. Moler, 2009, “Mechanics of individual isolated vortices in a cuprate superconductor,” *Nat. Phys.* **5**, 35–39.
- Avcı, S., Z. L. Xiao, J. Hua, A. Imre, R. Divan, J. Pearson, U. Welp, W. K. Kwok, and G. W. Crabtree, 2010, “Matching effect and dynamic phases of vortex matter in $\text{Bi}_2\text{Sr}_2\text{CaCu}_2\text{O}_8$ nanoribbon with a periodic array of holes,” *Appl. Phys. Lett.* **97**, 042511.
- Avraham, N., *et al.*, 2001, “‘Inverse’ melting of a vortex lattice,” *Nature (London)* **411**, 451–454.
- Back, C., *et al.*, 2020, “The 2020 skyrmionics roadmap,” *J. Phys. D* **53**, 363001.
- Baert, M., V. V. Metlushko, R. Jonckheere, V. V. Moshchalkov, and Y. Bruynseraede, 1995, “Composite Flux-Line Lattices Stabilized in Superconducting Films by a Regular Array of Artificial Defects,” *Phys. Rev. Lett.* **74**, 3269–3272.
- Bag, B., G. Shaw, S. S. Banerjee, S. Majumdar, A. K. Sood, and A. K. Grover, 2017, “Negative velocity fluctuations and non-equilibrium fluctuation relation for a driven high critical current vortex state,” *Sci. Rep.* **7**, 5531.
- Bak, P., 1982, “Commensurate phases, incommensurate phases and the Devil’s staircase,” *Rep. Prog. Phys.* **45**, 587–629.
- Bak, P., C. Tang, and K. Wiesenfeld, 1988, “Self-organized criticality,” *Phys. Rev. A* **38**, 364–374.
- Balents, L., M. C. Marchetti, and L. Radzihovsky, 1998, “Nonequilibrium steady states of driven periodic media,” *Phys. Rev. B* **57**, 7705–7739.
- Banerjee, S. S., *et al.*, 2000, “Peak effect, plateau effect, and fishtail anomaly: The reentrant amorphization of vortex matter in $2H\text{-NbSe}_2$,” *Phys. Rev. B* **62**, 11838–11845.
- Barker, J., and O. A. Tretiakov, 2016, “Static and Dynamical Properties of Antiferromagnetic Skyrmions in the Presence of Applied Current and Temperature,” *Phys. Rev. Lett.* **116**, 147203.
- Barkhausen, H., 1919, “Two phenomena discovered with the help of the new amplifiers,” *Z. Phys.* **20**, 401.

- Baumard, J., J. Cayssol, F. S. Bergeret, and A. Buzdin, 2019, "Generation of a superconducting vortex via Néel skyrmions," *Phys. Rev. B* **99**, 014511.
- Beg, M., *et al.*, 2017, "Dynamics of skyrmionic states in confined helimagnetic nanostructures," *Phys. Rev. B* **95**, 014433.
- Benassi, A., A. Vanossi, and E. Tosatti, 2011, "Nanofriction in cold ion traps," *Nat. Commun.* **2**, 236.
- Benz, S. P., M. S. Rzechowski, M. Tinkham, and C. J. Lobb, 1990, "Fractional Giant Shapiro Steps and Spatially Correlated Phase Motion in 2D Josephson Arrays," *Phys. Rev. Lett.* **64**, 693–696.
- Berdiyrov, G. R., M. V. Milošević, and F. M. Peeters, 2006, "Novel Commensurability Effects in Superconducting Films with Antidot Arrays," *Phys. Rev. Lett.* **96**, 207001.
- Berger, L., 1970, "Side-jump mechanism for the Hall effect of ferromagnets," *Phys. Rev. B* **2**, 4559–4566.
- Bertotti, G., G. Durin, and A. Magni, 1994, "Scaling aspects of domain wall dynamics and Barkhausen effect in ferromagnetic materials," *J. Appl. Phys.* **75**, 5490.
- Bhattacharya, S., and M. J. Higgins, 1993, "Dynamics of a Disordered Flux Line Lattice," *Phys. Rev. Lett.* **70**, 2617–2620.
- Bhatti, S., and S. N. Piramanayagam, 2019, "Effect of Dzyaloshinskii-Moriya interaction energy confinement on current-driven dynamics of skyrmions," *Phys. Status Solidi RRL* **13**, 1900090.
- Birch, M. T., *et al.*, 2020, "Real-space imaging of confined magnetic skyrmion tubes," *Nat. Commun.* **11**, 1726.
- Blatter, G., M. V. Feigel'man, V. B. Geshkenbein, A. I. Larkin, and V. M. Vinokur, 1994, "Vortices in high-temperature superconductors," *Rev. Mod. Phys.* **66**, 1125–1388.
- Bloom, I., A. C. Marley, and M. B. Weissman, 1993, "Nonequilibrium Dynamics of Discrete Fluctuators in Charge-Density Waves in NbSe₃," *Phys. Rev. Lett.* **71**, 4385–4388.
- Bogdanov, A. N., and C. Panagopoulos, 2020, "Physical foundations and basic properties of magnetic skyrmions," *Nat. Rev. Phys.* **2**, 492–498.
- Bogdanov, A. N., and D. A. Yablonskii, 1989, "Thermodynamically stable 'vortices' in magnetically ordered crystals. The mixed state of magnets," *Sov. Phys. JETP* **68**, 101–103, http://jetp.ras.ru/cgi-bin/dn/e_068_01_0101.pdf.
- Bohlein, T., and C. Bechinger, 2012, "Experimental Observation of Directional Locking and Dynamical Ordering of Colloidal Monolayers Driven across Quasiperiodic Substrates," *Phys. Rev. Lett.* **109**, 058301.
- Bohlein, T., J. Mikhael, and C. Bechinger, 2012, "Observation of kinks and antikinks in colloidal monolayers driven across ordered surfaces," *Nat. Mater.* **11**, 126–130.
- Bömerich, T., L. Heinen, and A. Rosch, 2020, "Skyrmion and tetarton lattices in twisted bilayer graphene," *Phys. Rev. B* **102**, 100408.
- Boulle, O., *et al.*, 2016, "Room-temperature chiral magnetic skyrmions in ultrathin magnetic nanostructures," *Nat. Nanotechnol.* **11**, 449–454.
- Braun, H.-B., 2012, "Topological effects in nanomagnetism: From superparamagnetism to chiral quantum solitons," *Adv. Phys.* **61**, 1–116.
- Braun, O. M., and Y. S. Kivshar, 1998, "Nonlinear dynamics of the Frenkel-Kontorova model," *Phys. Rep.* **306**, 1–108.
- Brearton, R., L. A. Turnbull, J. A. T. Verezhak, G. Balakrishnan, P. D. Hatton, G. van der Laan, and T. Hesjedal, 2021, "Deriving the skyrmion Hall angle from skyrmion lattice dynamics," *Nat. Commun.* **12**, 2723.
- Brey, L., H. A. Fertig, R. Côté, and A. H. MacDonald, 1995, "Skyrme Crystal in a Two-Dimensional Electron Gas," *Phys. Rev. Lett.* **75**, 2562–2565.
- Brown, B. L., U. C. Täuber, and M. Pleimling, 2018, "Effect of the Magnus force on skyrmion relaxation dynamics," *Phys. Rev. B* **97**, 020405.
- Brunner, M., and C. Bechinger, 2002, "Phase Behavior of Colloidal Molecular Crystals on Triangular Light Lattices," *Phys. Rev. Lett.* **88**, 248302.
- Büchler, H. P., G. Blatter, and W. Zwerger, 2003, "Commensurate-Incommensurate Transition of Cold Atoms in an Optical Lattice," *Phys. Rev. Lett.* **90**, 130401.
- Büttner, F., *et al.*, 2015, "Dynamics and inertia of skyrmionic spin structures," *Nat. Phys.* **11**, 225–228.
- Carlson, J. M., J. S. Langer, and B. E. Shaw, 1994, "Dynamics of earthquake faults," *Rev. Mod. Phys.* **66**, 657–670.
- Casiraghi, A., H. Corte-León, V. Vafae, F. Garcia-Sanchez, G. Durin, M. Pasquale, G. Jakob, M. Kläui, and O. Kazakova, 2019, "Individual skyrmion manipulation by local magnetic field gradients," *Commun. Phys.* **2**, 145.
- Castell-Queralt, J., L. Gonzalez-Gomez, N. Del-Valle, A. Sanchez, and C. Navau, 2019, "Accelerating, guiding, and compressing skyrmions by defect rails," *Nanoscale* **11**, 12589–12594.
- Cha, M.-C., and H. A. Fertig, 1994, "Topological defects, orientational order, and depinning of the electron solid in a random potential," *Phys. Rev. B* **50**, 14368–14380.
- Cha, M.-C., and H. A. Fertig, 1995, "Disorder-Induced Phase Transitions in Two-Dimensional Crystals," *Phys. Rev. Lett.* **74**, 4867–4870.
- Cha, M.-C., and H. A. Fertig, 1998, "Peak Effect and the Transition from Elastic to Plastic Depinning," *Phys. Rev. Lett.* **80**, 3851–3854.
- Chai, Y., *et al.*, 2021, "Probe of skyrmion phases and dynamics in MnSi via the magnetoelectric effect in a composite configuration," *Phys. Rev. B* **104**, L100413.
- Chen, Q.-H., and X. Hu, 2003, "Nonequilibrium Phase Transitions of Vortex Matter in Three-Dimensional Layered Superconductors," *Phys. Rev. Lett.* **90**, 117005.
- Chen, R., Y. Li, V. F. Pavlidis, and C. Moutafis, 2020, "Skyrmionic interconnect device," *Phys. Rev. Research* **2**, 043312.
- Chen, W., L. Liu, Y. Ji, and Y. Zheng, 2019, "Skyrmion ratchet effect driven by a biharmonic force," *Phys. Rev. B* **99**, 064431.
- Chen, W., L. Liu, and Y. Zheng, 2020, "Ultrafast Ratchet Dynamics of Skyrmions by Defect Engineering in Materials with Poor Conductivity under Gigahertz Magnetic Fields," *Phys. Rev. Applied* **14**, 064014.
- Choi, H. C., S.-Z. Lin, and J.-X. Zhu, 2016, "Density functional theory study of skyrmion pinning by atomic defects in MnSi," *Phys. Rev. B* **93**, 115112.
- Chudnovsky, E. M., and D. A. Garanin, 2018, "Skyrmion glass in a 2D Heisenberg ferromagnet with quenched disorder," *New J. Phys.* **20**, 033006.
- Civale, L., 1997, "Vortex pinning and creep in high-temperature superconductors with columnar defects," *Supercond. Sci. Technol.* **10**, A11–A28.
- Coey, J. M. D., 2010, *Magnetism and Magnetic Materials* (Cambridge University Press, Cambridge, England).
- Coppersmith, S. N., and P. B. Littlewood, 1986, "Interference Phenomena and Mode Locking in the Model of Deformable Sliding Charge-Density Waves," *Phys. Rev. Lett.* **57**, 1927–1930.
- Cote, P. J., and L. V. Meisel, 1991, "Self-Organized Criticality and the Barkhausen Effect," *Phys. Rev. Lett.* **67**, 1334–1337.
- Crabtree, G. W., and D. R. Nelson, 1997, "Vortex physics in high-temperature superconductors," *Phys. Today* **50**, No. 4, 38–45.
- Cubitt, R., *et al.*, 1993, "Direct observation of magnetic flux lattice melting and decomposition in the high- T_c superconductor Bi_{2.15}Sr_{1.95}CaCu₂O_{8+x}," *Nature (London)* **365**, 407–411.

- Dahir, S. M., A. F. Volkov, and I. M. Eremin, 2019, “Interaction of Skyrmions and Pearl Vortices in Superconductor-Chiral Ferromagnet Heterostructures,” *Phys. Rev. Lett.* **122**, 097001.
- D’Anna, G., P. L. Gammel, H. Safar, G. B. Alers, D. J. Bishop, J. Giapintzakis, and D. M. Ginsberg, 1995, “Vortex-Motion-Induced Voltage Noise in $\text{YBa}_2\text{Cu}_3\text{O}_{7-\delta}$ Single Crystals,” *Phys. Rev. Lett.* **75**, 3521–3524.
- Danneau, R., A. Ayari, D. Rideau, H. Requardt, J. E. Lorenzo, L. Ortega, P. Monceau, R. Currat, and G. Grübel, 2002, “Motional Ordering of a Charge-Density Wave in the Sliding State,” *Phys. Rev. Lett.* **89**, 106404.
- Das, S., *et al.*, 2019, “Observation of room-temperature polar skyrmions,” *Nature (London)* **568**, 368–372.
- Davis, T. J., D. Janoschka, P. Dreher, B. Frank, F.-J. M. zu Heringdorf, and H. Giessen, 2020, “Ultrafast vector imaging of plasmonic skyrmion dynamics with deep subwavelength resolution,” *Science* **368**, eaba6415.
- Denisov, K. S., I. V. Rozhansky, N. S. Averkiev, and E. Lähderanta, 2017, “A nontrivial crossover in topological Hall effect regimes,” *Sci. Rep.* **7**, 17204.
- Denisov, K. S., I. V. Rozhansky, N. S. Averkiev, and E. Lähderanta, 2018, “General theory of the topological Hall effect in systems with chiral spin textures,” *Phys. Rev. B* **98**, 195439.
- Desplat, L., J.-V. Kim, and R. L. Stamps, 2019, “Paths to annihilation of first- and second-order (anti)skyrmions via (anti)meron nucleation on the frustrated square lattice,” *Phys. Rev. B* **99**, 174409.
- Desplat, L., D. Suess, J.-V. Kim, and R. L. Stamps, 2018, “Thermal stability of metastable magnetic skyrmions: Entropic narrowing and significance of internal eigenmodes,” *Phys. Rev. B* **98**, 134407.
- Deutschländer, S., T. Horn, H. Löwen, G. Maret, and P. Keim, 2013, “Two-Dimensional Melting under Quenched Disorder,” *Phys. Rev. Lett.* **111**, 098301.
- Díaz, S. A., C. Reichhardt, D. P. Arovas, A. Saxena, and C. J. O. Reichhardt, 2018, “Avalanches and Criticality in Driven Magnetic Skyrmions,” *Phys. Rev. Lett.* **120**, 117203.
- Díaz, S. A., C. J. O. Reichhardt, D. P. Arovas, A. Saxena, and C. Reichhardt, 2017, “Fluctuations and noise signatures of driven magnetic skyrmions,” *Phys. Rev. B* **96**, 085106.
- Ding, J., X. Yang, and T. Zhu, 2015, “Manipulating current induced motion of magnetic skyrmions in the magnetic nanotrack,” *J. Phys. D* **48**, 115004.
- Di Scala, N., E. Olive, Y. Lansac, Y. Fily, and J. C. Soret, 2012, “The elastic depinning transition of vortex lattices in two dimensions,” *New J. Phys.* **14**, 123027.
- Dobramysl, U., M. Pleimling, and U. C. Täuber, 2014, “Pinning time statistics for vortex lines in disordered environments,” *Phys. Rev. E* **90**, 062108.
- Dobrovolskiy, O. V., and M. Huth, 2015, “Dual cut-off direct current-tunable microwave low-pass filter on superconducting Nb microstrips with asymmetric nanogrooves,” *Appl. Phys. Lett.* **106**, 142601.
- Dohi, T., S. DuttaGupta, S. Fukami, and H. Ohno, 2019, “Formation and current-induced motion of synthetic antiferromagnetic skyrmion bubbles,” *Nat. Commun.* **10**, 5153.
- Dreyfus, R., Y. Xu, T. Still, L. A. Hough, A. G. Yodh, and S. Torquato, 2015, “Diagnosing hyperuniformity in two-dimensional, disordered, jammed packings of soft spheres,” *Phys. Rev. E* **91**, 012302.
- Du, C. H., Y. R. Lee, C. Y. Lo, H. H. Lin, S. L. Chang, M. T. Tang, Y. P. Stetsko, and J. J. Lee, 2006, “Direct measurement of spatial distortions of charge density waves in $\text{K}_{0.3}\text{MoO}_3$,” *Appl. Phys. Lett.* **88**, 241916.
- Du, H., *et al.*, 2018, “Interaction of Individual Skyrmions in a Nanostructured Cubic Chiral Magnet,” *Phys. Rev. Lett.* **120**, 197203.
- Durán, C. A., P. L. Gammel, R. Wolfe, V. J. Fratello, D. J. Bishop, J. P. Rice, and D. M. Ginsberg, 1992, “Real-time imaging of the magnetic flux distribution in superconducting $\text{YBa}_2\text{Cu}_3\text{O}_{7-\delta}$,” *Nature (London)* **357**, 474–477.
- Duzgun, A., C. Nisoli, C. J. O. Reichhardt, and C. Reichhardt, 2020, “Commensurate states and pattern switching via liquid crystal skyrmions trapped in a square lattice,” *Soft Matter* **16**, 3338–3343.
- Duzgun, A., J. V. Selinger, and A. Saxena, 2018, “Comparing skyrmions and merons in chiral liquid crystals and magnets,” *Phys. Rev. E* **97**, 062706.
- Eichhorn, R., P. Reimann, and P. Hänggi, 2002, “Brownian Motion Exhibiting Absolute Negative Mobility,” *Phys. Rev. Lett.* **88**, 190601.
- Ertaş, D., and M. Kardar, 1996, “Anisotropic scaling in threshold critical dynamics of driven directed lines,” *Phys. Rev. B* **53**, 3520–3542.
- Everschor-Sitte, K., J. Masell, R. M. Reeve, and M. Kläui, 2018, “Perspective: Magnetic skyrmions—Overview of recent progress in an active research field,” *J. Appl. Phys.* **124**, 240901.
- Everschor-Sitte, K., and M. Sitte, 2014, “Real-space Berry phases: Skyrmion soccer (invited),” *J. Appl. Phys.* **115**, 172602.
- Fangohr, H., S. J. Cox, and P. A. J. de Groot, 2001, “Vortex dynamics in two-dimensional systems at high driving forces,” *Phys. Rev. B* **64**, 064505.
- Fassbender, J., J. Grenzer, O. Roshchupkina, Y. Choi, J. S. Jiang, and S. D. Bader, 2009, “The effect of ion irradiation and annealing on exchange spring magnets,” *J. Appl. Phys.* **105**, 023902.
- Feigel’man, M. V., V. B. Geshkenbein, A. I. Larkin, and V. M. Vinokur, 1989, “Theory of Collective Flux Creep,” *Phys. Rev. Lett.* **63**, 2303–2306.
- Feilhauer, J., S. Saha, J. Tobik, M. Zelent, L. J. Heyderman, and M. Mruczkiewicz, 2020, “Controlled motion of skyrmions in a magnetic antidot lattice,” *Phys. Rev. B* **102**, 184425.
- Fernandes, I. L., J. Bouaziz, S. Blügel, and S. Lounis, 2018, “Universality of defect-skyrmion interaction profiles,” *Nat. Commun.* **9**, 4395.
- Fernandes, I. L., M. Bouhassoune, and S. Lounis, 2020, “Defect-implantation for the all-electrical detection of non-collinear spin-textures,” *Nat. Commun.* **11**, 1602.
- Fernandes, I. L., J. Chico, and S. Lounis, 2020, “Impurity-dependent gyrotropic motion, deflection and pinning of current-driven ultra-small skyrmions in PdFe/Ir(111) surface,” *J. Phys. Condens. Matter* **32**, 425802.
- Fert, A., V. Cros, and J. Sampaio, 2013, “Skyrmions on the track,” *Nat. Nanotechnol.* **8**, 152–156.
- Fert, A., N. Reyren, and V. Cros, 2017, “Magnetic skyrmions: Advances in physics and potential applications,” *Nat. Rev. Mater.* **2**, 17031.
- Fidler, J., and T. Schrefl, 2000, “Micromagnetic modelling—The current state of the art,” *J. Phys. D* **33**, R135.
- Fily, Y., E. Olive, N. Di Scala, and J. C. Soret, 2010, “Critical behavior of plastic depinning of vortex lattices in two dimensions: Molecular dynamics simulations,” *Phys. Rev. B* **82**, 134519.
- Finocchio, G., F. Büttner, R. Tomasello, M. Carpentieri, and M. Kläui, 2016, “Magnetic skyrmions: From fundamental to applications,” *J. Phys. D* **49**, 423001.
- Fiory, A. T., 1971, “Quantum Interference Effects of a Moving Vortex Lattice in Al Films,” *Phys. Rev. Lett.* **27**, 501–503.
- Fisher, D. S., 1985, “Sliding charge-density waves as a dynamic critical phenomenon,” *Phys. Rev. B* **31**, 1396–1427.

- Fisher, D. S., 1998, “Collective transport in random media: From superconductors to earthquakes,” *Phys. Rep.* **301**, 113–150.
- Fisher, D. S., M. P. A. Fisher, and D. A. Huse, 1991, “Thermal fluctuations, quenched disorder, phase transitions, and transport in type-II superconductors,” *Phys. Rev. B* **43**, 130–159.
- Foster, D., C. Kind, P. J. Ackerman, J.-S. B. Tai, M. R. Dennis, and I. I. Smalyukh, 2019, “Two-dimensional skyrmion bags in liquid crystals and ferromagnets,” *Nat. Phys.* **15**, 655.
- Franken, J. H., H. J. M. Swagten, and B. Koopmans, 2012, “Shift registers based on magnetic domain wall ratchets with perpendicular anisotropy,” *Nat. Nanotechnol.* **7**, 499–503.
- Fujishiro, Y., *et al.*, 2019, “Topological transitions among skyrmion- and hedgehog-lattice states in cubic chiral magnets,” *Nat. Commun.* **10**, 1059.
- Ganguli, S. C., H. Singh, G. Saraswat, R. Ganguly, V. Bagwe, P. Shirage, A. Thamizhavel, and P. Raychaudhuri, 2015, “Disordering of the vortex lattice through successive destruction of positional and orientational order in a weakly pinned $\text{Co}_{0.0075}\text{NbSe}_2$ single crystal,” *Sci. Rep.* **5**, 10613.
- Gao, S., *et al.*, 2020, “Fractional antiferromagnetic skyrmion lattice induced by anisotropic couplings,” *Nature (London)* **586**, 37.
- Garst, M., J. Waizner, and D. Grundler, 2017, “Collective spin excitations of helices and magnetic skyrmions: Review and perspectives of magnonics in non-centrosymmetric magnets,” *J. Phys. D* **50**, 293002.
- Giamarchi, T., and P. Le Doussal, 1995, “Elastic theory of flux lattices in the presence of weak disorder,” *Phys. Rev. B* **52**, 1242–1270.
- Giamarchi, T., and P. Le Doussal, 1996, “Moving Glass Phase of Driven Lattices,” *Phys. Rev. Lett.* **76**, 3408–3411.
- Gilbert, D. A., B. B. Maranville, A. L. Balk, B. J. Kirby, P. Fischer, D. T. Pierce, J. Unguris, J. A. Borchers, and K. Liu, 2015, “Realization of ground-state artificial skyrmion lattices at room temperature,” *Nat. Commun.* **6**, 8462.
- Gilbert, D. A., *et al.*, 2019, “Precipitating ordered skyrmion lattices from helical spaghetti and granular powders,” *Phys. Rev. Mater.* **3**, 014408.
- Giller, D., *et al.*, 1997, “Disorder-Induced Transition to Entangled Vortex Solid in Nd-Ce-Cu-O Crystal,” *Phys. Rev. Lett.* **79**, 2542–2545.
- Goa, P. E., H. Hauglin, M. Baziljevich, E. Il’yashenko, P. L. Gammel, and T. H. Johansen, 2001, “Real-time magneto-optical imaging of vortices in superconducting NbSe_2 ,” *Supercond. Sci. Technol.* **14**, 729–731.
- Göbel, B., J. Henk, and I. Mertig, 2019, “Forming individual magnetic biskyrmions by merging two skyrmions in a centrosymmetric nanodisk,” *Sci. Rep.* **9**, 9521.
- Göbel, B., and I. Mertig, 2021, “Skyrmion ratchet propagation: Utilizing the skyrmion Hall effect in ac racetrack storage devices,” *Sci. Rep.* **11**, 3020.
- Göbel, B., I. Mertig, and O. A. Tretiakov, 2021, “Beyond skyrmions: Review and perspectives of alternative magnetic quasiparticles,” *Phys. Rep.* **895**, 1.
- Gong, X., H. Y. Yuan, and X. R. Wang, 2020, “Current-driven skyrmion motion in granular films,” *Phys. Rev. B* **101**, 064421.
- Gotcheva, V., A. T. J. Wang, and S. Teitel, 2004, “Lattice Gas Dynamics: Application to Driven Vortices in Two Dimensional Superconductors,” *Phys. Rev. Lett.* **92**, 247005.
- Grigorenko, A. N., S. J. Bending, M. J. Van Bael, M. Lange, V. V. Moshchalkov, H. Fangohr, and P. A. J. de Groot, 2003, “Symmetry Locking and Commensurate Vortex Domain Formation in Periodic Pinning Arrays,” *Phys. Rev. Lett.* **90**, 237001.
- Grollier, J., D. Querlioz, K. Y. Camsari, K. Everschor-Sitte, S. Fukami, and M. D. Stiles, 2020, “Neuromorphic spintronics,” *Nat. Electron.* **3**, 360–370.
- Gross, I., *et al.*, 2018, “Skyrmion morphology in ultrathin magnetic films,” *Phys. Rev. Mater.* **2**, 024406.
- Grüner, G., A. Zawadowski, and P. M. Chaikin, 1981, “Nonlinear Conductivity and Noise due to Charge-Density-Wave Depinning in NbSe_3 ,” *Phys. Rev. Lett.* **46**, 511–515.
- Guillamón, I., R. Córdoba, J. Sesé, J. M. De Teresa, M. R. Ibarra, S. Vieira, and H. Suderow, 2014, “Enhancement of long-range correlations in a 2D vortex lattice by an incommensurate 1D disorder potential,” *Nat. Phys.* **10**, 851–856.
- Güngördü, U., R. Nepal, O. A. Tretiakov, K. Belashchenko, and A. A. Kovalev, 2016, “Stability of skyrmion lattices and symmetries of quasi-two-dimensional chiral magnets,” *Phys. Rev. B* **93**, 064428.
- Gutierrez, J., A. V. Silhanek, J. Van de Vondel, W. Gillijns, and V. V. Moshchalkov, 2009, “Transition from turbulent to nearly laminar vortex flow in superconductors with periodic pinning,” *Phys. Rev. B* **80**, 140514.
- Haberkorn, N., B. Maiorov, I. O. Usov, M. Weigand, W. Hirata, S. Miyasaka, S. Tajima, N. Chikumoto, K. Tanabe, and L. Civale, 2012, “Influence of random point defects introduced by proton irradiation on critical current density and vortex dynamics of $\text{Ba}(\text{Fe}_{0.925}\text{Co}_{0.075})_2\text{As}_2$ single crystals,” *Phys. Rev. B* **85**, 014522.
- Hals, K. M. D., M. Schechter, and M. S. Rudner, 2016, “Composite Topological Excitations in Ferromagnet-Superconductor Heterostructures,” *Phys. Rev. Lett.* **117**, 017001.
- Hänggi, P., and F. Marchesoni, 2009, “Artificial Brownian motors: Controlling transport on the nanoscale,” *Rev. Mod. Phys.* **81**, 387–442.
- Hanneken, C., A. Kubetzka, K. von Bergmann, and R. Wiesendanger, 2016, “Pinning and movement of individual nanoscale magnetic skyrmions via defects,” *New J. Phys.* **18**, 055009.
- Harada, K., O. Kamimura, H. Kasai, T. Matsuda, A. Tonomura, and V. V. Moshchalkov, 1996, “Direct observation of vortex dynamics in superconducting films with regular arrays of defects,” *Science* **274**, 1167–1170.
- Harris, J. M., N. P. Ong, R. Gagnon, and L. Taillefer, 1995, “Washboard Frequency of the Moving Vortex Lattice in $\text{YBa}_2\text{Cu}_3\text{O}_{6.93}$ Detected by ac-dc Interference,” *Phys. Rev. Lett.* **74**, 3684–3687.
- Heinze, S., K. von Bergmann, M. Menzel, J. Brede, A. Kubetzka, R. Wiesendanger, G. Bihlmayer, and S. Blügel, 2011, “Spontaneous atomic-scale magnetic skyrmion lattice in two dimensions,” *Nat. Phys.* **7**, 713–718.
- Henderson, W., E. Y. Andrei, M. J. Higgins, and S. Bhattacharya, 1996, “Metastability and Glassy Behavior of a Driven Flux-Line Lattice,” *Phys. Rev. Lett.* **77**, 2077–2080.
- Herrero-Albillos, J., *et al.*, 2018, “2D magnetic domain wall ratchet: The limit of submicromagnetic holes,” *Mater. Des.* **138**, 111–118.
- Hess, H. F., R. B. Robinson, R. C. Dynes, J. M. Valles, and J. V. Waszczak, 1989, “Scanning-Tunneling-Microscope Observation of the Abrikosov Flux Lattice and the Density of States near and inside a Fluxoid,” *Phys. Rev. Lett.* **62**, 214–216.
- Hirata, Y., *et al.*, 2019, “Vanishing skyrmion Hall effect at the angular momentum compensation temperature of a ferrimagnet,” *Nat. Nanotechnol.* **14**, 232–236.
- Hoffmann, M., B. Zimmermann, G. P. Müller, D. Schürhoff, N. S. Kiselev, C. Melcher, and S. Blügel, 2017, “Antiskyrmions stabilized at interfaces by anisotropic Dzyaloshinskii-Moriya interactions,” *Nat. Commun.* **8**, 308.
- Hoshino, S., and N. Nagaosa, 2018, “Theory of the magnetic skyrmion glass,” *Phys. Rev. B* **97**, 024413.

- Hrabec, A., J. Sampaio, M. Belmeguenai, I. Gross, R. Weil, S. M. Chérif, A. Stashkevich, V. Jacques, A. Thiaville, and S. Rohart, 2017, “Current-induced skyrmion generation and dynamics in symmetric bilayers,” *Nat. Commun.* **8**, 15765.
- Hsu, P.-J., *et al.*, 2018, “Inducing skyrmions in ultrathin Fe films by hydrogen exposure,” *Nat. Commun.* **9**, 1571.
- Hu, J., and R. M. Westervelt, 1995, “Collective transport in two-dimensional magnetic bubble arrays,” *Phys. Rev. B* **51**, 17279–17282.
- Huang, P., T. Schonenberger, M. Cantoni, L. Heinen, A. Magrez, A. Rosch, F. Carbone, and H. M. Rønnow, 2020, “Melting of a skyrmion lattice to a skyrmion liquid via a hexatic phase,” *Nat. Nanotechnol.* **15**, 761.
- Hwa, T., P. Le Doussal, D. R. Nelson, and V. M. Vinokur, 1993, “Flux Pinning and Forced Vortex Entanglement by Splayed Columnar Defects,” *Phys. Rev. Lett.* **71**, 3545–3548.
- Ikka, M., A. Takeuchi, and M. Mochizuki, 2018, “Resonance modes and microwave-driven translational motion of a skyrmion crystal under an inclined magnetic field,” *Phys. Rev. B* **98**, 184428.
- Iwasaki, J., W. Koshibae, and N. Nagaosa, 2014, “Colossal spin transfer torque effect on skyrmion along the edge,” *Nano Lett.* **14**, 4432–4437.
- Iwasaki, J., M. Mochizuki, and N. Nagaosa, 2013a, “Current-induced skyrmion dynamics in constricted geometries,” *Nat. Nanotechnol.* **8**, 742–747.
- Iwasaki, J., M. Mochizuki, and N. Nagaosa, 2013b, “Universal current-velocity relation of skyrmion motion in chiral magnets,” *Nat. Commun.* **4**, 1463.
- Jani, H., *et al.*, 2021, “Antiferromagnetic half-skyrmions and bimerons at room temperature,” *Nature (London)* **590**, 74.
- Jena, J., B. Göbel, T. Ma, V. Kumar, R. Saha, I. Mertig, C. Felser, and S. S. P. Parkin, 2020, “Elliptical Bloch skyrmion chiral twins in an antiskyrmion system,” *Nat. Commun.* **11**, 1115.
- Jensen, H. J., A. Brass, and A. J. Berlinsky, 1988, “Lattice Deformations and Plastic Flow through Bottlenecks in a Two-Dimensional Model for Flux Pinning in Type-II Superconductors,” *Phys. Rev. Lett.* **60**, 1676–1679.
- Jiang, W., G. Chen, K. Liu, J. Zang, S. G. E. te Velthuis, and A. Hoffmann, 2017, “Skyrmions in magnetic multilayers,” *Phys. Rep.* **704**, 1–49.
- Jiang, W., *et al.*, 2015, “Blowing magnetic skyrmion bubbles,” *Science* **349**, 283–286.
- Jiang, W., *et al.*, 2017, “Direct observation of the skyrmion Hall effect,” *Nat. Phys.* **13**, 162–169.
- Jin, Z., *et al.*, 2020, “Dynamics of antiferromagnetic skyrmions in the absence or presence of pinning defects,” *Phys. Rev. B* **102**, 054419.
- Jonietz, F., *et al.*, 2010, “Spin transfer torques in MnSi at ultralow current densities,” *Science* **330**, 1648–1651.
- Juge, R., *et al.*, 2019, “Current-Driven Skyrmion Dynamics and Drive-Dependent Skyrmion Hall Effect in an Ultrathin Film,” *Phys. Rev. Applied* **12**, 044007.
- Juge, R., *et al.*, 2021, “Helium ions put magnetic skyrmions on the track,” *Nano Lett.* **21**, 2989–2996.
- Juniper, M. P. N., A. V. Straube, R. Besseling, D. G. A. L. Aarts, and R. P. A. Dullens, 2015, “Microscopic dynamics of synchronization in driven colloids,” *Nat. Commun.* **6**, 7187.
- Kafri, Y., D. R. Nelson, and A. Polkovnikov, 2007, “Unzipping vortices in type-II superconductors,” *Phys. Rev. B* **76**, 144501.
- Kagawa, F., H. Oike, W. Koshibae, A. Kikkawa, Y. Okamura, Y. Taguchi, N. Nagaosa, and Y. Tokura, 2017, “Current-induced viscoelastic topological unwinding of metastable skyrmion strings,” *Nat. Commun.* **8**, 1332.
- Kang, W., Y. Huang, C. Zheng, W. Lv, N. Lei, Y. Zhang, X. Zhang, Y. Zhou, and W. Zhao, 2016, “Voltage controlled magnetic skyrmion motion for racetrack memory,” *Sci. Rep.* **6**, 23164.
- Kardar, M., 1998, “Nonequilibrium dynamics of interfaces and lines,” *Phys. Rep.* **301**, 85–112.
- Karube, K., *et al.*, 2016, “Robust metastable skyrmions and their triangular-square lattice structural transition in a high-temperature chiral magnet,” *Nat. Mater.* **15**, 1237–1242.
- Karube, K., *et al.*, 2018, “Disordered skyrmion phase stabilized by magnetic frustration in a chiral magnet,” *Sci. Adv.* **4**, eaar7043.
- Kemmler, M., C. Gürlich, A. Sterck, H. Pöhler, M. Neuhaus, M. Siegel, R. Kleiner, and D. Koelle, 2006, “Commensurability Effects in Superconducting Nb Films with Quasiperiodic Pinning Arrays,” *Phys. Rev. Lett.* **97**, 147003.
- Kent, N., *et al.*, 2021, “Creation and observation of hopfions in magnetic multilayer systems,” *Nat. Commun.* **12**, 1562.
- Kim, J.-V., and M.-W. Yoo, 2017, “Current-driven skyrmion dynamics in disordered films,” *Appl. Phys. Lett.* **110**, 132404.
- Kindervater, J., *et al.*, 2020, “Evolution of magnetocrystalline anisotropies in $\text{Mn}_{1-x}\text{Fe}_x\text{Si}$ and $\text{Mn}_{1-x}\text{Co}_x\text{Si}$ as inferred from small-angle neutron scattering and bulk properties,” *Phys. Rev. B* **101**, 104406.
- Kirkpatrick, S., C. D. Gelatt, and M. P. Vecchi, 1983, “Optimization by simulated annealing,” *Science* **220**, 671–680.
- Klein, T., I. Joumard, S. Blanchard, J. Marcus, R. Cubitt, T. Giamarchi, and P. Le Doussal, 2001, “A Bragg glass phase in the vortex lattice of a type II superconductor,” *Nature (London)* **413**, 404–406.
- Klongcheongsan, T., T. J. Bullard, and U. C. Täuber, 2010, “Nonequilibrium steady states of driven magnetic flux lines in disordered type-II superconductors,” *Supercond. Sci. Technol.* **23**, 025023.
- Kolesnikov, A. G., M. E. Stebliy, A. S. Samardak, and A. V. Ognev, 2018, “Skyrmionium—High velocity without the skyrmion Hall effect,” *Sci. Rep.* **8**, 16966.
- Kolton, A. B., D. Domínguez, and N. Grønbech-Jensen, 1999, “Hall Noise and Transverse Freezing in Driven Vortex Lattices,” *Phys. Rev. Lett.* **83**, 3061–3064.
- Kolton, A. B., R. Exartier, L. F. Cugliandolo, D. Domínguez, and N. Grønbech-Jensen, 2002, “Effective Temperature in Driven Vortex Lattices with Random Pinning,” *Phys. Rev. Lett.* **89**, 227001.
- Kong, L., and J. Zang, 2013, “Dynamics of an Insulating Skyrmion under a Temperature Gradient,” *Phys. Rev. Lett.* **111**, 067203.
- Korda, P. T., M. B. Taylor, and D. G. Grier, 2002, “Kinetically Locked-In Colloidal Transport in an Array of Optical Tweezers,” *Phys. Rev. Lett.* **89**, 128301.
- Koshelev, A. E., and V. M. Vinokur, 1994, “Dynamic Melting of the Vortex Lattice,” *Phys. Rev. Lett.* **73**, 3580–3583.
- Koshibae, W., and N. Nagaosa, 2018, “Theory of current-driven skyrmions in disordered magnets,” *Sci. Rep.* **8**, 6328.
- Koshibae, W., and N. Nagaosa, 2019, “Dynamics of skyrmion in disordered chiral magnet of thin film form,” *Sci. Rep.* **9**, 5111.
- Kosterlitz, J. M., and D. J. Thouless, 1973, “Ordering, metastability and phase-transitions in two-dimensional systems,” *J. Phys. C* **6**, 1181–1203.
- Koushik, R., S. Kumar, K. R. Amin, M. Mondal, J. Jesudasan, A. Bid, P. Raychaudhuri, and A. Ghosh, 2013, “Correlated Conductance Fluctuations close to the Berezinskii-Kosterlitz-Thouless Transition in Ultrathin NbN Films,” *Phys. Rev. Lett.* **111**, 197001.
- Kovalev, A. A., 2014, “Skyrmionic spin Seebeck effect via dissipative thermomagnonic torques,” *Phys. Rev. B* **89**, 241101.
- Kovalev, A. A., and S. Sandhoefner, 2018, “Skyrmions and anti-skyrmions in quasi-two-dimensional magnets,” *Front. Phys.* **6**, 98.

- Kruchkov, A. J., J. S. White, M. Bartkowiak, I. Živković, A. Magrez, and H. M. Rønnow, 2018, “Direct electric field control of the skyrmion phase in a magnetoelectric insulator,” *Sci. Rep.* **8**, 10466.
- Kumar, M., A. Laitinen, and P. Hakonen, 2018, “Unconventional fractional quantum Hall states and Wigner crystallization in suspended Corbino graphene,” *Nat. Commun.* **9**, 2776.
- Lai, P., G. P. Zhao, H. Tang, N. Ran, S. Q. Wu, J. Xia, X. Zhang, and Y. Zhou, 2017, “An improved racetrack structure for transporting a skyrmion,” *Sci. Rep.* **7**, 45330.
- Latimer, M. L., G. R. Berdiyrov, Z. L. Xiao, F. M. Peeters, and W. K. Kwok, 2013, “Realization of Artificial Ice Systems for Magnetic Vortices in a Superconducting MoGe Thin Film with Patterned Nanostructures,” *Phys. Rev. Lett.* **111**, 067001.
- Lavergne, F. A., A. Curran, D. G. A. L. Aarts, and R. P. A. Dullens, 2018, “Dislocation-controlled formation and kinetics of grain boundary loops in two-dimensional crystals,” *Proc. Natl. Acad. Sci. U.S.A.* **115**, 6922–6927.
- Lee, C. S., B. Jankó, I. Derényi, and A. L. Barabási, 1999, “Reducing vortex density in superconductors using the ‘ratchet effect,’” *Nature (London)* **400**, 337–340.
- Legrand, W., D. Maccariello, N. Reyren, K. Garcia, C. Moutafis, C. Moreau-Luchaire, S. Collin, K. Bouzouhane, V. Cros, and A. Fert, 2017, “Room-temperature current-induced generation and motion of sub-100 nm skyrmions,” *Nano Lett.* **17**, 2703–2712.
- Leliaert, J., M. Dvornik, J. Mulkers, J. De Clercq, M. V. Milošević, and B. Van Waeyenberge, 2018, “Fast micromagnetic simulations on GPU—recent advances made with mumax(3),” *J. Phys. D* **51**, 123002.
- Leliaert, J., P. Gypens, M. V. Milošević, B. Van Waeyenberge, and J. Mulkers, 2019, “Coupling of the skyrmion velocity to its breathing mode in periodically notched nanotracks,” *J. Phys. D* **52**, 024003.
- Leonov, A. O., and M. Mostovoy, 2015, “Multiply periodic states and isolated skyrmions in an anisotropic frustrated magnet,” *Nat. Commun.* **6**, 8275.
- Leonov, A. O., and C. Pappas, 2019, “Skyrmion clusters and conical droplets in bulk helimagnets with cubic anisotropy,” *Phys. Rev. B* **99**, 144410.
- Leroux, M., M. J. Stolt, S. Jin, D. V. Pete, C. Reichhardt, and B. Maiorov, 2018, “Skyrmion lattice topological Hall effect near room temperature,” *Sci. Rep.* **8**, 15510.
- Le Thien, Q., D. McDermott, C. J. O. Reichhardt, and C. Reichhardt, 2017, “Enhanced pinning for vortices in hyperuniform pinning arrays and emergent hyperuniform vortex configurations with quenched disorder,” *Phys. Rev. B* **96**, 094516.
- Levy, J., and M. S. Sherwin, 1991, “Poincaré Sections of Charge-Density-Wave Dynamics: Mode Locking,” *Phys. Rev. Lett.* **67**, 2846–2849.
- Li, B., and A. A. Kovalev, 2020, “Magnon Landau Levels and Spin Responses in Antiferromagnets,” *Phys. Rev. Lett.* **125**, 257201.
- Li, S., W. Kang, X. Zhang, T. Nie, Y. Zhou, K. L. Wang, and W. Zhao, 2021, “Magnetic skyrmions for unconventional computing,” *Mater. Horiz.* **8**, 854–868.
- Li, S., J. Xia, X. Zhang, M. Ezawa, W. Kang, X. Liu, Y. Zhou, and W. Zhao, 2018, “Dynamics of a magnetic skyrmionium driven by spin waves,” *Appl. Phys. Lett.* **112**, 142404.
- Li, Z.-A., F. Zheng, A. H. Tavabi, J. Caron, C. Jin, H. Du, A. Kovács, M. Tian, M. Farle, and R. E. Dunin-Borkowski, 2017, “Magnetic skyrmion formation at lattice defects and grain boundaries studied by quantitative off-axis electron holography,” *Nano Lett.* **17**, 1395–1401.
- Liang, D., J. P. DeGrave, M. J. Stolt, Y. Tokura, and S. Jin, 2015, “Current-driven dynamics of skyrmions stabilized in MnSi nanowires revealed by topological Hall effect,” *Nat. Commun.* **6**, 8217.
- Liang, X., G. Zhao, L. Shen, J. Xia, L. Zhao, X. Zhang, and Y. Zhou, 2019, “Dynamics of an antiferromagnetic skyrmion in a racetrack with a defect,” *Phys. Rev. B* **100**, 144439.
- Libál, A., C. J. Olson Reichhardt, and C. Reichhardt, 2009, “Creating Artificial Ice States Using Vortices in Nanostructured Superconductors,” *Phys. Rev. Lett.* **102**, 237004.
- Lin, N. S., T. W. Heitmann, K. Yu, B. L. T. Plourde, and V. R. Misko, 2011, “Rectification of vortex motion in a circular ratchet channel,” *Phys. Rev. B* **84**, 144511.
- Lin, S.-Z., 2016, “Edge instability in a chiral stripe domain under an electric current and skyrmion generation,” *Phys. Rev. B* **94**, 020402.
- Lin, S.-Z., and C. D. Batista, 2018, “Face Centered Cubic and Hexagonal Close Packed Skyrmion Crystals in Centrosymmetric Magnets,” *Phys. Rev. Lett.* **120**, 077202.
- Lin, S.-Z., C. D. Batista, C. Reichhardt, and A. Saxena, 2014, “ac Current Generation in Chiral Magnetic Insulators and Skyrmion Motion Induced by the Spin Seebeck Effect,” *Phys. Rev. Lett.* **112**, 187203.
- Lin, S.-Z., and S. Hayami, 2016, “Ginzburg-Landau theory for skyrmions in inversion-symmetric magnets with competing interactions,” *Phys. Rev. B* **93**, 064430.
- Lin, S.-Z., C. Reichhardt, C. D. Batista, and A. Saxena, 2013a, “Driven Skyrmions and Dynamical Transitions in Chiral Magnets,” *Phys. Rev. Lett.* **110**, 207202.
- Lin, S.-Z., C. Reichhardt, C. D. Batista, and A. Saxena, 2013b, “Particle model for skyrmions in metallic chiral magnets: Dynamics, pinning, and creep,” *Phys. Rev. B* **87**, 214419.
- Lin, S.-Z., and A. Saxena, 2016, “Dynamics of Dirac strings and monopolelike excitations in chiral magnets under a current drive,” *Phys. Rev. B* **93**, 060401.
- Lin, S.-Z., J.-X. Zhu, and A. Saxena, 2019, “Kelvin modes of a skyrmion line in chiral magnets and the associated magnon transport,” *Phys. Rev. B* **99**, 140408.
- Litzius, K., *et al.*, 2017, “Skyrmion Hall effect revealed by direct time-resolved x-ray microscopy,” *Nat. Phys.* **13**, 170–175.
- Litzius, K., *et al.*, 2020, “The role of temperature and drive current in skyrmion dynamics,” *Nat. Electron.* **3**, 30–36.
- Liu, L., W. Chen, and Y. Zheng, 2020, “Current-Driven Skyrmion Motion beyond Linear Regime: Interplay between Skyrmion Transport and Deformation,” *Phys. Rev. Applied* **14**, 024077.
- Liu, Y., W. Hou, X. Han, and J. Zang, 2020, “Three-Dimensional Dynamics of a Magnetic Hopfion Driven by Spin Transfer Torque,” *Phys. Rev. Lett.* **124**, 127204.
- Liu, Y., N. Lei, C. Wang, X. Zhang, W. Kang, D. Zhu, Y. Zhou, X. Liu, Y. Zhang, and W. Zhao, 2019, “Voltage-Driven High-Speed Skyrmion Motion in a Skyrmion-Shift Device,” *Phys. Rev. Applied* **11**, 014004.
- Liu, Y.-H., and Y.-Q. Li, 2013, “A mechanism to pin skyrmions in chiral magnets,” *J. Phys. Condens. Matter* **25**, 076005.
- Lonsky, M., and A. Hoffmann, 2020, “Dynamic excitations of chiral magnetic textures,” *APL Mater.* **8**, 100903.
- Loreto, R. P., X. Zhang, Y. Zhou, M. Ezawa, X. Liu, and C. I. L. de Araujo, 2019, “Manipulation of magnetic skyrmions in a locally modified synthetic antiferromagnetic racetrack,” *J. Magn. Magn. Mater.* **482**, 155–159.
- Loudon, J. C., A. O. Leonov, A. N. Bogdanov, M. Ciomaga Hatnean, and G. Balakrishnan, 2018, “Direct observation of attractive skyrmions and skyrmion clusters in the cubic helimagnet Cu₂OSeO₃,” *Phys. Rev. B* **97**, 134403.
- Luo, M.-B., and X. Hu, 2007, “Depinning and Creep Motion in Glass States of Flux Lines,” *Phys. Rev. Lett.* **98**, 267002.

- Luo, S., M. Song, X. Li, Y. Zhang, J. Hong, X. Yang, X. Zou, N. Xu, and L. You, 2018, “Reconfigurable skyrmion logic gates,” *Nano Lett.* **18**, 1180–1184.
- Luo, S., and L. You, 2021, “Skyrmion devices for memory and logic applications,” *APL Mater.* **9**, 050901.
- Luo, Y., S.-Z. Lin, D. M. Fobes, Z. Liu, E. D. Bauer, J. B. Betts, A. Migliori, J. D. Thompson, M. Janoschek, and B. Maiorov, 2018, “Anisotropic magnetocrystalline coupling of the skyrmion lattice in MnSi,” *Phys. Rev. B* **97**, 104423.
- Luo, Y., *et al.*, 2020, “Skyrmion lattice creep at ultra-low current densities,” *Commun. Mater.* **1**, 83.
- Ma, C., X. Zhang, J. Xia, M. Ezawa, W. Jiang, T. Ono, S. N. Piramanayagam, A. Morisako, Y. Zhou, and X. Liu, 2019, “Electric field-induced creation and directional motion of domain walls and skyrmion bubbles,” *Nano Lett.* **19**, 353–361.
- Ma, F., C. Reichhardt, W. Gan, C. J. O. Reichhardt, and W. S. Lew, 2016, “Emergent geometric frustration of artificial magnetic skyrmion crystals,” *Phys. Rev. B* **94**, 144405.
- Ma, X., C. J. Olson Reichhardt, and C. Reichhardt, 2017, “Reversible vector ratchets for skyrmion systems,” *Phys. Rev. B* **95**, 104401.
- Ma, X., C. J. O. Reichhardt, and C. Reichhardt, 2020, “Braiding Majorana fermions and creating quantum logic gates with vortices on a periodic pinning structure,” *Phys. Rev. B* **101**, 024514.
- Maccariello, D., W. Legrand, N. Reyren, K. Garcia, K. Bouzehouane, S. Collin, V. Cros, and A. Fert, 2018, “Electrical detection of single magnetic skyrmions in metallic multilayers at room temperature,” *Nat. Nanotechnol.* **13**, 233–237.
- MacDonald, M. P., G. C. Spalding, and K. Dholakia, 2003, “Microfluidic sorting in an optical lattice,” *Nature (London)* **426**, 421–424.
- MacKinnon, C. R., S. Lepadatu, T. Mercer, and P. R. Bissell, 2020, “Role of an additional interfacial spin-transfer torque for current-driven skyrmion dynamics in chiral magnetic layers,” *Phys. Rev. B* **102**, 214408.
- Mankalale, M. G., Z. Zhao, J.-P. Wang, and S. S. Sapatnekar, 2019, “SkyLogic—A proposal for a skyrmion logic device,” *IEEE Trans. Electron Devices* **66**, 1990–1996.
- Marchiori, E., P. J. Curran, J. Kim, N. Satchell, G. Burnell, and S. J. Bending, 2017, “Reconfigurable superconducting vortex pinning potential for magnetic disks in hybrid structures,” *Sci. Rep.* **7**, 45182.
- Marconi, V. I., A. B. Kolton, J. A. Capitán, J. A. Cuesta, A. Pérez-Junquera, M. Vélez, J. I. Martín, and J. M. R. Parrondo, 2011, “Crossed-ratchet effects and domain wall geometrical pinning,” *Phys. Rev. B* **83**, 214403.
- Marley, A. C., M. J. Higgins, and S. Bhattacharya, 1995, “Flux Flow Noise and Dynamical Transitions in a Flux Line Lattice,” *Phys. Rev. Lett.* **74**, 3029–3032.
- Marrows, C. H., and K. Zeissler, 2021, “Perspective on skyrmion spintronics,” *Appl. Phys. Lett.* **119**, 250502.
- Martín, J. I., M. Vélez, J. Nogués, and I. K. Schuller, 1997, “Flux Pinning in a Superconductor by an Array of Submicrometer Magnetic Dots,” *Phys. Rev. Lett.* **79**, 1929–1932.
- Martinez, J. C., W. S. Lew, W. L. Gan, and M. B. A. Jalil, 2018, “Theory of current-induced skyrmion dynamics close to a boundary,” *J. Magn. Magn. Mater.* **465**, 685–691.
- Martinoli, P., O. Daldini, C. Leemann, and E. Stocker, 1975, “ac quantum interference in superconducting films with periodically modulated thickness,” *Solid State Commun.* **17**, 205–209.
- Mascot, E., J. Bedow, M. Graham, S. Rachel, and D. K. Morr, 2021, “Topological superconductivity in skyrmion lattices,” *npj Quantum Mater.* **6**, 6.
- Masell, J., D. R. Rodrigues, B. F. McKeever, and K. Everschor-Sitte, 2020, “Spin-transfer torque driven motion, deformation, and instabilities of magnetic skyrmions at high currents,” *Phys. Rev. B* **101**, 214428.
- Matsuda, T., K. Harada, H. Kasai, O. Kamimura, and A. Tonomura, 1996, “Observation of dynamic interaction of vortices with pinning centers by Lorentz microscopy,” *Science* **271**, 1393–1395.
- Matsumoto, T., Y.-G. So, Y. Kohno, H. Sawada, Y. Ikuhara, and N. Shibata, 2016a, “Direct observation of $\Sigma 7$ domain boundary core structure in magnetic skyrmion lattice,” *Sci. Adv.* **2**, e1501280.
- Matsumoto, T., Y.-G. So, Y. Kohno, H. Sawada, R. Ishikawa, Y. Ikuhara, and N. Shibata, 2016b, “Jointed magnetic skyrmion lattices at a small-angle grain boundary directly visualized by advanced electron microscopy,” *Sci. Rep.* **6**, 35880.
- Mehta, A. P., A. C. Mills, K. A. Dahmen, and J. P. Sethna, 2002, “Universal pulse shape scaling function and exponents: Critical test for avalanche models applied to Barkhausen noise,” *Phys. Rev. E* **65**, 046139.
- Menezes, R. M., J. Mulkers, C. C. de Souza Silva, and M. V. Milošević, 2019, “Deflection of ferromagnetic and antiferromagnetic skyrmions at heterochiral interfaces,” *Phys. Rev. B* **99**, 104409.
- Menezes, R. M., J. F. S. Neto, C. C. de Souza Silva, and M. V. Milošević, 2019, “Manipulation of magnetic skyrmions by superconducting vortices in ferromagnet-superconductor heterostructures,” *Phys. Rev. B* **100**, 014431.
- Merithew, R. D., M. W. Rabin, M. B. Weissman, M. J. Higgins, and S. Bhattacharya, 1996, “Persistent Metastable States in Vortex Flow at the Peak Effect in NbSe₂,” *Phys. Rev. Lett.* **77**, 3197–3199.
- Migita, K., K. Yamada, and Y. Nakatani, 2020, “Controlling skyrmion motion in an angelfish-type racetrack memory by an ac magnetic field,” *Appl. Phys. Express* **13**, 073003.
- Mikhael, J., J. Roth, L. Helden, and C. Bechinger, 2008, “Archimedean-like tiling on decagonal quasicrystalline surfaces,” *Nature (London)* **454**, 501–504.
- Milde, P., *et al.*, 2013, “Unwinding of a skyrmion lattice by magnetic monopoles,” *Science* **340**, 1076–1080.
- Milošević, M. V., G. R. Berdiyrov, and F. M. Peeters, 2007, “Fluxonic cellular automata,” *Appl. Phys. Lett.* **91**, 212501.
- Mirebeau, I., N. Martin, M. Deutsch, L. J. Bannenberg, C. Pappas, G. Chaboussant, R. Cubitt, C. Decorse, and A. O. Leonov, 2018, “Spin textures induced by quenched disorder in a reentrant spin glass: Vortices versus ‘frustrated’ skyrmions,” *Phys. Rev. B* **98**, 014420.
- Mochizuki, M., X. Z. Yu, S. Seki, N. Kanazawa, W. Koshibae, J. Zang, M. Mostovoy, Y. Tokura, and N. Nagaosa, 2014, “Thermally driven ratchet motion of a skyrmion microcrystal and topological magnon Hall effect,” *Nat. Mater.* **13**, 241–246.
- Mohan, S., J. Sinha, S. S. Banerjee, A. K. Sood, S. Ramakrishnan, and A. K. Grover, 2009, “Large Low-Frequency Fluctuations in the Velocity of a Driven Vortex Lattice in a Single Crystal of 2H-NbSe₂ Superconductor,” *Phys. Rev. Lett.* **103**, 167001.
- Montoya, S. A., R. Tolley, I. Gilbert, S.-G. Je, M.-Y. Im, and E. E. Fullerton, 2018, “Spin-orbit torque induced dipole skyrmion motion at room temperature,” *Phys. Rev. B* **98**, 104432.
- Moon, K., R. T. Scalettar, and G. T. Zimányi, 1996, “Dynamical Phases of Driven Vortex Systems,” *Phys. Rev. Lett.* **77**, 2778–2781.
- Moreau-Luchaire, C., *et al.*, 2016, “Additive interfacial chiral interaction in multilayers for stabilization of small individual skyrmions at room temperature,” *Nat. Nanotechnol.* **11**, 444–448.
- Moretti, P., and M.-C. Miguel, 2009, “Irreversible flow of vortex matter: Polycrystal and amorphous phases,” *Phys. Rev. B* **80**, 224513.
- Morin, A., N. Desreumaux, J.-B. Caussin, and D. Bartolo, 2017, “Distortion and destruction of colloidal flocks in disordered environments,” *Nat. Phys.* **13**, 63–67.

- Mühlbauer, S., B. Binz, F. Jonietz, C. Pfleiderer, A. Rosch, A. Neubauer, R. Georgii, and P. Böni, 2009, “Skyrmion lattice in a chiral magnet,” *Science* **323**, 915–919.
- Müller, J., 2017, “Magnetic skyrmions on a two-lane racetrack,” *New J. Phys.* **19**, 025002.
- Müller, J., J. Rajeswari, P. Huang, Y. Murooka, H. M. Rønnow, F. Carbone, and A. Rosch, 2017, “Magnetic Skyrmions and Skyrmion Clusters in the Helical Phase of Cu_2OSeO_3 ,” *Phys. Rev. Lett.* **119**, 137201.
- Müller, J., and A. Rosch, 2015, “Capturing of a magnetic skyrmion with a hole,” *Phys. Rev. B* **91**, 054410.
- Nagaosa, N., and Y. Tokura, 2013, “Topological properties and dynamics of magnetic skyrmions,” *Nat. Nanotechnol.* **8**, 899–911.
- Nakajima, H., A. Kotani, M. Mochizuki, K. Harada, and S. Mori, 2017, “Formation process of skyrmion lattice domain boundaries: The role of grain boundaries,” *Appl. Phys. Lett.* **111**, 192401.
- Nakajima, T., H. Oike, A. Kikkawa, E. P. Gilbert, N. Booth, K. Kakurai, Y. Taguchi, Y. Tokura, F. Kagawa, and T. Arima, 2017, “Skyrmion lattice structural transition in MnSi,” *Sci. Adv.* **3**, e1602562.
- Nattermann, T., and S. Scheidl, 2000, “Vortex-glass phases in type-II superconductors,” *Adv. Phys.* **49**, 607–704.
- Navau, C., N. Del-Valle, and A. Sanchez, 2016, “Analytical trajectories of skyrmions in confined geometries: Skyrmionic racetracks and nano-oscillators,” *Phys. Rev. B* **94**, 184104.
- Navau, C., N. Del-Valle, and A. Sanchez, 2018, “Interaction of isolated skyrmions with point and linear defects,” *J. Magn. Magn. Mater.* **465**, 709–715.
- Nayak, A. K., V. Kumar, T. Ma, P. Werner, E. Pippel, R. Sahoo, F. Damay, U. K. Röbller, C. Felser, and S. S. P. Parkin, 2017, “Magnetic antiskyrmions above room temperature in tetragonal Heusler materials,” *Nature (London)* **548**, 561–566.
- Nelson, D. R., 1983, “Reentrant melting in solid films with quenched random impurities,” *Phys. Rev. B* **27**, 2902–2914.
- Nelson, D. R., 1988, “Vortex Entanglement in High- T_c Superconductors,” *Phys. Rev. Lett.* **60**, 1973–1976.
- Nelson, D. R., and B. I. Halperin, 1979, “Dislocation-mediated melting in two dimensions,” *Phys. Rev. B* **19**, 2457–2484.
- Nepal, R., U. Güngördü, and A. A. Kovalev, 2018, “Magnetic skyrmion bubble motion driven by surface acoustic waves,” *Appl. Phys. Lett.* **112**, 112404.
- Neubauer, A., C. Pfleiderer, B. Binz, A. Rosch, R. Ritz, P. G. Niklowitz, and P. Böni, 2009, “Topological Hall Effect in the A Phase of MnSi,” *Phys. Rev. Lett.* **102**, 186602.
- Nishikawa, Y., K. Hukushima, and W. Krauth, 2019, “Solid-liquid transition of skyrmions in a two-dimensional chiral magnet,” *Phys. Rev. B* **99**, 064435.
- Nozaki, T., Y. Jibiki, M. Goto, E. Tamura, T. Nozaki, H. Kubota, A. Fukushima, S. Yuasa, and Y. Suzuki, 2019, “Brownian motion of skyrmion bubbles and its control by voltage applications,” *Appl. Phys. Lett.* **114**, 012402.
- Nych, A., J. Fukuda, U. Ognysta, S. Žumer, and I. Mušević, 2017, “Spontaneous formation and dynamics of half-skyrmions in a chiral liquid-crystal film,” *Nat. Phys.* **13**, 1215.
- Ogawa, N., W. Koshibae, A. J. Beekman, N. Nagaosa, M. Kubota, M. Kawasaki, and Y. Tokura, 2015, “Photodrive of magnetic bubbles via magnetoelastic waves,” *Proc. Natl. Acad. Sci. U.S.A.* **112**, 8977–8981.
- O’Hern, C. S., L. E. Silbert, A. J. Liu, and S. R. Nagel, 2003, “Jamming at zero temperature and zero applied stress: The epitome of disorder,” *Phys. Rev. E* **68**, 011306.
- Okuma, S., H. Imaizumi, D. Shimamoto, and N. Kokubo, 2011, “Quantum melting and lattice orientation of driven vortex matter,” *Phys. Rev. B* **83**, 064520.
- Okuma, S., J. Inoue, and N. Kokubo, 2007, “Suppression of broadband noise at mode locking in driven vortex matter,” *Phys. Rev. B* **76**, 172503.
- Okuyama, D., *et al.*, 2019, “Deformation of the moving magnetic skyrmion lattice in MnSi under electric current flow,” *Commun. Phys.* **2**, 79.
- Olive, E., and J. C. Soret, 2006, “Chaotic Dynamics of Superconductor Vortices in the Plastic Phase,” *Phys. Rev. Lett.* **96**, 027002.
- Olson, C. J., C. Reichhardt, and F. Nori, 1998a, “Fractal Networks, Braiding Channels, and Voltage Noise in Intermittently Flowing Rivers of Quantized Magnetic Flux,” *Phys. Rev. Lett.* **80**, 2197–2200.
- Olson, C. J., C. Reichhardt, and F. Nori, 1998b, “Nonequilibrium Dynamic Phase Diagram for Vortex Lattices,” *Phys. Rev. Lett.* **81**, 3757–3760.
- Olson, C. J., C. Reichhardt, R. T. Scalettar, G. T. Zimányi, and N. Grønbech-Jensen, 2003, “Metastability and transient effects in vortex matter near a decoupling transition,” *Phys. Rev. B* **67**, 184523.
- Olson, C. J., G. T. Zimányi, A. B. Kolton, and N. Grønbech-Jensen, 2000, “Static and Dynamic Coupling Transitions of Vortex Lattices in Disordered Anisotropic Superconductors,” *Phys. Rev. Lett.* **85**, 5416–5419.
- Olszewski, M. W., M. R. Eskildsen, C. Reichhardt, and C. J. O. Reichhardt, 2018, “Structural transitions in vortex systems with anisotropic interactions,” *New J. Phys.* **20**, 023005.
- Onose, Y., Y. Okamura, S. Seki, S. Ishiwata, and Y. Tokura, 2012, “Observation of Magnetic Excitations of Skyrmion Crystal in a Helimagnetic Insulator Cu_2OSeO_3 ,” *Phys. Rev. Lett.* **109**, 037603.
- Ortiz-Ambriz, A., and P. Tierno, 2016, “Engineering of frustration in colloidal artificial ices realized on microfeatured grooved lattices,” *Nat. Commun.* **7**, 10575.
- Palermo, X., *et al.*, 2020, “Tailored Flux Pinning in Superconductor-Ferromagnet Multilayers with Engineered Magnetic Domain Morphology from Stripes to Skyrmions,” *Phys. Rev. Applied* **13**, 014043.
- Paltiel, Y., E. Zeldov, Y. N. Myasoedov, H. Shtrikman, S. Bhattacharya, M. J. Higgins, Z. L. Xiao, E. Y. Andrei, P. L. Gammel, and D. J. Bishop, 2000, “Dynamic instabilities and memory effects in vortex matter,” *Nature (London)* **403**, 398–401.
- Pardo, F., F. de la Cruz, P. L. Gammel, E. Bucher, and D. J. Bishop, 1998, “Observation of smectic and moving-Bragg-glass phases in flowing vortex lattices,” *Nature (London)* **396**, 348–350.
- Park, H. S., *et al.*, 2014, “Observation of the magnetic flux and three-dimensional structure of skyrmion lattices by electron holography,” *Nat. Nanotechnol.* **9**, 337–342.
- Pasquini, G., D. Pérez Daroca, C. Chilotte, G. S. Lozano, and V. Bekeris, 2008, “Ordered, Disordered, and Coexistent Stable Vortex Lattices in NbSe_2 Single Crystals,” *Phys. Rev. Lett.* **100**, 247003.
- Pathak, S. A., and R. Hertel, 2021, “Geometrically constrained skyrmions,” *Magnetochemistry* **7**, 26.
- Peng, L., R. Takagi, W. Koshibae, K. Shibata, K. Nakajima, T. Arima, N. Nagaosa, S. Seki, X. Yu, and Y. Tokura, 2020, “Controlled transformation of skyrmions and antiskyrmions in a non-centrosymmetric magnet,” *Nat. Nanotechnol.* **15**, 181.
- Perković, O., K. Dahmen, and J. P. Sethna, 1995, “Avalanches, Barkhausen Noise, and Plain Old Criticality,” *Phys. Rev. Lett.* **75**, 4528–4531.

- Pertsinidis, A., and X. S. Ling, 2008, “Statics and Dynamics of 2D Colloidal Crystals in a Random Pinning Potential,” *Phys. Rev. Lett.* **100**, 028303.
- Petrović, A. P., *et al.*, 2021, “Skyrmion-(Anti)Vortex Coupling in a Chiral Magnet-Superconductor Heterostructure,” *Phys. Rev. Lett.* **126**, 117205.
- Pinna, D., F. Abreu Araujo, J.-V. Kim, V. Cros, D. Querlioz, P. Bessiere, J. Droulez, and J. Grollier, 2018, “Skyrmion Gas Manipulation for Probabilistic Computing,” *Phys. Rev. Applied* **9**, 064018.
- Pinsolle, E., N. Kirova, V. L. R. Jacques, A. A. Sinchenko, and D. Le Bolloc’h, 2012, “Creep, Flow, and Phase Slippage Regimes: An Extensive View of the Sliding Charge-Density Wave Revealed by Coherent X-Ray Diffraction,” *Phys. Rev. Lett.* **109**, 256402.
- Plettenberg, J., M. Stier, and M. Thorwart, 2020, “Steering of the Skyrmion Hall Angle by Gate Voltages,” *Phys. Rev. Lett.* **124**, 207202.
- Pöllath, S., *et al.*, 2017, “Dynamical Defects in Rotating Magnetic Skyrmion Lattices,” *Phys. Rev. Lett.* **118**, 207205.
- Prychynenko, D., M. Sitte, K. Litzius, B. Krüger, G. Bourianoff, M. Kläui, J. Sinova, and K. Everschor-Sitte, 2018, “Magnetic Skyrmion as a Nonlinear Resistive Element: A Potential Building Block for Reservoir Computing,” *Phys. Rev. Applied* **9**, 014034.
- Psaroudaki, C., and D. Loss, 2018, “Skyrmions Driven by Intrinsic Magnons,” *Phys. Rev. Lett.* **120**, 237203.
- Puertas, A. M., and T. Voigtman, 2014, “Microrheology of colloidal systems,” *J. Phys. Condens. Matter* **26**, 243101.
- Purnama, I., W. L. Gan, D. W. Wong, and W. S. Lew, 2015, “Guided current-induced skyrmion motion in 1D potential well,” *Sci. Rep.* **5**, 10620.
- Purnama, I., C. S. Murapaka, W. S. Lew, and T. Ono, 2014, “Remote driving of multiple magnetic domain walls due to topological interaction,” *Appl. Phys. Lett.* **104**, 092414.
- Rajeswari, J., *et al.*, 2015, “Filming the formation and fluctuation of skyrmion domains by cryo-Lorentz transmission electron microscopy,” *Proc. Natl. Acad. Sci. U.S.A.* **112**, 14212–14217.
- Raju, M., A. Yagil, A. Soumyanarayanan, A. K. C. Tan, A. Almoalem, F. Ma, O. M. Auslaender, and C. Panagopoulos, 2019, “The evolution of skyrmions in Ir/Fe/Co/Pt multilayers and their topological Hall signature,” *Nat. Commun.* **10**, 696.
- Ralph, D. C., and M. D. Stiles, 2008, “Spin transfer torques,” *J. Magn. Magn. Mater.* **320**, 1190–1216.
- Reichhardt, C., and F. Nori, 1999, “Phase Locking, Devil’s Staircases, Farey Trees, and Arnold Tongues in Driven Vortex Lattices with Periodic Pinning,” *Phys. Rev. Lett.* **82**, 414–417.
- Reichhardt, C., C. J. Olson, N. Grønbech-Jensen, and F. Nori, 2001, “Moving Wigner Glasses and Smectics: Dynamics of Disordered Wigner Crystals,” *Phys. Rev. Lett.* **86**, 4354–4357.
- Reichhardt, C., C. J. Olson, and F. Nori, 1997, “Dynamic Phases of Vortices in Superconductors with Periodic Pinning,” *Phys. Rev. Lett.* **78**, 2648–2651.
- Reichhardt, C., C. J. Olson, and F. Nori, 1998, “Commensurate and incommensurate vortex states in superconductors with periodic pinning arrays,” *Phys. Rev. B* **57**, 7937–7943.
- Reichhardt, C., and C. J. Olson Reichhardt, 2015, “Shapiro steps for skyrmion motion on a washboard potential with longitudinal and transverse ac drives,” *Phys. Rev. B* **92**, 224432.
- Reichhardt, C., and C. J. Olson Reichhardt, 2016, “Magnus-induced dynamics of driven skyrmions on a quasi-one-dimensional periodic substrate,” *Phys. Rev. B* **94**, 094413.
- Reichhardt, C., D. Ray, and C. J. Olson Reichhardt, 2015, “Magnus-induced ratchet effects for skyrmions interacting with asymmetric substrates,” *New J. Phys.* **17**, 073034.
- Reichhardt, C., D. Ray, and C. J. O. Reichhardt, 2015a, “Collective Transport Properties of Driven Skyrmions with Random Disorder,” *Phys. Rev. Lett.* **114**, 217202.
- Reichhardt, C., D. Ray, and C. J. O. Reichhardt, 2015b, “Quantized transport for a skyrmion moving on a two-dimensional periodic substrate,” *Phys. Rev. B* **91**, 104426.
- Reichhardt, C., D. Ray, and C. J. O. Reichhardt, 2018, “Nonequilibrium phases and segregation for skyrmions on periodic pinning arrays,” *Phys. Rev. B* **98**, 134418.
- Reichhardt, C., and C. J. O. Reichhardt, 2016, “Noise fluctuations and drive dependence of the skyrmion Hall effect in disordered systems,” *New J. Phys.* **18**, 095005.
- Reichhardt, C., and C. J. O. Reichhardt, 2017a, “Depinning and nonequilibrium dynamic phases of particle assemblies driven over random and ordered substrates: A review,” *Rep. Prog. Phys.* **80**, 026501.
- Reichhardt, C., and C. J. O. Reichhardt, 2017b, “Shapiro spikes and negative mobility for skyrmion motion on quasi-one-dimensional periodic substrates,” *Phys. Rev. B* **95**, 014412.
- Reichhardt, C., and C. J. O. Reichhardt, 2019a, “Nonlinear transport, dynamic ordering, and clustering for driven skyrmions on random pinning,” *Phys. Rev. B* **99**, 104418.
- Reichhardt, C., and C. J. O. Reichhardt, 2019b, “Thermal creep and the skyrmion Hall angle in driven skyrmion crystals,” *J. Phys. Condens. Matter* **31**, 07LT01.
- Reijnders, J. W., and R. A. Duine, 2004, “Pinning of Vortices in a Bose-Einstein Condensate by an Optical Lattice,” *Phys. Rev. Lett.* **93**, 060401.
- Reimann, P., 2002, “Brownian motors: Noisy transport far from equilibrium,” *Phys. Rep.* **361**, 57–265.
- Rex, S., I. V. Gornyi, and A. D. Mirlin, 2019, “Majorana bound states in magnetic skyrmions imposed onto a superconductor,” *Phys. Rev. B* **100**, 064504.
- Risbud, S. R., and G. Drazer, 2014, “Directional locking in deterministic lateral-displacement microfluidic separation systems,” *Phys. Rev. E* **90**, 012302.
- Ritzmann, U., L. Desplat, B. Dupé, R. E. Camley, and J.-V. Kim, 2020, “Asymmetric skyrmion-antiskyrmion production in ultrathin ferromagnetic films,” *Phys. Rev. B* **102**, 174409.
- Ritzmann, U., S. von Malottki, J.-V. Kim, S. Heinze, J. Sinova, and B. Dupé, 2018, “Trochoidal motion and pair generation in skyrmion and antiskyrmion dynamics under spin-orbit torques,” *Nat. Electron.* **1**, 451–457.
- Romming, N., C. Hanneken, M. Menzel, J. E. Bickel, B. Wolter, K. von Bergmann, A. Kubetzka, and R. Wiesendanger, 2013, “Writing and deleting single magnetic skyrmions,” *Science* **341**, 636–639.
- Ros, A., R. Eichhorn, J. Regtmeier, T. T. Duong, P. Reimann, and D. Anselmetti, 2005, “Brownian motion—Absolute negative particle mobility,” *Nature (London)* **436**, 928.
- Rößler, U. K., A. N. Bogdanov, and C. Pfleiderer, 2006, “Spontaneous skyrmion ground states in magnetic metals,” *Nature (London)* **442**, 797–801.
- Rousselet, J., L. Salome, A. Ajdari, and J. Prost, 1994, “Directional motion of Brownian particles induced by a periodic asymmetric potential,” *Nature (London)* **370**, 446–448.
- Rózsa, L., A. Deák, E. Simon, R. Yanes, L. Udvardi, L. Szunyogh, and U. Nowak, 2016, “Skyrmions with Attractive Interactions in an Ultrathin Magnetic Film,” *Phys. Rev. Lett.* **117**, 157205.
- Rybakov, F. N., A. B. Borisov, S. Blügel, and N. S. Kiselev, 2015, “New Type of Stable Particlelike States in Chiral Magnets,” *Phys. Rev. Lett.* **115**, 117201.

- Rybakov, F. N., A. B. Borisov, S. Blügel, and N. S. Kiselev, 2016, "New spiral state and skyrmion lattice in 3D model of chiral magnets," *New J. Phys.* **18**, 045002.
- Rybakov, F. N., and N. S. Kiselev, 2019, "Chiral magnetic skyrmions with arbitrary topological charge," *Phys. Rev. B* **99**, 064437.
- Sadr-Lahijany, M. R., P. Ray, and H. E. Stanley, 1997, "Dispersivity-Driven Melting Transition in Two-Dimensional Solids," *Phys. Rev. Lett.* **79**, 3206–3209.
- Safar, H., P. L. Gammel, D. A. Huse, D. J. Bishop, J. P. Rice, and D. M. Ginsberg, 1992, "Experimental Evidence for a First-Order Vortex-Lattice-Melting Transition in Untwinned, Single Crystal $\text{YBa}_2\text{Cu}_3\text{O}_7$," *Phys. Rev. Lett.* **69**, 824–827.
- Saha, S., *et al.*, 2019, "Formation of Néel-type skyrmions in an antidot lattice with perpendicular magnetic anisotropy," *Phys. Rev. B* **100**, 144435.
- Salger, T., S. Kling, T. Hecking, C. Geckeler, L. Morales-Molina, and M. Weitz, 2009, "Directed transport of atoms in a Hamiltonian quantum ratchet," *Science* **326**, 1241–1243.
- Salimath, A., A. About, A. Brataas, and A. Manchon, 2019, "Current-driven skyrmion depinning in magnetic granular films," *Phys. Rev. B* **99**, 104416.
- Salomaa, M. M., and G. E. Volovik, 1987, "Quantized vortices in superfluid ^3He ," *Rev. Mod. Phys.* **59**, 533–613.
- Sampaio, J., V. Cros, S. Rohart, A. Thiaville, and A. Fert, 2013, "Nucleation, stability and current-induced motion of isolated magnetic skyrmions in nanostructures," *Nat. Nanotechnol.* **8**, 839–844.
- Sato, T., A. Kikkawa, Y. Taguchi, Y. Tokura, and F. Kagawa, 2020, "Mode locking phenomena of the current-induced skyrmion-lattice motion in microfabricated MnSi ," *Phys. Rev. B* **102**, 180411.
- Sato, T., W. Koshibae, A. Kikkawa, T. Yokouchi, H. Oike, Y. Taguchi, N. Nagaosa, Y. Tokura, and F. Kagawa, 2019, "Slow steady flow of a skyrmion lattice in a confined geometry probed by narrow-band resistance noise," *Phys. Rev. B* **100**, 094410.
- Schulz, T., R. Ritz, A. Bauer, M. Halder, M. Wagner, C. Franz, C. Pfleiderer, K. Everschor, M. Garst, and A. Rosch, 2012, "Emergent electrodynamic skyrmions in a chiral magnet," *Nat. Phys.* **8**, 301–304.
- Schütte, C., J. Iwasaki, A. Rosch, and N. Nagaosa, 2014, "Inertia, diffusion, and dynamics of a driven skyrmion," *Phys. Rev. B* **90**, 174434.
- Schütte, C., and A. Rosch, 2014, "Dynamics and energetics of emergent magnetic monopoles in chiral magnets," *Phys. Rev. B* **90**, 174432.
- Seki, S., M. Garst, J. Waizner, R. Takagi, N. D. Khanh, Y. Okamura, K. Kondou, F. Kagawa, Y. Otani, and Y. Tokura, 2020, "Propagation dynamics of spin excitations along skyrmion strings," *Nat. Commun.* **11**, 256.
- Seki, S., X. Z. Yu, S. Ishiwata, and Y. Tokura, 2012, "Observation of skyrmions in a multiferroic material," *Science* **336**, 198–201.
- Sengupta, A., S. Sengupta, and G. I. Menon, 2010, "Driven disordered polymorphic solids: Phases and phase transitions, dynamical coexistence and peak effect anomalies," *Phys. Rev. B* **81**, 144521.
- Sethna, J. P., K. Dahmen, S. Kartha, J. A. Krumhansl, B. W. Roberts, and J. D. Shore, 1993, "Hysteresis and Hierarchies: Dynamics of Disorder-Driven First-Order Phase Transformations," *Phys. Rev. Lett.* **70**, 3347–3350.
- Sethna, J. P., K. A. Dahmen, and C. R. Myers, 2001, "Crackling noise," *Nature (London)* **410**, 242–250.
- Shapiro, S., 1963, "Josephson Currents in Superconducting Tunneling: The Effect of Microwaves and Other Observations," *Phys. Rev. Lett.* **11**, 80–82.
- Shaw, G., P. Mandal, S. S. Banerjee, A. Niazi, A. K. Rastogi, A. K. Sood, S. Ramakrishnan, and A. K. Grover, 2012, "Critical behavior at depinning of driven disordered vortex matter in $2H\text{-NbS}_2$," *Phys. Rev. B* **85**, 174517.
- Shen, L. C., J. Xia, G. P. Zhao, X. C. Zhang, M. Ezawa, O. A. Tretiakov, X. X. Liu, and Y. Zhou, 2018, "Dynamics of the antiferromagnetic skyrmion induced by a magnetic anisotropy gradient," *Phys. Rev. B* **98**, 134448.
- Shen, M., Y. Zhang, J. Ou-Yang, X. Yang, and L. You, 2018, "Motion of a skyrmionium driven by spin wave," *Appl. Phys. Lett.* **112**, 062403.
- Shibata, K., T. Tanigaki, T. Akashi, H. Shinada, K. Harada, K. Niitsu, D. Shindo, N. Kanazawa, Y. Tokura, and T. Arima, 2018, "Current-driven motion of domain boundaries between skyrmion lattice and helical magnetic structure," *Nano Lett.* **18**, 929–933.
- Shklovskij, V. A., V. V. Sosedkin, and O. V. Dobrovolskiy, 2014, "Vortex ratchet reversal in an asymmetric washboard pinning potential subject to combined dc and ac stimuli," *J. Phys. Condens. Matter* **26**, 025703.
- Silva, R. L., L. D. Secchin, W. A. Moura-Melo, A. R. Pereira, and R. L. Stamps, 2014, "Emergence of skyrmion lattices and bimerons in chiral magnetic thin films with nonmagnetic impurities," *Phys. Rev. B* **89**, 054434.
- Singh, A., *et al.*, 2019, "Scaling of domain cascades in stripe and skyrmion phases," *Nat. Commun.* **10**, 1988.
- Skyrme, T. H., 1961, "A non-linear field theory," *Proc. R. Soc. A* **260**, 127.
- Skyrme, T. H. R., 1962, "A unified field theory of mesons and baryons," *Nucl. Phys.* **31**, 556.
- Sondhi, S. L., A. Karlhede, S. A. Kivelson, and E. H. Rezayi, 1993, "Skyrmions and the crossover from the integer to fractional quantum Hall effect at small Zeeman energies," *Phys. Rev. B* **47**, 16419–16426.
- Song, K. M., *et al.*, 2020, "Skyrmion-based artificial synapses for neuromorphic computing," *Nat. Electron.* **3**, 148–155.
- Soumyanarayanan, A., *et al.*, 2017, "Tunable room-temperature magnetic skyrmions in Ir/Fe/Co/Pt multilayers," *Nat. Mater.* **16**, 898–904.
- Stier, M., R. Strobel, S. Krause, W. Häusler, and M. Thorwart, 2021, "Role of impurity clusters for the current-driven motion of magnetic skyrmions," *Phys. Rev. B* **103**, 054420.
- Stosic, D., T. B. Ludermir, and M. V. Milošević, 2017, "Pinning of magnetic skyrmions in a monolayer Co film on Pt(111): Theoretical characterization and exemplified utilization," *Phys. Rev. B* **96**, 214403.
- Strandburg, K. J., 1988, "Two-dimensional melting," *Rev. Mod. Phys.* **60**, 161–207.
- Straver, E. W. J., J. E. Hoffman, O. M. Auslaender, D. Rugar, and K. A. Moler, 2008, "Controlled manipulation of individual vortices in a superconductor," *Appl. Phys. Lett.* **93**, 172514.
- Suess, D., C. Vogler, F. Bruckner, P. Heistracher, and C. Abert, 2018, "A repulsive skyrmion chain as a guiding track for a racetrack memory," *AIP Adv.* **8**, 115301.
- Suess, D., C. Vogler, F. Bruckner, P. Heistracher, F. Slanovc, and C. Abert, 2019, "Spin torque efficiency and analytic error rate estimates of skyrmion racetrack memory," *Sci. Rep.* **9**, 4827.
- Sun, L., R. X. Cao, B. F. Miao, Z. Feng, B. You, D. Wu, W. Zhang, A. Hu, and H. F. Ding, 2013, "Creating an Artificial Two-Dimensional Skyrmion Crystal by Nanopatterning," *Phys. Rev. Lett.* **110**, 167201.
- Sun, L., H. Z. Wu, B. F. Miao, D. Wu, and H. F. Ding, 2018, "Tuning the stability and the skyrmion Hall effect in magnetic skyrmions by

- adjusting their exchange strengths with magnetic disks,” *J. Magn. Mater.* **455**, 39.
- Tagaki, R., Y. Yamasaki, T. Yokouchi, V. Ukleev, Y. Yokoyama, H. Nakao, T. Arima, Y. Tokura, and S. Seki, 2020, “Particle-size dependent structural transformation of skyrmion lattice,” *Nat. Commun.* **11**, 5685.
- Tagaki, R., X. Z. Yu, J. S. White, K. Shibata, Y. Kaneko, G. Tatara, H. M. Rønnow, Y. Tokura, and S. Seki, 2018, “Low-Field Bi-Skyrmion Formation in a Noncentrosymmetric Chimney Ladder Ferromagnet,” *Phys. Rev. Lett.* **120**, 037203.
- Tatara, G., H. Kohno, and J. Shibata, 2008, “Microscopic approach to current-driven domain wall dynamics,” *Phys. Rep.* **468**, 213–301.
- Thiele, A. A., 1973, “Steady-State Motion of Magnetic Domains,” *Phys. Rev. Lett.* **30**, 230–233.
- Thorneywork, A. L., J. L. Abbott, D. G. A. L. Aarts, and R. P. A. Dullens, 2017, “Two-Dimensional Melting of Colloidal Hard Spheres,” *Phys. Rev. Lett.* **118**, 158001.
- Tierno, P., 2012, “Depinning and Collective Dynamics of Magnetically Driven Colloidal Monolayers,” *Phys. Rev. Lett.* **109**, 198304.
- Toft-Petersen, R., A. B. Abrahamsen, S. Balog, L. Porcar, and M. Laver, 2018, “Decomposing the Bragg glass and the peak effect in a type-II superconductor,” *Nat. Commun.* **9**, 901.
- Togawa, Y., R. Abiru, K. Iwaya, H. Kitano, and A. Maeda, 2000, “Direct Observation of the Washboard Noise of a Driven Vortex Lattice in a High-Temperature Superconductor, $\text{Bi}_2\text{Sr}_2\text{CaCu}_2\text{O}_y$,” *Phys. Rev. Lett.* **85**, 3716–3719.
- Tokunaga, Y., X. Z. Yu, J. S. White, H. M. Rønnow, D. Morikawa, Y. Taguchi, and Y. Tokura, 2015, “A new class of chiral materials hosting magnetic skyrmions beyond room temperature,” *Nat. Commun.* **6**, 7638.
- Tokura, Y., and N. Kanazawa, 2021, “Magnetic skyrmion materials,” *Chem. Rev.* **121**, 2857–2897.
- Tolley, R., S. A. Montoya, and E. E. Fullerton, 2018, “Room-temperature observation and current control of skyrmions in Pt/Co/Os/Pt thin films,” *Phys. Rev. Mater.* **2**, 044404.
- Tomasello, R., E. Martinez, R. Zivieri, L. Torres, M. Carpentieri, and G. Finocchio, 2014, “A strategy for the design of skyrmion racetrack memories,” *Sci. Rep.* **4**, 6784.
- Tomasello, R., *et al.*, 2018, “Micromagnetic understanding of the skyrmion Hall angle current dependence in perpendicularly magnetized ferromagnets,” *Phys. Rev. B* **98**, 224418.
- Tong, Q., F. Liu, J. Xiao, and W. Yao, 2018, “Skyrmions in the moiré of van der Waals 2D magnets,” *Nano Lett.* **18**, 7194–7199.
- Torquato, S., 2016, “Hyperuniformity and its generalizations,” *Phys. Rev. E* **94**, 022122.
- Toscano, D., S. A. Leonel, P. Z. Coura, and F. Sato, 2019, “Building traps for skyrmions by the incorporation of magnetic defects into nanomagnets: Pinning and scattering traps by magnetic properties engineering,” *J. Magn. Mater.* **480**, 171–185.
- Travesset, A., R. A. White, and K. A. Dahmen, 2002, “Crackling noise, power spectra, and disorder-induced critical scaling,” *Phys. Rev. B* **66**, 024430.
- Troncoso, R. E., and A. S. Núñez, 2014, “Thermally assisted current-driven skyrmion motion,” *Phys. Rev. B* **89**, 224403.
- Tsesses, S., E. Ostrovsky, K. Cohen, B. Gjonaj, N. H. Lindner, and G. Bartal, 2018, “Optical skyrmion lattice in evanescent electromagnetic fields,” *Science* **361**, 993–996.
- Tsoi, M., R. E. Fontana, and S. S. P. Parkin, 2003, “Magnetic domain wall motion triggered by an electric current,” *Appl. Phys. Lett.* **83**, 2617–2619.
- Tung, S., V. Schweikhard, and E. A. Cornell, 2006, “Observation of Vortex Pinning in Bose-Einstein Condensates,” *Phys. Rev. Lett.* **97**, 240402.
- Vakili, H., *et al.*, 2021, “Skyrmionics—Computing and memory technologies based on topological excitations in magnets,” *J. Appl. Phys.* **130**, 070908.
- Van Look, L., E. Rosseel, M. J. Van Bael, K. Temst, V. V. Moshchalkov, and Y. Bruynseraede, 1999, “Shapiro steps in a superconducting film with an antidot lattice,” *Phys. Rev. B* **60**, R6998–R7000.
- Vanossi, A., N. Manini, M. Urbakh, S. Zapperi, and E. Tosatti, 2013, “Colloquium: Modeling friction: From nanoscale to mesoscale,” *Rev. Mod. Phys.* **85**, 529–552.
- Villegas, J. E., M. I. Montero, C.-P. Li, and I. K. Schuller, 2006, “Correlation Length of Quasiperiodic Vortex Lattices,” *Phys. Rev. Lett.* **97**, 027002.
- Villegas, J. E., S. Savel’ev, F. Nori, E. M. Gonzalez, J. V. Anguita, R. García, and J. L. Vicent, 2003, “A superconducting reversible rectifier that controls the motion of magnetic flux quanta,” *Science* **302**, 1188–1191.
- Vizarim, N. P., C. Reichhardt, C. J. O. Reichhardt, and P. A. Venegas, 2020, “Skyrmion dynamics and topological sorting on periodic obstacle arrays,” *New J. Phys.* **22**, 053025.
- Vizarim, N. P., C. J. O. Reichhardt, P. A. Venegas, and C. Reichhardt, 2020, “Skyrmion pinball and directed motion on obstacle arrays,” *J. Phys. Commun.* **4**, 085001.
- Vlasko-Vlasov, V. K., L. A. Dorosinskii, A. A. Polyanskii, V. I. Nikitenko, U. Welp, B. W. Veal, and G. W. Crabtree, 1994, “Study of the Influence of Individual Twin Boundaries on the Magnetic Flux Penetration in $\text{YBa}_2\text{Cu}_3\text{O}_{7-\delta}$,” *Phys. Rev. Lett.* **72**, 3246–3249.
- Wang, C., D. Xiao, X. Chen, Y. Zhou, and Y. Liu, 2017, “Manipulating and trapping skyrmions by magnetic field gradients,” *New J. Phys.* **19**, 083008.
- Wang, L., *et al.*, 2018, “Ferroelectrically tunable magnetic skyrmions in ultrathin oxide heterostructures,” *Nat. Mater.* **17**, 1087–1094.
- Wang, L., *et al.*, 2019, “Construction of a room-temperature Pt/Co/Ta multilayer film with ultrahigh-density skyrmions for memory application,” *ACS Appl. Mater. Interfaces* **11**, 12098–12104.
- Wang, W., M. Beg, B. Zhang, W. Kuch, and H. Fangohr, 2015, “Driving magnetic skyrmions with microwave fields,” *Phys. Rev. B* **92**, 020403(R).
- Wang, W., *et al.*, 2016, “A centrosymmetric hexagonal magnet with superstable biskyrmion magnetic nanodomains in a wide temperature range of 100–340 K,” *Adv. Mater.* **28**, 6887.
- Wang, X. S., A. Qaiumzadeh, and A. Brataas, 2019, “Current-Driven Dynamics of Magnetic Hopfions,” *Phys. Rev. Lett.* **123**, 147203.
- Wang, X.-G., L. Chotorlishvili, V. K. Dugaev, A. Ernst, I. V. Maznichenko, N. Arnold, C. Jia, J. Berakdar, I. Mertig, and J. Barnaś, 2020, “The optical tweezer of skyrmions,” *npj Comput. Mater.* **6**, 140.
- Wang, Y. J., *et al.*, 2020, “Polar meron lattice in strained oxide ferroelectrics,” *Nat. Mater.* **19**, 881.
- Wang, Y.-L., X. Ma, J. Xu, Z.-L. Xiao, A. Snezhko, R. Divan, L. E. Ocola, J. E. Pearson, B. Jánko, and W.-K. Kwok, 2018, “Switchable geometric frustration in an artificial-spin-ice-superconductor heterosystem,” *Nat. Nanotechnol.* **13**, 560.
- Wang, Z., *et al.*, 2020, “Thermal generation, manipulation and thermoelectric detection of skyrmions,” *Nat. Electron.* **3**, 672.
- Wei, Q.-H., C. Bechinger, D. Rudhardt, and P. Leiderer, 1998, “Experimental Study of Laser-Induced Melting in Two-Dimensional Colloids,” *Phys. Rev. Lett.* **81**, 2606–2609.
- Weiss, J. A., A. E. Larsen, and D. G. Grier, 1998, “Interactions, dynamics, and elasticity in charge-stabilized colloidal crystals,” *J. Chem. Phys.* **109**, 8659–8666.

- Weissman, M. B., 1988, “ $1/f$ noise and other slow, nonexponential kinetics in condensed matter,” *Rev. Mod. Phys.* **60**, 537–571.
- White, J. S., *et al.*, 2014, “Electric-Field-Induced Skyrmion Distortion and Giant Lattice Rotation in the Magnetoelectric Insulator Cu_2OSeO_3 ,” *Phys. Rev. Lett.* **113**, 107203.
- Wiesendanger, R., 2016, “Nanoscale magnetic skyrmions in metallic films and multilayers: A new twist for spintronics,” *Nat. Rev. Mater.* **1**, 16044.
- Williams, F. I. B., *et al.*, 1991, “Conduction Threshold and Pinning Frequency of Magnetically Induced Wigner Solid,” *Phys. Rev. Lett.* **66**, 3285–3288.
- Wolf, D., S. Schneider, U. K. Rößler, A. Kovács, M. Schmidt, R. E. Dunin-Borkowski, B. Büchner, B. Rellinghaus, and A. Lubk, 2022, “Unveiling the three-dimensional magnetic texture of skyrmion tubes,” *Nat. Nanotechnol.* **17**, 250–255.
- Woo, S., *et al.*, 2016, “Observation of room-temperature magnetic skyrmions and their current-driven dynamics in ultrathin metallic ferromagnets,” *Nat. Mater.* **15**, 501–506.
- Woo, S., *et al.*, 2018, “Current-driven dynamics and inhibition of the skyrmion Hall effect of ferrimagnetic skyrmions in GdFeCo films,” *Nat. Commun.* **9**, 959.
- Xia, J., X. Zhang, M. Ezawa, Q. Shao, X. Liu, and Y. Zhou, 2020, “Dynamics of an elliptical ferromagnetic skyrmion driven by the spin-orbit torque,” *Appl. Phys. Lett.* **116**, 022407.
- Xia, J., X. Zhang, K.-Y. Mak, M. Ezawa, O. A. Tretiakov, Y. Zhou, G. Zhao, and X. Liu, 2021, “Current-induced dynamics of skyrmion tubes in synthetic antiferromagnetic multilayers,” *Phys. Rev. B* **103**, 174408.
- Xiao, K., Y. Roichman, and D. G. Grier, 2011, “Two-dimensional optical thermal ratchets based on Fibonacci spirals,” *Phys. Rev. E* **84**, 011131.
- Xiao, Z. L., E. Y. Andrei, and M. J. Higgins, 1999, “Flow Induced Organization and Memory of a Vortex Lattice,” *Phys. Rev. Lett.* **83**, 1664–1667.
- Xing, X., J. Åkerman, and Y. Zhou, 2020, “Enhanced skyrmion motion via strip domain wall,” *Phys. Rev. B* **101**, 214432.
- Xu, X. B., H. Fangohr, Z. H. Wang, M. Gu, S. L. Liu, D. Q. Shi, and S. X. Dou, 2011, “Vortex dynamics for low- κ type-II superconductors,” *Phys. Rev. B* **84**, 014515.
- Yang, G., P. Stano, J. Klinovaja, and D. Loss, 2016, “Majorana bound states in magnetic skyrmions,” *Phys. Rev. B* **93**, 224505.
- Yang, H., A. Thiaville, S. Rohart, A. Fert, and M. Chshiev, 2015, “Anatomy of Dzyaloshinskii-Moriya Interaction at Co/Pt Interfaces,” *Phys. Rev. Lett.* **115**, 267210.
- Yang, S., K.-W. Moon, C. Kim, D.-H. Kim, J. Shin, J. Hong, S. K. Kim, and C. Hwang, 2021, “Control of the half-skyrmion Hall effect and its application to adder-subtractor,” *Adv. Quantum Technol.* **4**, 2000060.
- Yi, S. D., S. Onoda, N. Nagaosa, and J. H. Han, 2009, “Skyrmions and anomalous Hall effect in a Dzyaloshinskii-Moriya spiral magnet,” *Phys. Rev. B* **80**, 054416.
- Yokouchi, T., S. Sugimoto, B. Rana, S. Seki, N. Ogawa, S. Kasai, and Y. Otani, 2020, “Creation of magnetic skyrmions by surface acoustic waves,” *Nat. Nanotechnol.* **15**, 361–366.
- Yokouchi, T., *et al.*, 2018, “Current-induced dynamics of skyrmion strings,” *Sci. Adv.* **4**, eaat1115.
- Young, A. P., 1979, “Melting and the vector Coulomb gas in two dimensions,” *Phys. Rev. B* **19**, 1855–1866.
- Yu, X., 2021, “Magnetic imaging of various topological spin textures and their dynamics,” *J. Magn. Magn. Mater.* **539**, 168332.
- Yu, X., D. Morikawa, T. Yokouchi, K. Shibata, N. Kanazawa, F. Kagawa, T. Arima, and Y. Tokura, 2018, “Aggregation and collapse dynamics of skyrmions in a non-equilibrium state,” *Nat. Phys.* **14**, 832.
- Yu, X., *et al.*, 2017, “Current-induced nucleation and annihilation of magnetic skyrmions at room temperature in a chiral magnet,” *Adv. Mater.* **29**, 1606178.
- Yu, X., *et al.*, 2020, “Real-space observation of topological defects in extended skyrmion-strings,” *Nano Lett.* **20**, 7313–7320.
- Yu, X. Z., N. Kanazawa, Y. Onose, K. Kimoto, W. Z. Zhang, S. Ishiwata, Y. Matsui, and Y. Tokura, 2011, “Near room-temperature formation of a skyrmion crystal in thin-films of the helimagnet FeGe ,” *Nat. Mater.* **10**, 106–109.
- Yu, X. Z., N. Kanazawa, W. Z. Zhang, T. Nagai, T. Hara, K. Kimoto, Y. Matsui, Y. Onose, and Y. Tokura, 2012, “Skyrmion flow near room temperature in an ultralow current density,” *Nat. Commun.* **3**, 988.
- Yu, X. Z., W. Koshibae, Y. Tokunaga, K. Shibata, Y. Taguchi, N. Nagaosa, and Y. Tokura, 2018, “Transformation between meron and skyrmion topological spin textures in a chiral magnet,” *Nature (London)* **564**, 95–98.
- Yu, X. Z., D. Morikawa, K. Nakajima, K. Shibata, N. Kanazawa, T. Arima, N. Nagaosa, and Y. Tokura, 2020, “Motion tracking of 80-nm-size skyrmions upon directional current injections,” *Sci. Adv.* **6**, eaaz9744.
- Yu, X. Z., Y. Onose, N. Kanazawa, J. H. Park, J. H. Han, Y. Matsui, N. Nagaosa, and Y. Tokura, 2010, “Real-space observation of a two-dimensional skyrmion crystal,” *Nature (London)* **465**, 901–904.
- Yu, X. Z., Y. Tokunaga, Y. Kaneko, W. Z. Zhang, K. Kimoto, Y. Matsui, Y. Taguchi, and Y. Tokura, 2014, “Biskyrmion states and their current-driven motion in a layered manganite,” *Nat. Commun.* **5**, 3198.
- Yuan, H. Y., X. S. Wang, M.-H. Yung, and X. R. Wang, 2019, “Wiggling skyrmion propagation under parametric pumping,” *Phys. Rev. B* **99**, 014428.
- Zahn, K., R. Lenke, and G. Maret, 1999, “Two-Stage Melting of Paramagnetic Colloidal Crystals in Two Dimensions,” *Phys. Rev. Lett.* **82**, 2721–2724.
- Zang, J., M. Mostovoy, J. H. Han, and N. Nagaosa, 2011, “Dynamics of Skyrmion Crystals in Metallic Thin Films,” *Phys. Rev. Lett.* **107**, 136804.
- Zapperi, S., C. Castellano, F. Colaiori, and G. Durin, 2005, “Signature of effective mass in crackling-noise asymmetry,” *Nat. Phys.* **1**, 46–49.
- Zapperi, S., P. Cizeau, G. Durin, and H. E. Stanley, 1998, “Dynamics of a ferromagnetic domain wall: Avalanches, depinning transition, and the Barkhausen effect,” *Phys. Rev. B* **58**, 6353–6366.
- Zázvorka, J., F. Dittrich, Y. Ge, N. Kerber, K. Raab, T. Winkler, K. Litzius, M. Veis, P. Virnau, and M. Kläui, 2020, “Skyrmion lattice phases in thin film multilayer,” *Adv. Funct. Mater.* **30**, 2004037.
- Zázvorka, J., *et al.*, 2019, “Thermal skyrmion diffusion used in a reshuffler device,” *Nat. Nanotechnol.* **14**, 658–661.
- Zeissler, K., *et al.*, 2017, “Pinning and hysteresis in the field dependent diameter evolution of skyrmions in $\text{Pt}/\text{Co}/\text{Ir}$ superlattice stacks,” *Sci. Rep.* **7**, 15125.
- Zeissler, K., *et al.*, 2018, “Discrete Hall resistivity contribution from Néel skyrmions in multilayer nanodiscs,” *Nat. Nanotechnol.* **13**, 1161–1166.
- Zeissler, K., *et al.*, 2020, “Diameter-independent skyrmion Hall angle observed in chiral magnetic multilayers,” *Nat. Commun.* **11**, 428.
- Zeldov, E., D. Majer, M. Konczykowski, V. B. Geshkenbein, V. M. Vinokur, and H. Shtrikman, 1995, “Thermodynamic observation of first-order vortex-lattice melting transition in $\text{Bi}_2\text{Sr}_2\text{CaCu}_2\text{O}_8$,” *Nature (London)* **375**, 373–376.

- Zhang, S., F. Kronast, G. van der Laan, and T. Hesjedal, 2018, “Real-space observation of skyrmionium in a ferromagnet-magnetic topological insulator heterostructure,” *Nano Lett.* **18**, 1057.
- Zhang, S., A. K. Petford-Long, and C. Phatak, 2016, “Creation of artificial skyrmions and antiskyrmions by anisotropy engineering,” *Sci. Rep.* **6**, 31248.
- Zhang, S., G. van der Laan, J. Müller, L. Heinen, M. Garst, A. Bauer, H. Berger, C. Pfleiderer, and T. Hesjedal, 2018, “Reciprocal space tomography of 3D skyrmion lattice order in a chiral magnet,” *Proc. Natl. Acad. Sci. U.S.A.* **115**, 6386–6391.
- Zhang, S., J. Zhang, Y. Wen, E. M. Chudnovsky, and X. Zhang, 2018, “Determination of chirality and density control of Néel-type skyrmions with in-plane magnetic field,” *Commun. Phys.* **1**, 36.
- Zhang, S., *et al.*, 2020, “Direct imaging of an inhomogeneous electric current distribution using the trajectory of magnetic half-skyrmions,” *Sci. Adv.* **6**, eaay1876.
- Zhang, S. L., A. Bauer, H. Berger, C. Pfleiderer, G. van der Laan, and T. Hesjedal, 2016, “Imaging and manipulation of skyrmion lattice domains in Cu_2OSeO_3 ,” *Appl. Phys. Lett.* **109**, 192406.
- Zhang, S. L., W. W. Wang, D. M. Burn, H. Peng, H. Berger, A. Bauer, C. Pfleiderer, G. van der Laan, and T. Hesjedal, 2018, “Manipulation of skyrmion motion by magnetic field gradients,” *Nat. Commun.* **9**, 2115.
- Zhang, X., M. Ezawa, D. Xiao, G. P. Zhao, Y. Liu, and Y. Zhou, 2015, “All-magnetic control of skyrmions in nanowires by a spin wave,” *Nanotechnology* **26**, 225701.
- Zhang, X., M. Ezawa, and Y. Zhou, 2015, “Magnetic skyrmion logic gates: Conversion, duplication and merging of skyrmions,” *Sci. Rep.* **5**, 9400.
- Zhang, X., M. Ezawa, and Y. Zhou, 2016, “Thermally stable magnetic skyrmions in multilayer synthetic antiferromagnetic racetracks,” *Phys. Rev. B* **94**, 064406.
- Zhang, X., J. Müller, J. Xia, M. Garst, X. Liu, and Y. Zhou, 2017, “Motion of skyrmions in nanowires driven by magnonic momentum-transfer forces,” *New J. Phys.* **19**, 065001.
- Zhang, X., J. Xia, M. Ezawa, O. A. Tretiakov, H. T. Diep, G. Zhao, X. Liu, and Y. Zhou, 2021, “A frustrated bimeronium: Static structure and dynamics,” *Appl. Phys. Lett.* **118**, 052411.
- Zhang, X., J. Xia, L. Shen, M. Ezawa, O. A. Tretiakov, G. Zhao, X. Liu, and Y. Zhou, 2020, “Static and dynamic properties of bimerons in a frustrated ferromagnetic monolayer,” *Phys. Rev. B* **101**, 144435.
- Zhang, X., J. Xia, G. P. Zhao, X. Liu, and Y. Zhou, 2017, “Magnetic skyrmion transport in a nanotrack with spatially varying damping and non-adiabatic torque,” *IEEE Trans. Magn.* **53**, 1500206.
- Zhang, X., J. Xia, Y. Zhou, X. Liu, H. Zhang, and M. Ezawa, 2017, “Skyrmion dynamics in a frustrated ferromagnetic film and current-induced helicity locking-unlocking transition,” *Nat. Commun.* **8**, 1717.
- Zhang, X., J. Xia, Y. Zhou, D. Wang, X. Liu, W. Zhao, and M. Ezawa, 2016, “Control and manipulation of a magnetic skyrmionium in nanostructures,” *Phys. Rev. B* **94**, 094420.
- Zhang, X., Y. Zhou, and M. Ezawa, 2016a, “Antiferromagnetic skyrmion: Stability, creation and manipulation,” *Sci. Rep.* **6**, 24795.
- Zhang, X., Y. Zhou, and M. Ezawa, 2016b, “Magnetic bilayer-skyrmions without skyrmion Hall effect,” *Nat. Commun.* **7**, 10293.
- Zhang, X., Y. Zhou, M. Ezawa, G. P. Zhao, and W. Zhao, 2015, “Magnetic skyrmion transistor: Skyrmion motion in a voltage-gated nanotrack,” *Sci. Rep.* **5**, 11369.
- Zhang, X., Y. Zhou, K. M. Song, T.-E. Park, J. Xia, M. Ezawa, X. Liu, W. Zhao, G. Zhao, and S. Woo, 2020, “Skyrmion-electronics: Writing, deleting, reading and processing magnetic skyrmions toward spintronic applications,” *J. Phys. Condens. Matter* **32**, 143001.
- Zhang, X.-X., A. S. Mishchenko, G. De Filippis, and N. Nagaosa, 2016, “Electric transport in three-dimensional skyrmion/monopole crystal,” *Phys. Rev. B* **94**, 174428.
- Zhao, H. J., V. R. Misko, and F. M. Peeters, 2013, “Dynamics of self-organized driven particles with competing range interaction,” *Phys. Rev. E* **88**, 022914.
- Zhao, H. J., W. Wu, Wei Zhou, Z. X. Shi, V. R. Misko, and F. M. Peeters, 2016, “Reentrant dynamics of driven pancake vortices in layered superconductors,” *Phys. Rev. B* **94**, 024514.
- Zhao, L., *et al.*, 2020, “Topology-Dependent Brownian Gyromotion of a Single Skyrmion,” *Phys. Rev. Lett.* **125**, 027206.
- Zheng, F., *et al.*, 2018, “Experimental observation of chiral magnetic bobbles in B20-type FeGe,” *Nat. Nanotechnol.* **13**, 451–455.
- Zhou, H., H. Polshyn, T. Taniguchi, K. Watanabe, and A. F. Young, 2020, “Solids of quantum Hall skyrmions in graphene,” *Nat. Phys.* **16**, 154.
- Zhou, L., R. Qin, Y.-Q. Zheng, and Y. Wang, 2019, “Skyrmion Hall effect with spatially modulated Dzyaloshinskii-Moriya interaction,” *Front. Phys.* **14**, 53602.
- Zhou, Y., R. Mansell, and S. van Dijken, 2019, “Driven gyrotropic skyrmion motion through steps in magnetic anisotropy,” *Sci. Rep.* **9**, 6525.
- Zou, J., S. Zhang, and Y. Tserkovnyak, 2020, “Topological Transport of Deconfined Hedgehogs in Magnets,” *Phys. Rev. Lett.* **125**, 267201.
- Zvezdin, A. K., V. I. Belotelov, and K. A. Zvezdin, 2008, “Gyroscopic force acting on the magnetic vortex in a weak ferromagnet,” *JETP Lett.* **87**, 381–384.